

N7678027



N7678027

**DEVELOPMENT
OF A
FAIL SAFE DESIGN
OXIDATION RESISTANT
REINFORCED CARBON SYSTEM
FOR THE
WING LEADING EDGE
OF A
SPACE SHUTTLE VEHICLE**

NASA-JSC CONTRACT NAS9-12763

**PHASE III FINAL REPORT
VOLUME V
APPENDIX C
THERMAL ANALYSES**

VSD REPORT NO. T143-5R-30008



VOUGHT SYSTEMS DIVISION
LTV AEROSPACE CORPORATION

P.O. BOX 5907 • DALLAS TEXAS 75222

REPRODUCED BY:
U.S. Department of Commerce
National Technical Information Service
Springfield, Virginia 22161



APPENDIX C

THERMAL DESIGN INFORMATION RELEASES (DIRS)

CONTENTS

T143-DIR-2-03	Ablation Analysis of Bare RPP on Shuttle Wing Leading Edge
T143-DIR-2-07	Predicted Temperature Distribution for the Wing Leading Edge Skin and Rib
T143-DIR-2-11	Predicted Temperature Distribution for the Windward Side Leading Edge Support Joint and Bracket
T143-DIR-2-18	Support Lug Thermal Test - Predicted Temperature Distribution
T143-DIR-2-19 and Rev. A	Fail Safe Leading Edge Thermal Analysis
T143-DIR-3-02	Gap Heating Test

174-10174

DESIGN INFORMATION REQUEST-RELEASE

6-15-72

REL. (S) AND EFF. ABLATION ANALYSIS OF BARE RPP ON SHUTTLE WING LEADING EDGE		DIR. NO. T143-DIR-2-03		REV.	
		DATE 5 June 1972	PAGE 1	OF 6	
SYSTEM PHASE III SHUTTLE LEADING EDGE		REF. O. O. NUMBER 3357-AA-1160			
Fill in block below for Information Request			Fill in block below for Information Release		
GROUP			IN REPLY TO DIR. NUMBER		
GROUP			REL. TO D.M. While		
BY			PREPARED BY J. Medford		
ISON			DATE 6/5/72		
ONLY <input type="checkbox"/> EWR <input type="checkbox"/> BUWEP <input type="checkbox"/> <input type="checkbox"/>			GROUP APP. J Medford		
			DATE 6/5/72		
			PROJ OFFICE While		
			DATE 6/5/72		
T. Esenwein, W.E. Agan, B.A. Forcht, I.E. Harder, E.C. Matza, F.D. Tarsia					

- REFERENCES:
- (1) "Thermal Analysis Development Plan, Phase III Shuttle Leading Edge", Memorandum No. T143-5M-00144, 4 May 1972
 - (2) "Development of a Reinforced Carbonaceous and Ablative Composite for Entry Heat Protection of Manned Spacecraft", VMSC Report No. 330.17, July, 1963
 - (3) "Development of a Thermal Protection System for the Wing of a Space Shuttle Vehicle", Phase II Final Report, VMSC Report No. T143-5R-00124, 30 April 1972.
 - (4) "Thermal Evaluation Tests of Oxidation Inhibited Carbonaceous Materials in the MSC 1.5 MW Arc Heated Tunnel", NASA Memorandum No. ES5/5-21 (0)/108M, 20 May 1970.
 - (5) "Thermal Evaluation Tests of Reinforced Pyrolyzed Plastic (RPP) Materials in the MSC 1.5 MW and 10 MW Arc-Heated Facilities", NASA Memorandum No. ES5/11-12(9) 1287M, 12 November 1969.

INTRODUCTION:

A reentry oxidation analysis was performed, as required by Reference (1), to determine the reentry thickness loss of bare RPP in the event of coating loss prior to reentry. This data will be used, in conjunction with structural analyses, to define the total skin thickness required to provide a fail safe design.

APPROACH:

Surface recession rates were computed at ten locations around the leading edge periphery using a VMSC one-dimensional ablation routine which accounts for reaction rate control, transition and diffusion control oxidation mechanisms. Oxidation characteristics of bare RPP were based upon plasma arc test data as reported in Reference (2). Emittance and specific heat of bare RPP were also taken from Reference (2), while thermal conductivity was assumed equal to that of coated RPP and was taken from final characterization data in Reference (3).

Effects of cross radiation were included in the oxidation analysis by permitting the inside surface of the skin to participate in radiant interchange with a surface of specified time variant temperature equal to the average temperature within the leading edge cavity. This cavity temperature was taken from Phase II cross radiation analysis results as reported in Reference (3). Since the average cavity temperature could conceivably be different for the thick skin fail safe design than for the thin skin Phase II design, a comparison was made of peak inside skin temperatures from Phase II cross radiation analyses and from the current ablation analyses to determine if a correction was required to the Phase II cavity temperature.

RESULTS:

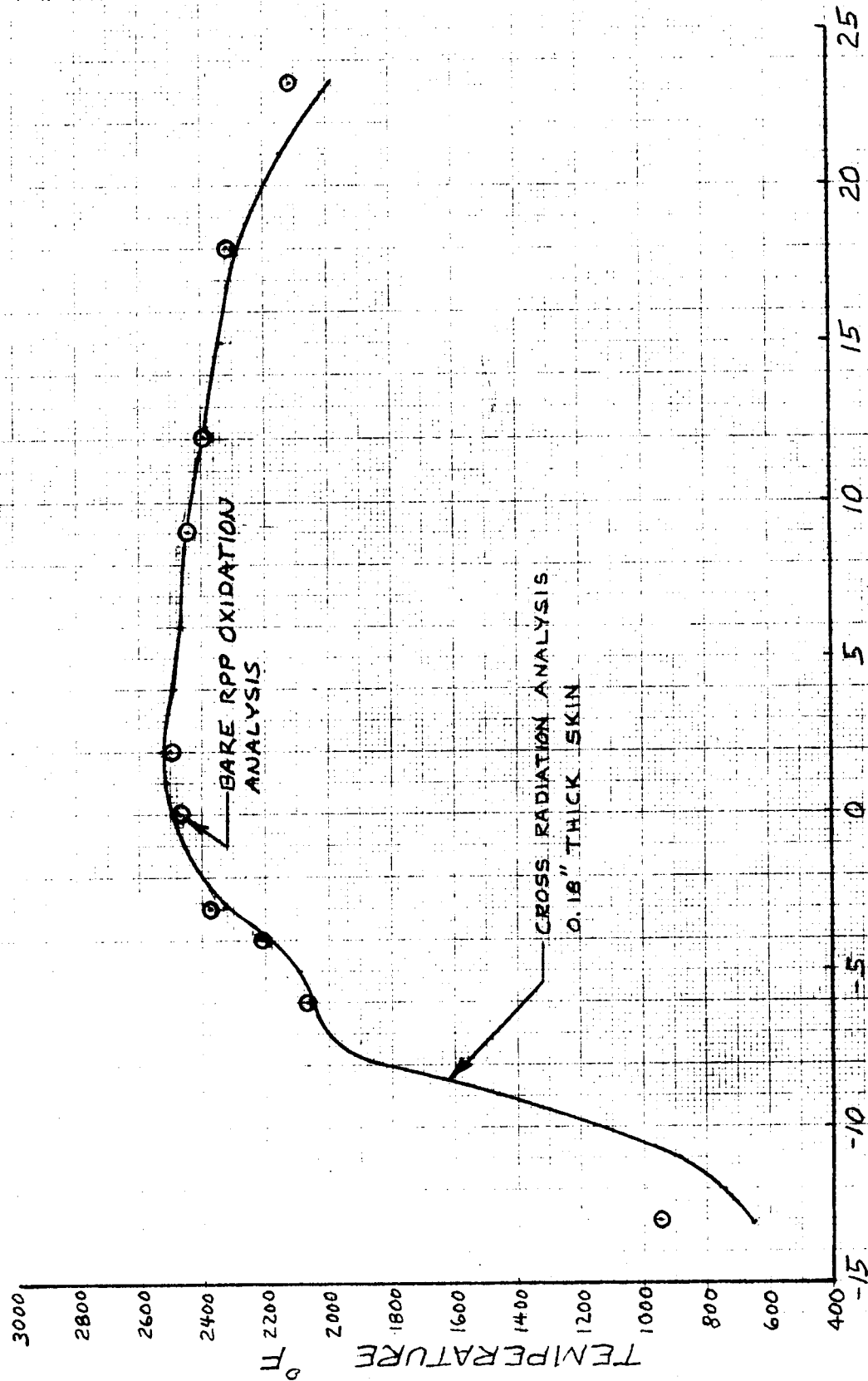
Computed maximum inside skin temperatures are presented as a function of location on the leading edge in Figure 1, and are compared with Phase II cross radiation analysis results. The close agreement indicates that the average cavity temperature obtained from Phase II analyses and used in the current ablation analyses for determining cross radiation effects upon skin temperatures is quite reasonable.

Oxidation results are presented in Figures 2 and 3. Thickness losses for ten locations on the leading edge are shown in Figure 2 as a function of entry time. The maximum thickness loss from these curves is cross plotted as a function of location on the leading edge in Figure 3. It is seen that the peak thickness loss at the stagnation line is 0.236 inch, and that this drops to 0.076 inch on the windward side trailing edge and to essentially no recession on the leeward side trailing edge.

RECOMMENDATIONS:

It is recommended that 20% additional thickness be added to the surface recession values in Figure 3 for margin. This value is based upon plasma arc data scatter about theoretical oxidation losses in References (2), (4), and (5) and in the recent wing tip model tests at NASA-MSC.

FIGURE 1
COMPARISON OF SKIN INSIDE TEMPERATURES



"WETTED" DISTANCE FROM LEADING EDGE, INCHES

FIGURE 2
THICKNESS LOSS VERSUS TIME

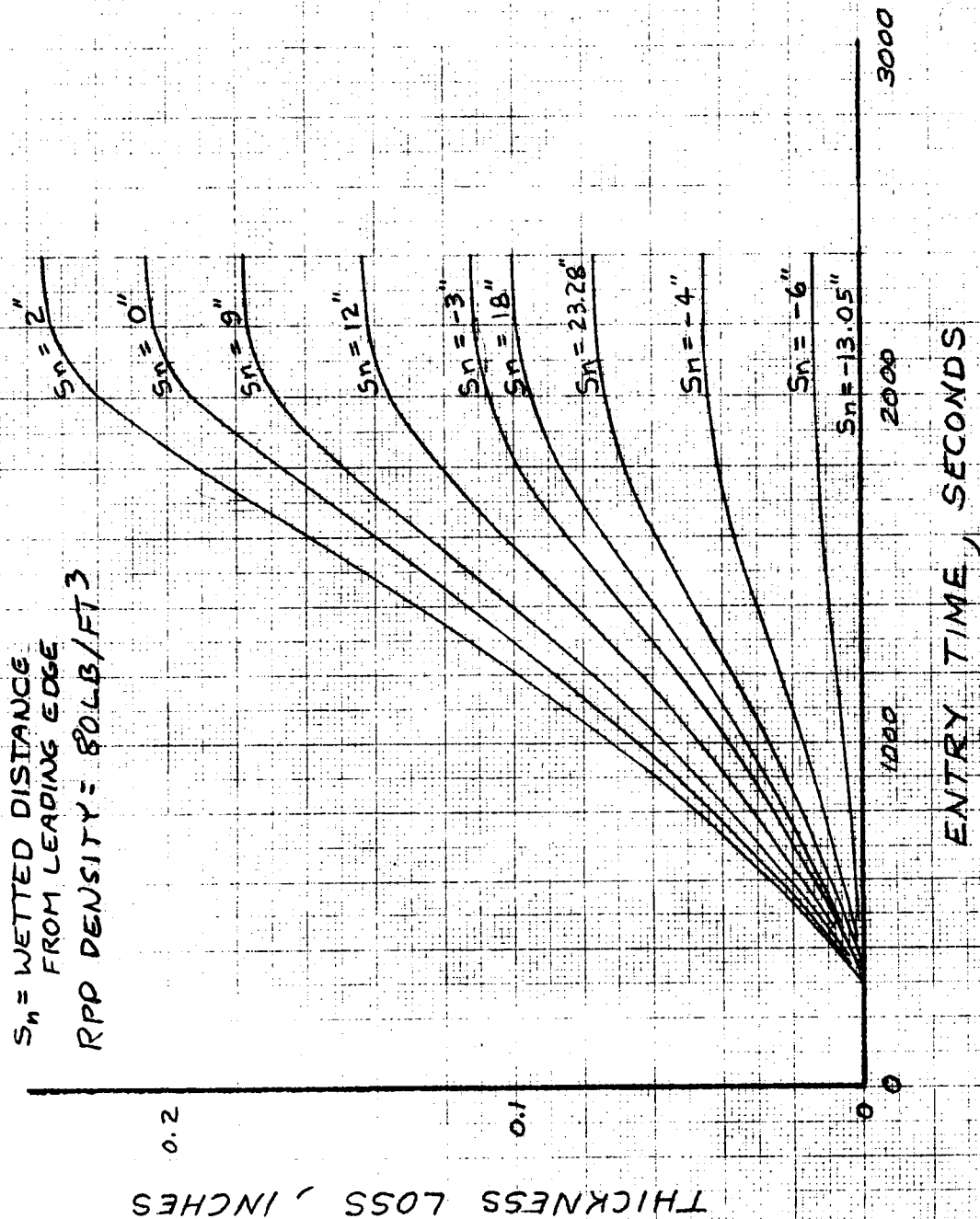
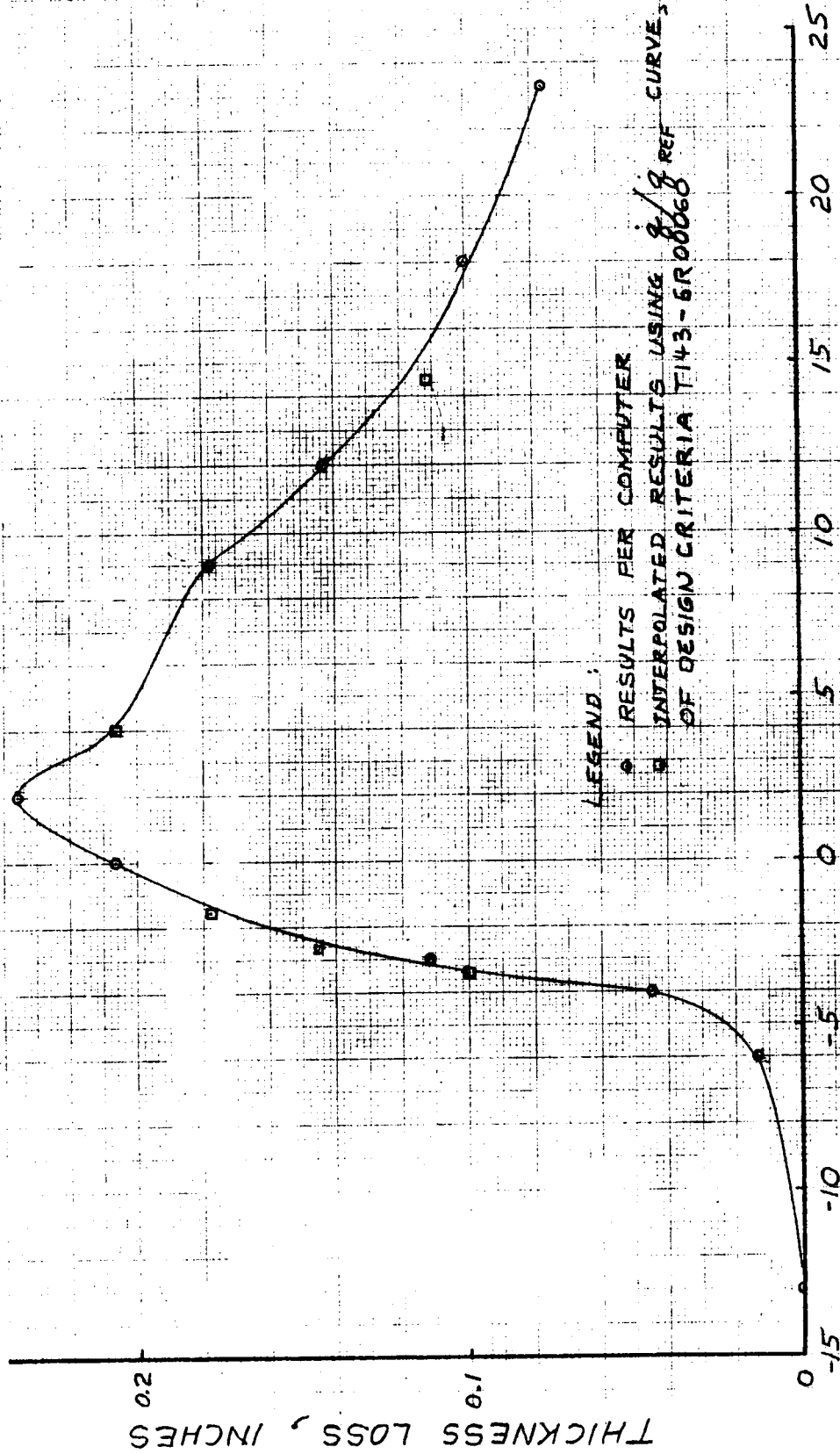


FIGURE 3

THICKNESS LOSS FOR 2400 SECONDS
RPP DENSITY = 80 LB/FT³



LEGEND:

● RESULTS PER COMPUTER

□ INTERPOLATED RESULTS USING 8/8 REF CURVE, FIGURE 11 OF DESIGN CRITERIA T143-6R00060

"WETTED" DISTANCE FROM LEADING EDGE, INCHES

DESIGN INFORMATION REQUEST - RELEASE

7-17-72

REL (S) AND EFF. PREDICTED TEMPERATURE DISTRIBUTION FOR THE WING		DIR. NO. T143-DIR-2-07		REV.
LEADING EDGE SKIN AND RIB		DATE 13 July 72	PAGE 1	OF 27
SYSTEM Phase III Shuttle Lead. Edge		REF. G. G. NUMBER 3357-AA-1160		
Fill in block below for Information Request		Fill in block below for Information Release		
 GROUP _____ BY _____ SON _____ ONLY <input type="checkbox"/> BWR <input type="checkbox"/> BUWEPs <input type="checkbox"/> 		IN REPLY TO DIR. NUMBER _____ REL. TO D.M. While GROUP 3-52000 PREPARED BY W.A. Whitten DATE 14 JULY 1972 CHECKED BY J.E.M. GROUP APP. J.E. Medford DATE 14 July 1972 PROJ OFFICE _____ DATE 7/15/72		

F.T. Esenwein, R.J. Copeland, W.E. Agan, E. Matza, B. A. Forcht

IGN INFORMATION:

References: 1. "Ablation Analysis of Bare RPP on Shuttle Wing Leading Edge",
T143-DIR-2-03, 5 June 1972

2. "Development of a Thermal Protection System for the Wing of a Space Shuttle Vehicle", Report No. T143-5R-00124, 30 April 1972.

3. "Space Shuttle Wing Leading Edge Design Criteria, Phase III",
Report No. T143-5R00060, 19 May 1972

INTRODUCTION

Thermal analyses were conducted to determine the predicted temperature distribution in the leading edge skin and rib of the space shuttle vehicle wing.

This analysis is part of Phase III of the "Development of a Thermal Protection System for the Wing of a Space Shuttle Vehicle", NASA-MSC Contract No. NAS9-11224. In this phase a thicker laminate leading edge is examined in an effort to achieve a one mission return capability in the event of coating failure. In addition the heat shield insulation design goal is to protect wing structure having a 350°F temperature limitation, compared with the 650°F limit of Phase II.

The thermal analyses were performed using VMSC computer routine which accounted for cross radiation, conduction and heat sink effects. Only the first 660 seconds of the reentry portion of the mission starting from an altitude of 400,000 feet was considered since both peak temperature and temperature gradients occur during this

period. An initial temperature of -170°F was used in order to obtain worst case thermal gradients (change in temperature per unit of length) in the material.

Discussion of the analysis is divided into three parts. The leading edge skin temperature results are discussed first, followed by discussion of results for the ribs in the cavity area and in the support joint area.

CONFIGURATION DEFINITION

Figure 1 shows a cross section of the leading edge and the insert shows a typical leading edge panel and rib and sealing strip. The thermal analysis for the leading edge skin used a two-dimensional model of the cross section. The analysis for the rib used separate two-dimensional models for each of six locations in the uninsulated cavity area and two support joint areas. Details of the individual thermal models will be discussed in the following sections.

Thermal property data used in the analysis are presented in Tables I through IV, and are based upon SRI data from Reference 2.

THERMAL ANALYSIS OF LEADING EDGE SKIN

The two-dimensional thermal model used in the analysis of the leading edge skin is shown in Figure 2. The substructure insulation surface was represented by an adiabatic surface since the insulation design has not been firmed. This results in slightly conservative (high) computed insulation surface temperatures.

The thickness of the leading edge skin is designed for a one-mission return capability in the event of coating failure. The thickness loss with coating failure for 2400 seconds was determined in Reference 1 and 120% of this loss was added to the structural thickness requirement of 0.13". The resulting thickness is shown on Figure 3. The leading edge was divided into three nodes through the thickness for the high thickness loss region, and into two nodes for the low-loss region as shown on the thermal model of Figure 2. Node locations were chosen so as to obtain temperatures at the centerline of the elements to be used in the structural analysis.

The recovery temperature and the convection heat transfer coefficients used in the analysis for the maximum heating location are presented in Table V. These are the same as those used in the Phase II analysis of Reference 2. The convection coefficient was modified for use at the other locations to account for the reduced heat flux away from the maximum heating location. The modification used for the various exterior surface nodes of Figure 2 are presented in Table VI, based upon the heating distribution from Reference 3. Also given on Table VI is the location of the exterior nodes relative to the most forward point on the leading edge.

The predicted temperature at the peak heating location is presented as a function of time on Figure 4. The temperature of the leading edge reaches a peak of 2547°F at a time of 660 seconds. Temperatures at the other locations for this time are presented on Figures 5 and 6. The predicted surface temperature distribution around the leading edge at 660 seconds is presented graphically on Figure 5. Comparing these results to those of the Phase II analysis shows lower maximum temperatures for the present study. The maximum temperature of the skin is 2547°F compared to 2592°F for Phase II, and the maximum temperature of the insulation is 2272°F compared to 2396°F for Phase II. The lower temperatures for this study are the result of two factors: (1) higher skin emissivity (Table III values versus 0.85), (2) higher circumferential heat conduction due to thicker skin. These two factors offset the reduction in cross radiation effect due to a thicker skin. Comparing the current temperatures with radiation equilibrium values based upon the Table III emittance data shows that the temperature reduction due to cross radiation and heat conduction for the fail safe skin is 123°F, compared to 148°F for the thinner skin analyzed in Phase II.

One of the primary purposes of the thermal analyses was to determine the location and magnitude of the maximum thermal gradients in the leading edge. In order to determine the maximum gradient around the periphery of the leading edge the temperatures at various times were plotted as shown on Figure 7. From this data it was determined that the maximum gradient of 541°F/inch occurs between nodes 12 and 14 on the leeward side, where the wing support insulation begins, at a time of 400 seconds. This gradient is higher than the Phase II computed value of 325°F/inch. A finer nodal network was used in the current analysis in the vicinity of the peak gradient in order to more accurately define the magnitude of the gradient.

The maximum thermal gradient through the thickness of the leading edge is 697°F/inch and occurs at the maximum heating location at a time of 300 seconds.

THERMAL ANALYSIS OF RIBS IN CAVITY AREA

Temperatures in the ribs were predicted for six locations around the leading edge: 2", 9", and 18" wetted distance on the windward side, and 2", 5", and 8" wetted distance on the leeward side.

The sealing strip between the leading edge panels was included in the thermal model. The thickness of the seal strip lip was taken as the minimum of 0.13" or 120% of the thickness loss with coating failure.

The two dimensional thermal model for the rib included the rib, one half of the sealing strip, surrounding radiating structure, and approximately five inches of the panel skin. Node dimensions in the rib were selected to correspond to the grid points used in the structural analysis model. Figure 8 is a sketch of the model. Subsequent analysis verified that including only five inches of the panel skin was adequate since the temperature difference between the skin nodes farthest away from the rib was negligible.

The temperature of the radiating structure node was input as a function of time, as shown on Figure 9. The temperature-time profile was determined as the average temperature of the insulation nodes from the leading edge skin analysis.

Predicted temperatures for the rib and adjacent skin are presented on Figure 10 for a time of 660.0 seconds. Results of the leading edge skin analysis are included on the figure and agree very well with the predicted skin temperatures obtained in the rib analysis. This indicates that the use of a single temperature curve, Figure 9, to represent radiating structure adequately accounts for cross radiation effects.

The rib temperature at the maximum heating location is presented in Figure 11 for several times during entry. From the figure it is seen that the maximum temperature drop across the rib occurs at a time of 260 seconds. The maximum temperature drop is 346°F compared to 300°F computed in Phase II. This is due to the lower thermal conductivity used in the current analysis as compared to the Phase II design value. The current conductivity is based upon the Southern Research Institute data from Phase II (Reference 2). The temperature distribution across the rib and adjacent skin at this time is shown in Figure 12 for six locations around the periphery of the leading edge. Similar data is presented in Figure 13 for an entry time of 400 seconds, corresponding to the time of maximum temperature gradient around the periphery of the leading edge skin.

The rib temperatures presented in Figures 10 - 13 apply to the major portion of the rib which is free to participate in cross-radiation with skin and other structure. These results do not apply in the support joint areas where the rib and adjacent skin are covered with insulation. Temperatures in the support joint areas are discussed in the following section.

THERMAL ANALYSIS OF RIBS IN SUPPORT JOINT AREA

The windward and leeward side support joint area rib temperatures were analyzed using 70 node three dimensional thermal models. These models included heat conduction along the skin and carbon-carbon rib, across the fused silica insulators and into the steel bolt and Haynes 188 support fitting. Cross

radiation from the skin and surrounding structure to the portion of the rib outside of the bulk insulation was considered, as was heat conduction through the bulk insulation and into the support joint. The carbon-carbon rib portions of the windward and leeward side models are shown in Figures 14 and 15, respectively.

Computed temperatures in the windward side support joint are shown in Figures 16 and 17 for entry times of 260 and 400 seconds, respectively. These are the times of peak temperature drop across the rib in the cavity area and of peak skin temperature gradient, respectively. Similar temperatures for the leeward side are shown in Figures 18 and 19. It is seen that the temperature drop across the rib for the windward side, between nodes 6 and 37 is 1191°F at 400 secs. This temperature drop peaks at 380 seconds at a value of 1205°F , as shown in Figure 20 which presents the temperature distribution in the rib under the support lug. This compares to a value of 1100°F computed in Phase II. This drop is considerably higher than that in the cavity area because,

- ° Heat transfer from skin to rib is by conduction only, since bulk insulation suppresses cross radiation.
- ° The rib height is higher in the support joint area than in the cavity area.
- ° Attachment hardware at the inboard side of the rib serves as a heat sink to maintain relatively low temperatures.

TABLE I
SPECIFIC HEAT OF RPP

TEMP., °F	-200.	200.	500.	1000.	1500.	2000.	2500.	3000.
C _p , BTU/LB °F	.105	.2	.26	.322	.37	.395	.415	.426

TABLE II
THERMAL CONDUCTIVITY OF RPP (NORMAL DIRECTION)*

TEMP., °F	-250.	0.	330.	500.	750.	1000.	1500.	1940.	3000.
K, BTU-IN/HR FT ² °F	14.6	30.	40.	44.	48.2	50.2	50.3	50.	44.6

TABLE III
EMISSIVITY OF RPP

TEMP., °F	-200.	500.	1000.	1500.	2000.	2500.	3000.
ε	.85	.85	.893	.925	.94	.935	.898

TABLE IV
DENSITY OF RPP

TEMP., °F	-250.	3000.
ρ, LB/FT ³	85.	85.

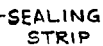
* Conductivity for parallel direction is 1.90 times these values.

TABLE V

RECOVERY TEMPERATURE AND CONVECTION COEFFICIENT MAXIMUM HEATING LOCATION		
TIME SECONDS	RECOVERY TEMP °F	CONVECTION COEFFICIENT BTU/HR FT ² °F
0.0	49540.	.038
100.	49540.	.19
200.	49540.	.57
250.	49540.	1.14
300.	49540.	2.36
350.	49540.	3.2
400.	48740.	3.36
450.	47940.	3.35
500.	46640.	3.44
600.	44940.	3.58
700.	42640.	3.78
800.	40540.	3.99
1000.	35040.	4.57
1200.	29790.	5.06
1400.	23940.	5.55
1600.	18090.	5.89
1800.	12840.	6.26
2000.	8280.	6.51
2200.	4440.	8.03
2400.	1690.	8.03
2600.	332.	7.26
2800.	15.	8.63
3200.	3.	9.82
3600.	69.	12.8

TABLE VI

MULTIPLICATION FACTORS FOR CONVECTION COEFFICIENTS			
NODE NO. (FIGURE 2)	MULTIPLICATION FACTOR	x_n INCHES	s_n INCHES
2	.04	6.71	-13.17
4	.04	6.32	-12.69
6	.04	5.8	-12.15
8	.04	5.43	-11.53
10	.04	4.86	-10.81
12	.044	4.19	- 9.91
14	.05	3.43	- 8.91
16	.06	2.76	- 7.91
18	.073	2.15	- 6.91
20	.1	1.61	- 5.91
22	.128	1.12	- 4.91
24	.235	.71	- 3.91
27	.571	.37	- 2.91
30	.757	.15	- 1.91
33	.844	.03	- .94
36	.9	.0	0
39	.95	.075	.97
42	1.	.26	1.97
45	.942	.57	2.95
48	.89	1.0	3.92
51	.865	1.53	4.92
54	.841	2.11	5.90
57	.825	2.74	6.89
60	.814	3.4	7.87
63	.8	4.19	8.87
66	.762	4.99	9.87
69	.708	5.82	10.87
72	.664	6.65	11.87
75	.626	7.56	12.87
78	.591	8.44	13.87
81	.563	9.36	14.87
84	.533	10.25	15.87
87	.507	11.25	16.87
90	.482	12.13	17.85
93	.466	13.06	18.84
96	.45	14.01	19.82
99	.441	14.94	20.81
102	.424	15.88	21.74
105	.416	16.58	22.46
108	.411	17.13	23.03
111	.406	17.59	23.51



TYPICAL PANEL AND SEALING STRIP



FIGURE 1 LEADING EDGE CONFIGURATION

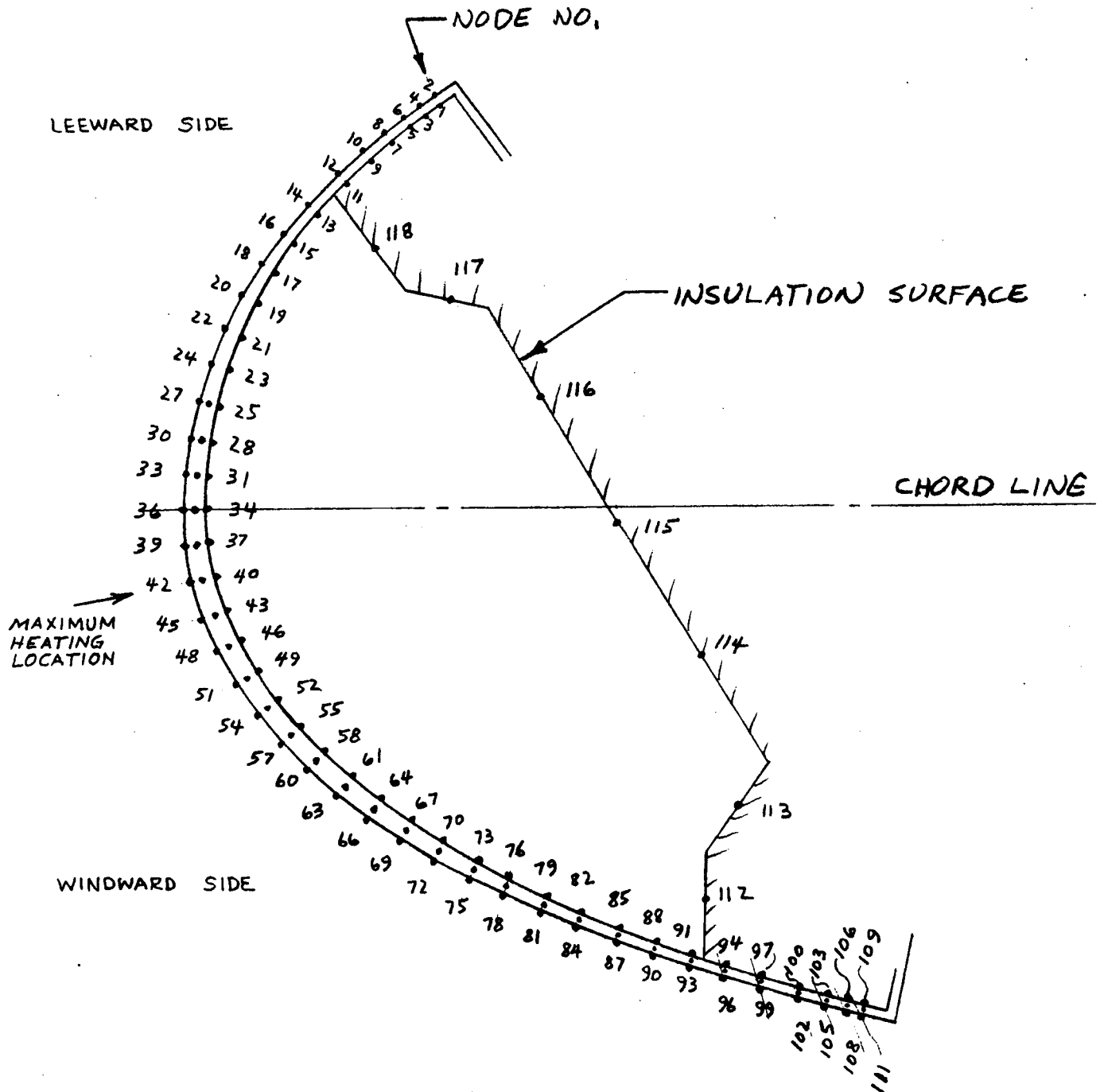


FIGURE 2 THERMAL MODEL OF LEADING
EDGE SKIN

FIGURE 3 SKIN THICKNESS DISTRIBUTION

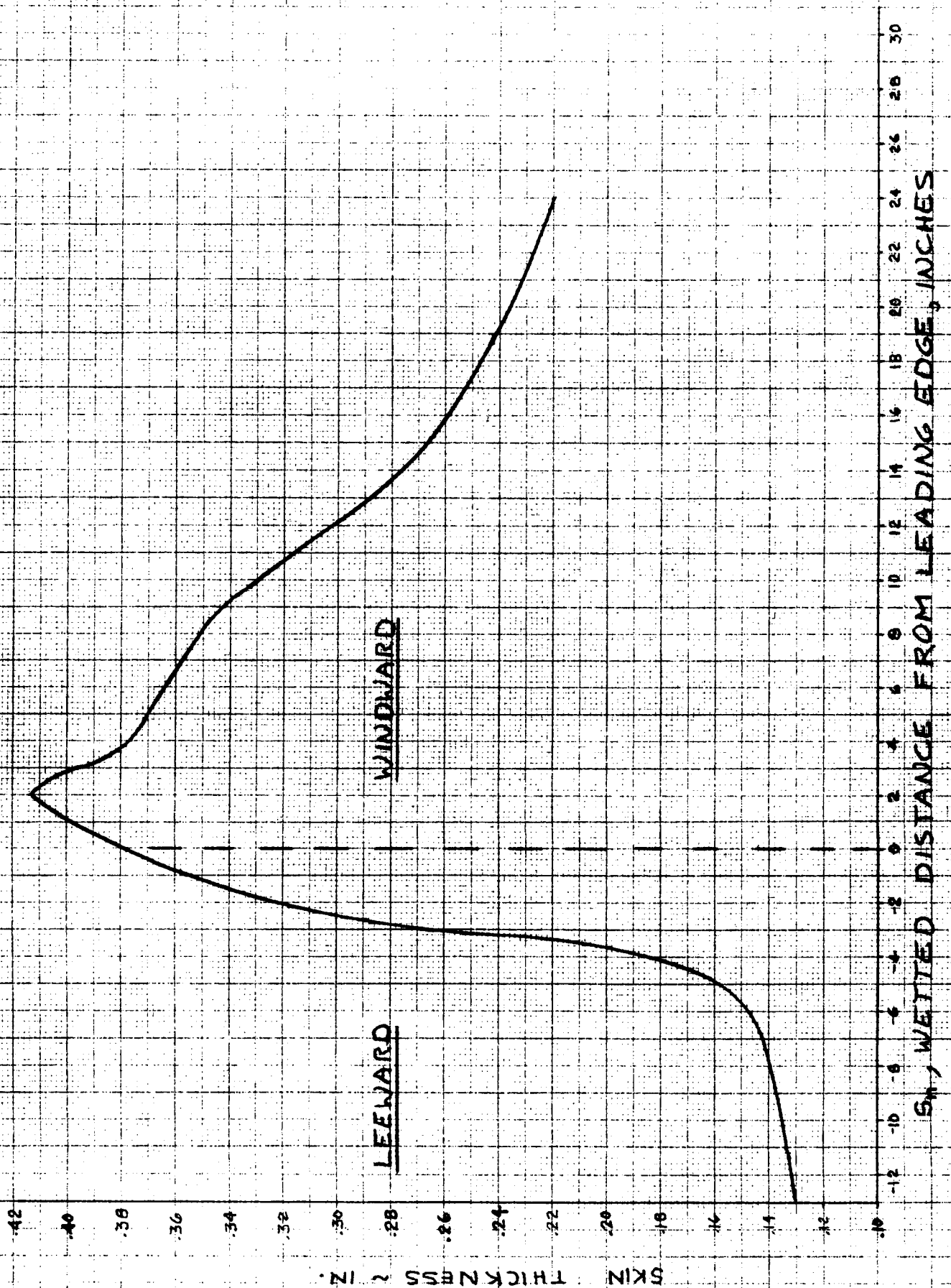


FIGURE 4

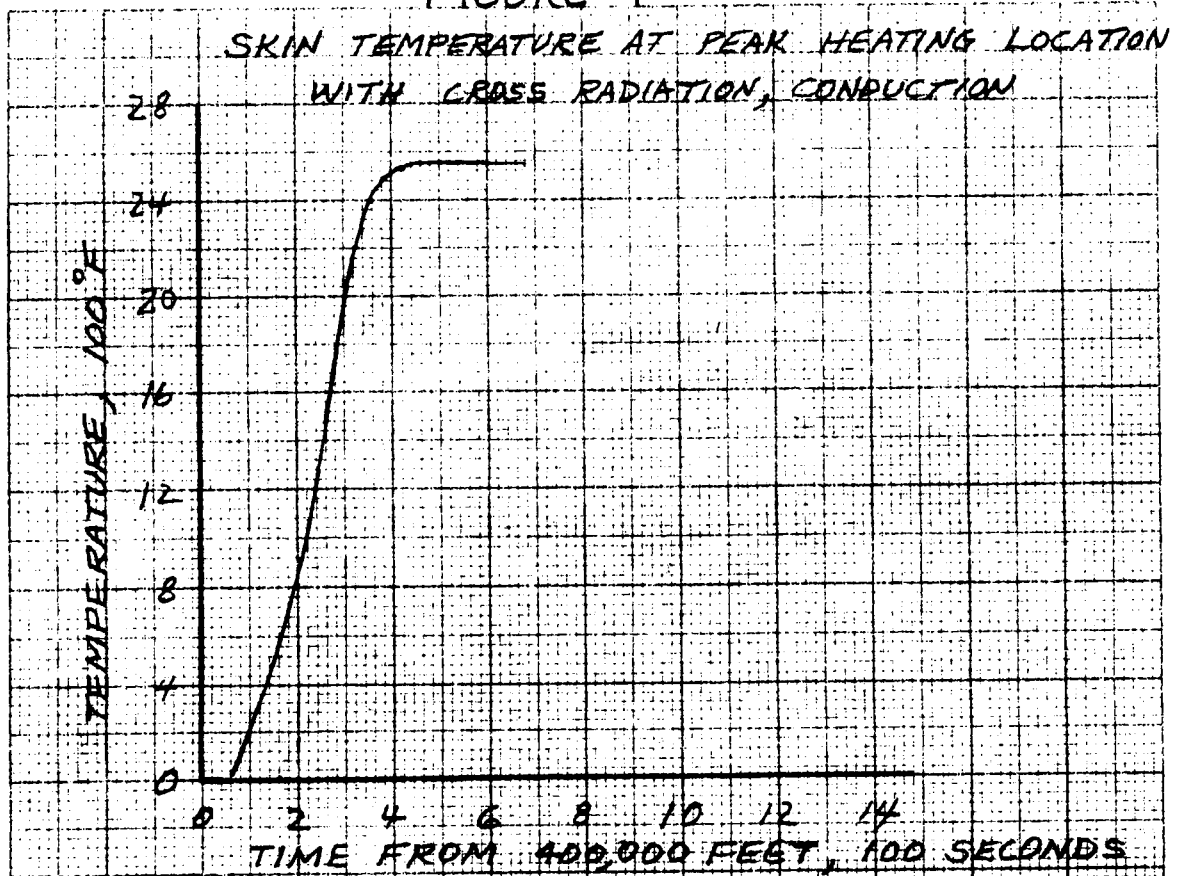
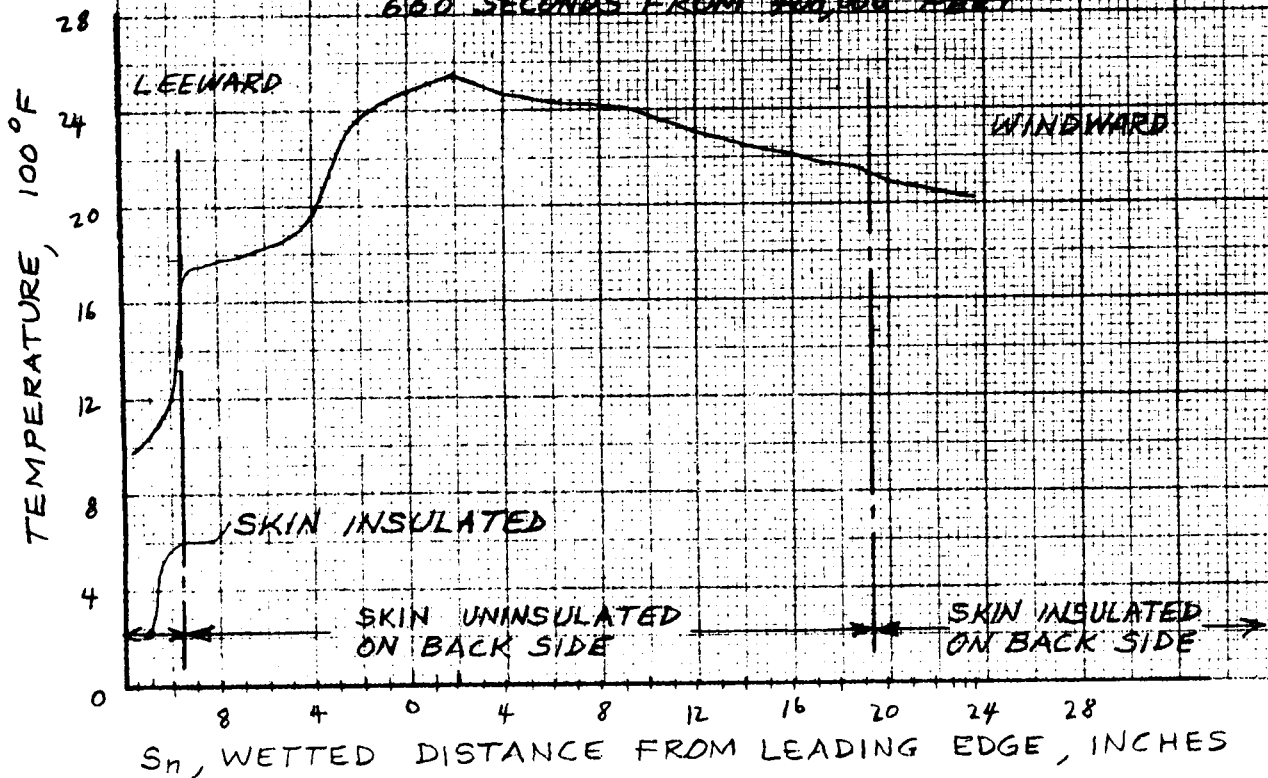


FIGURE 5
SKIN TEMPERATURE DISTRIBUTION
WITH CROSS RADIATION, CONDUCTION
SURFACE TEMPERATURES
660 SECONDS FROM 400,000 FEET



NOTE: TEMPERATURES SHOWN
IN PARENTHESES ARE °F AND
OCCUR AT 660 SECONDS
FROM 400,000 FEET.

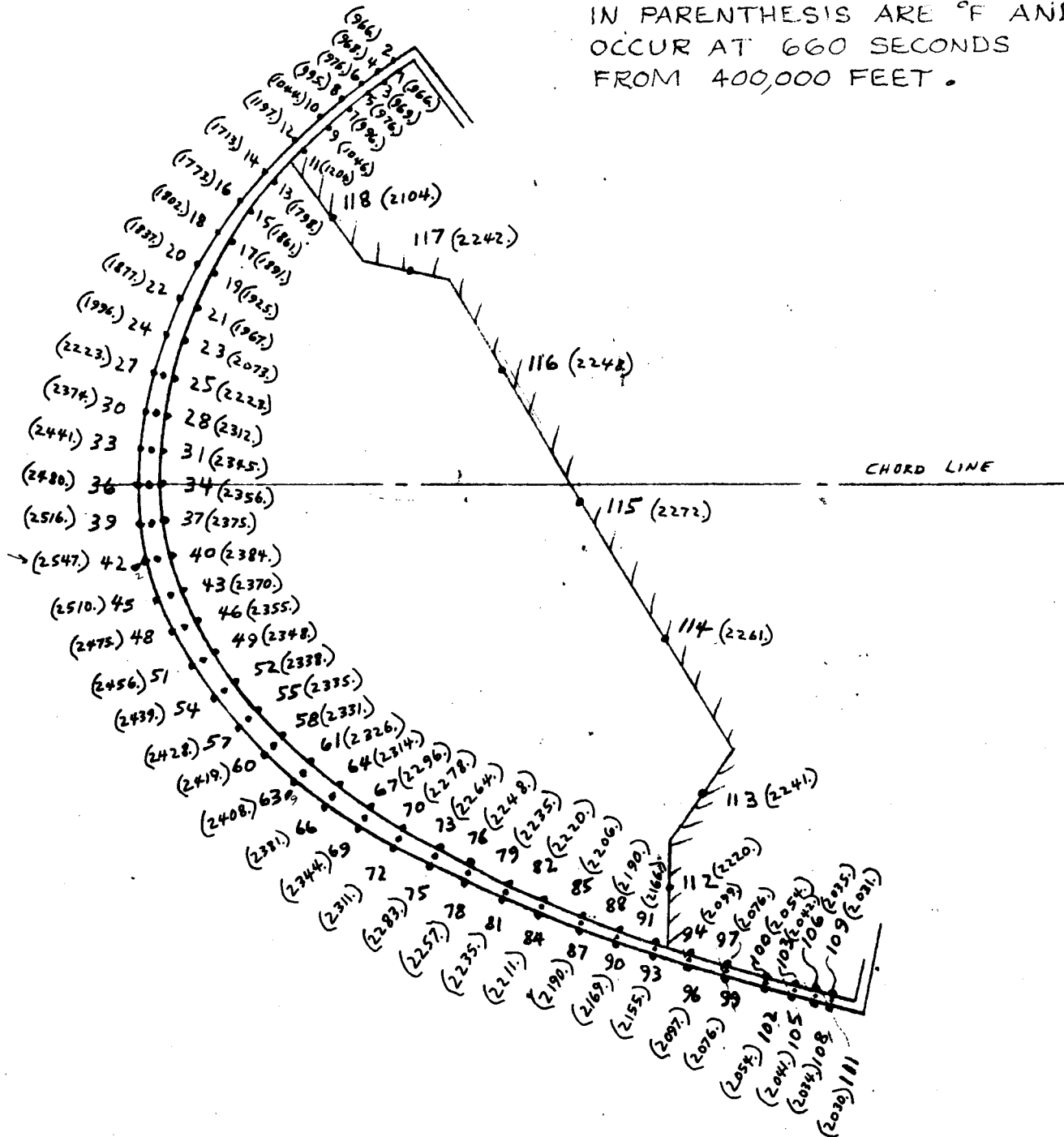
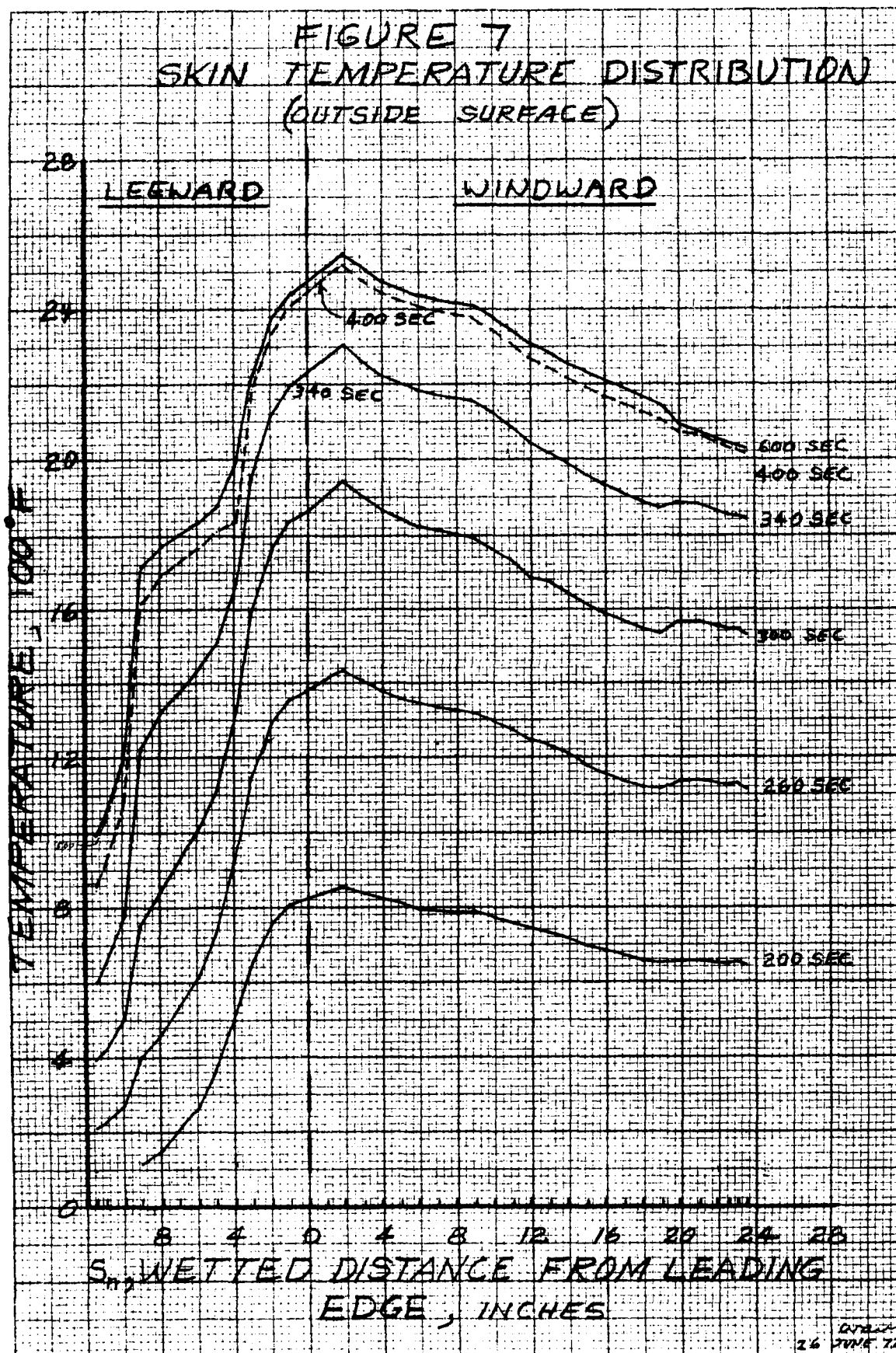


FIGURE 6 SKIN AND INSULATION TEMPERATURES



LOCATION	DIMENSIONS (INCHES)			
	X_h	H	T1	T2
2" WINDWARD	0.26	1.65	0.283	0.413
9" "	4.19	1.12	0.213	0.345
18" "	12.13	1.50	0.13	0.247
2" LEEWARD	0.15	1.82	0.192	0.321
5" "	1.12	1.88	0.13	0.159
8" "	2.76	1.95	0.13	0.14

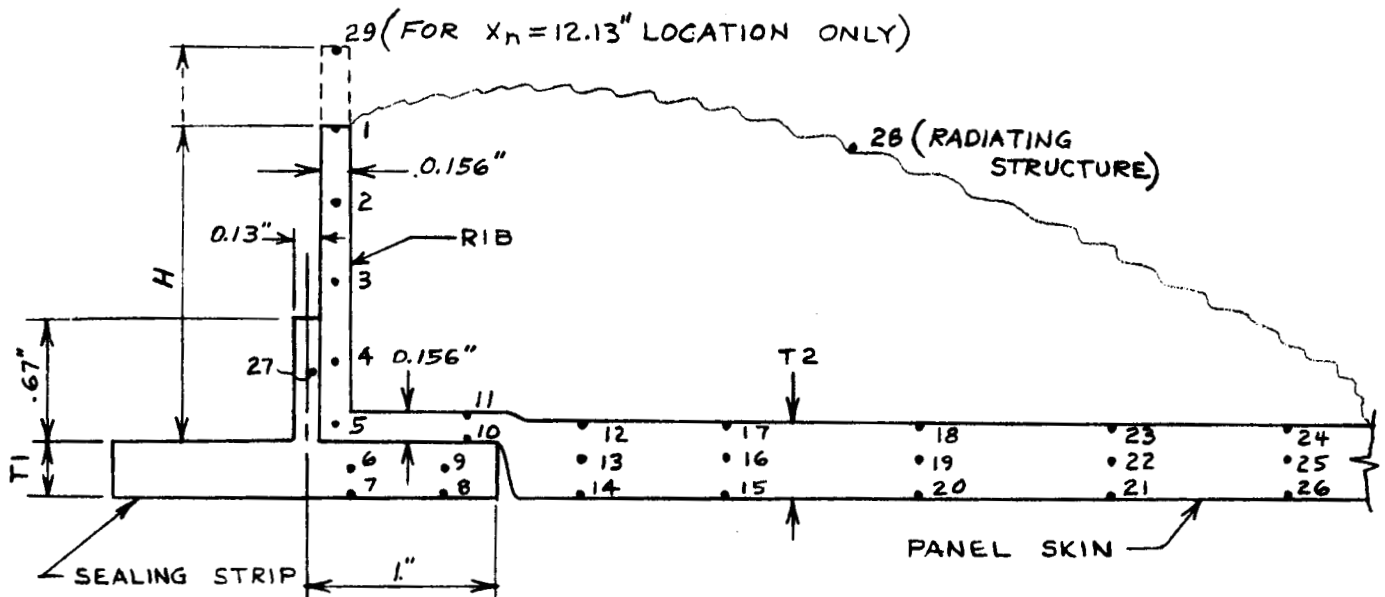
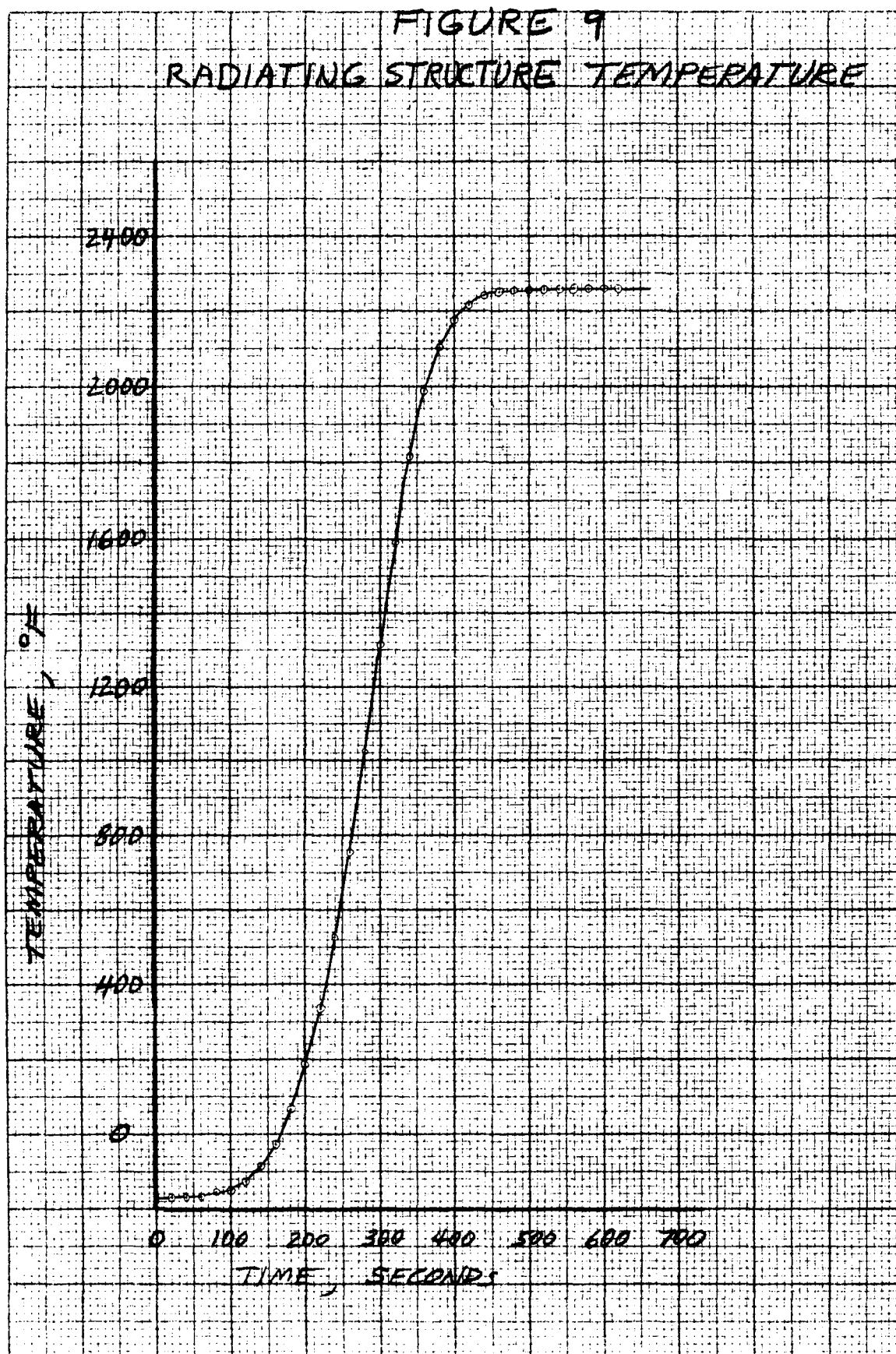


FIGURE 8 RIB THERMAL MODEL



TIME FROM 409000 FEET = 660 SEC.

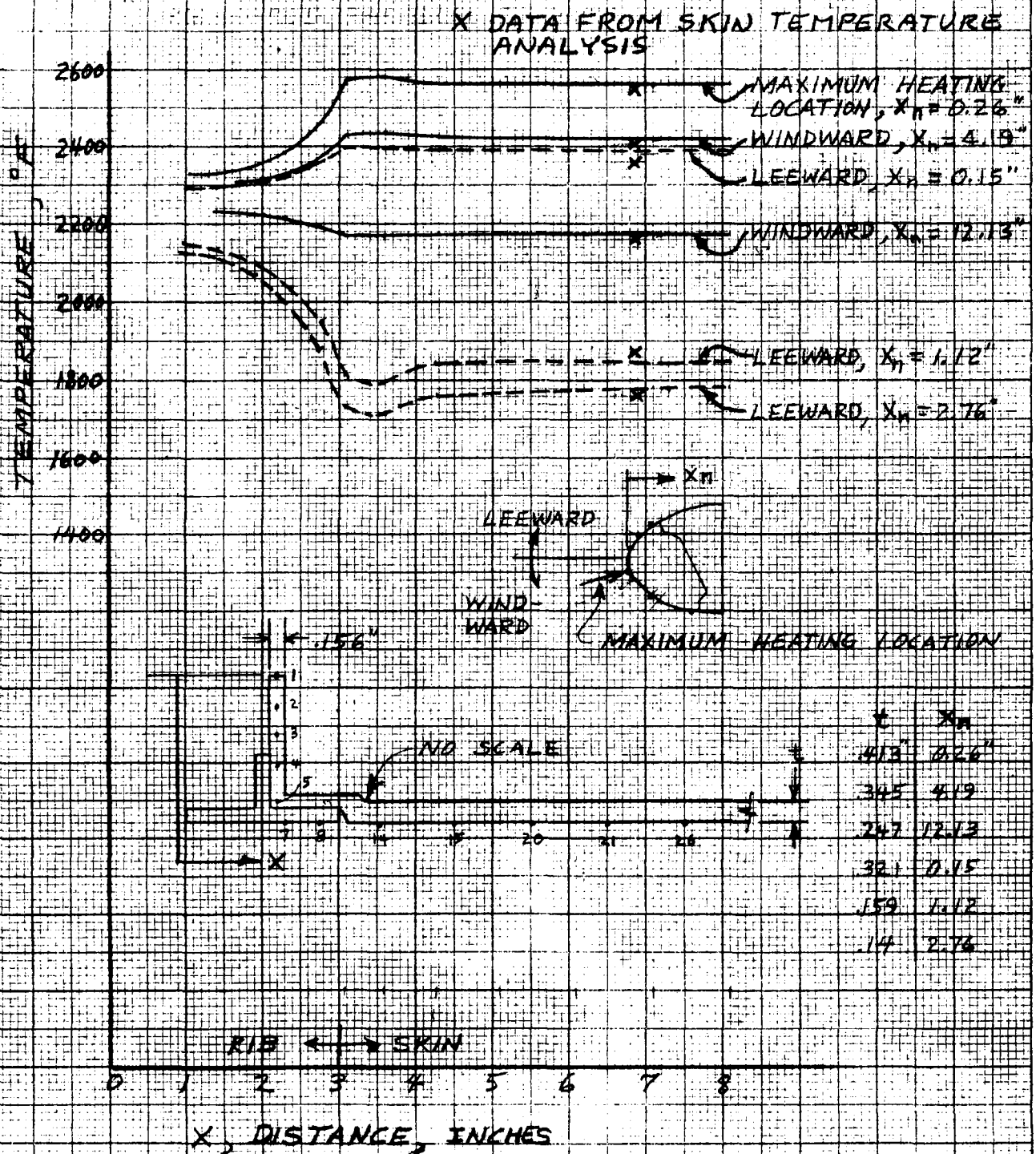
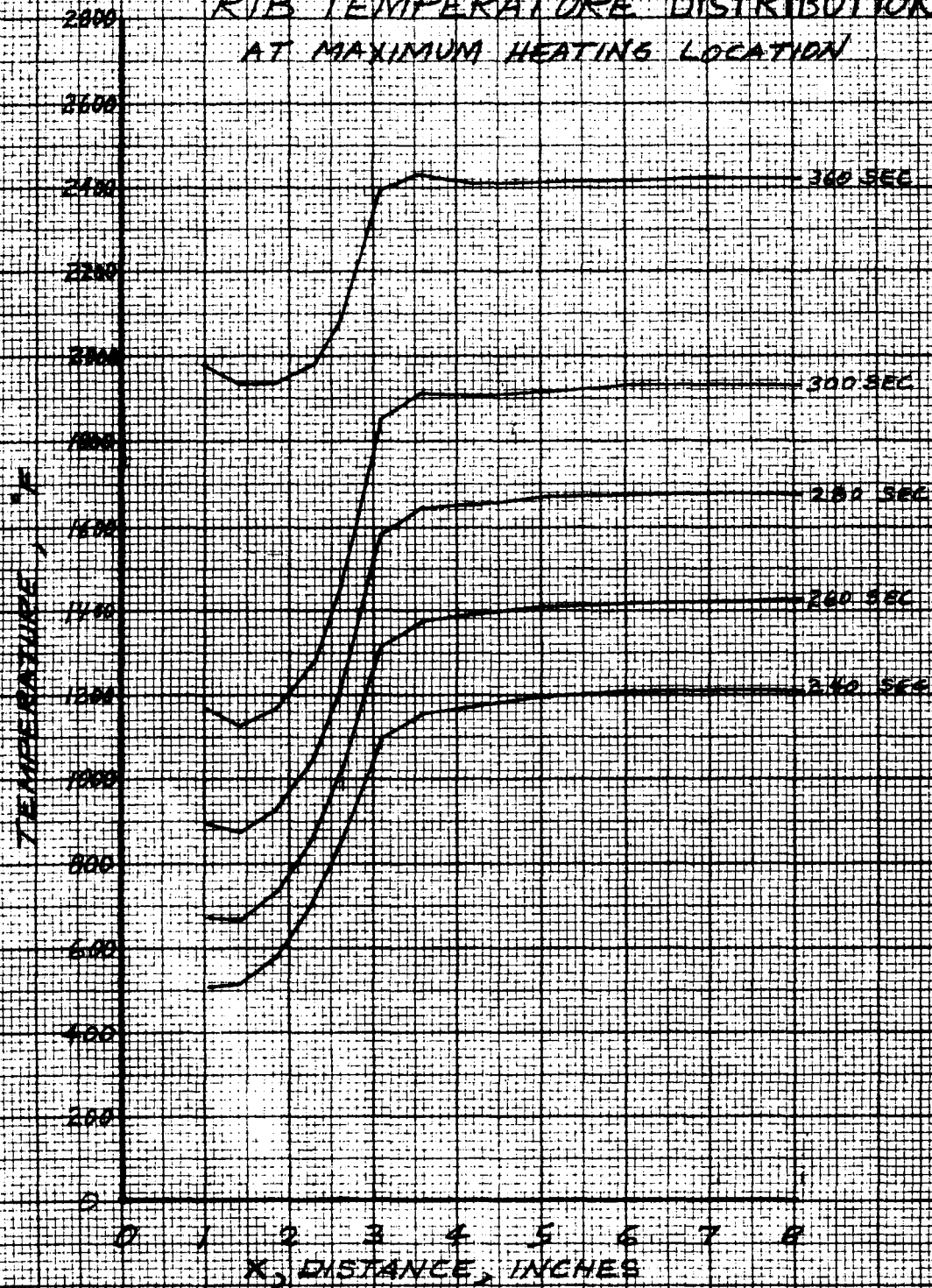
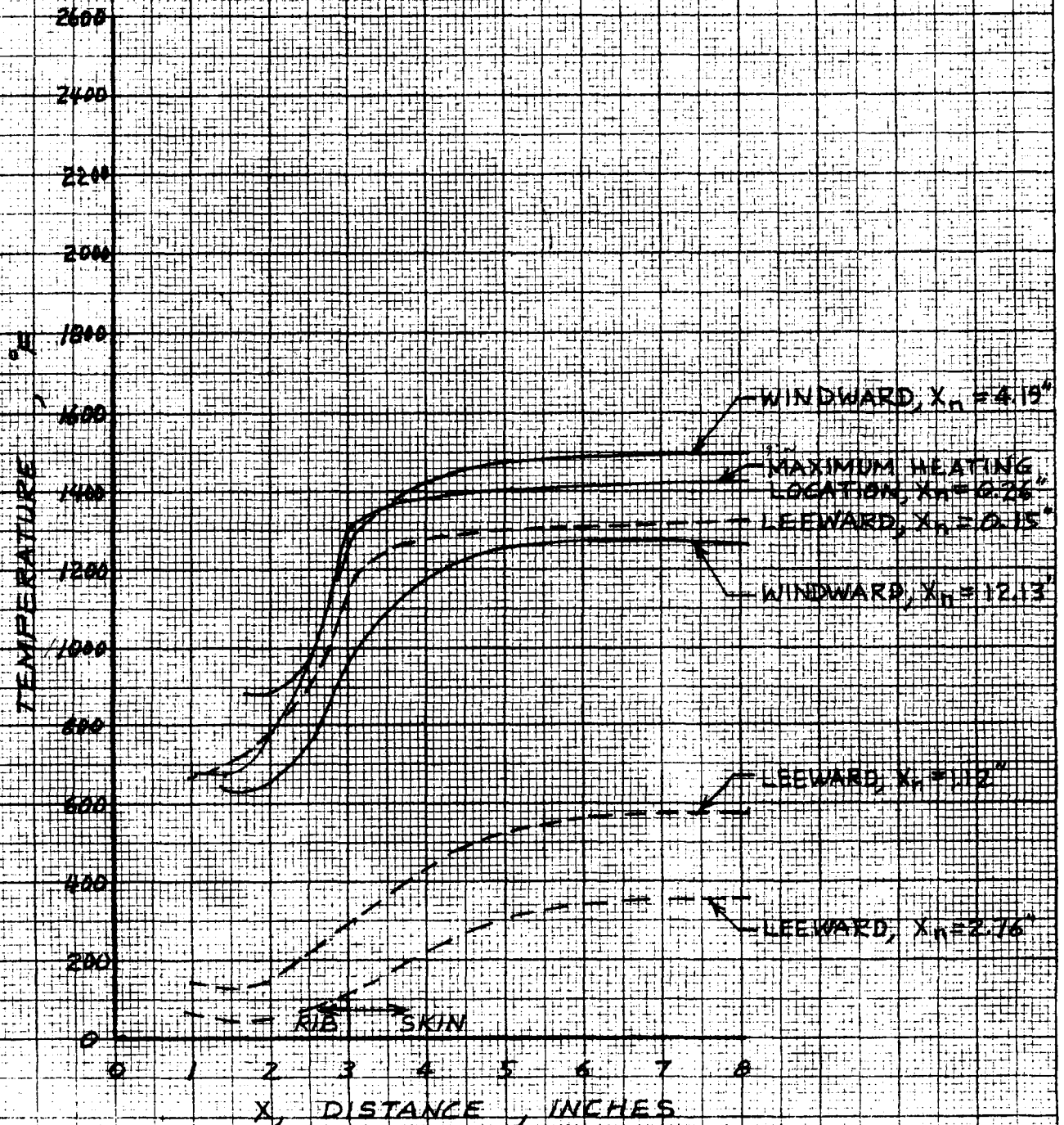
RIB TEMPERATURE DISTRIBUTION
FIGURE 10

FIGURE II
RIB TEMPERATURE DISTRIBUTION
AT MAXIMUM HEATING LOCATION



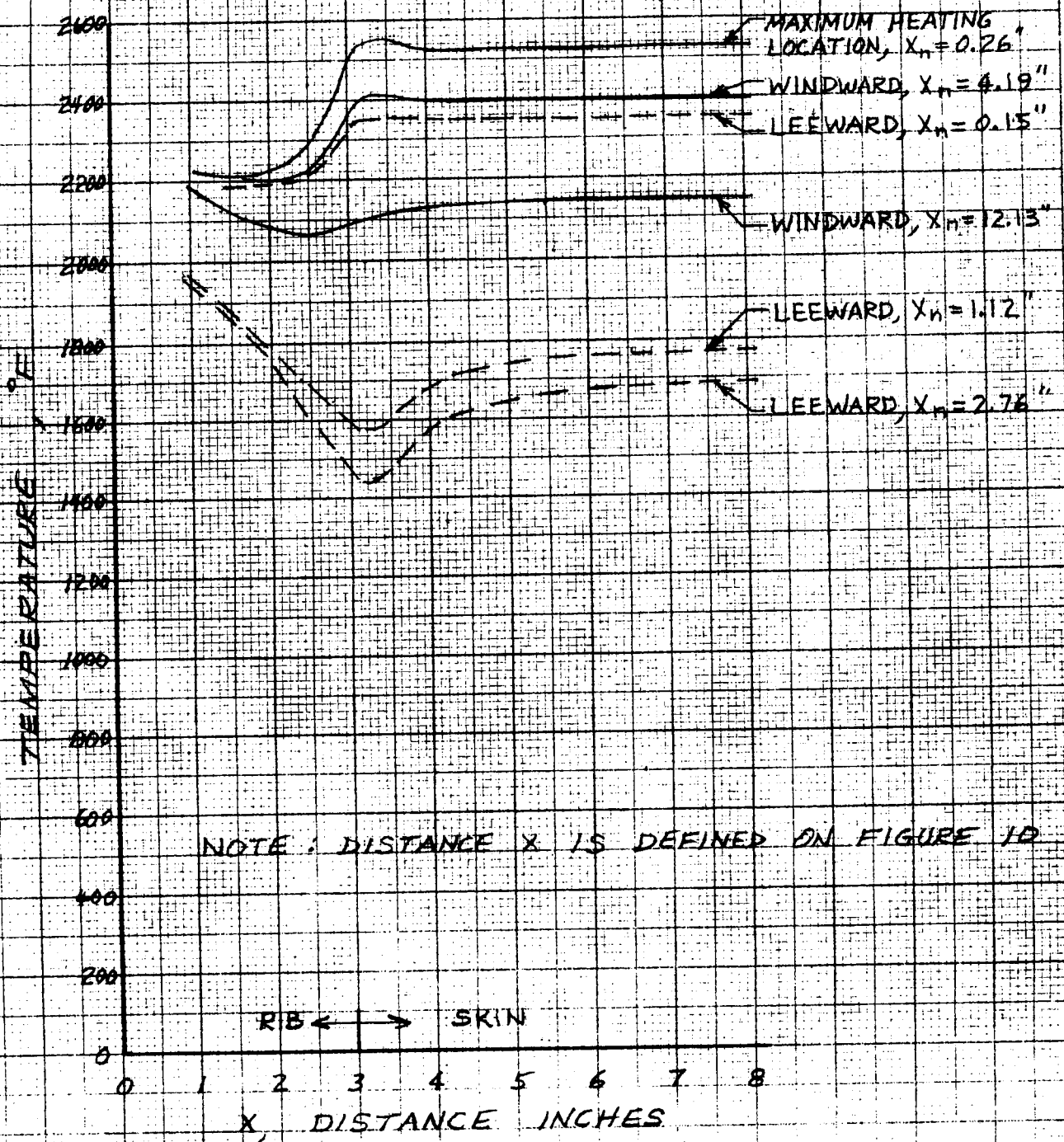
TIME FROM 400,000 FEET = 260 SECONDS

NOTE: DISTANCE X IS DEFINED ON FIGURE 10



RIB TEMPERATURE DISTRIBUTION, 260 SECONDS
FIGURE 12

TIME FROM 400,000 FEET = 400 SECONDS



RIB TEMPERATURE DISTRIBUTION, 400 SECONDS
FIGURE 13

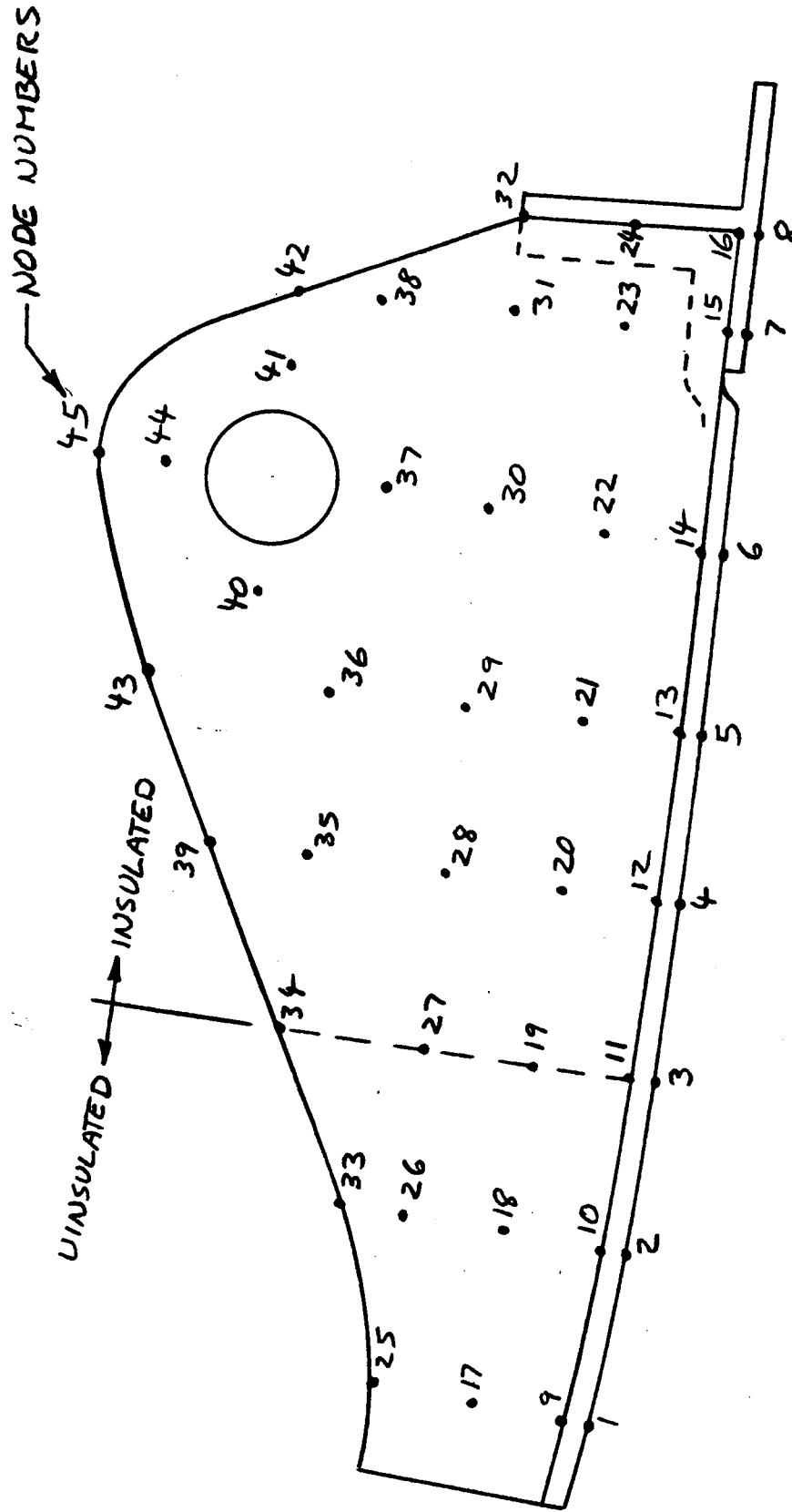


FIGURE 14 WINDWARD SIDE SUPPORT JOINT THERMAL
MODEL, CARBON-CARBON RIB NODES

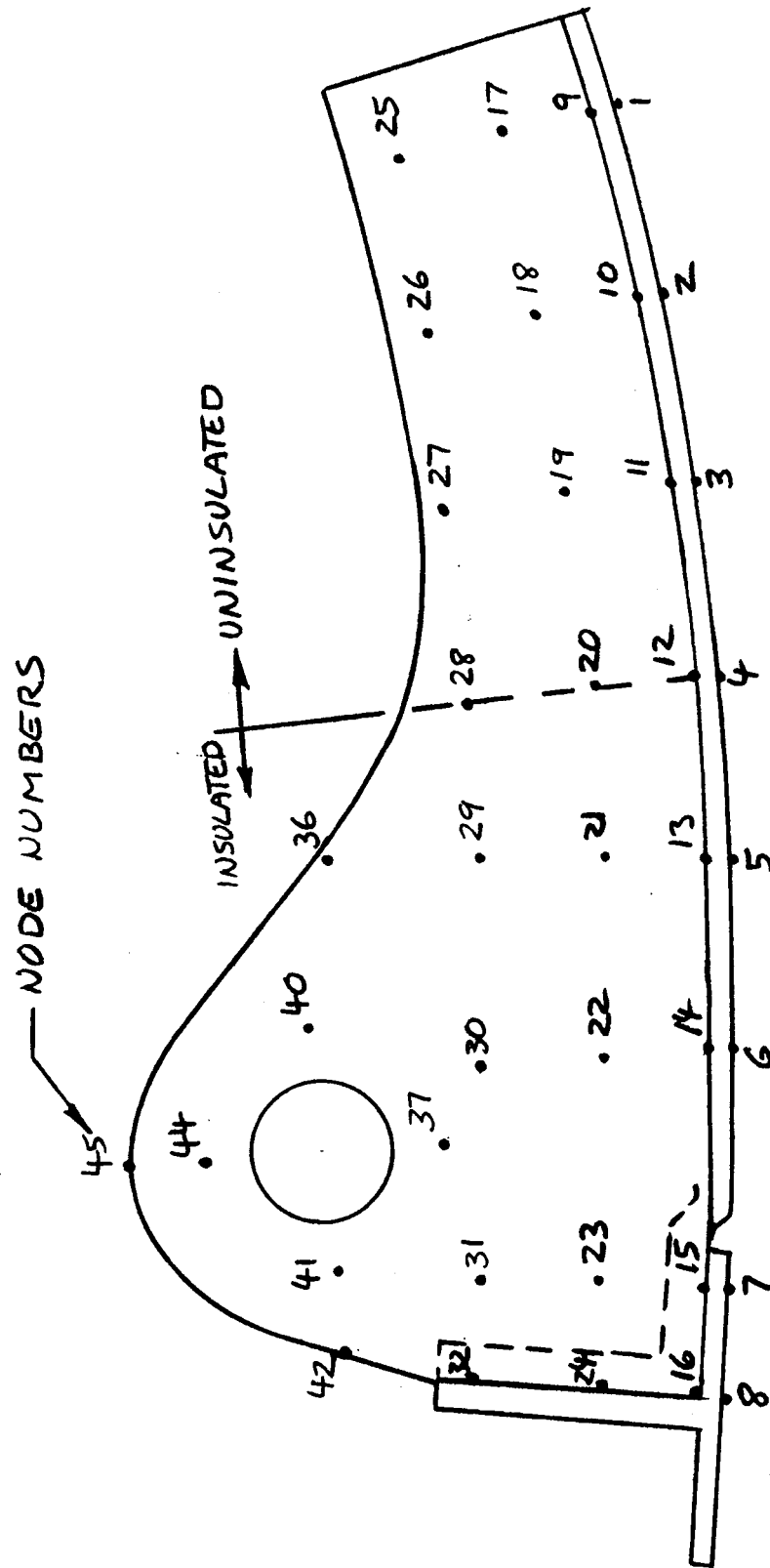


FIGURE 15 LEEWARD SIDE SUPPORT JOINT THERMAL
MODEL, CARBON-CARBON RIB NODES

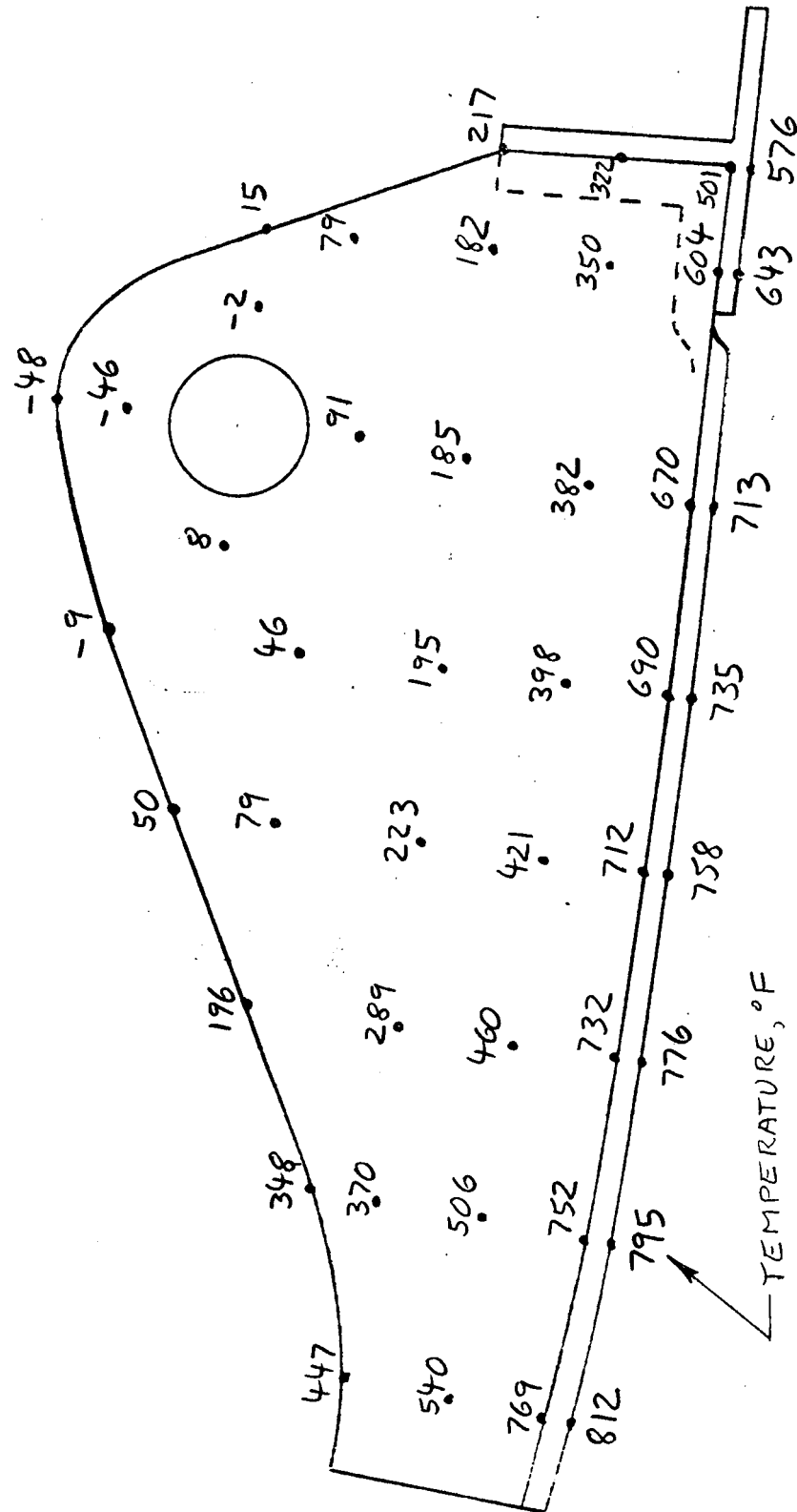


FIGURE 16 WINDWARD SIDE SUPPORT JOINT TEMPERATURES
ENTRY TIME = 260 SECONDS

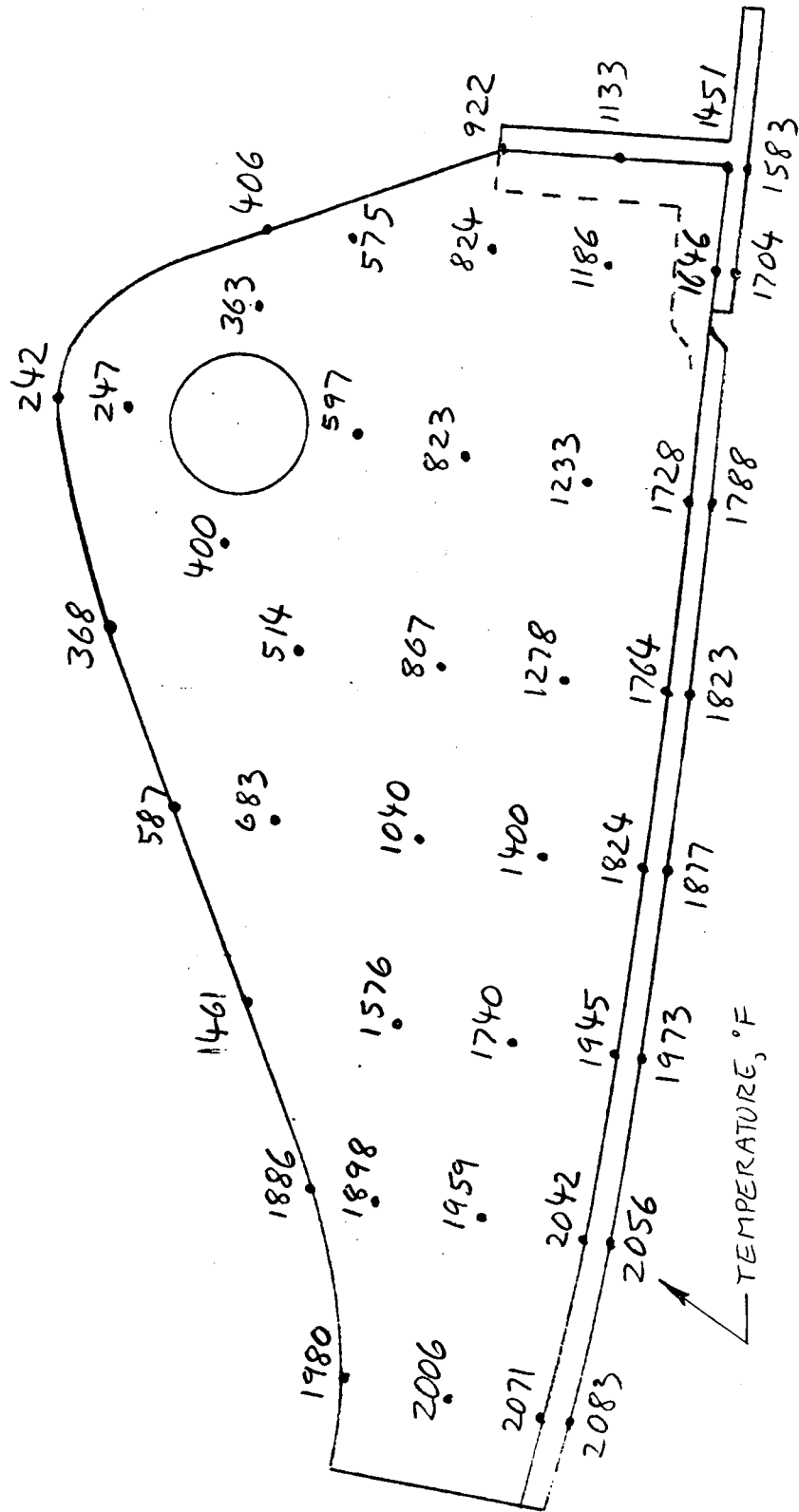


FIGURE 17 WINDWARD SIDE SUPPORT JOINT TEMPERATURES
ENTRY TIME = 400 SECONDS

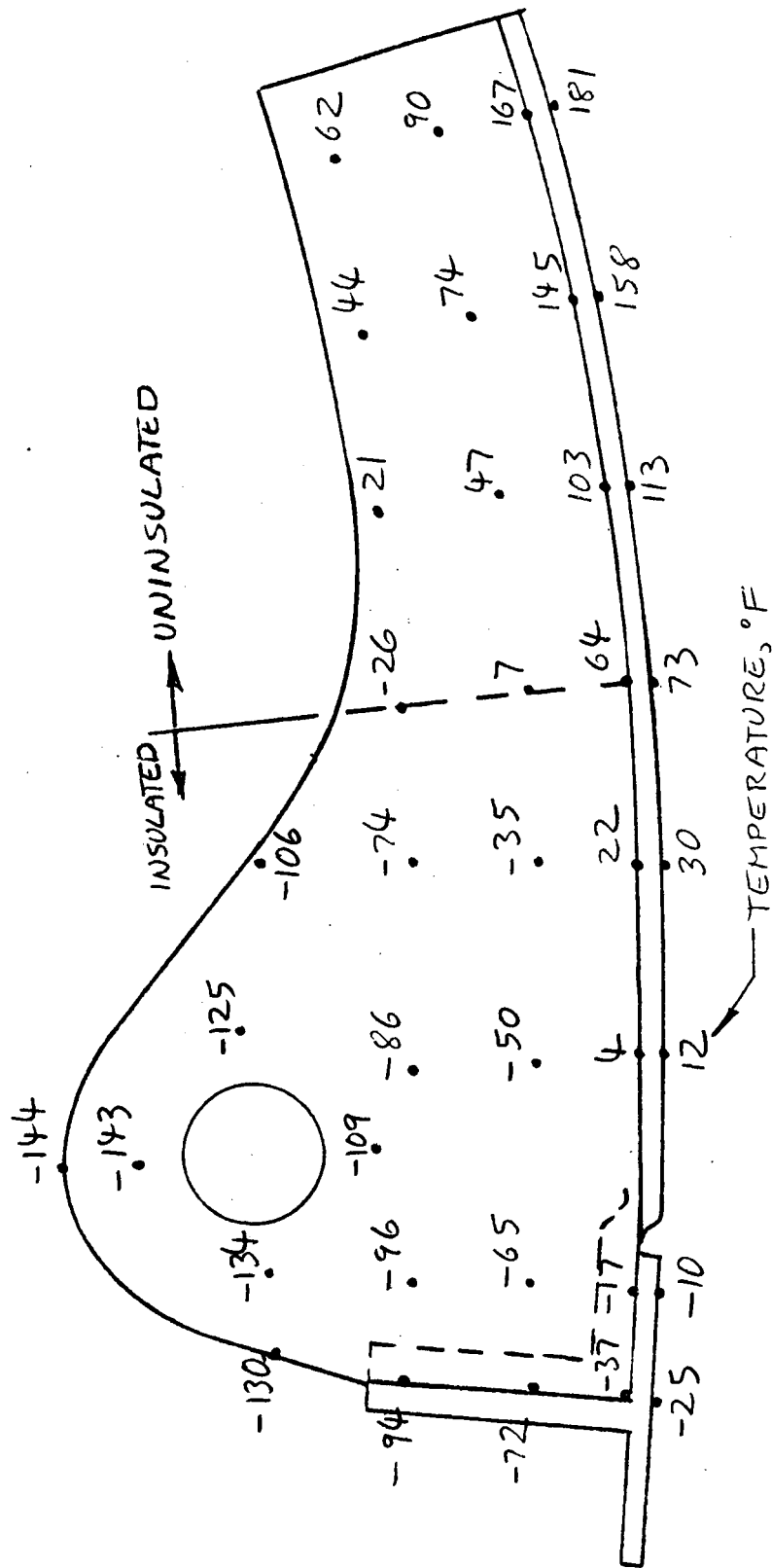


FIGURE 18 LEEWARD SIDE SUPPORT JOINT TEMPERATURES
ENTRY TIME = 260 SECONDS

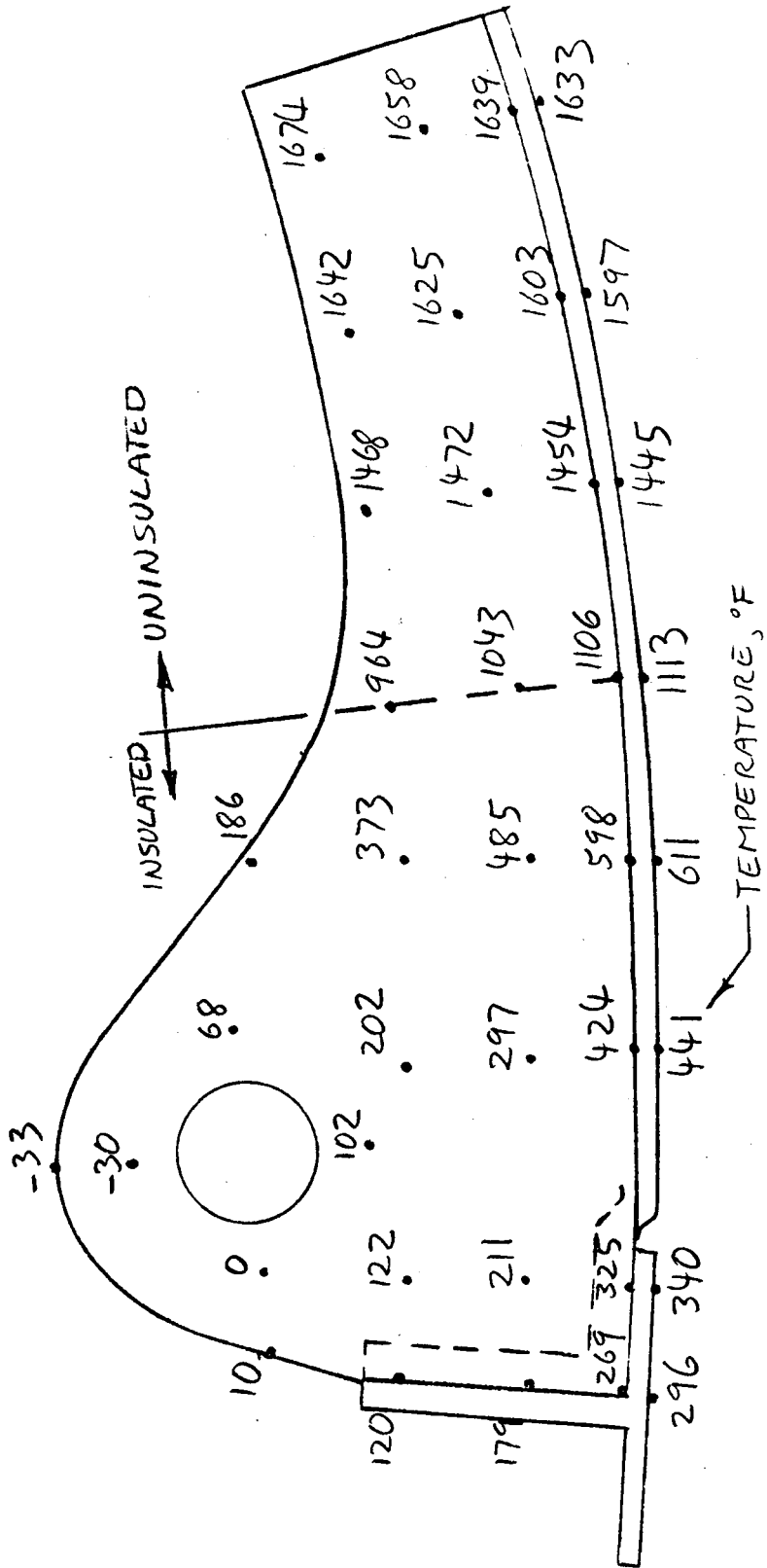
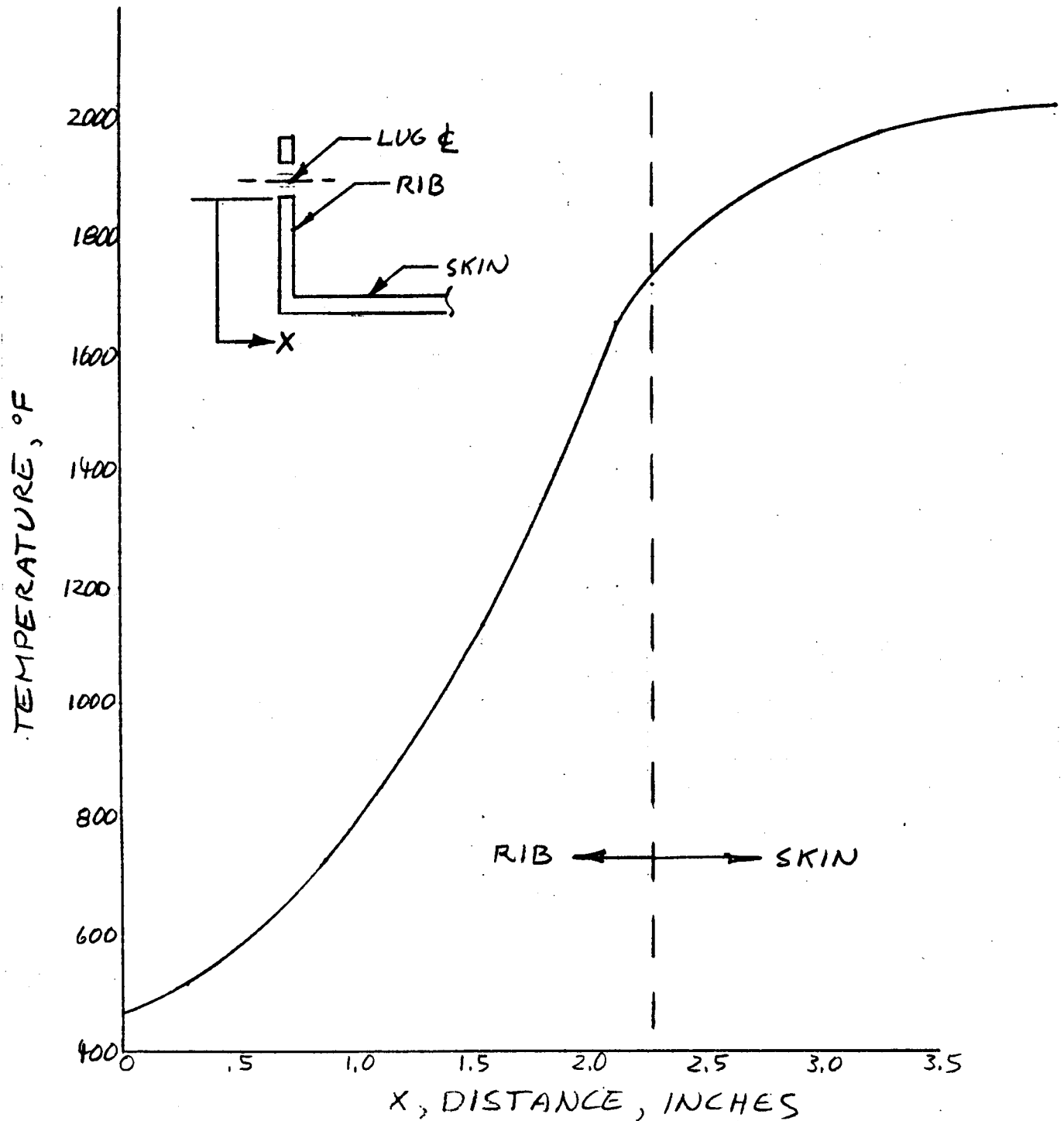


FIGURE 19 LEEWARD SIDE SUPPORT JOINT TEMPERATURES
ENTRY TIME = 400 SECONDS

FIGURE 20, RIB TEMPERATURE
DROP, SUPPORT JOINT AREA

WINDWARD SIDE
TIME = 380 SECONDS



DESIGN INFORMATION REQUEST - RELEASE

8-10-72

TITL (S) AND EFF.		DIR. NO.		REV.	
PREDICTED TEMPERATURE DISTRIBUTION FOR THE WINDWARD		T143-DIR-2-11			
SIDE LEADING EDGE SUPPORT JOINT AND BRACKET		DATE	PAGE	OF	
		8/9/72	1	39	
SYSTEM		REF. G. O. NUMBER			
		3357-AA-1160			

Fill in block below for Information Request		Fill in block below for Information Release	
BY _____ GROUP _____ SON _____ GROUP _____ ONLY <input type="checkbox"/> BWR <input type="checkbox"/> BUWPS <input type="checkbox"/>		IN REPLY TO DIR. NUMBER _____ REL. TO D. M. While GROUP 3-52000 PREPARED BY W.A. Whitten DATE 8-8-72 GROUP APP. J.E. Medford DATE 8-8-72 CHECKED BY E. Matza DATE 8-8-72 PROJ OFFICE D.M. While DATE 8/10/72	

F.T. Esenwein, R.J. Copeland, W.E. Agan, E. Matza, B.A. Forcht

REFERENCES:

- "Development of a Thermal Protection System for the Wing of A Space Shuttle Vehicle," VMSC Report No. T143-5R-00124, 30 April 1972.
- "Predicted Temperature Distribution for the Wing Leading Edge Skin and Rib", VMSC Design Information Release No. T143-DIR-2-07, 13 July 1972.

INTRODUCTION:

The leading edge is attached to brackets bolted to the wing box as illustrated in Figure 1. Analyses were performed during Phase II (Reference 1) to determine the insulation required to protect the wing structure having a 650°F temperature limitation. The temperature limitation has been changed to 350°F for Phase III analysis.

The purpose of the present analysis is to determine the attachment configuration required to protect the wing structure from temperatures above 350°F. A number of attachment options are considered and the results of the thermal analysis were used to help guide in selection of the attachment configuration to be ground tested. Pre-test predictions for selected configuration are presented. Only the windward side attachment was considered.

The thermal analyses were performed using a three-dimensional thermal model and a VMSC computer routine which accounted for heat conduction along the skin and RPP rib, across the hard insulators at the support joint, the steel bolt, the bracket, and across the insulation into the aluminum wing structure. Cross radiation from the skin to the portion of the RPP rib outside the bulk insulation was also considered, as was the heat conduction through the bulk insulation and into the support joint.

CONFIGURATION DEFINITION

Two types of attachments were considered. Attachment number 1, the baseline, has a one-piece bracket between the attachment bolt and the aluminum structure; and attachment number 2 has a two-piece bracket. A number of variations were considered for each type of attachment.

The three-dimensional thermal model used in the analysis is shown in Figures 2 through 8. The model for the rib area is similar to that which was used in Reference 2 to predict temperatures of the ribs in the support joint area. The aluminum structure is represented by a block of aluminum with adiabatic boundaries except at the bracket. Also the effect of the titanium brace (Figure 1) upon the bracket is neglected for this analysis.

THERMAL ANALYSIS

The recovery temperature and the convection heat transfer coefficients used for the external skin nodes were the same as those used in the rib analysis of Reference 2. The external temperature of the bulk insulation was input as a function of time as given in Figure 9. Thermal property data used in the analysis is presented in the Appendix.

All the analysis except that for the ground test predictions is based upon an initial temperature distribution obtained from Grumman Aircraft Corporation. The temperatures varied from 275°F at the exterior surface to 180°F at the aluminum structure. This distribution represents worst-case conditions where the shuttle makes a single orbit before landing; and consequently, the structural temperatures remain high at time of entry due to residual boost heating. At this stage in the shuttle development, the possibility of such high initial temperatures at the time of reentry is not known. Near the completion of the analysis, North American Rockwell suggested using an initial temperature of 130°F, so the last run (predictions for the ground test of the lug) uses 130°F.

A summary of the results is presented in Tables I and II. The type of insulation used in the different configurations is also indicated on the tables. The individual runs will be discussed in the following paragraphs in the order listed in the tables.

Computed temperatures as a function of entry time for attachment No. 1 (one piece bracket shown in Figure 5), variation 1 are shown in Figure 10. Temperature of the RPP rib at its interface with the silica insulator peaks at 1721°F which is tolerable for the fused silica. The steel bolt temperature peaks at 1209°F, and the peak temperature of the Haynes bracket is 754°F; both of which are tolerable. The aluminum temperature is 385°F and rising at the end of the run (4500 seconds). Since the aluminum temperature was already over the 350°F limit the run was not continued. Extrapolation of the available data yields a maximum expected aluminum temperature not greater than 422°F. Note that these peak

temperatures are summarized on Tables I and II for each run. Also the number of the figure containing the detailed results for each run (Figures 10 through 22) is included on the tables for ready reference.

Variations 2 and 3 of attachment type 1 considered additional aluminum heat sink in place of the silica insulation at the cold end of the Haynes bracket. The results of variation 3 show that the temperature of the aluminum can be kept below 350°F by using sufficient additional heat sink (1.526" x 1.8" x 2.85").

The results using variations 4 and 5 show that a thickness of approximately 0.6" silicone laminate insulation at the bracket-aluminum interface is required to hold the aluminum temperature to below 350°F. All the previous runs have been made for silica hard insulation at the bolt connecting the RPP rib to the bracket. Changing the bolt insulation from silica to high density zirconia makes it necessary to use thicker (approximately 0.3" more) silicone laminate insulation at the bracket-aluminum interface, as shown by the results for variation 6.

The results for the one-piece bracket showed that relatively thick insulation is required at the bracket-aluminum interface. These thicknesses require long bolts which introduce possible structures problems. Because of this a two-piece bracket (called attachment Type 2 - see Figure 6) was investigated.

The results of the analysis for attachment type 2 are summarized in Table II. Variation 1 utilized 0.25 inch thick silica between the hot end and cold end of the Haynes bracket. This configuration is unsatisfactory because the peak aluminum temperature may be as high as 429°F.

In variation 2 of attachment type 2 most of the silica insulation was replaced with lower thermal conductivity Dyna-flex; with the silica retained only at the bolts. Although this arrangement lowered the conductance between the hot and cold ends of the Haynes bracket, the peak temperature of the aluminum increased slightly, since the heat capacity of the insulation had been reduced. (The density of silica is 118 lb/ft³ compared to 6. lb/ft³ for the Dyna-flex).

In variations 3 through 7 of attachment type 2 the cold end of the bracket is made from glass silicone laminate. Computed temperatures as a function of entry time for variation 3 are shown in Figure 17. Temperature of the RPP rib at its interface with the silica insulators peak at 1721°F. The steel bolt temperature peaks at 1208°F, and the peak temperature of the Haynes steel bracket is 768°F. The peak temperature at the interface between the Haynes and the silica laminate is 645°F and the peak aluminum temperature is 292°F. All these temperatures are tolerable.

Variation number 5 was investigated to determine the effect of changing the bolt insulation from silica to zirconia which has a greater thermal conductivity. For this configuration the peak temperature of the interface between the silicone laminate and the Haynes bracket reaches 800°F which is considered excessive. For this reason the run was not continued and hence the peak aluminum temperature was not obtained.

Two methods were considered for reducing the interface temperature to a tolerable value for zirconia insulators at the bolt. First, the thickness of the Haynes bracket was reduced from 0.2" to 0.1" - variation 6. This gave even worse results than before because of the reduced heat capacity of the bracket. The second method proved to be satisfactory because

the peak interface temperature was reduced to 700°F and the peak aluminum temperature is only 284°F. This method used the 0.1" thick bracket of variation 6, but the thickness of the bracket at the interface location was increased to 0.4" to provide more heat sink at that location. Although this may not be a practical way to build the bracket it does indicate that with proper location of the mass of the bracket zirconia insulators may be used at the bolt.

Attachment type 2 was selected for the test configuration because in addition to providing adequate thermal margin it avoids thick insulators with long bolts, and is very flexible with respect to design changes. Two test configurations were analyzed: a preliminary configuration (Figure 7), and a final configuration (Figure 8) which incorporated required structural changes.

The predicted temperatures for the preliminary design of the lug test configuration are shown in Figure 21. The thermal model for this bracket is shown in Figure 7 and utilizes a polyimide fiberglass piece at the cold end of the bracket and Inconel 718 at the hot end of the bracket. The predicted temperatures plotted on Figure 21 show that the aluminum temperature has increased only slightly for the first 4500 seconds of entry time. Comparing the trends of the temperatures to those for previous runs indicates the peak aluminum temperature would probably be less than 300°F for this configuration, and all of the temperatures are tolerable. This run was not continued because final details of the test configuration became available so the thermal model was changed to agree with the test configuration.

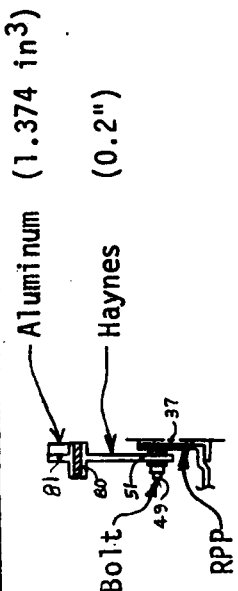
The thermal model of the test bracket is shown in Figure 8. The thickness of the Inconel was increased to give more support area at the bolt insulators, and aluminum angles were added at the cold end of the bracket.

Predicted temperatures for the final configuration are shown in Figure 22. The aluminum temperature increases only 13°F in 9000 seconds of time. Extrapolation of the data indicates the peak aluminum temperature will not be greater than 241°F. All the peak temperatures for this configuration are below the allowables.

SUMMARY:

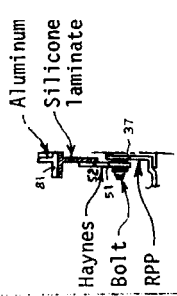
- (1) A two piece attachment bracket was selected for the test configuration (see Figure 8).
- (2) Predicted peak temperature of the aluminum substructure for the selected attachment configuration is 241°F, which is well below the 350°F allowed.
- (3) Changing from silica to high density zirconia bolt insulators at the RPP lug increases the heat conduction through the insulators, for a given insulator design. Results for variations 5 and 6 of attachment type 1 show that approximately 0.3 inch thicker insulation is required at the bracket - aluminum interface in order for the zirconia design to yield the same aluminum temperature as the silica design.

TABLE I
SUPPORT JOINT PEAK TEMPERATURES, °F
ATTACHMENT NUMBER 1

CONFIGURATION:							
VARIATION NUMBER		1	2	3	4	5	6
1) Insulation used at Haynes Aluminum interface		0.25" Silica	0.25" Aluminum	1.526" Aluminum	0.25" Silicone laminate	0.6" Silicone laminate	0.8" Silicone laminate
2) Insulation used at Bolt		Silica	Silica	Silica	Silica	Silica	Zirconia
PEAK TEMPERATURES (See Figure)		Figure 10	Figure 11	Figure 12	Figure 13	Figure 14	Figure 15
1) Attachment Bolt (Node 49)		1209.	1208.	1207.	1209.	1209.	1244.
2) RPP/Insulation Interface (Node 37)		1721.	1721.	1721.	1721.	1721.	1567.
3) Aluminum (Node 81)		388-422.	434	322-326	≈ 415.*	359.	374.
4) Haynes Support Bracket							
Hot end (Node 51)		754.	747.	739.	754.	755.	969.
Cold end (Node 80)		399-422	≈ 434	≈ 326	415.	399.	477

*Using increased convection coefficients after 2400 seconds yielded 402°F.

TABLE II
SUPPORT JOINT PEAK TEMPERATURES, °F
ATTACHMENT NUMBER 2

CONFIGURATION:											See Figure 7	See Figure 8
	VARIATION NUMBER	1	2	3	4	5	6	7	8	9		
1) Insulation used at cold end of Haynes bracket	0.25" Silica	0.25" Silica and Dyna-flex	0.2" Silica laminate	0.34" Silica laminate	0.2" Silica laminate	0.2" Silica laminate	0.2" Silica laminate	0.2" Silica laminate	0.42" Polyimide F.G.	0.25" Polyimide F.G.		
2) Insulation used at bolt	Silica	Silica	Silica	Silica	Zirconia	Zirconia	Zirconia	Zirconia	Silica	Silica		
PEAK TEMPERATURES	Figure 16	Figure 17	No Figure	No Figure	Figure 18	Figure 19	Figure 20	Figure 21	Figure 22			
1) Attachment bolt (Node 49)	1196.	1198.	1208.	1210.	1243.	1369.	1338.	1227.	1178.			
2) RPP/Insulation Interface (Node 37)	1720.	1720.	1721.	1721.	1566.	1617.	1608.	1711.	1699.			
3) Aluminum (Node 81)	≈ 429.	≈ 439.	292.	276.	Not Available	Not Available	284.	Not Available	Not Available	≈ 241.		
4) Haynes Support Bracket Hot end (Node 51)	702.	711.	768.	≈ 768.	980.	1166.	1096.	733.	604.			
Interface with insulation (Node 52)	≈ 429.	≈ 439.	645.	≈ 645.	800.	851.	700.	523.	446.			

* Haynes 188 support fitting thickness reduced from 0.2" to 0.1"

** Same as variation 6 except node 52 is 0.4" thick to provide more heat sink at Haynes/Silicone interface.

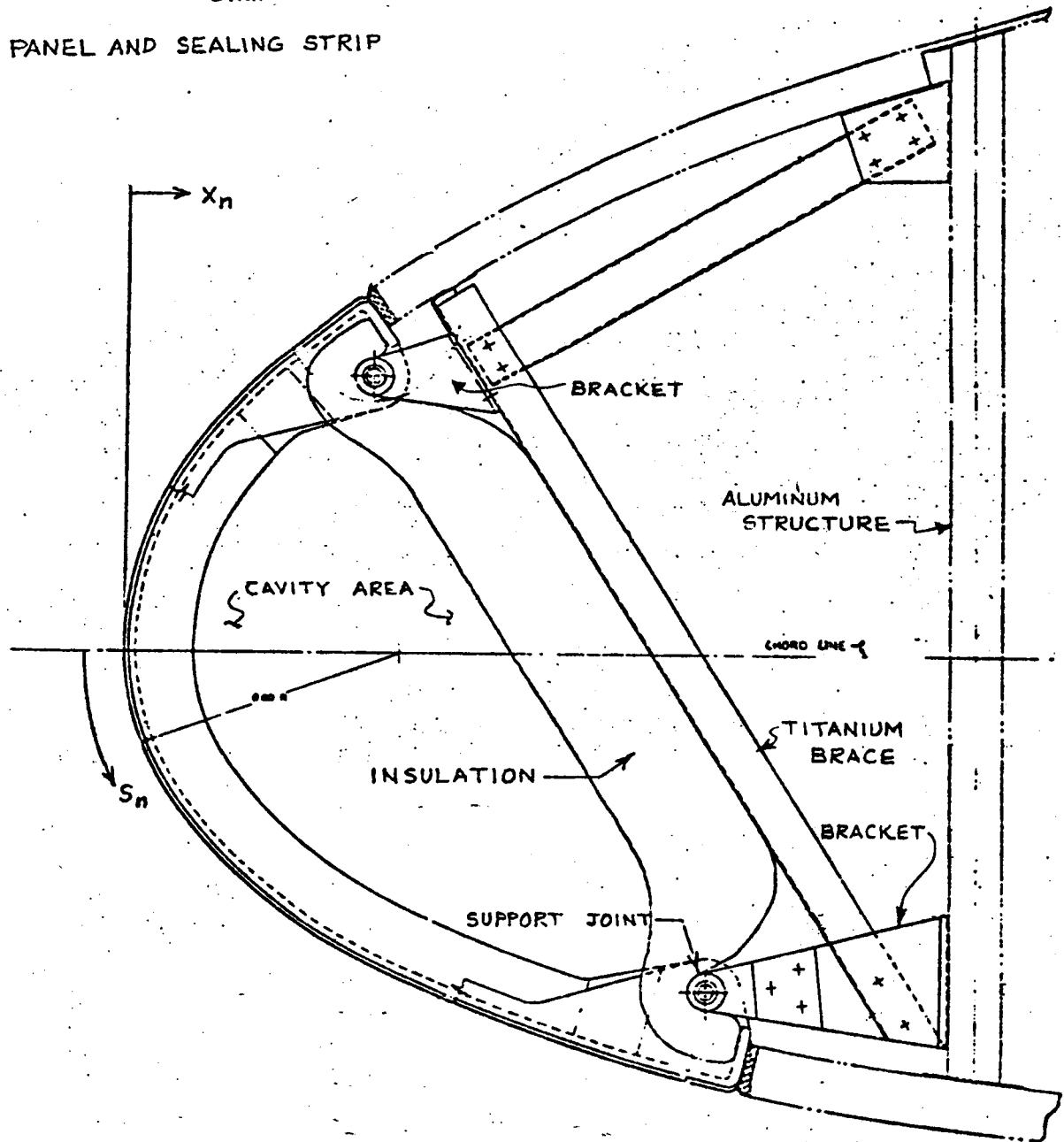
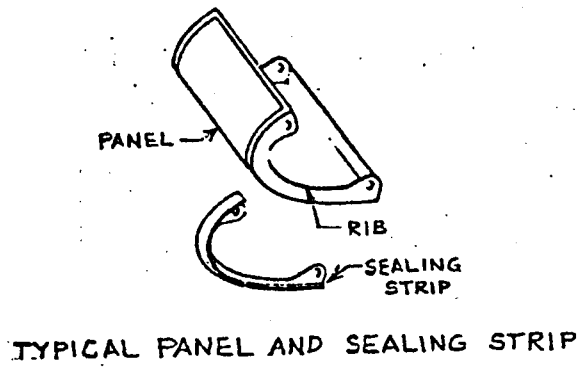


FIGURE 1 LEADING EDGE CONFIGURATION

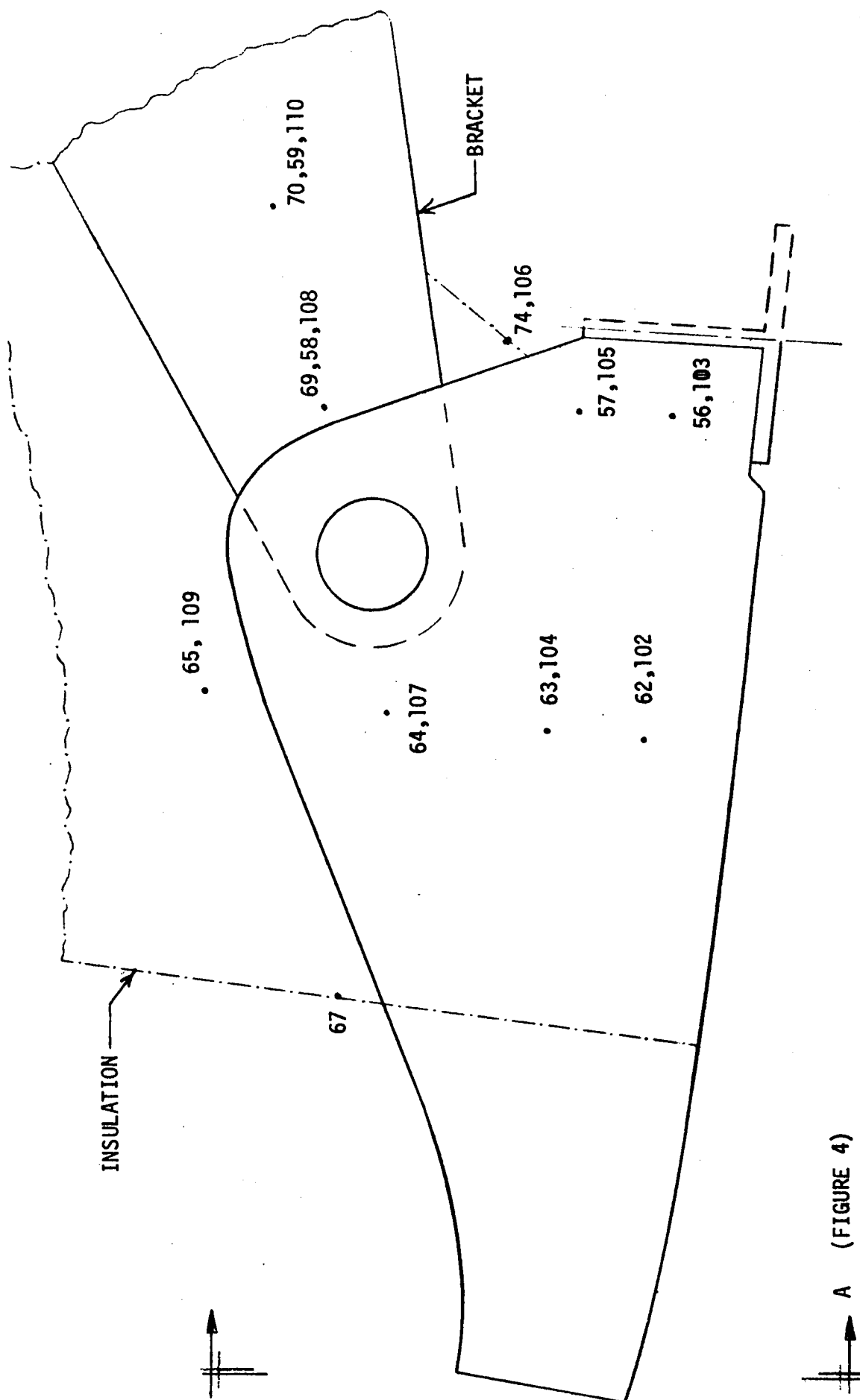


FIGURE 3 - THERMAL MODEL OF BULK INSULATION

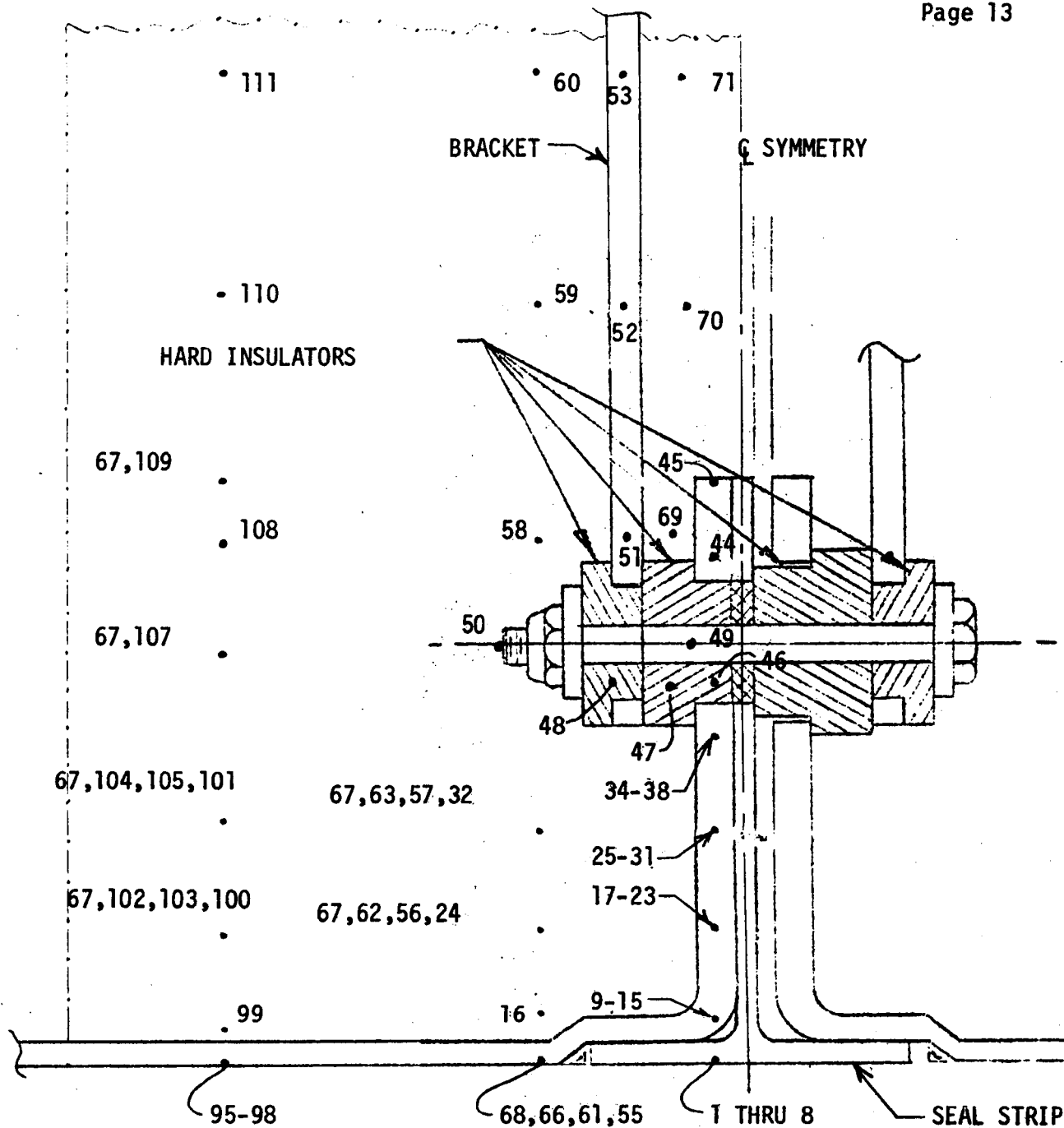


FIGURE 4 - THERMAL MODEL - SECTION A-A

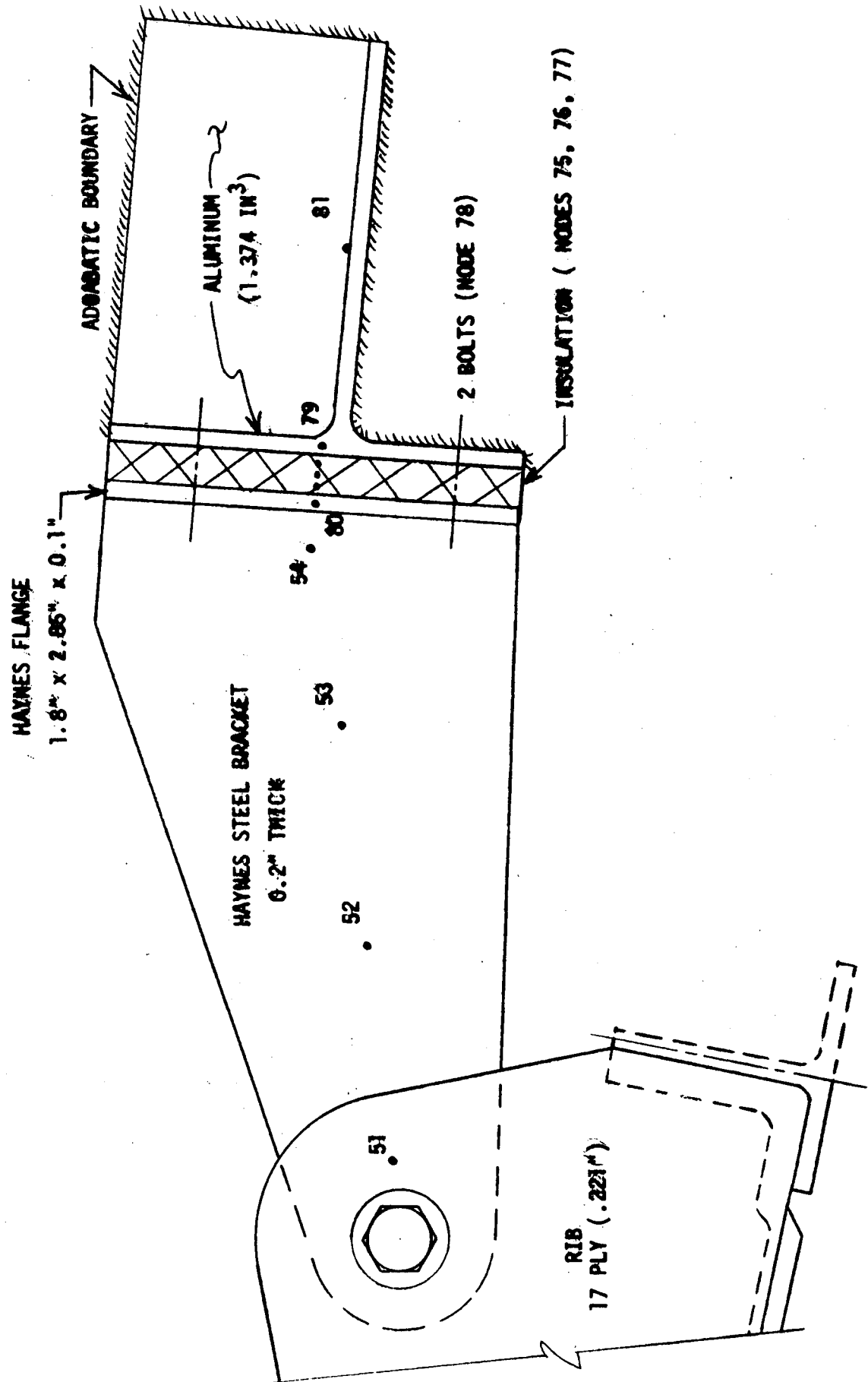


FIGURE 5 THERMAL MODEL ATTACHMENT TYPE 1 BRACKET

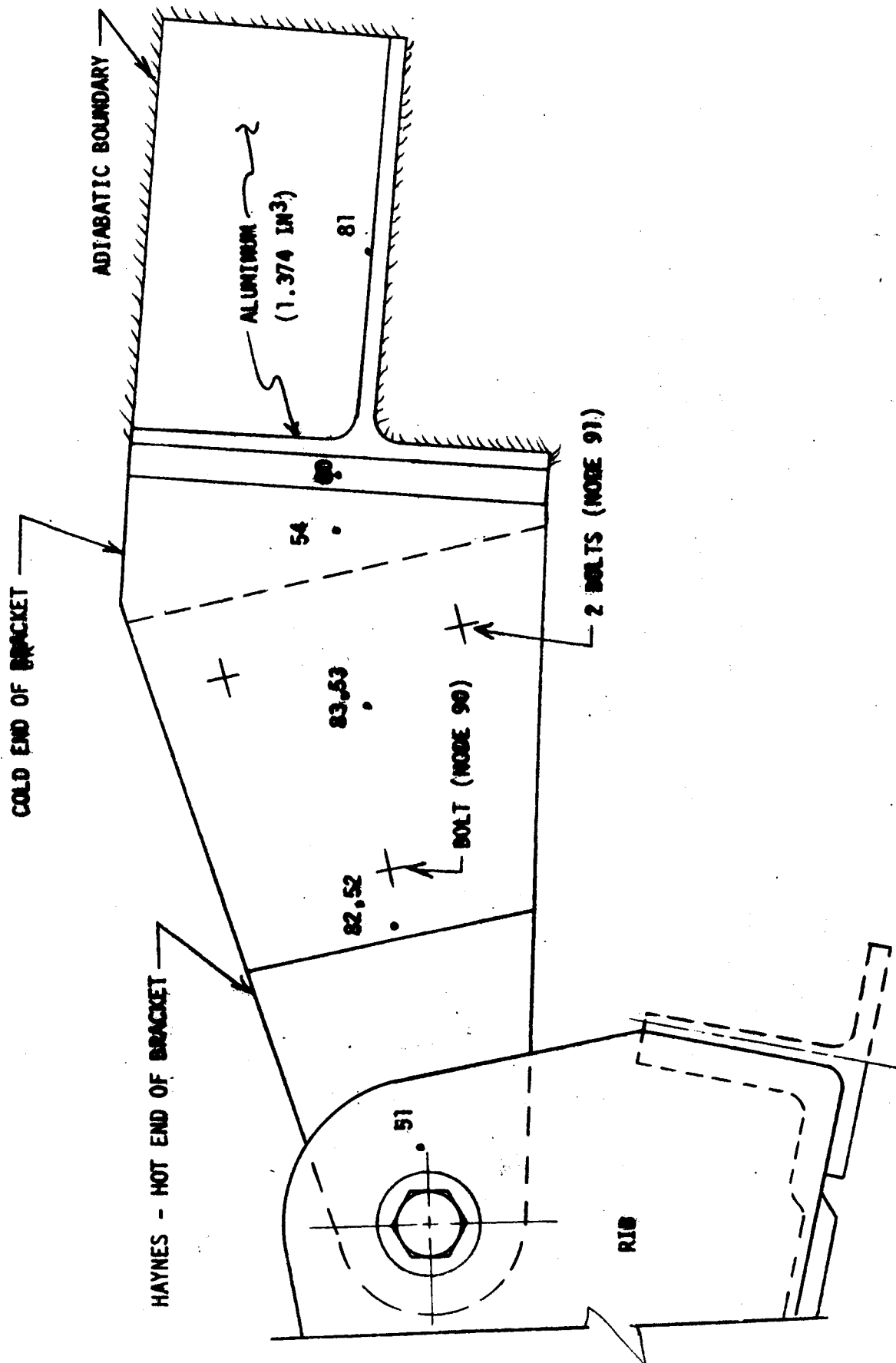


FIGURE 6 THERMAL MODEL ATTACHMENT TYPE 2 BRACKET

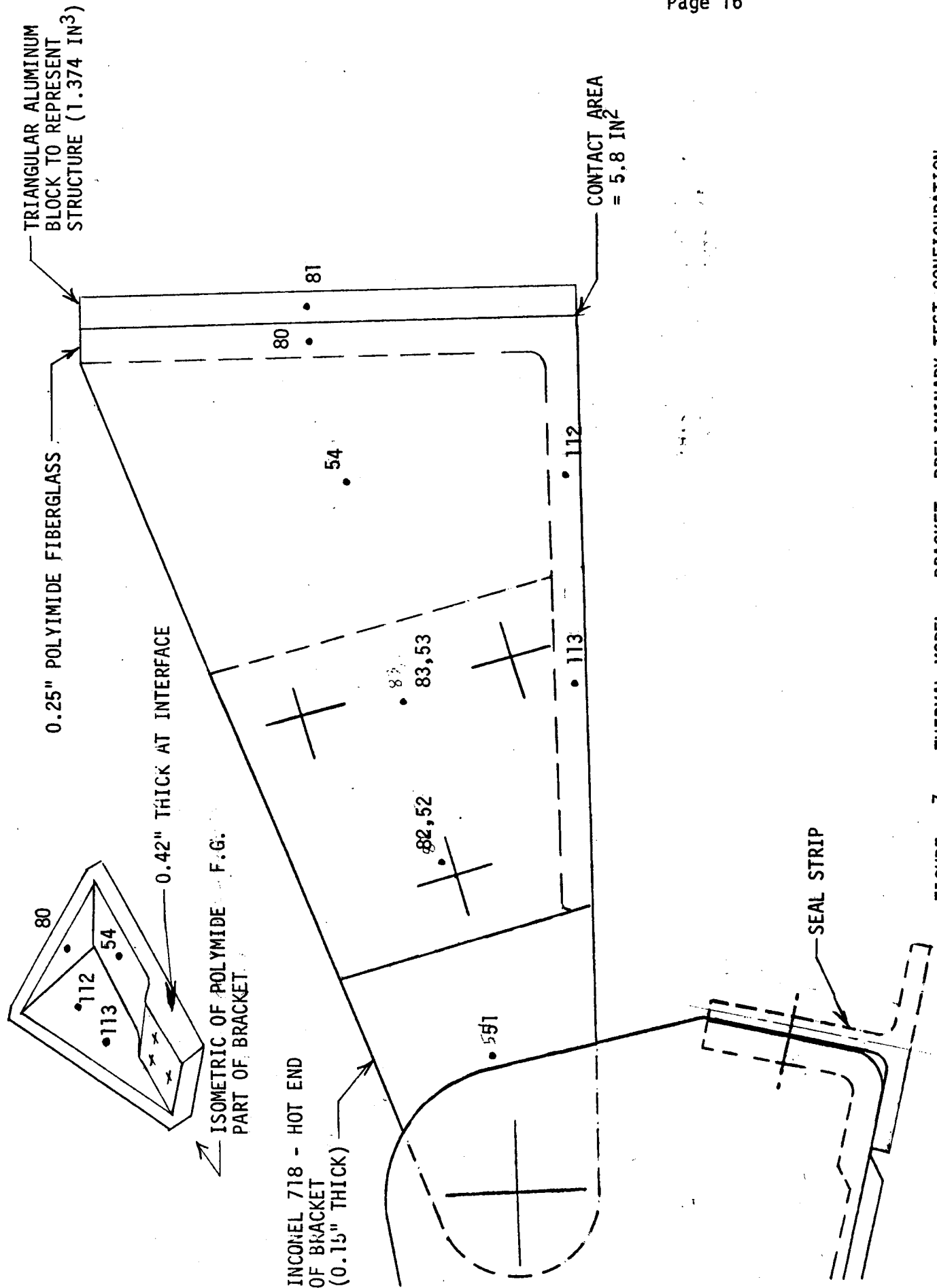


FIGURE 7 - THERMAL MODEL - BRACKET, PRELIMINARY TEST CONFIGURATION

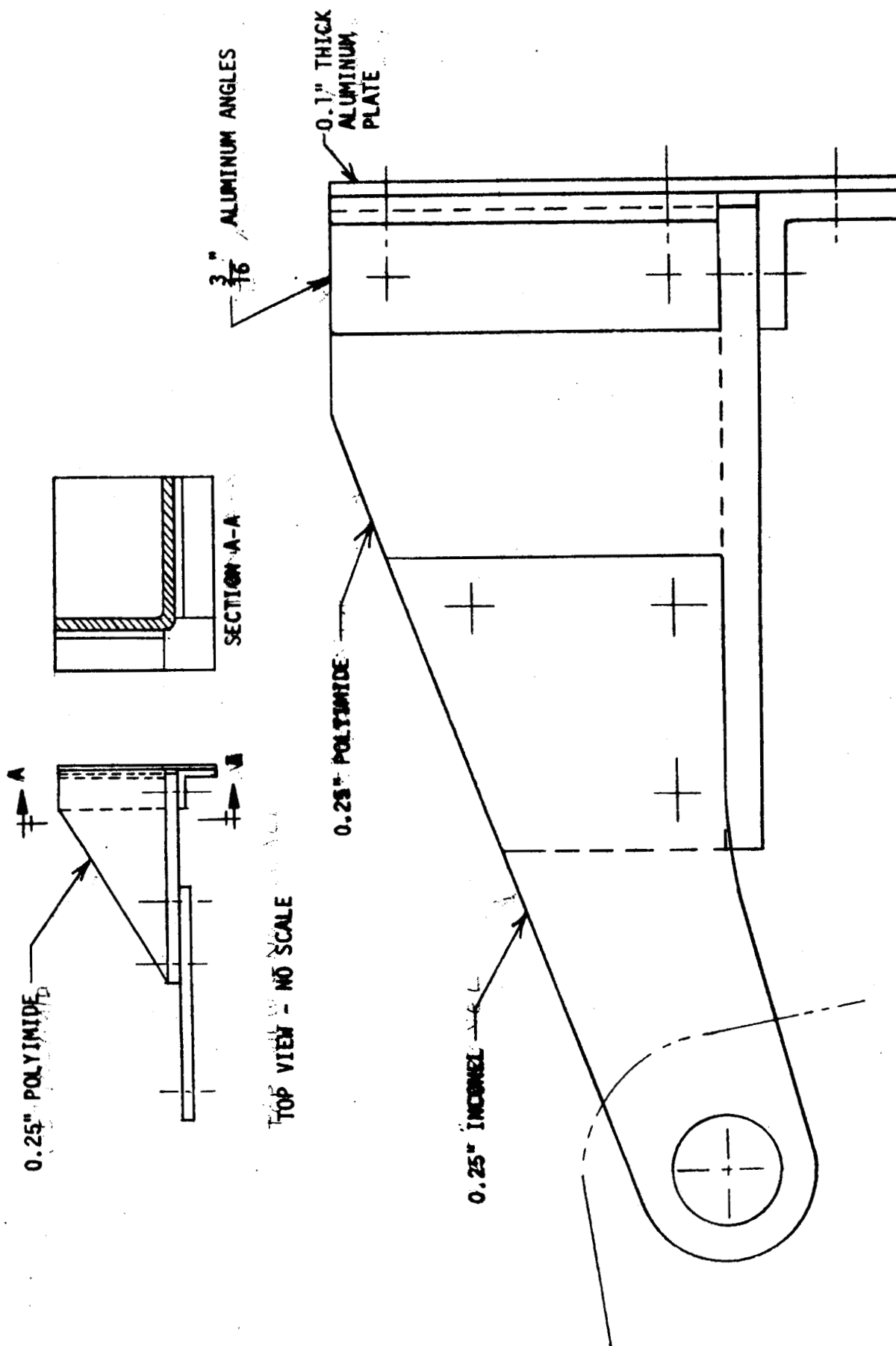


FIGURE 8 THERMAL MODEL - BRACKET FOR GROUND TEST

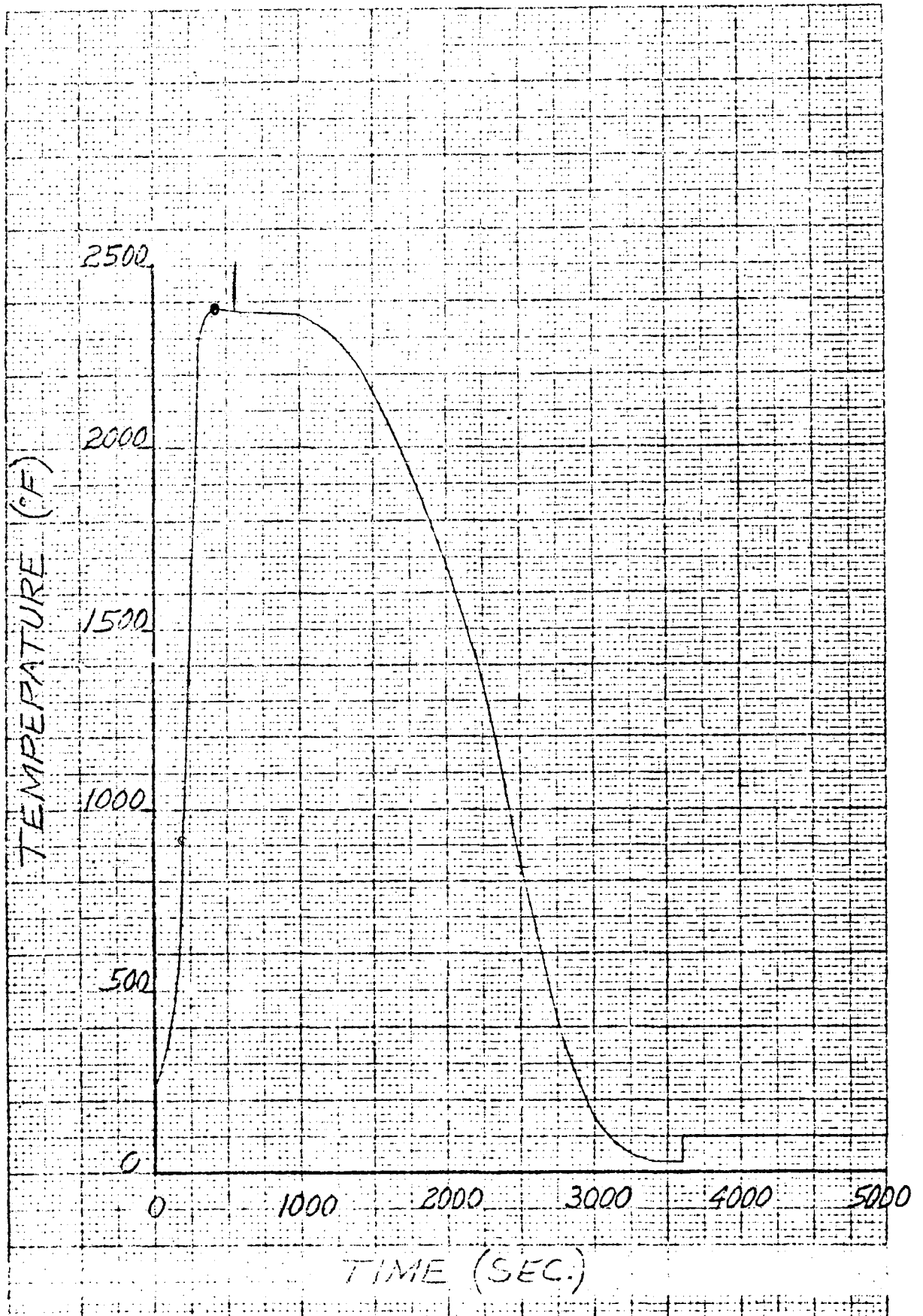
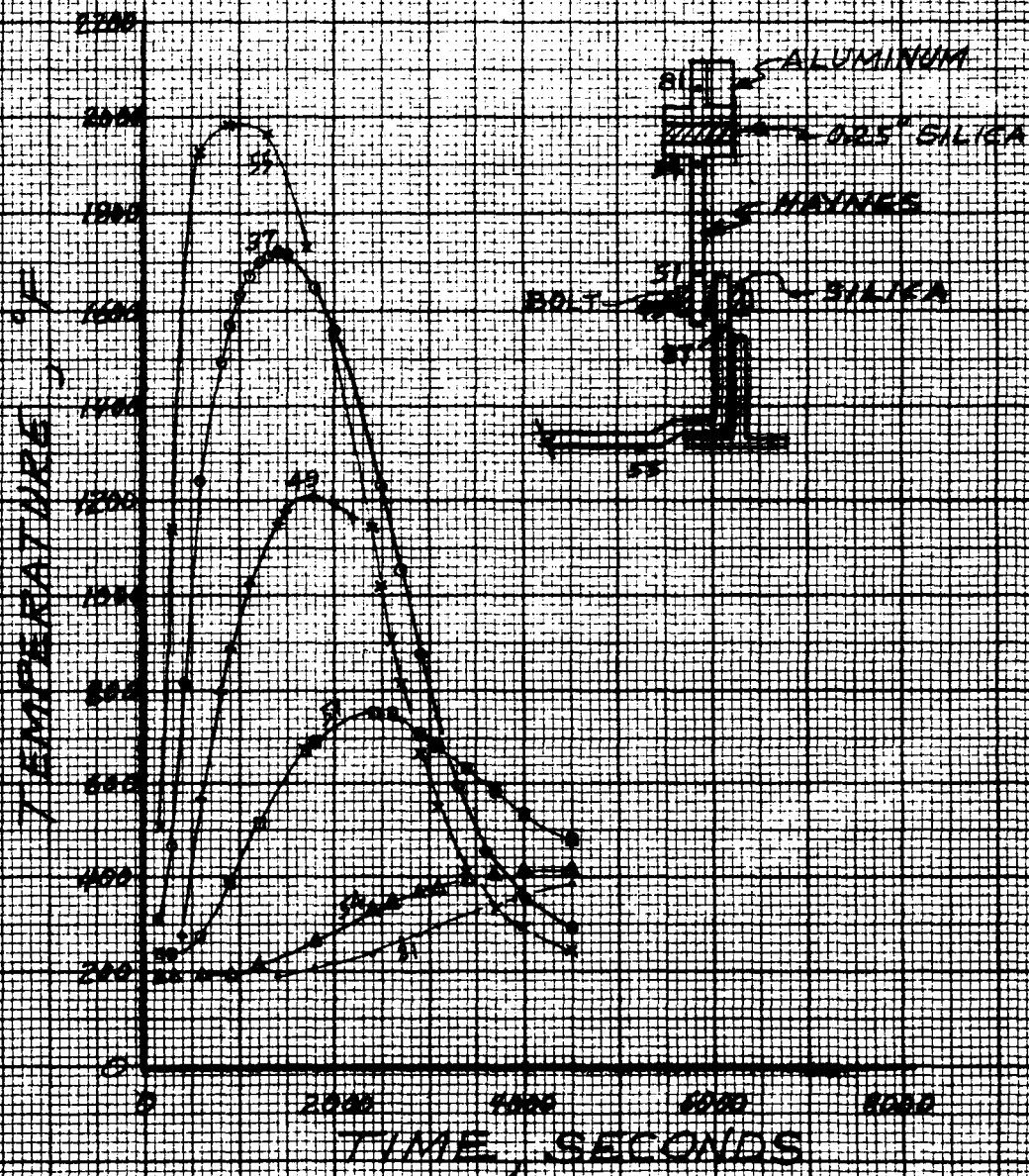


FIGURE 9 RADIATING STRUCTURE TEMPERATURE

FIGURE 10
PREDICTED TEMPERATURES
ATTACHMENT 1 - VARIATION 1



Handwritten signature and date: 10/1/77

FIGURE 11
PREDICTED TEMPERATURES
ATTACHMENT 1 - VARIATION 2

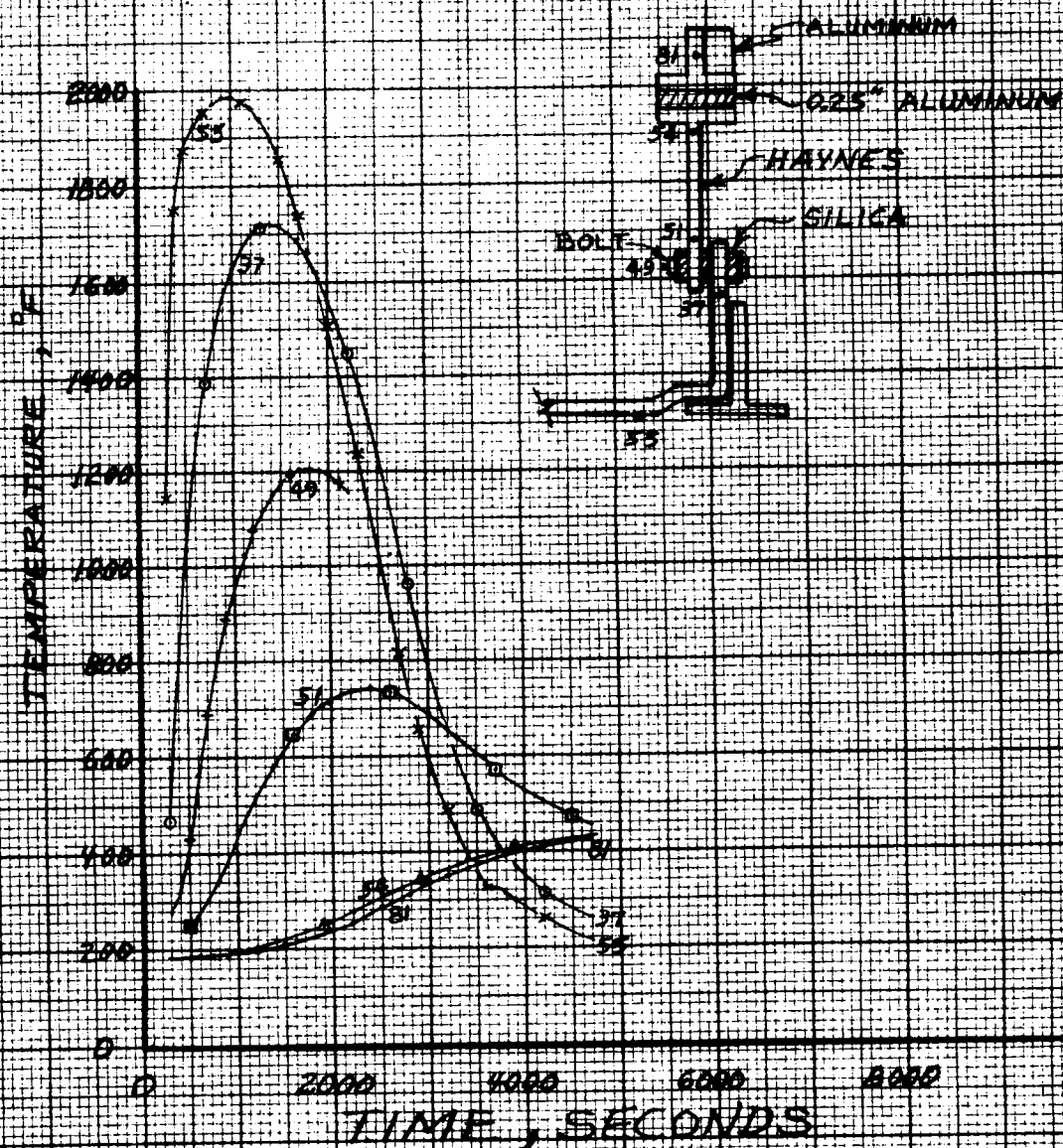


FIGURE 12
PREDICTED TEMPERATURES
ATTACHMENT 1 - VARIATION 3

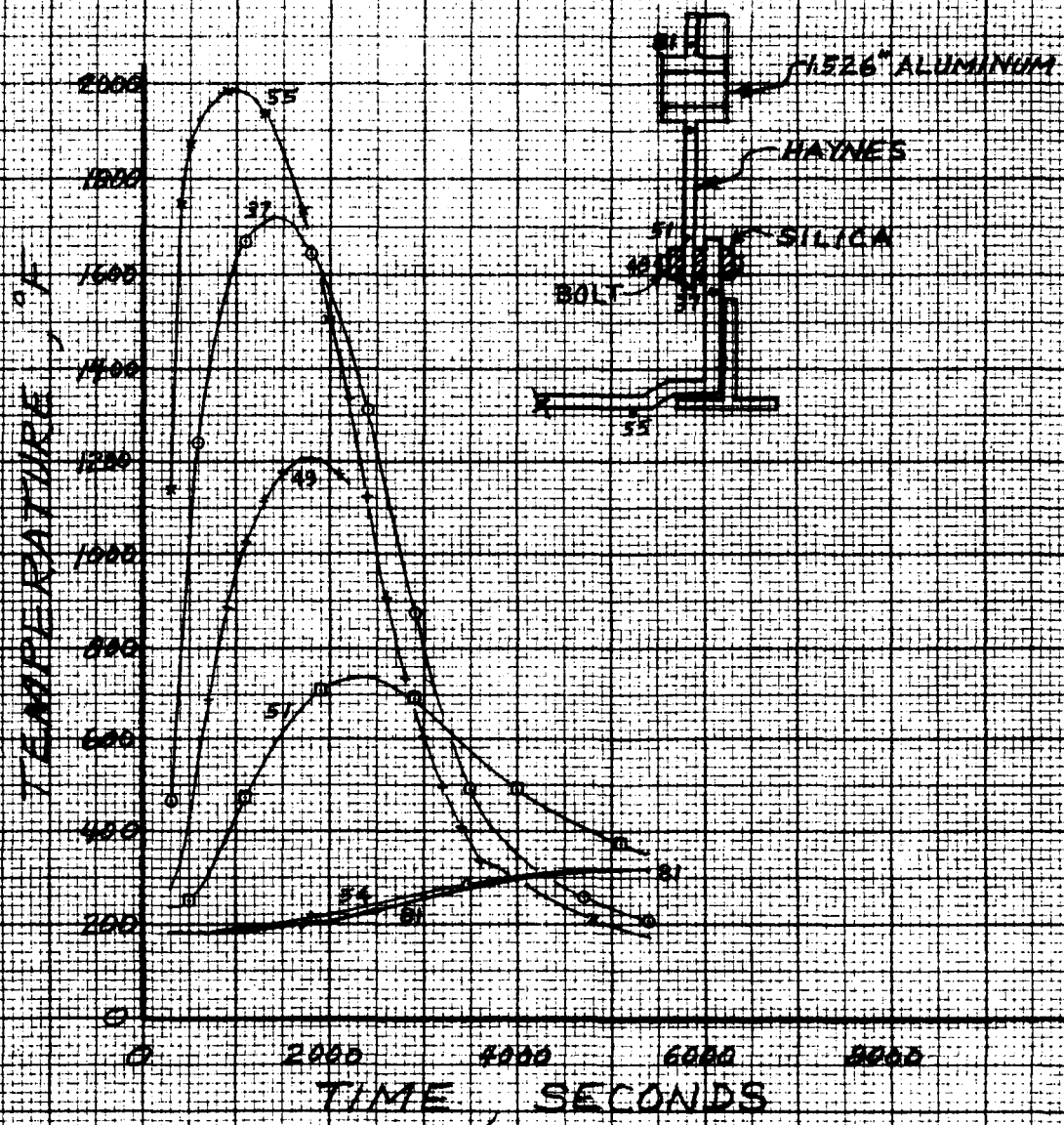


FIGURE 13
PREDICTED TEMPERATURES
ATTACHMENT 1-VARIATION 4

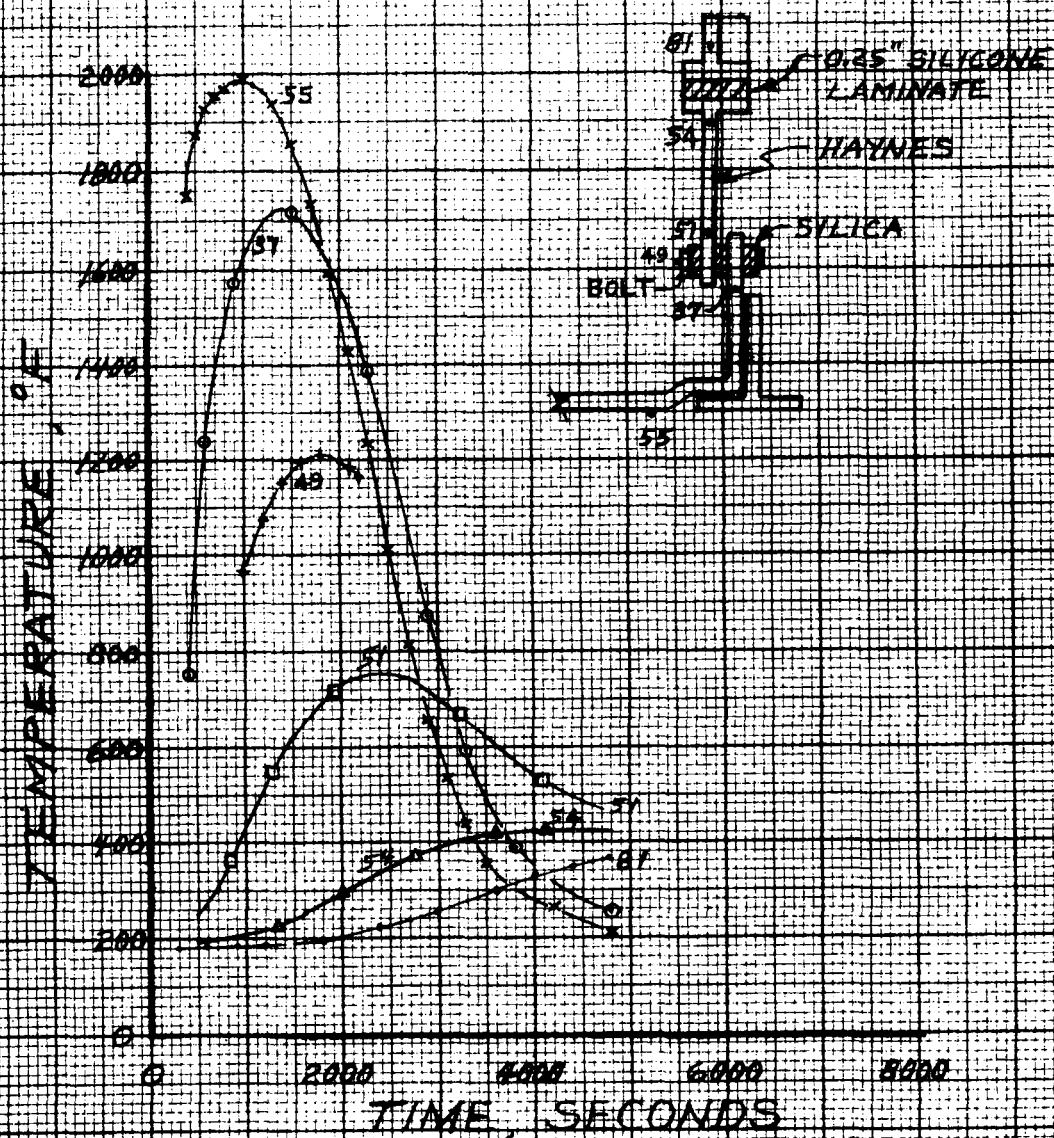


FIGURE 14
PREDICTED TEMPERATURES
ATTACHMENT 1 - VARIATION 5

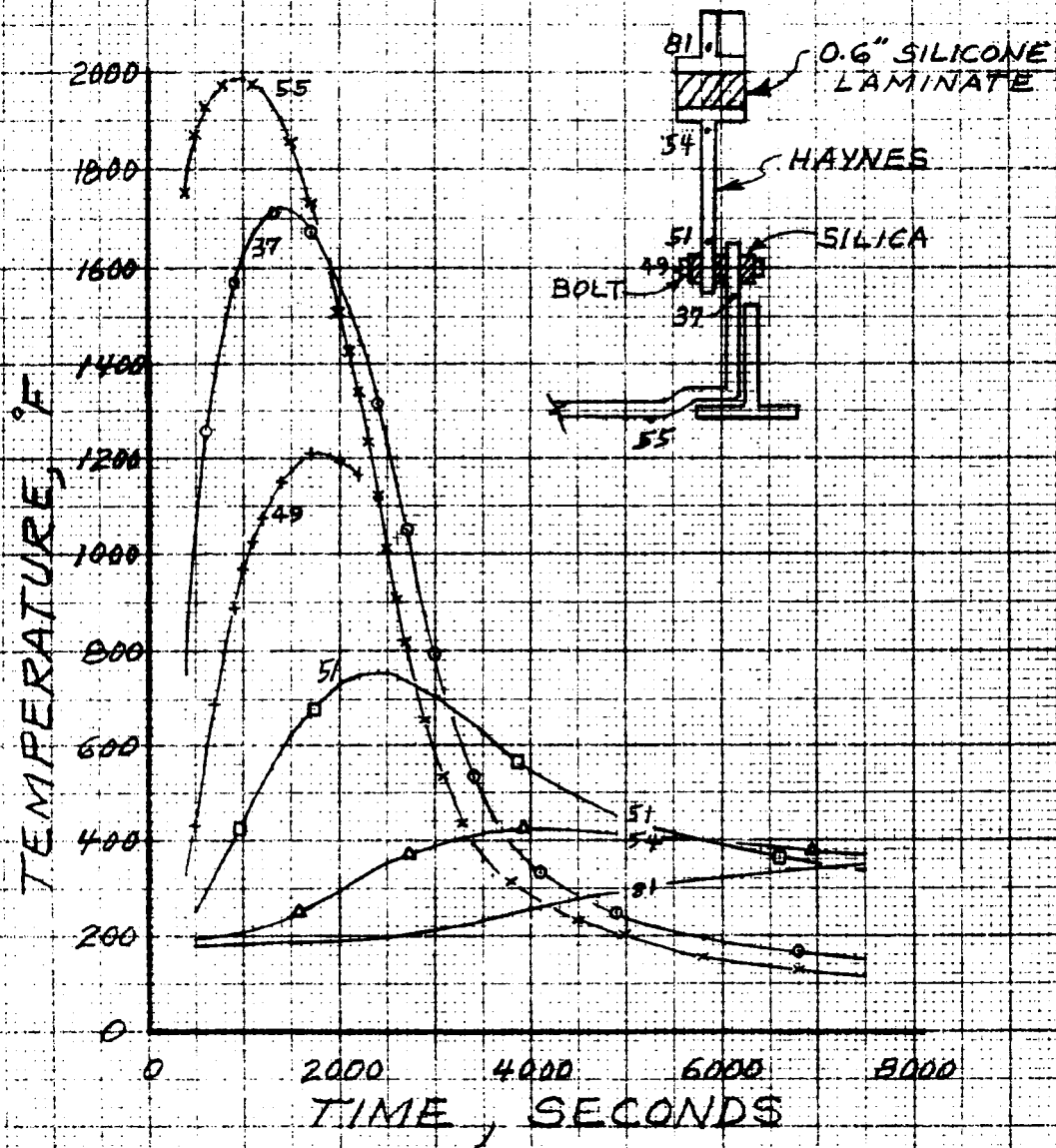


FIGURE 15
PREDICTED TEMPERATURES
ATTACHMENT 1 - VARIATION 6

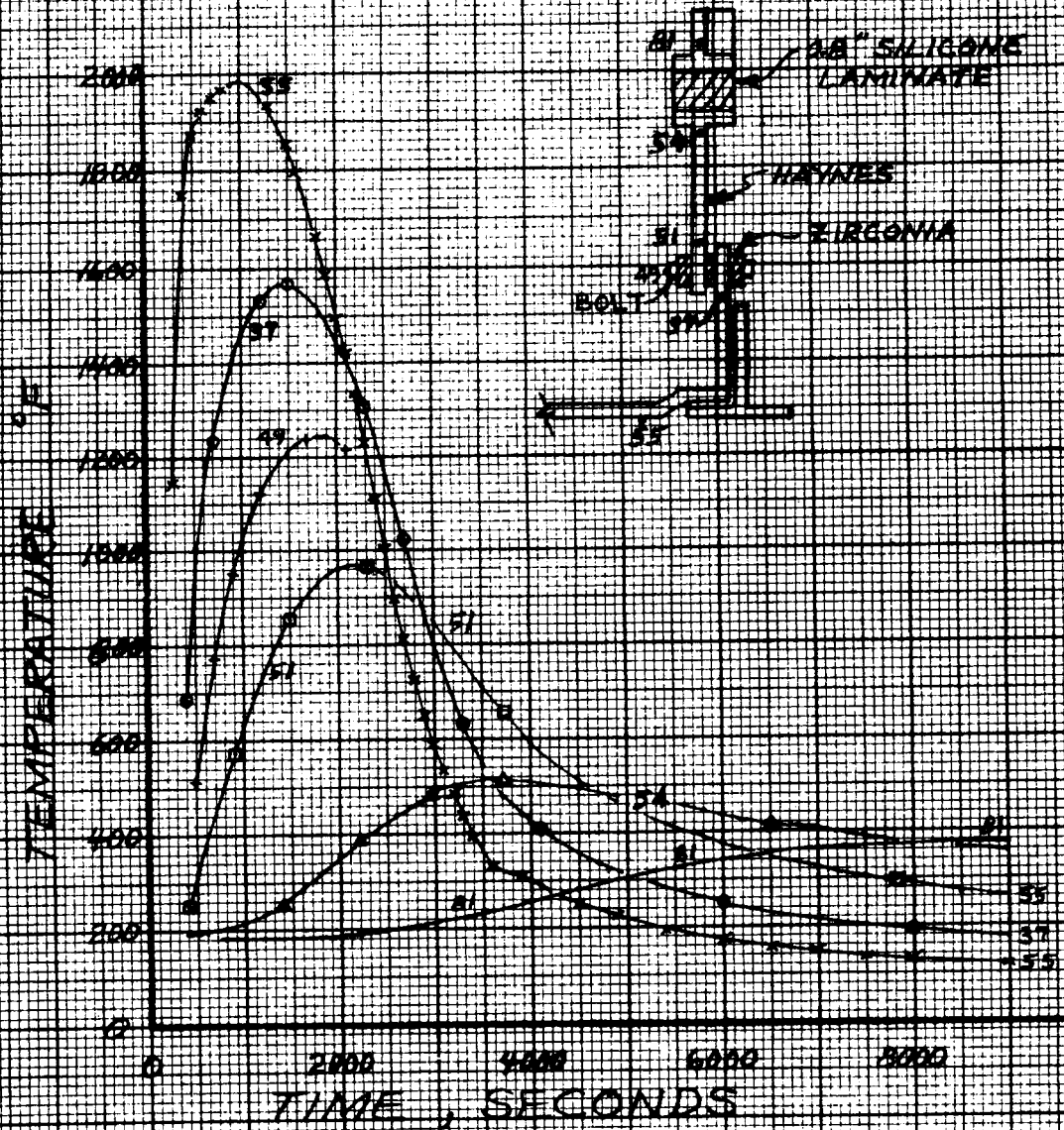


FIGURE 16
PREDICTED TEMPERATURES
ATTACHMENT 2-VARIATION 1

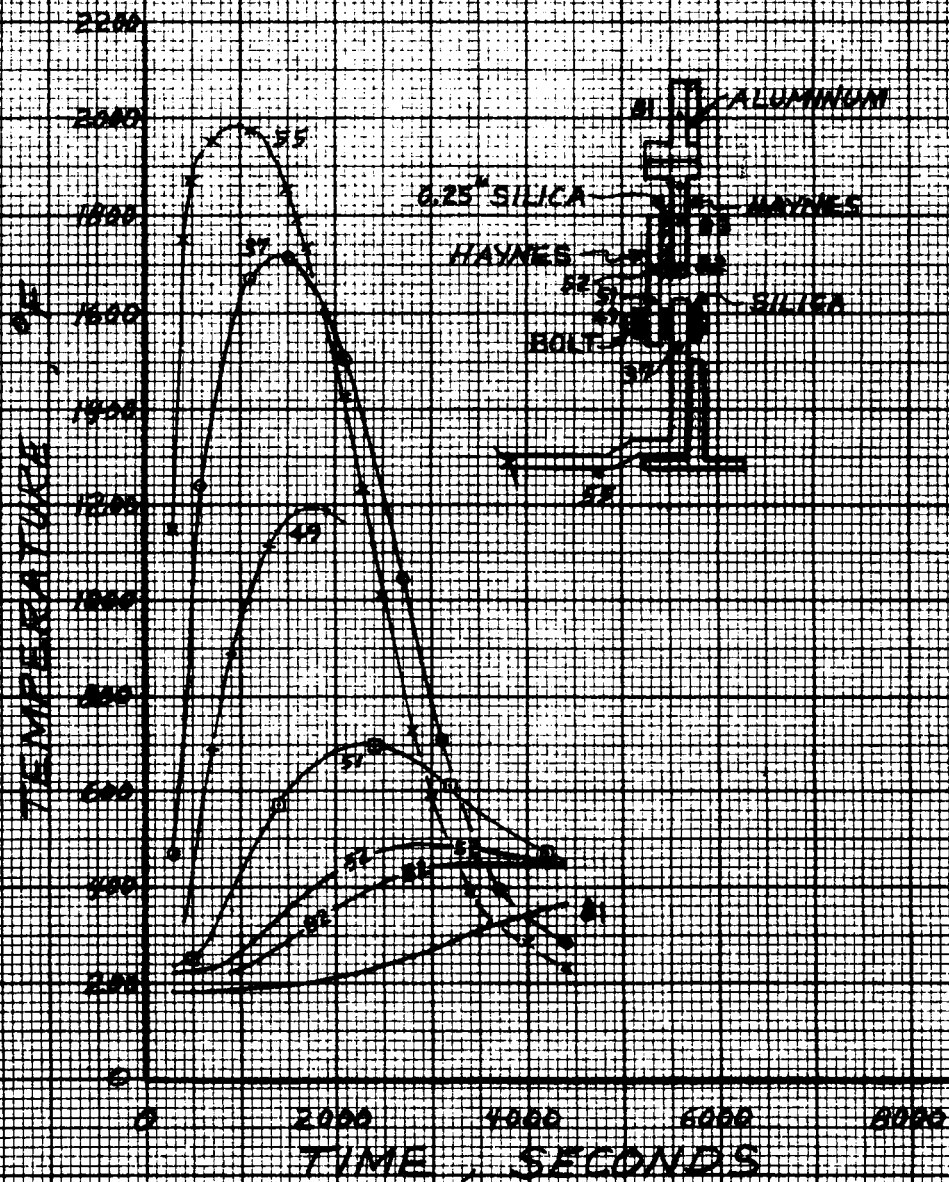
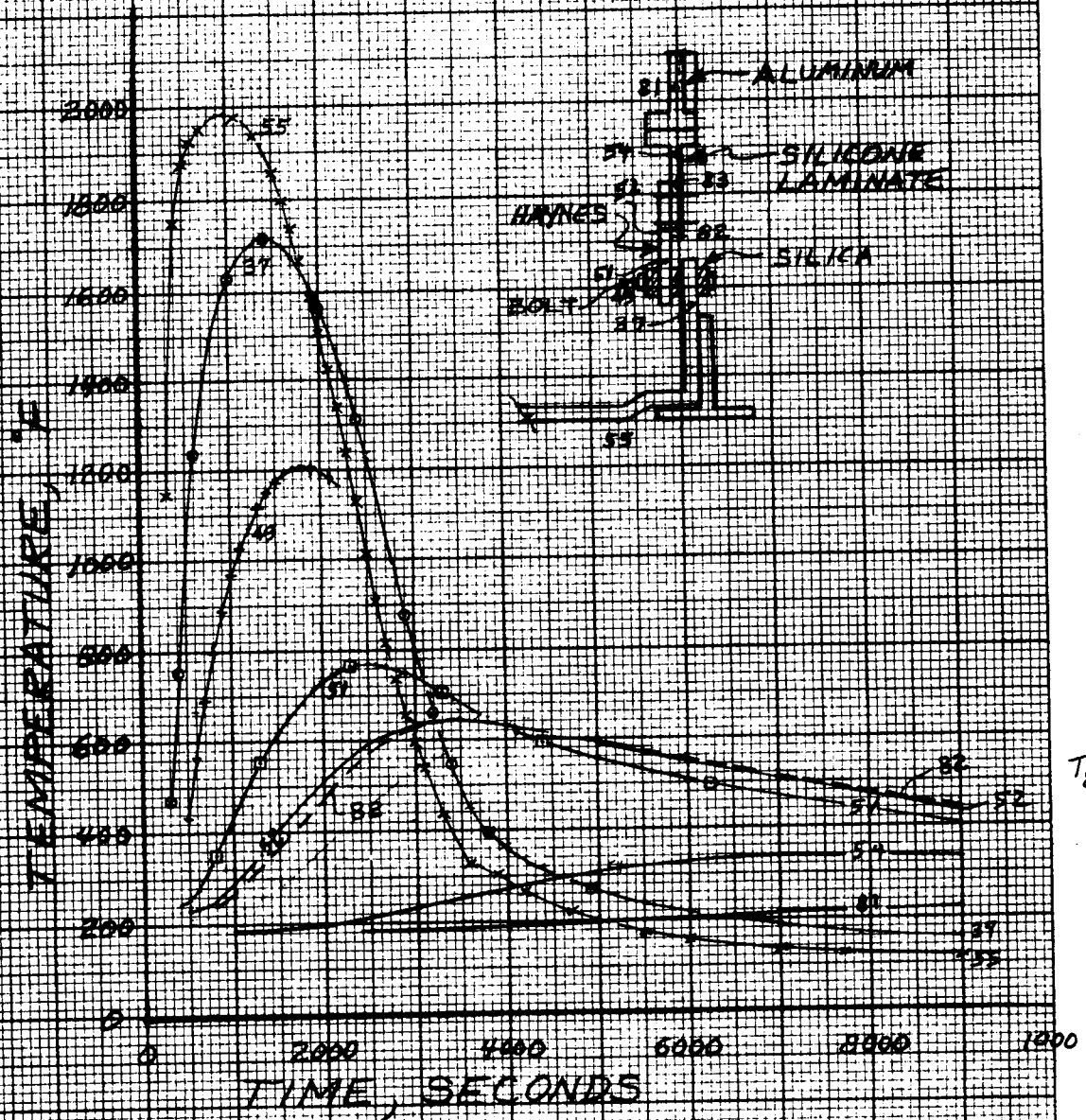


FIGURE 17
PREDICTED TEMPERATURES
ATTACHMENT 2 - VARIATION 3



$T_{81 \text{ MAX}} \leq 292^\circ$

FIGURE 1B
PREDICTED TEMPERATURES
ATTACHMENT 2 - VARIATION 5

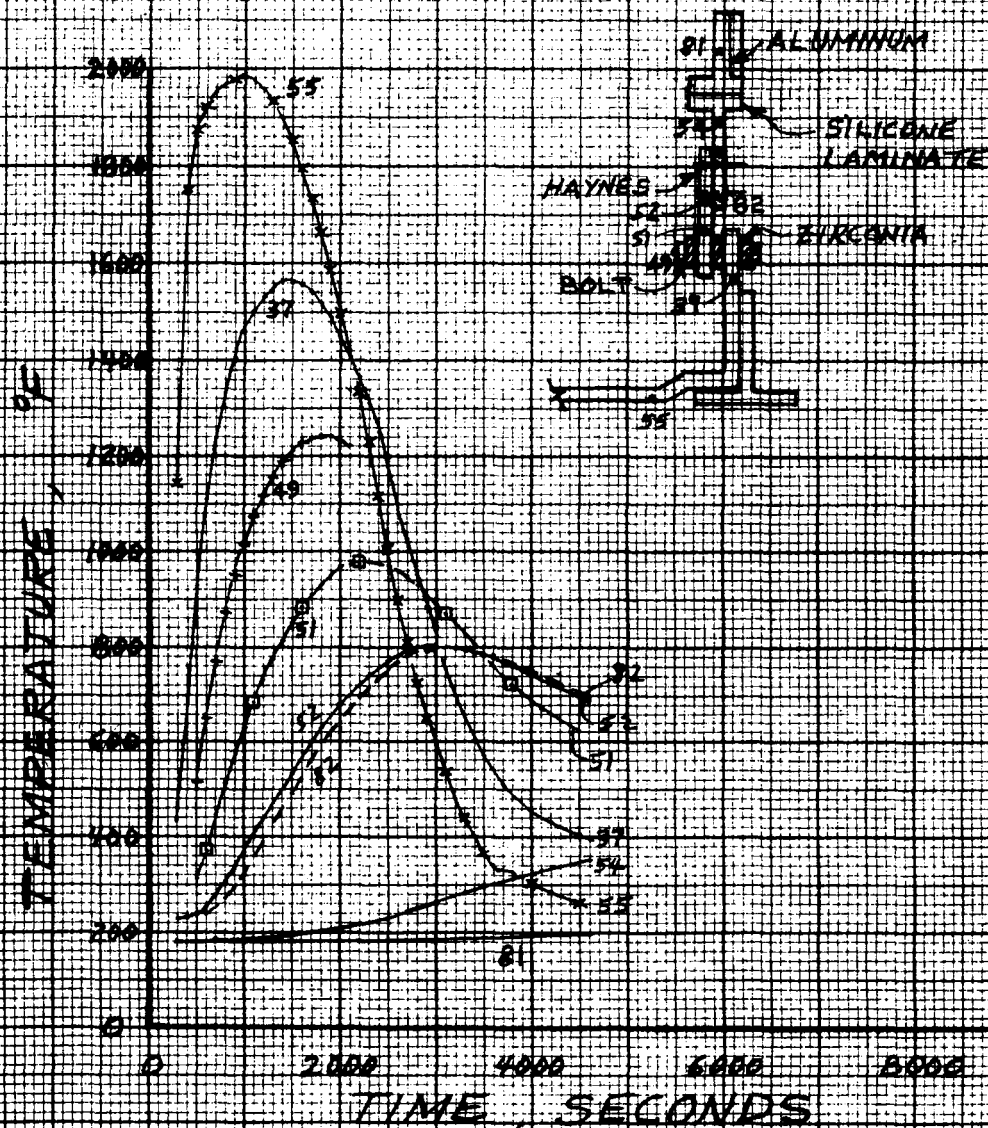


FIGURE 19
PREDICTED TEMPERATURES
ATTACHMENT 2 - VARIATION 6

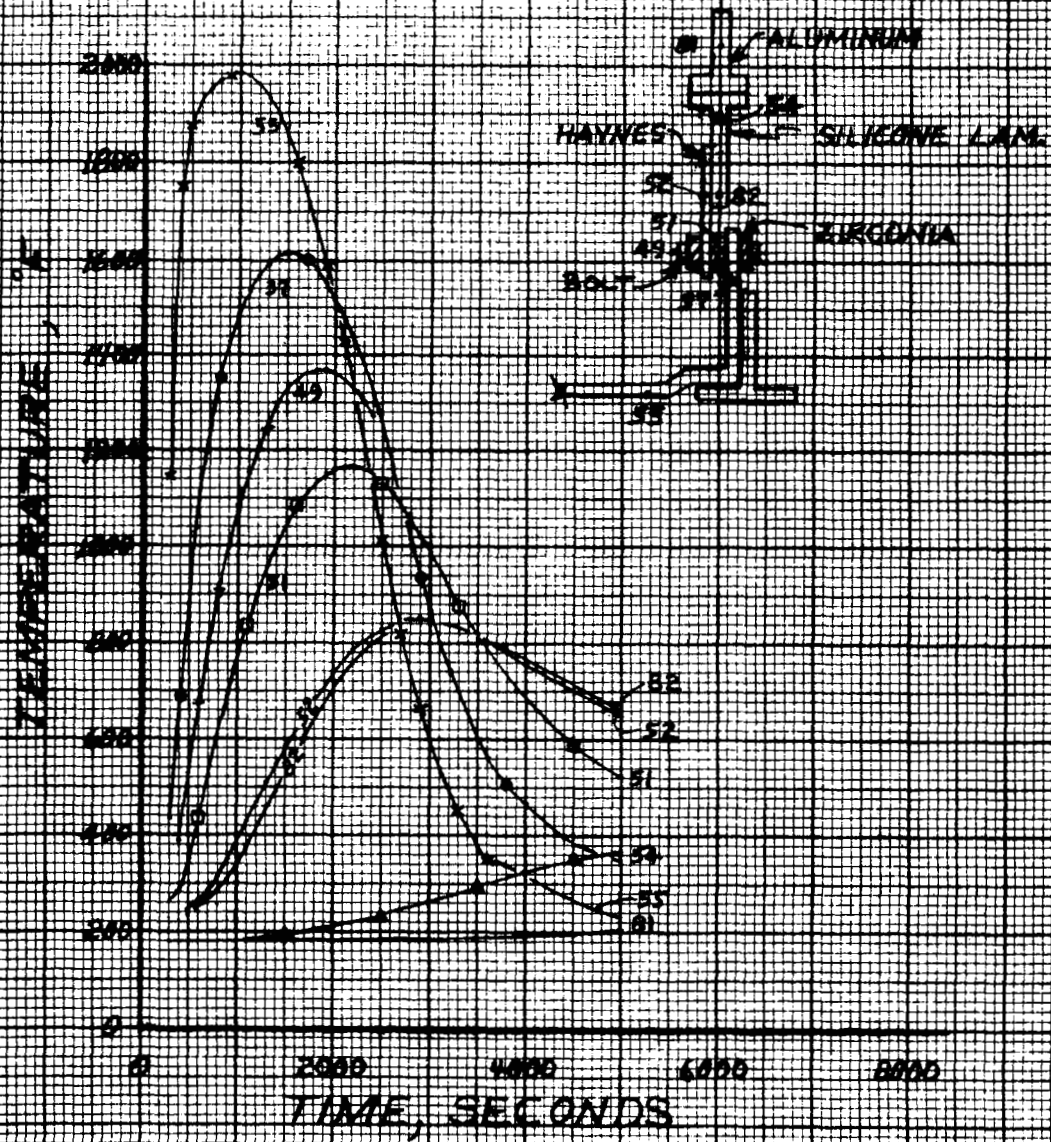


FIGURE 20
PREDICTED TEMPERATURES
ATTACHMENT 2 - VARIATION 7

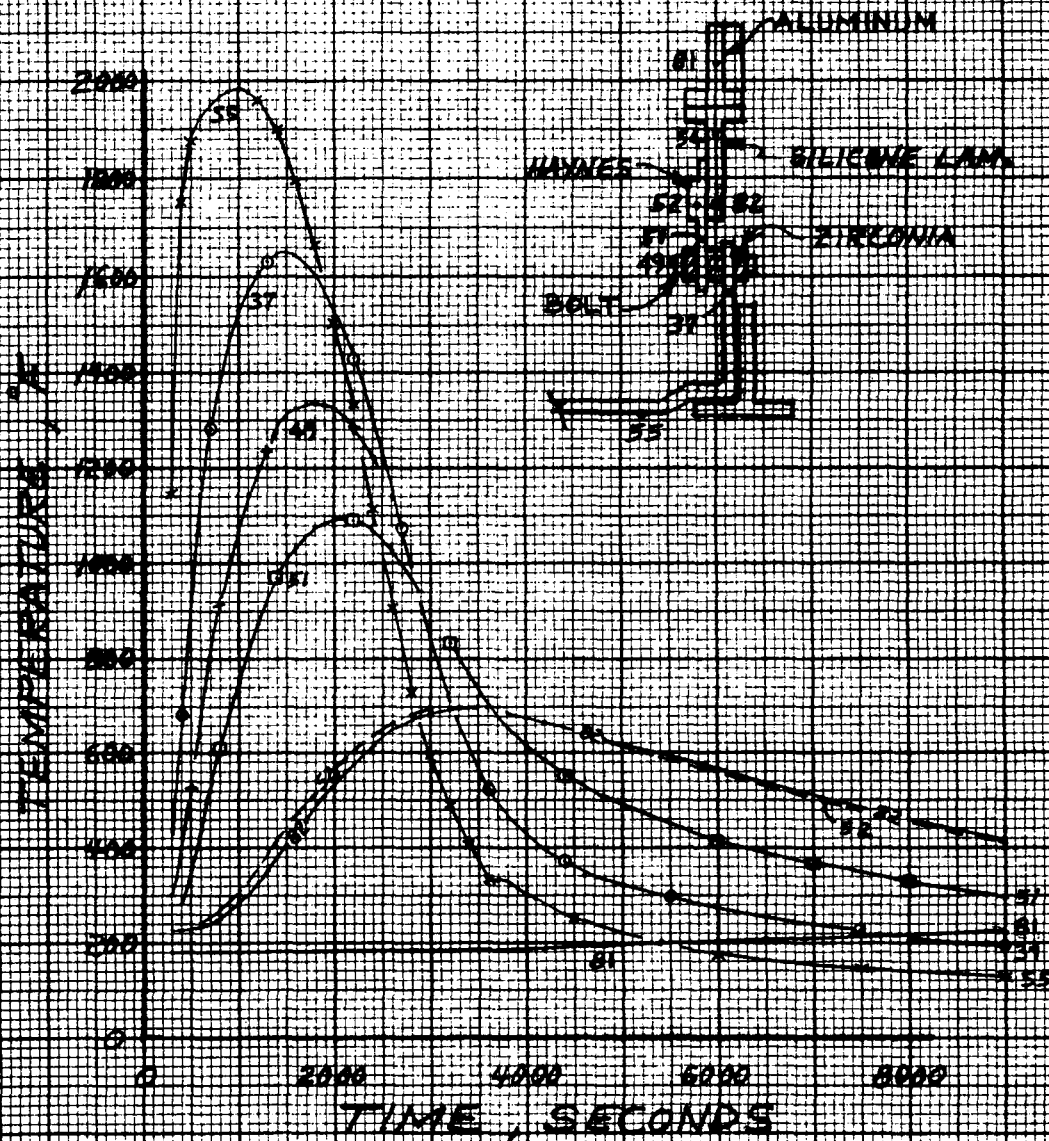


FIGURE 21
PREDICTED TEMPERATURES
GROUND TEST OF LUG AREA
PRELIMINARY CONFIGURATION

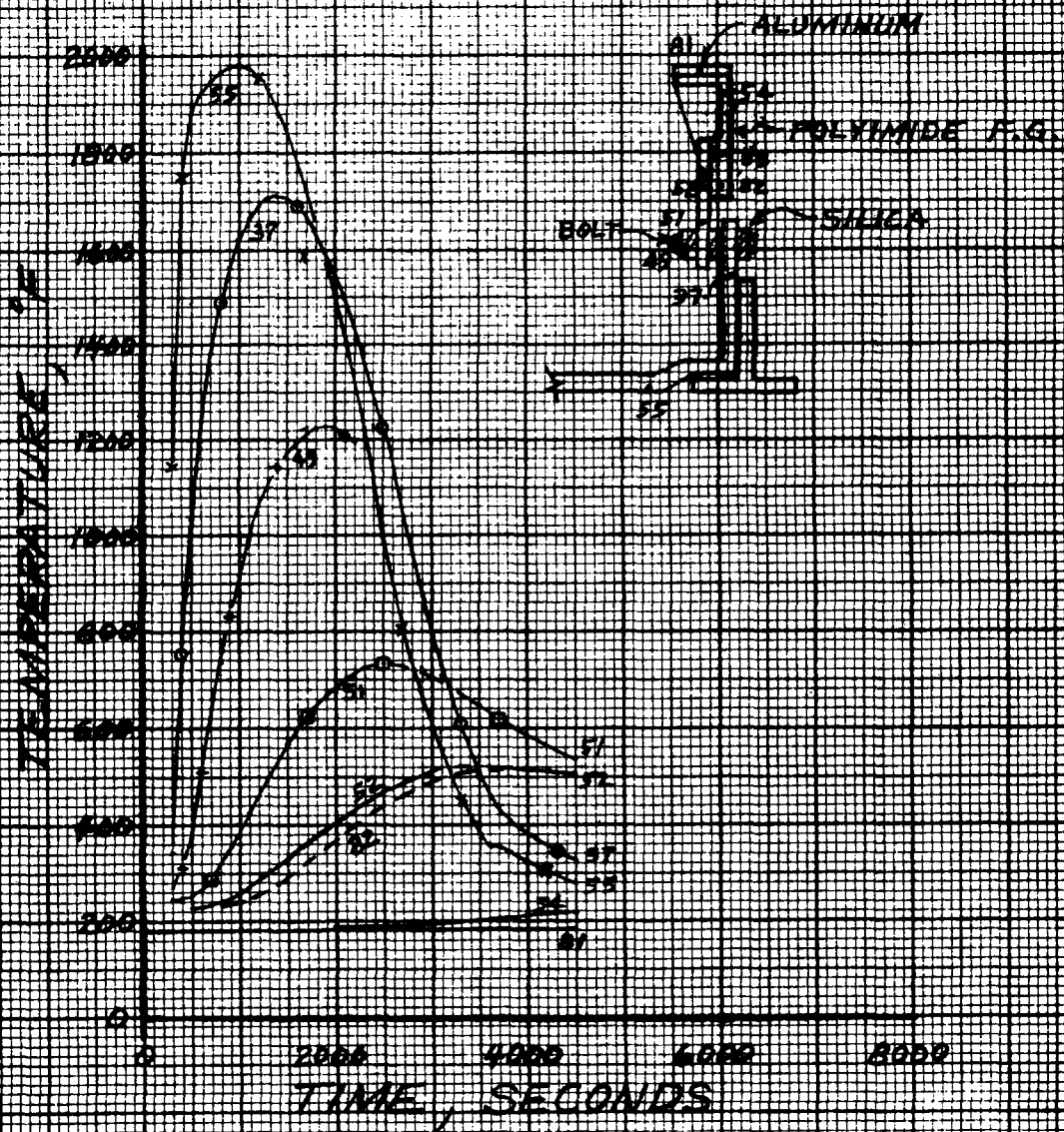
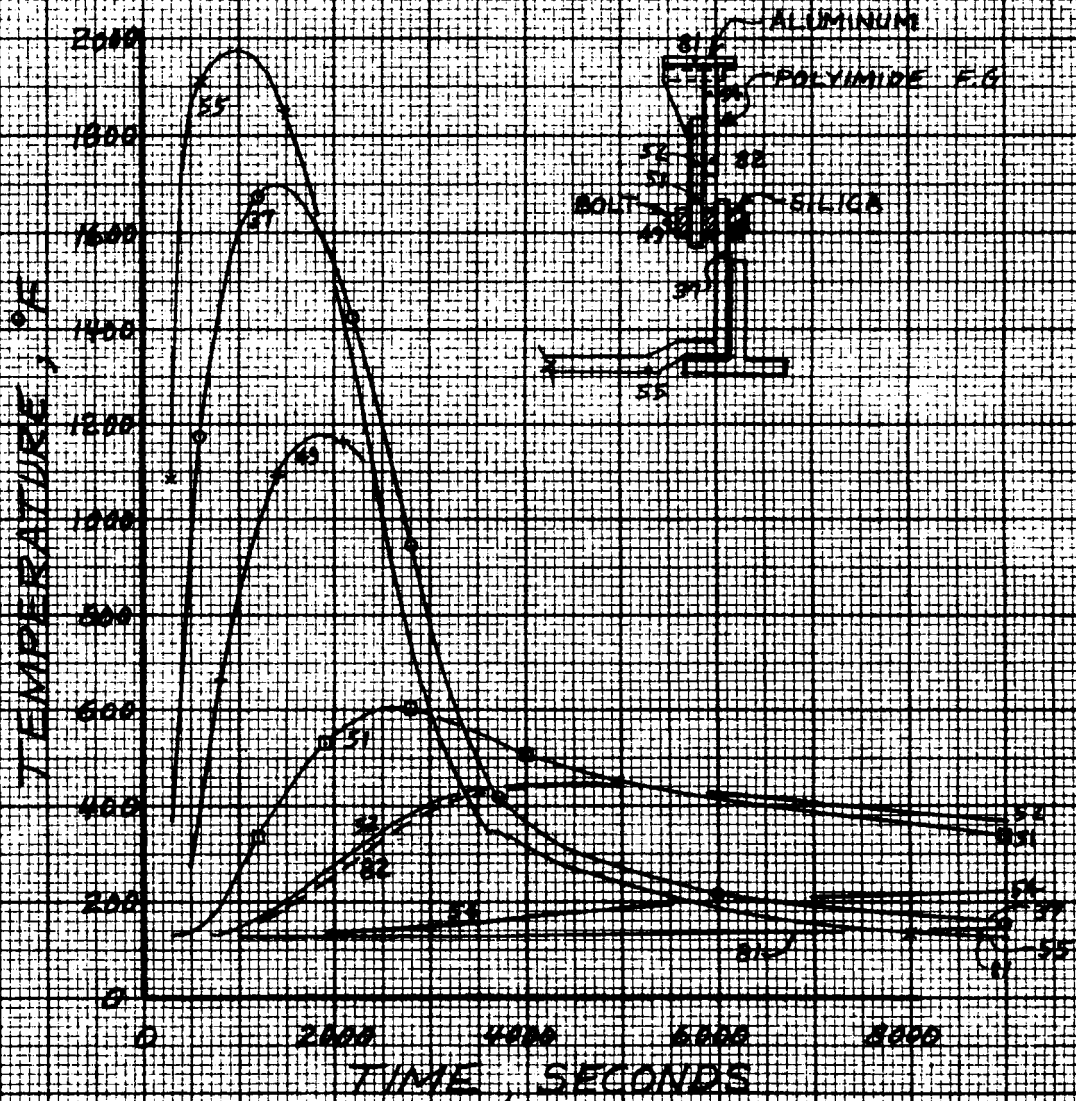


FIGURE 22
PREDICTED TEMPERATURES
GROUND TEST OF LUG AREA
FINAL CONFIGURATION



APPENDIX

MATERIAL THERMAL PROPERTIES

Thermal property data used in the analyses are presented herein. Part of the data is based upon SRI data from Reference 1. Material densities are presented in Table 1. Note also that Table 1 is an index to the other tables.

MATERIAL THERMAL PROPERTIES

MATERIAL	DENSITY $\rho = \text{LB/FT}^3$	SPECIFIC HEAT $C_p = \text{BTU/LB } ^\circ\text{F}$ OR TABLE NUMBER	THERMAL CONDUCTIVITY $K = \text{BTU-IN/HR FT}^2 \text{ } ^\circ\text{F}$ OR TABLE NUMBER
Aluminum	175.	Table 2	Table 3
Dyna-flex	6.	.25	Table 4
Dyna-Quartz	6.2	Table 5	Table 6
Fused Silica	118.	Table 7	Table 8
Glass Silicone Laminate	119.	.252	Table 9
Haynes 188	575.	Table 10	Table 11
High Density Zirconia	334.	Table 12	Table 13
Rene	500.	.104	Table 14
RPP*	84.5	Table 15	Table 16
Stainless Steel	498.	Table 18	Table 19
Fiberfrax H	8	Table 20	Table 21
Inconel 718	513.	Table 22	Table 23
LI 1500 Insulation	15.	Table 24	Table 25
Polyimide	109.	Table 26	Table 27

TABLE 2

SPECIFIC HEAT OF ALUMINUM

TEMP., $^\circ\text{F}$	-330.	-200.	0.	100.	200.	300.	400.	600.	800.
C_p , BTU/LB $^\circ\text{F}$.112	.152	.192	.204	.214	.224	.23	.251	.278

TABLE 3

THERMAL CONDUCTIVITY OF ALUMINUM

TEMP., $^\circ\text{F}$	-200	300.	400.	500.	800.
K , BTU-IN/HR $\text{FT}^2 \text{ } ^\circ\text{F}$	600.	1000.	1200.	1260.	1200.

*Emissivity of RPP is given in Table 17.

TABLE 4

THERMAL CONDUCTIVITY OF DYNAFLEX

TEMP., °F	-400.	200.	400.	600.	900.	1200.
K, BTU-IN/HR FT ² °F	.29	.29	.41	.55	.79	1.09
TEMP	1400.	1500.	1600.	1800.	1900.	2000.
K	1.33	1.47	1.61	1.94	2.12	2.31

TABLE 5

SPECIFIC HEAT OF DYNA-QUARTZ

TEMP., °F	-460	0.	400.	1000.	1800.	2800.
Cp, BTU/LB °F	.2	.2	.299	.272	.292	.292

TABLE 6

THERMAL CONDUCTIVITY OF DYNA-QUARTZ

TEMP., °F	-200.	0.	200.	400.	600.	800.	1000.	1200.
K, BTU-IN/HR FT ² °F	.216	.24	.264	.3	.342	.39	.45	.521
TEMP	1400.	1600.	1800.	2000.	2200.	2400.	2600.	2800.
K	.611	.738	.888	1.09	1.4	1.9	2.5	2.87

TABLE 7

SPECIFIC HEAT OF FUSED SILICA

TEMP., °F	-400.	0.	500.	1000.	1500.	2000.	2500.
Cp, BTU/LB °F	.195	.195	.24	.268	.286	2.96	.3

TABLE 8

THERMAL CONDUCTIVITY OF FUSED SILICA

TEMP., °F	-460.	100.	400.	800.	1200.	1400.	1600.	1800.	2200.	2500.
K, BTU-IN/HR FT ² °F	0.	1.5	2.75	3.55	4.2	4.65	5.45	6.9	8.3	9.08

TABLE 9

THERMAL CONDUCTIVITY OF GLASS SILICONE LAMINATE

TEMP., °F	-400.	0.	110.	220.	450.	600.	1000.
K, BTU-IN/HR FT ² °F	1.	1.	1.2	1.32	1.38	1.54	2.43

TABLE 10

SPECIFIC HEAT OF HAYNES 188

TEMP., °F	-460.	32.	283.	860.	930.	1470.	3000.
C _p , BTU/LB °F	0.	0.092	.097	.153	.119	.1363	.1363

TABLE 11

THERMAL CONDUCTIVITY OF HAYNES 188

TEMP., °F	-460.	268.	300.	400.	600.	800.	1000.	2000.
K, BTU-IN/HR FT ² °F	109.	109.	123.	133.	151.	168.	182.	182.

TABLE 12

SPECIFIC HEAT OF HIGH DENSITY ZIRCONIA

TEMP., °F	-400.	0.	100.	200.	400.	700.	1000.	2200.	2201.	3000.
C _p , BTU/LB °F	.1	.1	.11	.117	.127	.138	.144	.155	.144	.144

TABLE 13

THERMAL CONDUCTIVITY OF HIGH DENSITY ZIRCONIA

TEMP., °F	-400.	0.	900.	2300.	3000.
K, BTU-IN/HR FT ² °F	11.4	11.46	12.3	14.4	15.6

TABLE 14

THERMAL CONDUCTIVITY OF RENE

TEMP., °F	-460.	400.	1200.	1800.	2500.
K, BTU-IN/HR FT ² °F	74.	74.	116.	151.	151.

TABLE 15

SPECIFIC HEAT OF RPP

TEMP., °F	-460.	100.	500.	1000.	1500.	200.	2500.	3000.	4000.
C _p , BTU/LB °F	0.	.204	.272	.341	.39	.419	.436	.447	.447

TABLE 16

THERMAL CONDUCTIVITY OF RPP PARALLEL DIRECTION

TEMP., °F	-250.	0.	250.	500.	1000.	1500.	2000.	2500.	3000.	4000.
K, BTU-IN/HR FT ² °F	40.	62.	75.	80.	86.	89.	94.	102.	113.	113.

TABLE 17
EMISSIVITY OF RPP

TEMP., °F	-200.	500.	1000.	1500.	2000.	2500.	3000.
ϵ	.85	.85	.893	.925	.94	.935	.898

TABLE 18
SPECIFIC HEAT OF STAINLESS STEEL

TEMP., °F	-400.	0.	200.	400.	800.	1200.	1560.	4000.
C_p , BTU/LB °F	.06	.105	.118	.126	.137	.143	.152	.152

TABLE 19
THERMAL CONDUCTIVITY OF STAINLESS STEEL

TEMP., °F	-400.	0.	200.	400.	800.	1200.	1500.	4000.
K , BTU/LB °F	96.	98.3	101.7	110.	139.	167.	186.	186.

TABLE 20
SPECIFIC HEAT OF FIBERFRAX H

TEMP., °F	-210.	40.	240.	540.	1040.	1540.	2040.	2540.
C_p , BTU/LB °F	.1	.172	.214	.25	.28	.295	.3	.3

TABLE 21										
THERMAL CONDUCTIVITY OF FIBERFRAX H										
TEMP., °F	-200.	70.	400.	600.	800.	1000.	1200.			
K, BTU-IN HR FT ² °F	.2	.25	.3	.35	.45	.55	.65			
TEMP	1400.	1600.	1800.	2000.	2200	2400.				
K	.8	.95	1.2	1.5	1.8	2.2				

TABLE 22										
SPECIFIC HEAT OF INCONEL 718										
TEMP. °F	-400.	0.	300.	1000.	1500.	3000.				
C _p , BTU/LB °F	.06	.098	.114	.13	.152	.152				

TABLE 23										
THERMAL CONDUCTIVITY OF INCONEL 718										
TEMP. °F	-460.	100.	1600.	3000.						
K, BTU-IN/HR FT ² °F	0.	78.3	173.	200.						

TABLE 24

SPECIFIC HEAT OF LI-1500 INSULATION

TEMP., °F	-100.	8.	260.	440.	620.	800.	980.	1340.	1700.
C _p , BTU/LB °F	.0716	.151	.198	.234	.263	.28	.287	.294	.306
TEMP	2060.	2430.							
C _p	.316	.32							

TABLE 25

THERMAL CONDUCTIVITY OF LI-1500 INSULATION

TEMP., °F	0.	300.	700.	1400.	2000.	2500.
K, BTU-IN/HR FT ² °F	.28	.31	.35	.60	1.02	1.35

TABLE 26

SPECIFIC HEAT OF POLYIMIDE F.G. LAMINATE

TEMP., °F	-400.	100.	1100.
C _p , BTU/LB °F	.21	.21	.28

TABLE 27

THERMAL CONDUCTIVITY OF POLYIMIDE F.G. LAMINATE

TEMP., °F	0.	1000.
K, BTU-IN/HR FT ² °F	2.0	3.37

DESIGN INFORMATION REQUEST RELEASE

OCCAS AND EFF.		DIR. NO.		REV	
SUPPORT LUG THERMAL TEST - PREDICTED TEMPERATURE		T143-DIR-2-18			
DISTRIBUTION		DATE	PAGE	OF	
		4 Dec. 1972	1	58	
SYSTEM		REF. EWA			
SHUTTLE LEADING EDGE		3357-CA-1160			
Fill in block below for Information Request			Fill in block below for Information Release		
D. _____ GROUP _____ EQ. BY _____ GROUP _____ EASCH _____ V. ONLY <input type="checkbox"/> BWR <input type="checkbox"/> BUWEPs <input type="checkbox"/>			IN REPLY TO DIR. NUMBER _____ REL. TO D.M. While GROUP 3-52000 PREPARED BY W.A. Whitten 15 Dec 1972 DATE W.A. Whitten 11-4-72 GROUP APP. J.B. Medford 12/15/72 DATE CHECKED BY J.E.M. 12-15-72 DATE PROJ OFFICE DATE		

F.T. Esenwein, E. Matza, B.A. Forcht, W.E. Agan, I.E. Harder

DESIGN INFORMATION:

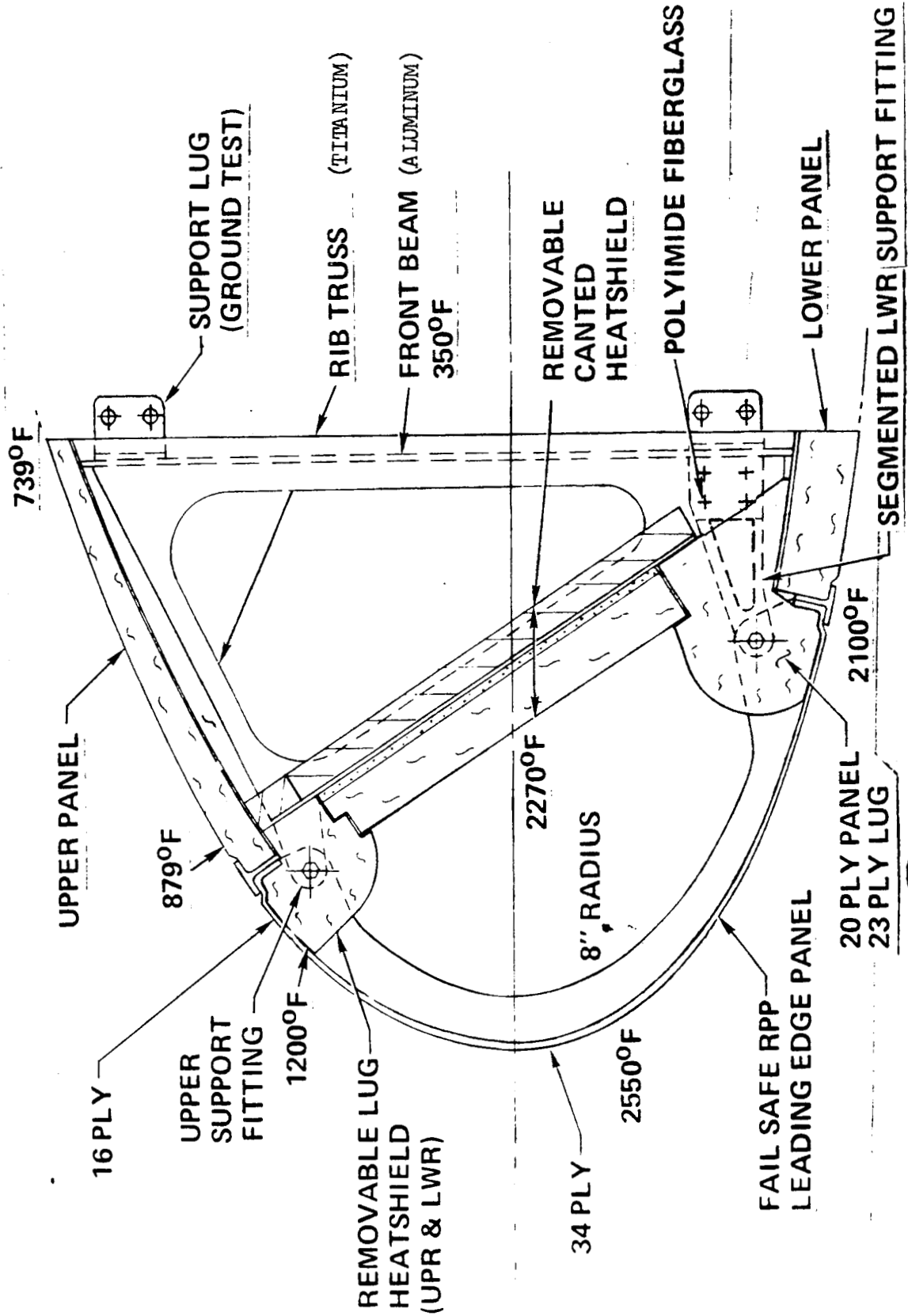
REFERENCES:

- (1) "Development of a Thermal Protection System for the Wing of a Space Shuttle Vehicle , VMSC Report No. T143-5R-00124, 30 April 1972.
- (2) "Predicted Temperature Distribution for the Windward Side Leading Edge Support Joint and Bracket", VMSC Report T143-DIR-2-11, 9 August 1972.
- (3) "Thermal and Structural Test of Prototype Support Joint Concept", VMSC Test Request T143-TRA-235, 19 July 1972.
- (4) "Thermal and Structural Retest of Prototype Support Joint Concept", 3 October 1972, VMSC Test Request T143-TRA-239.
- (5) "Predicted Temperature Distribution for the Wing Leading Edge Skin and Rib", VMSC Design Information Release No. T143-DIR-2-07, 13 July 1972.
- (6) "Investigation of Insulative Heat Shield Attachment Systems", Technical Report AFFDL-TR-65-55, April 1965.

INTRODUCTION

The work reported herein was performed under NASA Manned Spacecraft Center (MSC) Contract NAS9-12763-2S. The wing leading edge of the space shuttle vehicle is to be attached to brackets bolted to the wing box as illustrated in Figure 1. Only the windward side attachment is considered in this study. Analyses were performed during Phase II (Reference 1) to determine the insulation required to

THE DESIGN



VOUGHT MISSILES
AND SPACE COMPANY

protect the wing structure having a 650°F temperature limitation. The temperature limitation has been changed to 350°F for Phase III analyses.

A number of attachment concepts were considered and the results of thermal analyses were used to help guide in the selection of the attachment configuration to be ground tested. Thermal analyses performed prior to the ground tests of the support lug were reported in Reference 2.

A test of the support lug performed on 29 September 1972 resulted in excessive temperatures at the aluminum structure and the polyimide fiberglass part of the bracket. Results of the September test were used to help in redesigning the bracket so as to keep the temperatures of the polyimide and aluminum below their maximum allowables.

Two tests were performed with the redesigned bracket. Both tests (November 3 and 8) were performed in the Space Environment Simulator at 10 mm Hg pressure. This was done to have better control of the cooldown portion of the test so as to avoid overheating due to convection and/or combustion effects experienced in the 29 September test, which was done at ambient conditions.

All temperatures for the two tests performed on the redesigned bracket were well below their allowed maximums. But since the actual temperature of the polyimide fiberglass was considerably above that predicted with the thermal model of the test article, post-test analysis was performed to improve the thermal model. Two major modifications were made to the thermal model so as to make it yield better agreement with the test results. These changes consisted of increasing the thermal conductivity of the inconel parts of the bracket by 20%, and making the coefficient at the support joints a function of the temperature at the joint.

TEST CONFIGURATION DEFINITION

Three tests were performed for the support lug. The first test was performed 29 September 1972 at ambient conditions per Reference 3. The other two tests were performed on a redesigned bracket 3 November and 8 November per Reference 4 in the Space Environment Simulator at 10 mm Hg conditions to simulate the average

entry pressure during the high temperature portion of the trajectory.

The test model included RPP skin and attachment flange, T-seal, bulk insulation, joint bolt, support fitting (bracket), and primary structure (See Figures 1 and 2).

The test article was heated through a single temperature-time cycle representative of flight conditions. Heat input was controlled at two locations, (1) on the outside of the RPP skin panels and (2) on the surface of the insulation as defined in References 3 and 4, and on Figure 2.

First Test - 29 September 1972

The test arrangement is shown on Figure 2. A total of nine thermocouples were installed on the test article as shown on the figure. A cooling air duct was located as shown on the figure in order to provide air to be used in the cooldown portion of the test. Graphite heaters were placed as shown to provide the heat input. Dynaflex (12 PCF) was used to simulate insulation around the lug.

Figure 3 shows the details of the support joint bracket, and Fig. 4 shows the details of the support joint area.

First Retest - 3 November 1972

Figure 5 shows the details of the redesigned support bracket. The following major modifications were made to the design of the bracket to prevent excessive temperatures at the aluminum and the polyimide fiberglass.

1. The contact area between the Inconel bracket and the sleeve was reduced. (The bracket thickness was reduced from 0.25" to 0.156".)
2. The length of the Inconel bracket was increased to provide a long conduction path and reduced fiberglass temperature.
3. The conduction area through the Inconel bracket was kept to a minimum by removing the low stressed area as shown in Figure 5.

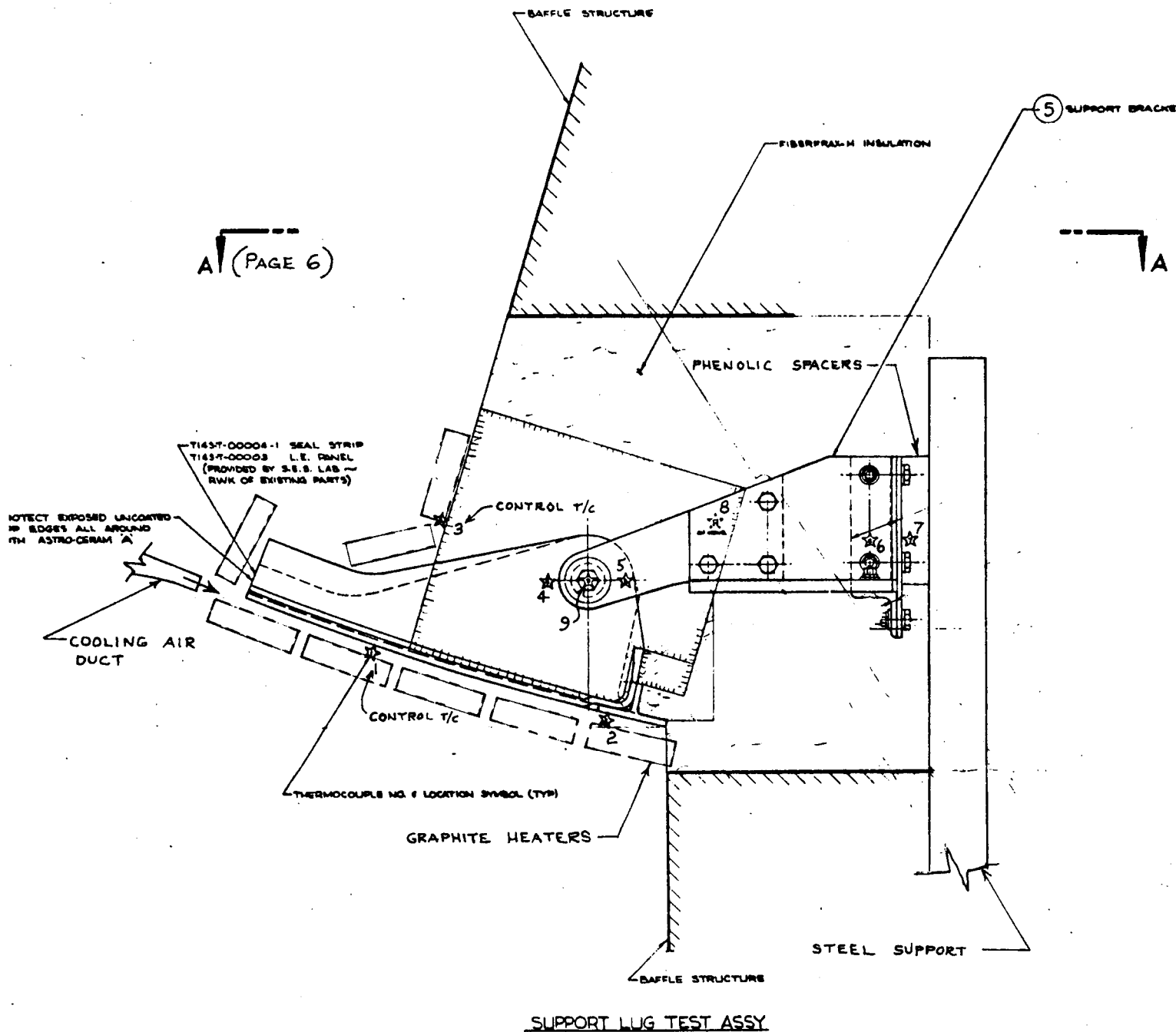
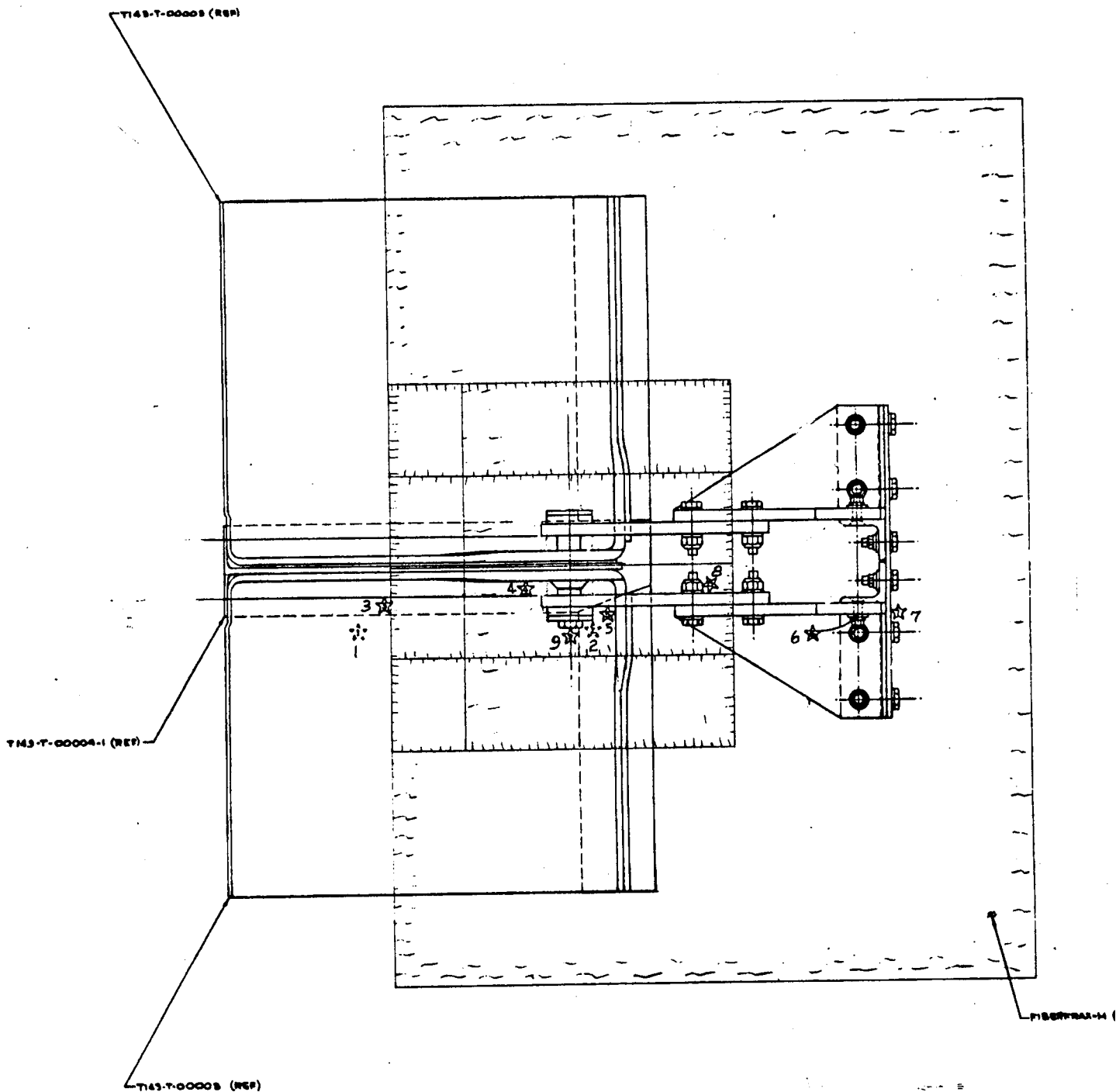


FIGURE 2 - TEST CONFIGURATION



VIEW A-A

FIGURE 2 (Cont'd.) TEST CONFIGURATION

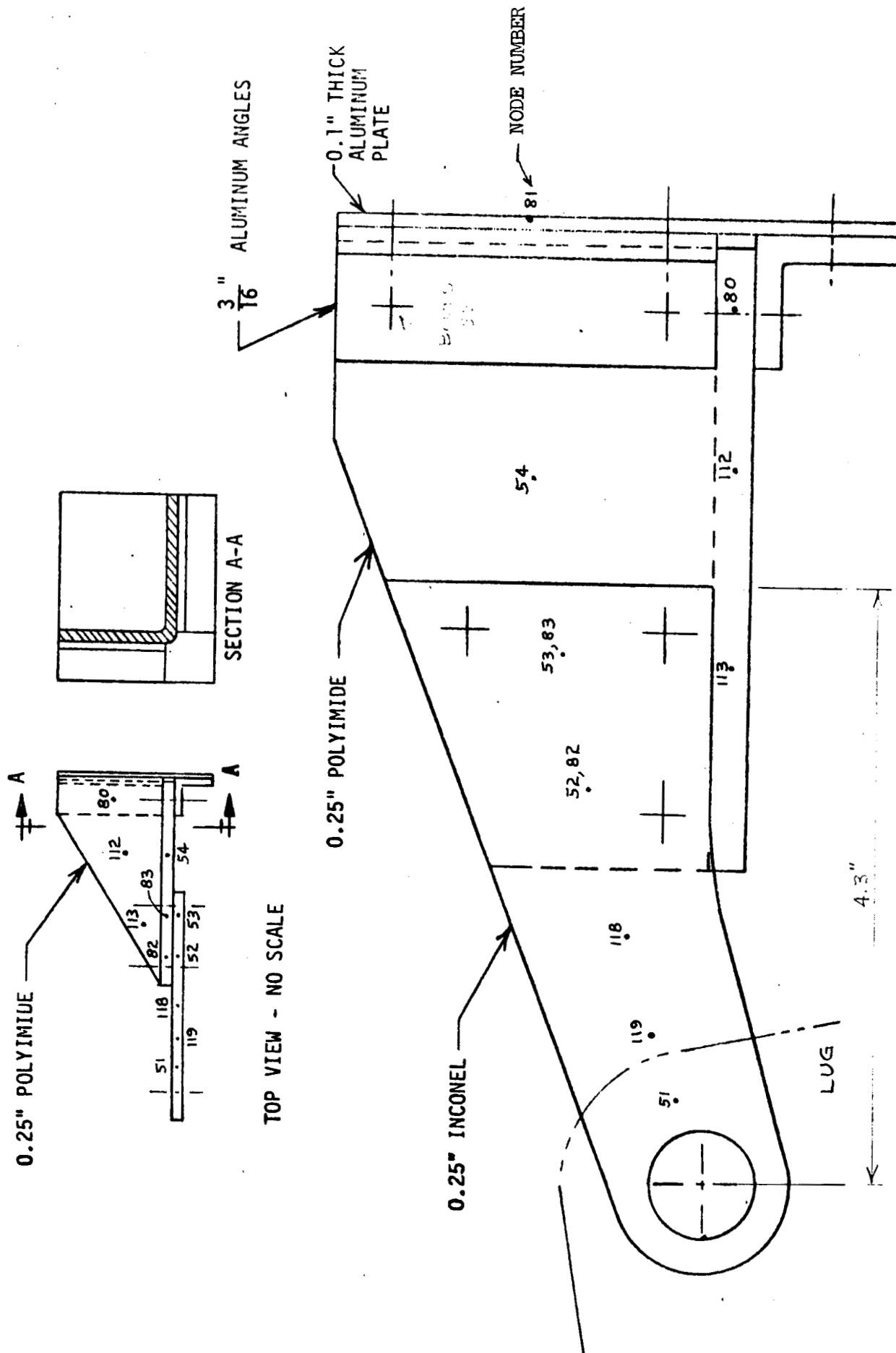


FIGURE 3 THERMAL MODEL - BRACKET FOR SEPTEMBER TEST

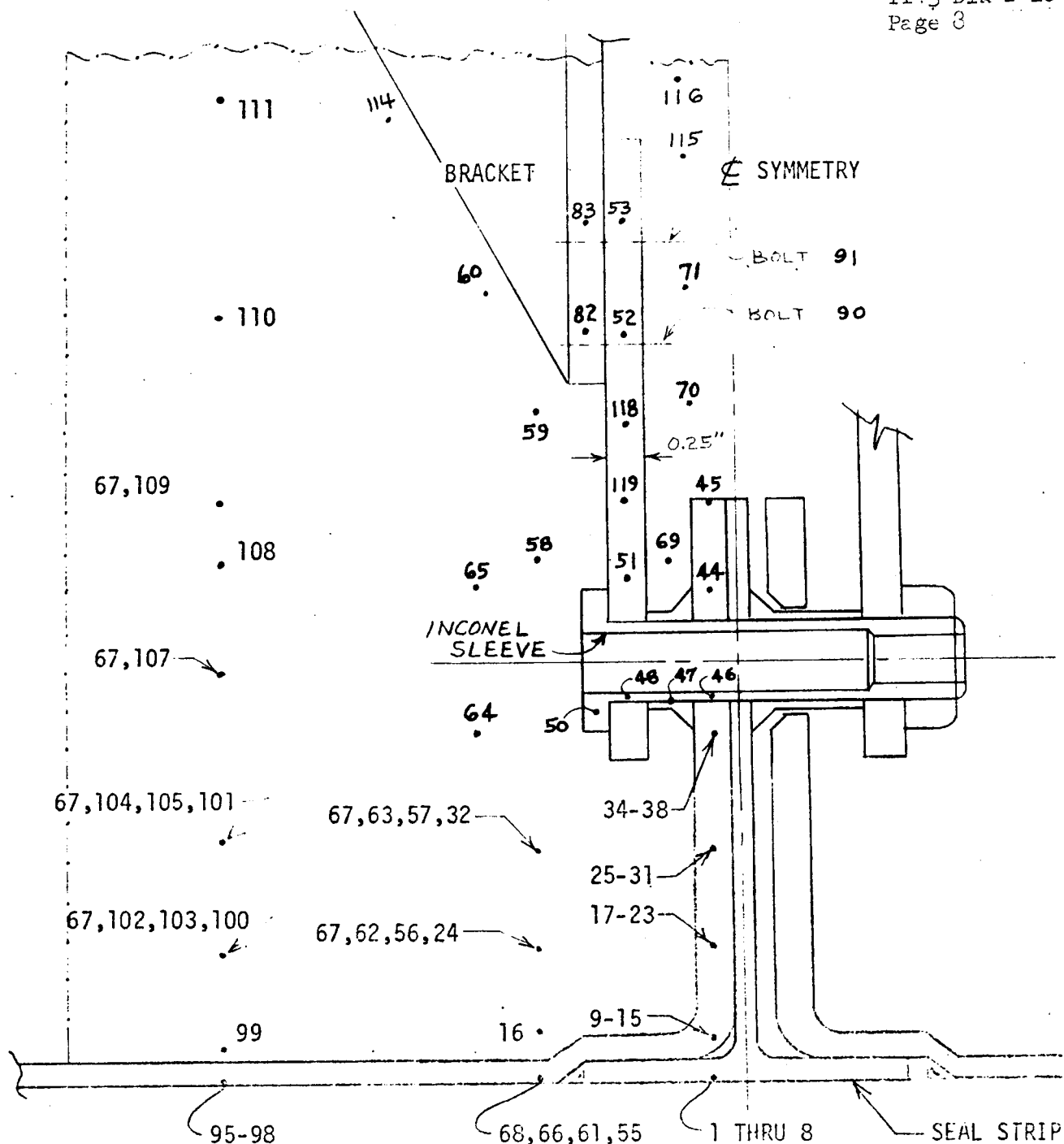


FIGURE 4 - THERMAL MODEL - SUPPORT JOINT AREA
SEPTEMBER TEST

NODE NUMBERS
127 (INSULATION)

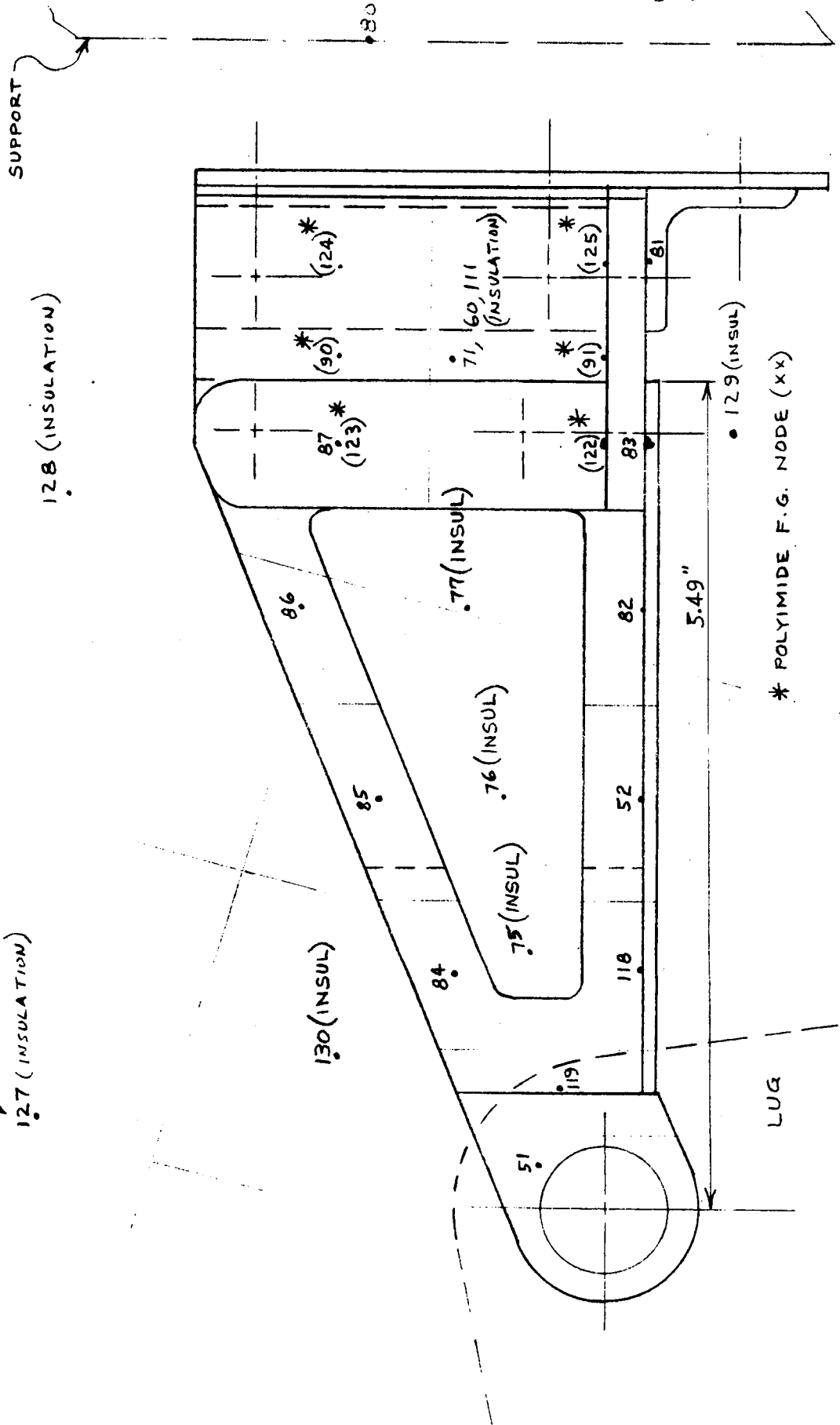


FIGURE 5 THERMAL MODEL-BRACKET SIDE VIEW (RETEST)

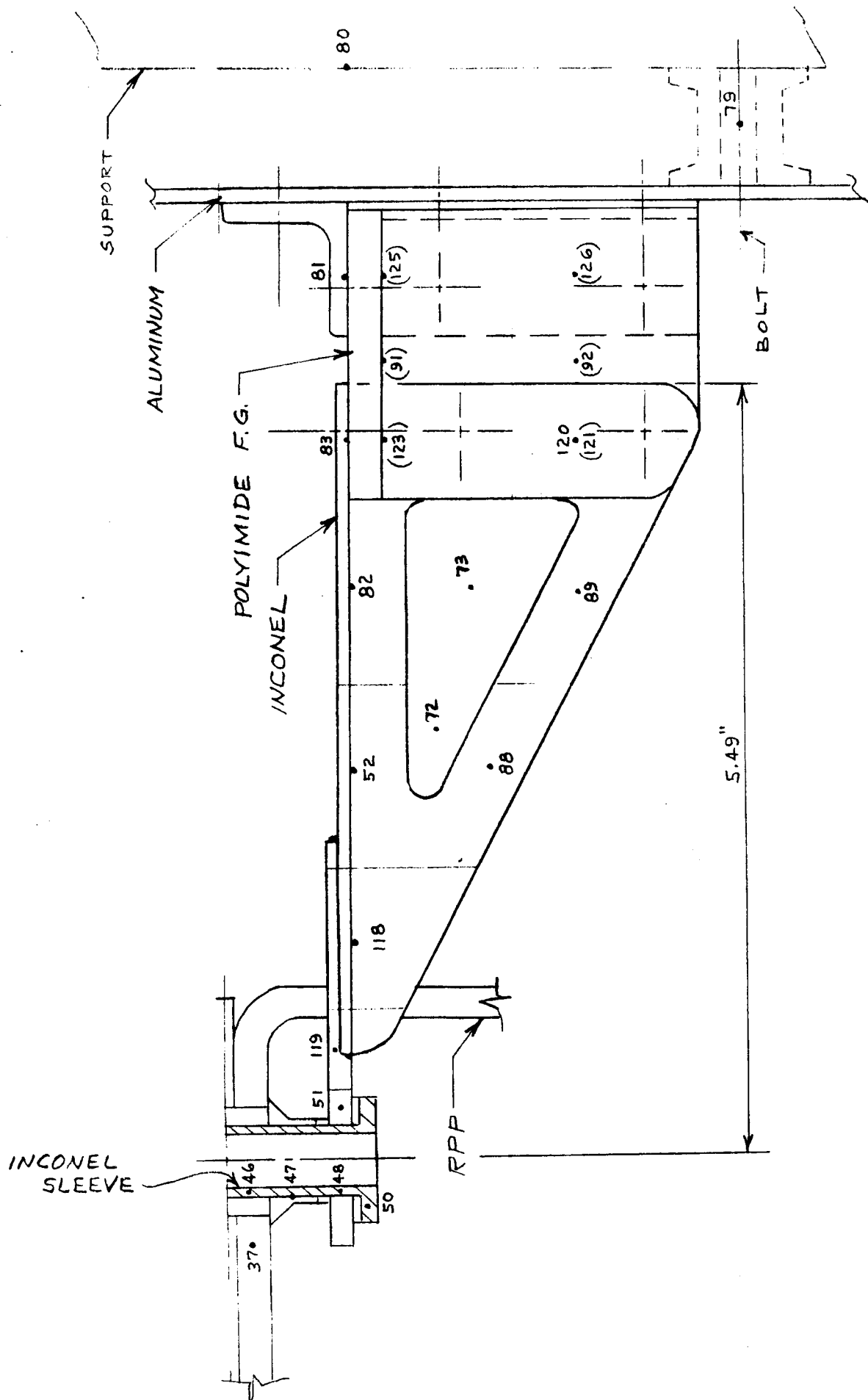


FIGURE 5 CON'T THERMAL MODEL - BRACKET TOP VIEW (RETEST)

4. Volume of the simulated aluminum front beam was increased from 3.04 in³ to 4.0 in³ to be more representative and include part of the 0.1" thick aluminum plate behind the insulation. This new value is probably still conservative from a thermal standpoint since it is assumed that the aft side of the plate is an adiabatic surface.

Other differences between the test set-up for this test and the September test are:

1. Retest was done inside the Space Simulator as mentioned previously.
2. No cooling air was used for the retest.
3. Insulation at the backside of the graphite heaters for the RPP surface was moved away from the heaters in order to have better control of the cooldown portion of the test, and avoid part of the overheating experienced in the last test. Calibration data showed that close control could be achieved through at least the first 40 minutes of the test. Beyond this, when the temperature of the heater is below about 1200°F, some conservatism will exist (heat input will be too great). However, analysis showed high thermal margins, so the extra heat input was tolerated.
4. Dynaquartz (10 PCF) insulation was substituted for Dynaflex in the lug area to be more representative of planned design.
5. More thermocouples were used. A total of 26 thermocouples were installed on the test article as shown on Figure 6.
6. The aluminum panel was better isolated from the supporting structure. Figure 7 shows details of the fiberglass phenolic isolators.
7. Greater care was taken in installing the insulation in the lug area so that direct radiation could not occur from the RPP lug to the inconel bracket.

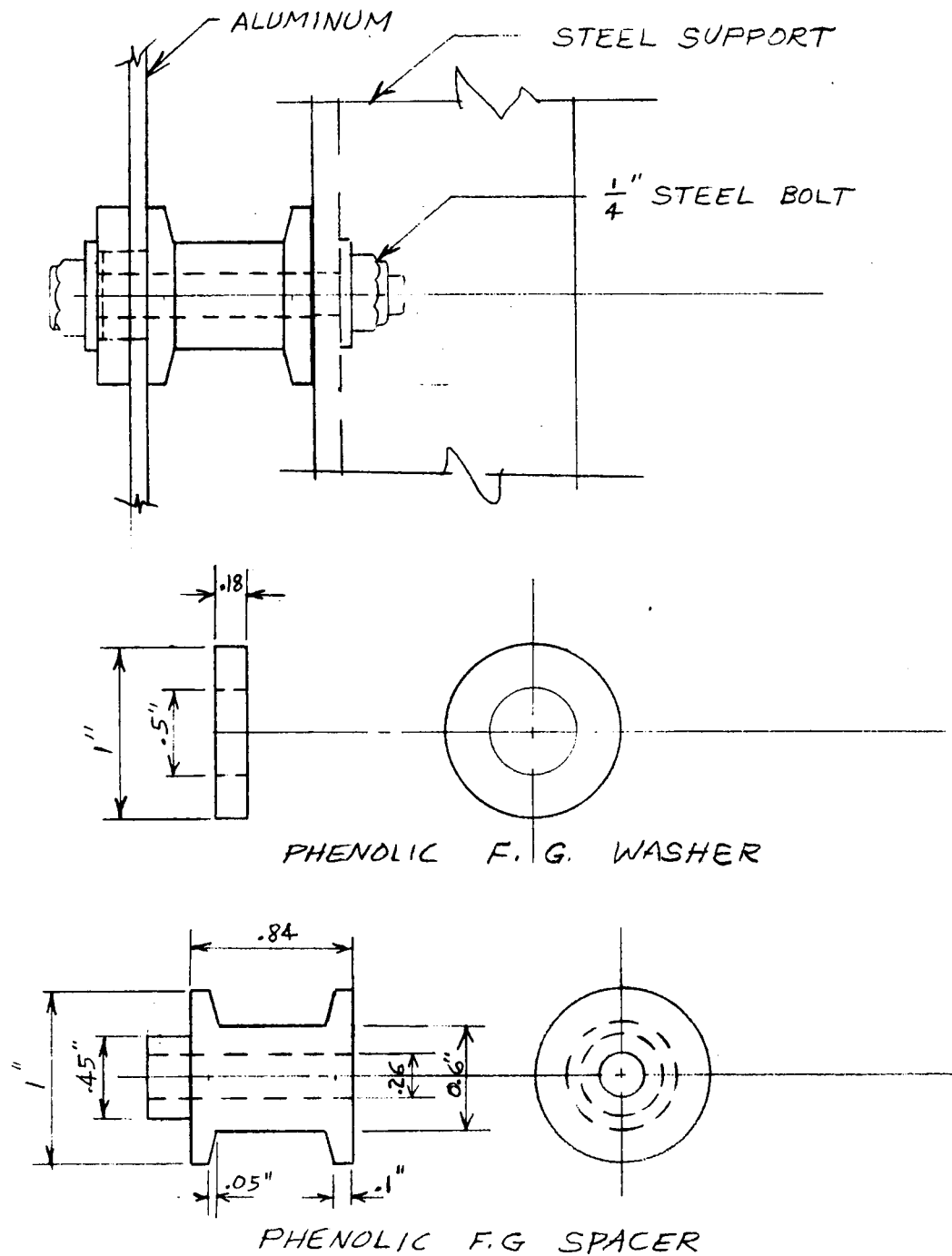


FIGURE 7 ISOLATORS USED IN RETESTS

Second Retest - 8 November 1972

The test setup for this test was the same as for the 3 November test, except for the following:

- 1) Insulation was installed inside the cutouts in the inconel brackets. This was done to prevent thermal radiation from the hot end to the cold end of the bracket.
- 2) Thermocouple number 16 was moved from the front of the insulation to the side of the insulation as shown in Figure 6.

TEST RESULTS

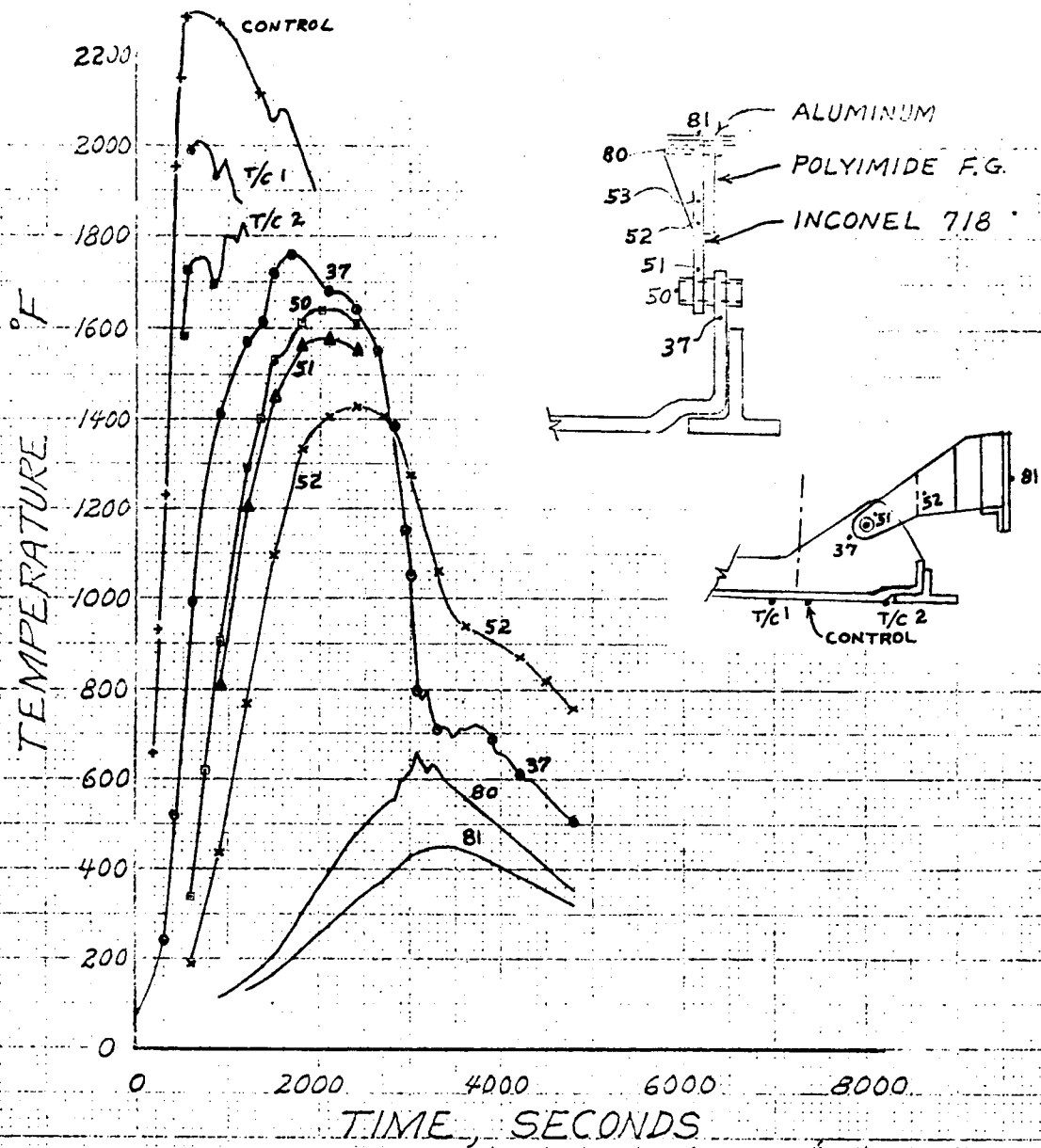
All three tests will be discussed in this section but major emphasis will be placed on the second retest since the total heat input for it most closely represents flight conditions.

First Test - 29 September 1972

Excessive temperatures occurred on the polyimide fiberglass and on the simulated aluminum front beam. Maximum temperatures were 1640°F on the support joint bolt, 1426°F for the fiberglass, and 450°F for the aluminum (see Figure 8). The test and results were disappointing for a number of reasons:

- (1) Cooling air turned on at 1380 sec to assist in the cooldown at the temperature control points was able to flow past the insulation and supply additional unwanted heat to the Inconel lug joint. Thermocouple temperature rise in these areas corresponds to the initiation of air flow.
- (2) The air flow, while proving effective at lower temperatures during checkout, was ineffective at peak operating temperatures. The air flow enhanced the combustion of the red hot graphite heaters and contributed to a total heat load applied to the test article substantially in excess of that planned.

FIGURE 8
MEASURED TEMPERATURES
WINDWARD SIDE LUG AREA
SEPTEMBER TEST



- (3) The joint heat transfer coefficient actually experienced during the test was probably higher than that used for the pre-test predictions, especially at the higher temperatures. The joint coefficients used were extrapolated from test data generated on a previous RPP program at lower temperatures. Post-test analysis showed that the use of infinite joint coefficients compared to those used in the initial analysis (100 BTU/hr ft²°F) result in a 37°F increase in inconel bolt temperature, 96°F increase in fiberglass temperature, and 3°F increase*in the aluminum temperature. The joint coefficients will be discussed more fully during discussion of the second retest results.
- (4) The above problems resulted in overheating and degradation of a stainless steel nut (previously checked for 1500°F capability) on the Inconel hollow bolt, and overheating and charring of the hot end of the polyimide fiberglass. The Inconel parts appeared satisfactory as did the cool end of the polyimide. With all this the aluminum backface only reached 450°F.

Based on the analyses of the test results it is believed that the major reason for the excessive temperatures was the convection and/or combustion effects existing and noted during the test.

First Retest - 3 November 1972

All temperatures for this test were well below their maximum allowables. The peak temperature of the polyimide was 550°F and the peak temperature of the aluminum was 255°F.

Total heat input for this test was also considerably above the desired values as can be seen from a study of Figure 9. Test temperatures of thermocouples 2 and 10, which have more influence on the heat input to the joint than thermocouple number 1 does, were higher than desired during the peak heating time and also considerably higher after a time of about 2500 seconds. Heat input to the
* at a time of 1800 seconds

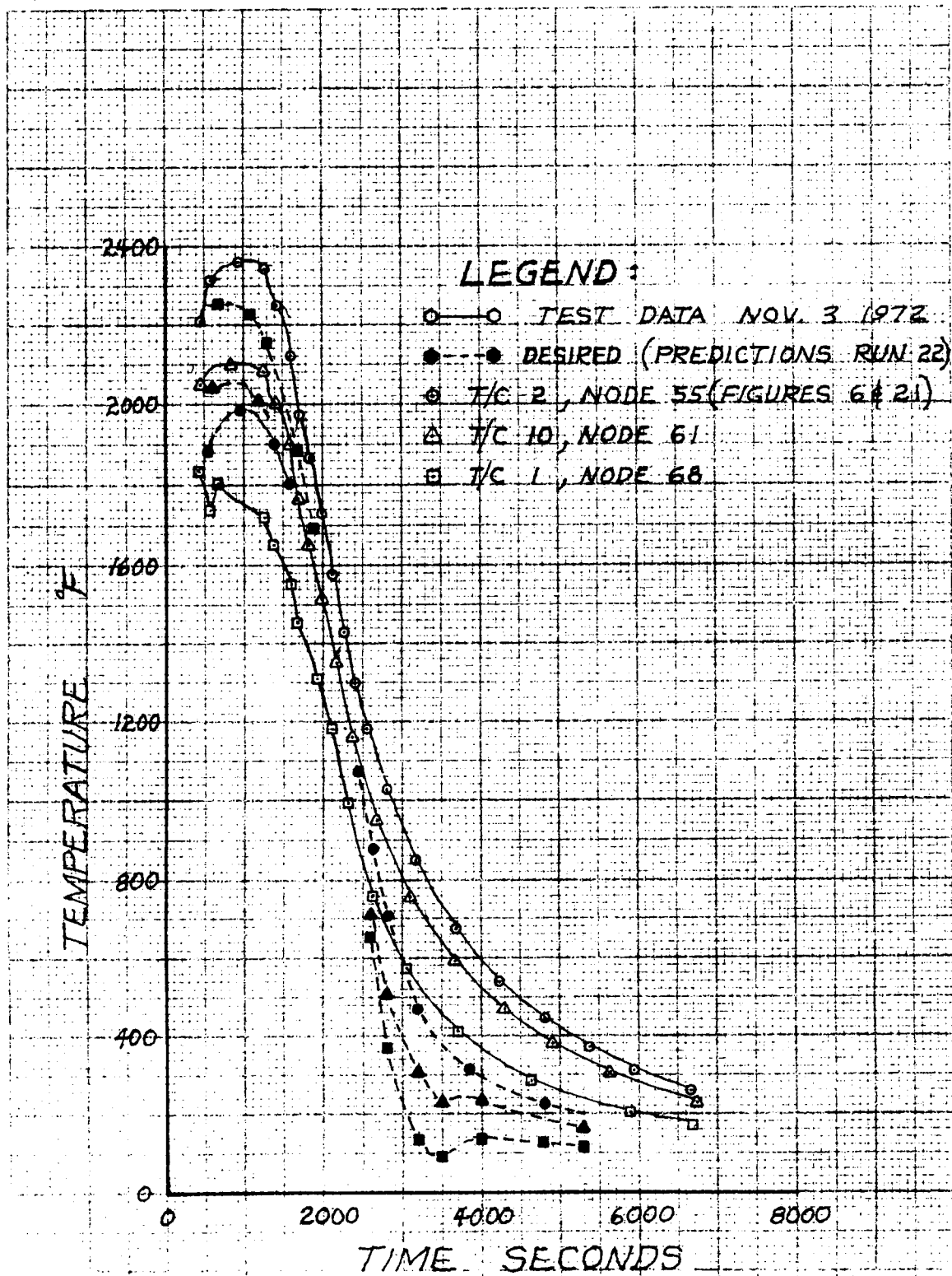


FIGURE 9 RPP SKIN TEMPERATURES
FIRST RETEST

insulation was also higher than desired; the peak temperatures of both thermocouples 3 and 16 were above 2500°F whereas only 2050°F was desired.

Test data for this test are presented in Figures 10 through 14.

Since the peak polyimide temperature was about 200°F greater than the pre-test prediction of 345°F, a close comparison was made between the actual test configuration and the thermal model used in making the predictions. Aside from the total heat input, the major difference was that the thermal model did not account for thermal radiation inside the cut-out areas of the inconel brackets. Although the total areas involved are small, the temperature difference between the hot end and cold end of the bracket is large so the heat transfer could be significant. The shape of the temperature curve for the cold end of the bracket (the test temperature increased much faster and peaked faster than predicted) also indicated that possibly a radiation effect rather than a conduction effect was responsible for the differences between test and predictions.

Another difference between the test article and the thermal model involves the symmetry at the centerline of the T-seal strip between the two leading edge panels. All the thermal analyses were done assuming symmetry and only the panel with the fixed lug was modeled. But the test results indicate that more than 50% of the total heat input to the aluminum entered through the side with the fixed lug. Thermocouples 5 and 8 were on the hot and cold ends, respectively, of the inconel bracket on the fixed panel; and thermocouples 22 and 23 were at corresponding locations on the bracket on the sliding panel. Maximum temperatures at the hot ends of the brackets were 1275°F for the fixed side and only 1175°F for the sliding side (see Figures 10 and 11). Temperature drop through the fixed side was 730°F and only 635° for the sliding side. Additional discussion of the pre-test and post-test analyses will be included in a later section, titled, "Thermal Model Definitions".

NOTE: Thermocouple locations are shown in
Figure 6.

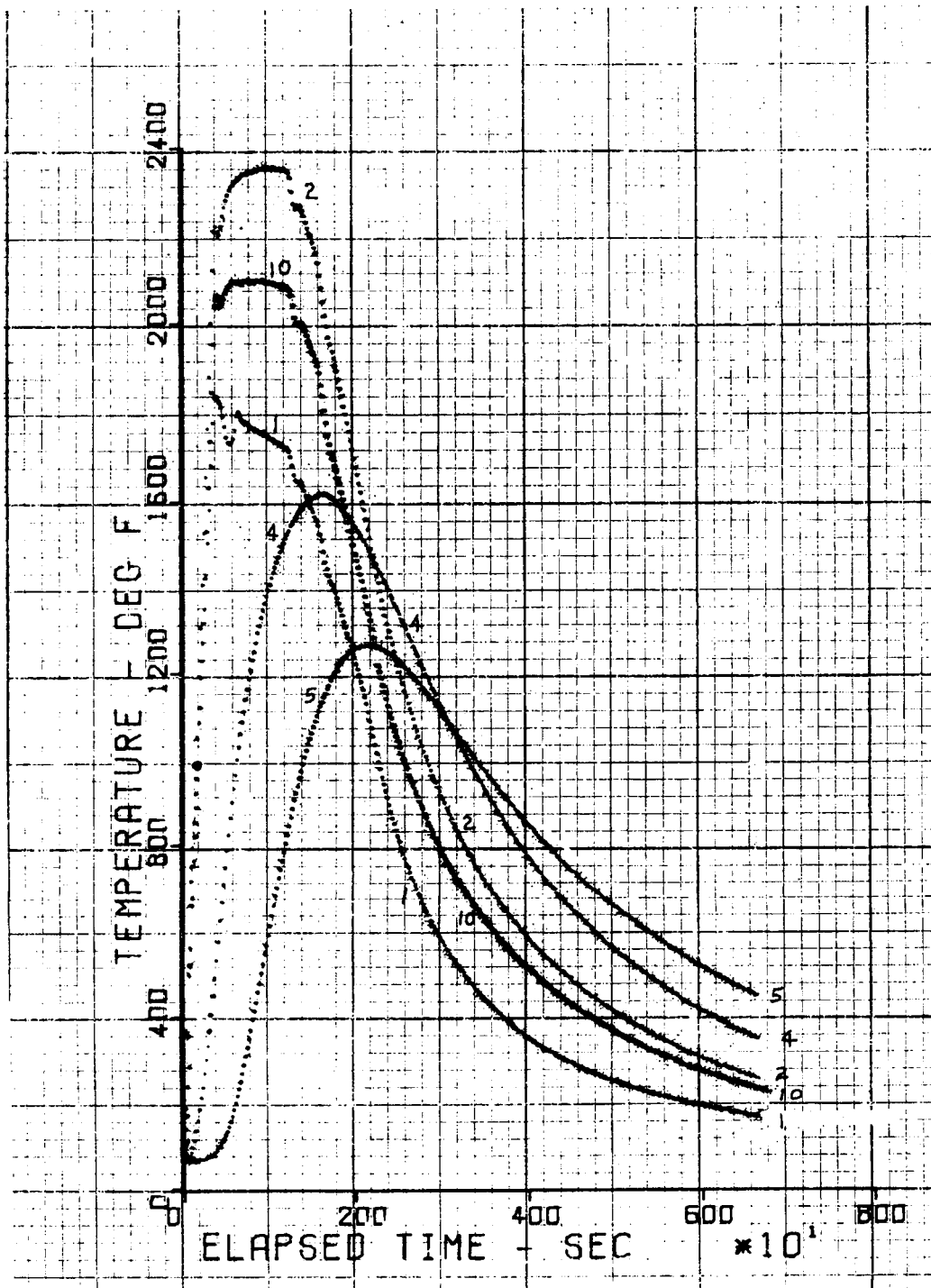


FIGURE 10

RPP WINDWARD SIDE LUG TEST - NOVEMBER 3, 1972

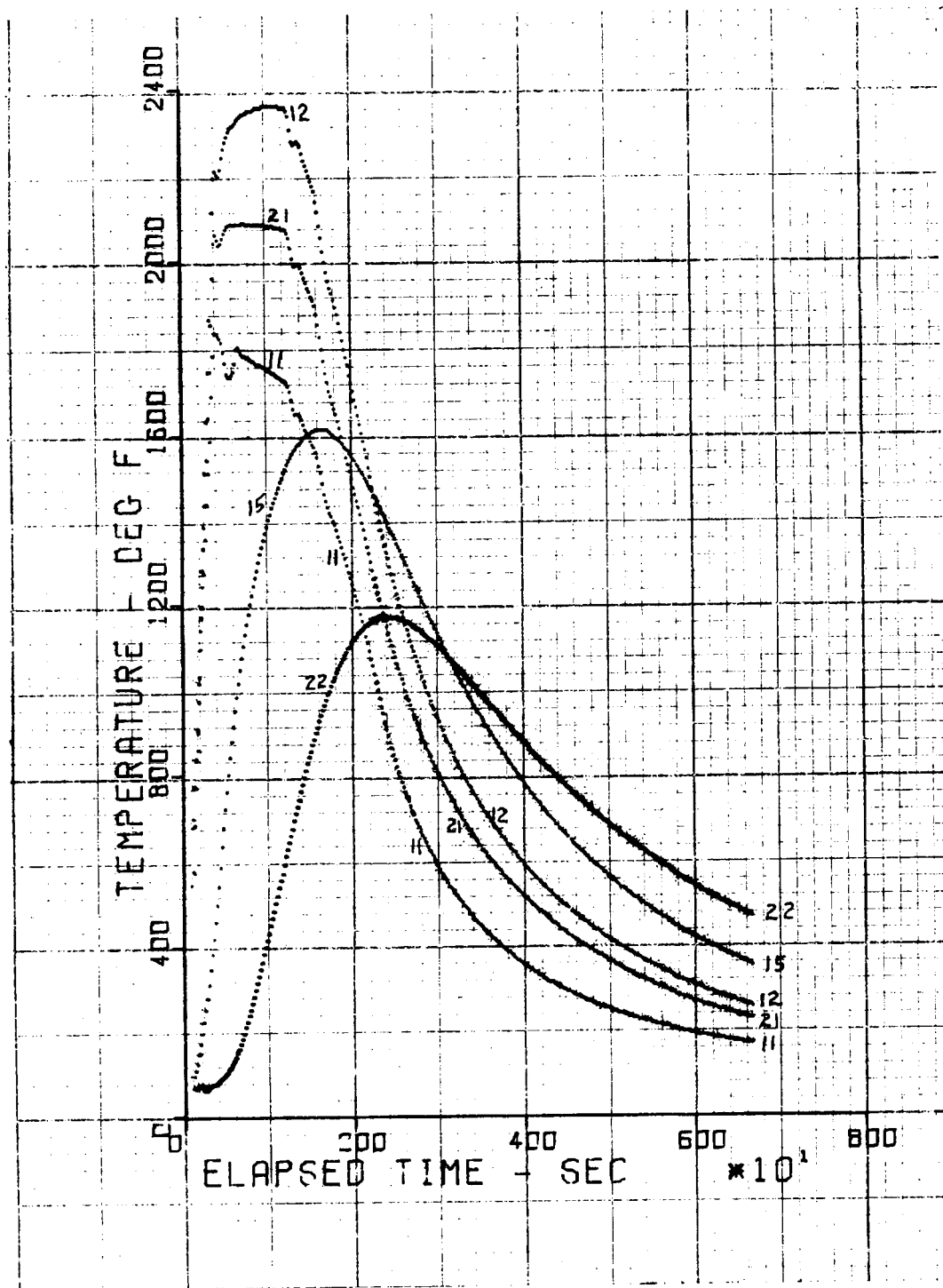


FIGURE 11

RPP WINDWARD SIDE LUG TEST - NOVEMBER 3, 1972

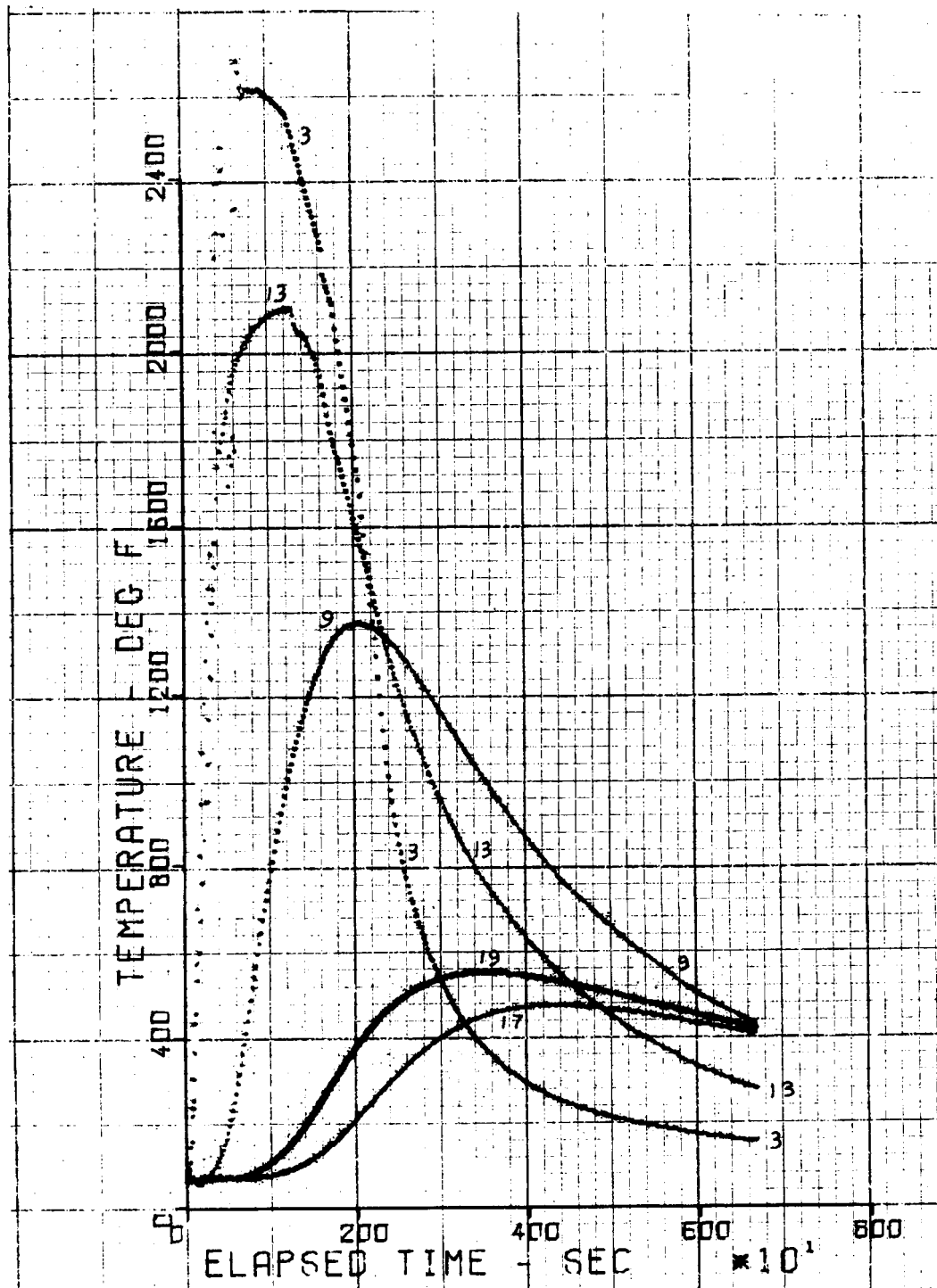


FIGURE 12

RPP WINDWARD SIDE LUG TEST - NOVEMBER 3, 1972

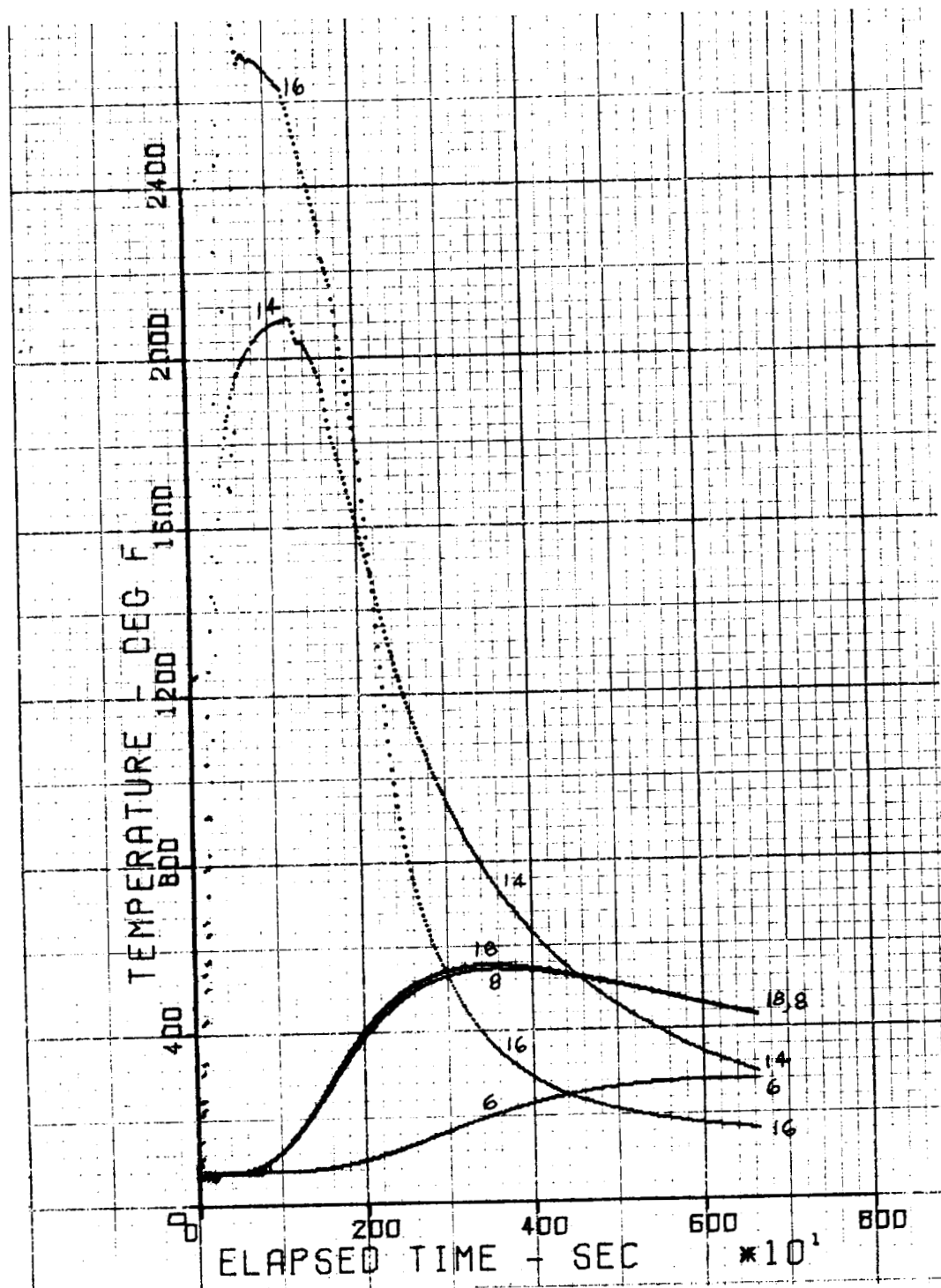


FIGURE 13

RPP WINLAWARD SIDE LUG TEST - NOVEMBER 3, 1972

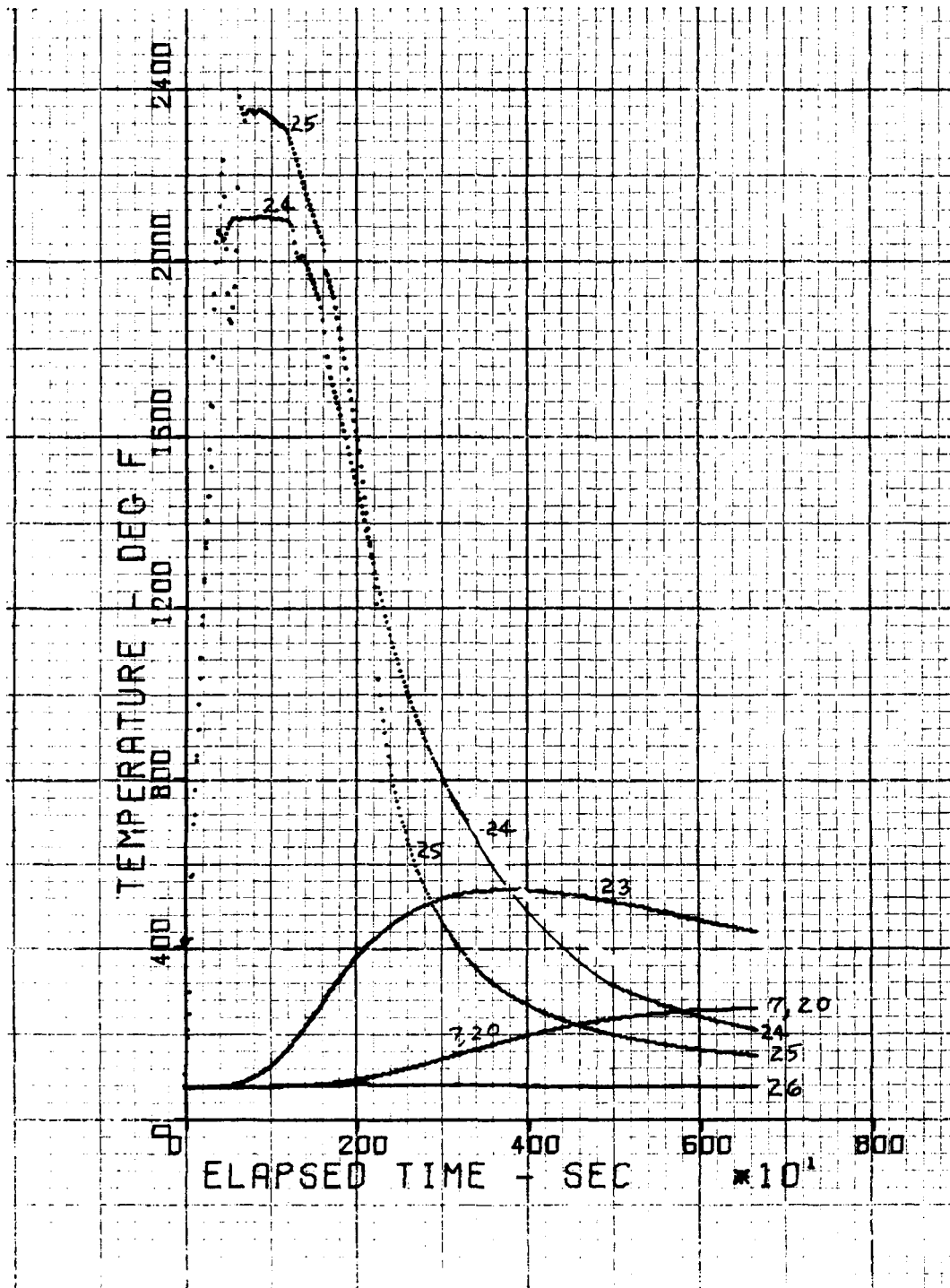


FIGURE 14
RPP WINDWARD SIDE LUG TEST - NOVEMBER 3, 1972

After a review of the test data, it was decided to retest with insulation installed inside the cut-outs of the brackets.

Second Retest - 8 November 1972

All temperatures for this test were well below their maximum allowables. The peak temperature of the polyimide was 450°F and the peak temperature of the aluminum was 231°F. These values were considerably closer to the pre-test predictions than they were for the previous test.

Total heat input for this test was much closer to the desired values during the peak heating time than it was for the previous test. Figure 15 shows the desired temperatures of the RPP surface compared to the test values. Although the temperatures of the more important thermocouples (2 and 10) were near the desired values during the first 2500 seconds the temperatures after that time are much greater than desired. The effect of these higher temperatures is to input more total heat into the specimen than desired; therefore, the temperatures of the bracket are conservative (greater than those for flight conditions).

Test results for this test are presented in Figures 16 through 20. Locations of the thermocouples are shown on Figure 6.

Two thermocouples (numbers 3 and 25) were located on the front of the insulation near the heaters and one (number 16) was located on the side of the insulation. Figures 18 and 20 show a large difference between the temperatures for thermocouples 3 and 25 although they were both on the front surface. A post test inspection of the thermocouple installation revealed the reason for the lower temperature of number 3. Thermocouple number 25 was located at the surface of the insulation directly facing a graphite heater, whereas thermocouple number 3 was buried 0.1" inside the insulation and was not directly facing a graphite heater. Peak temperatures were 2335°F for number 25 and 1730°F for number 3.

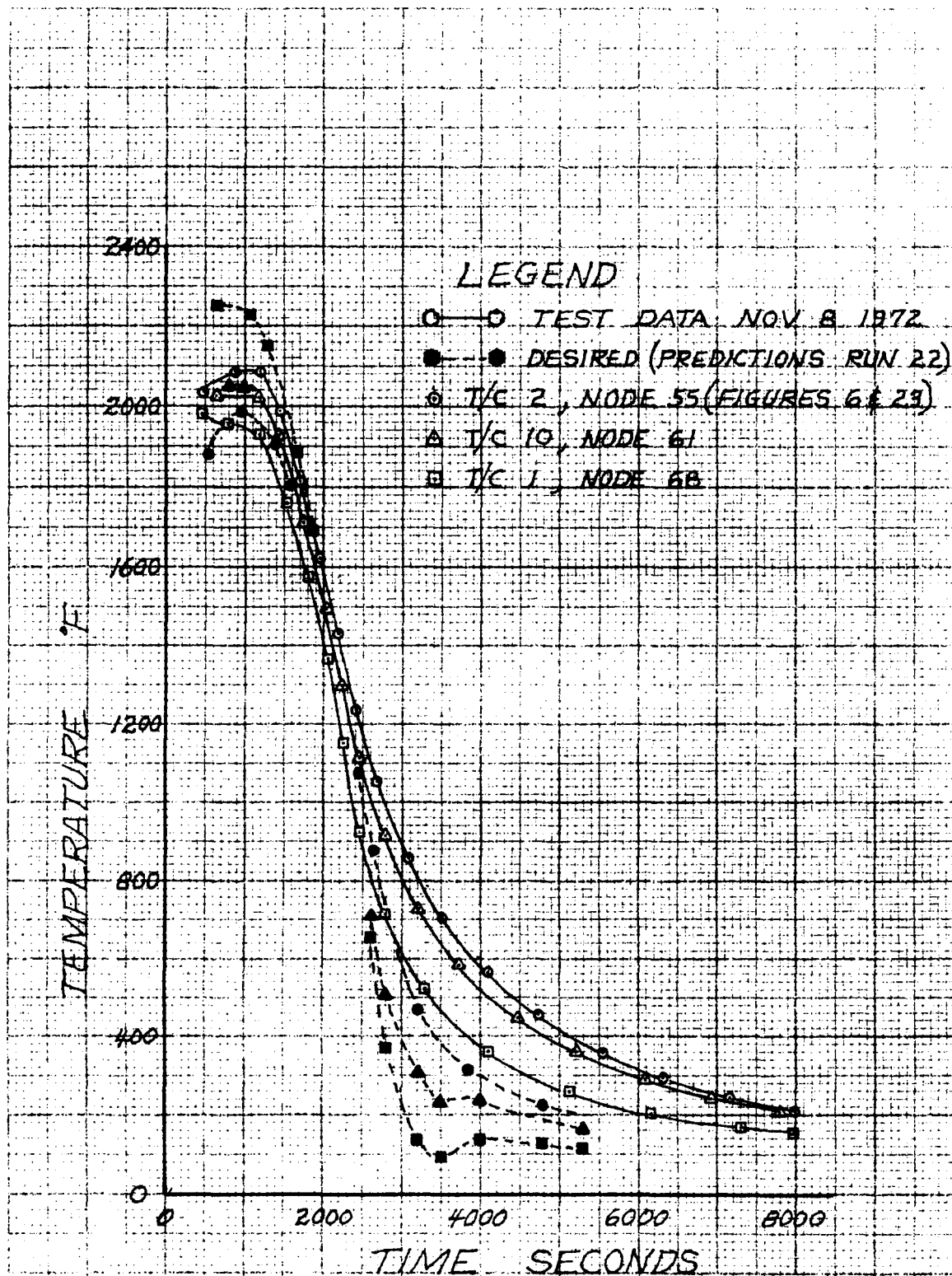


FIGURE 15 RPP SKIN TEMPERATURES
SECOND RETEST

NOTE: Thermocouple locations are shown in Figure 6

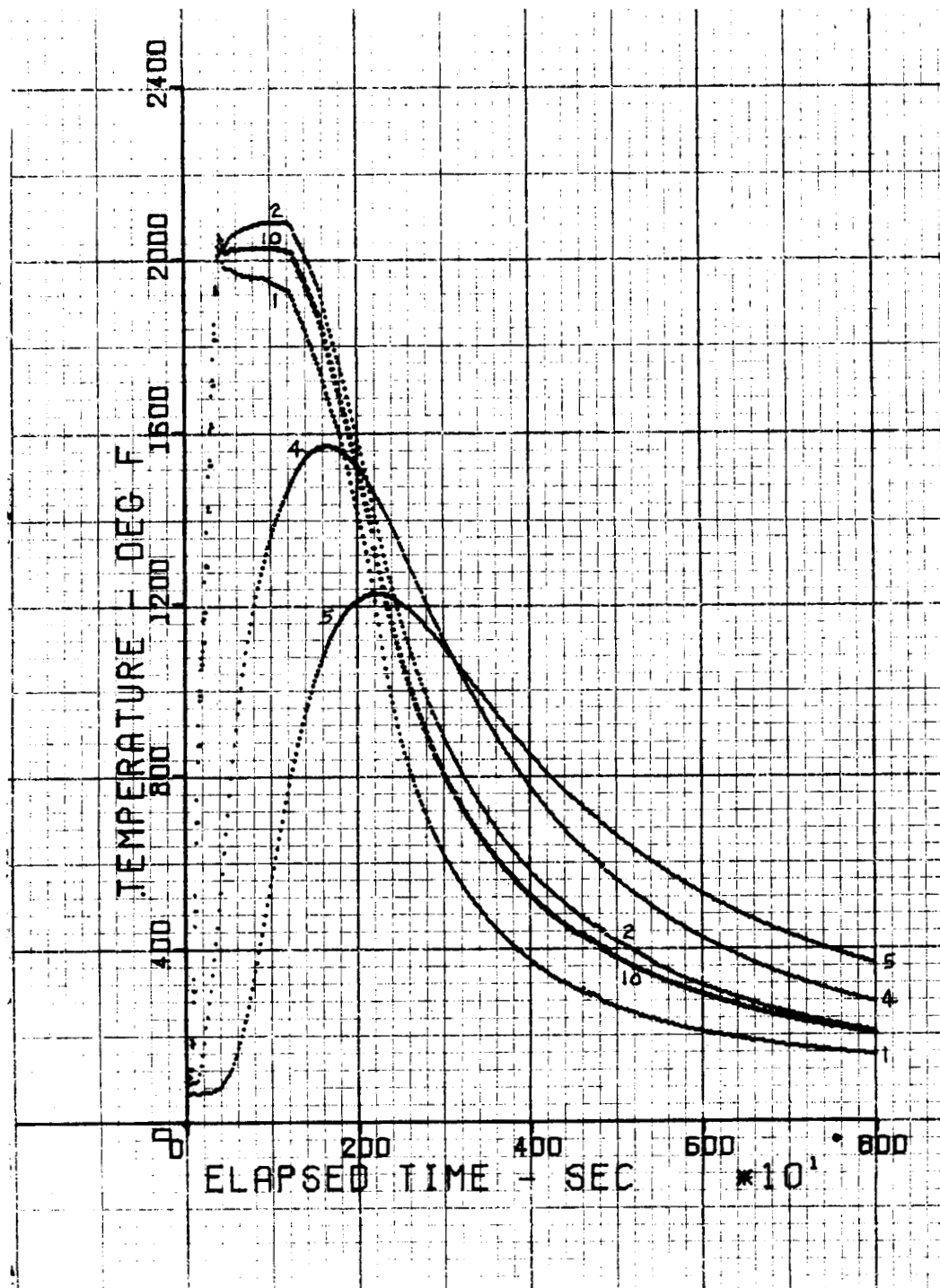


FIGURE 16

RPP WINDWARD SIDE LUG TEST - NOVEMBER 8, 1972

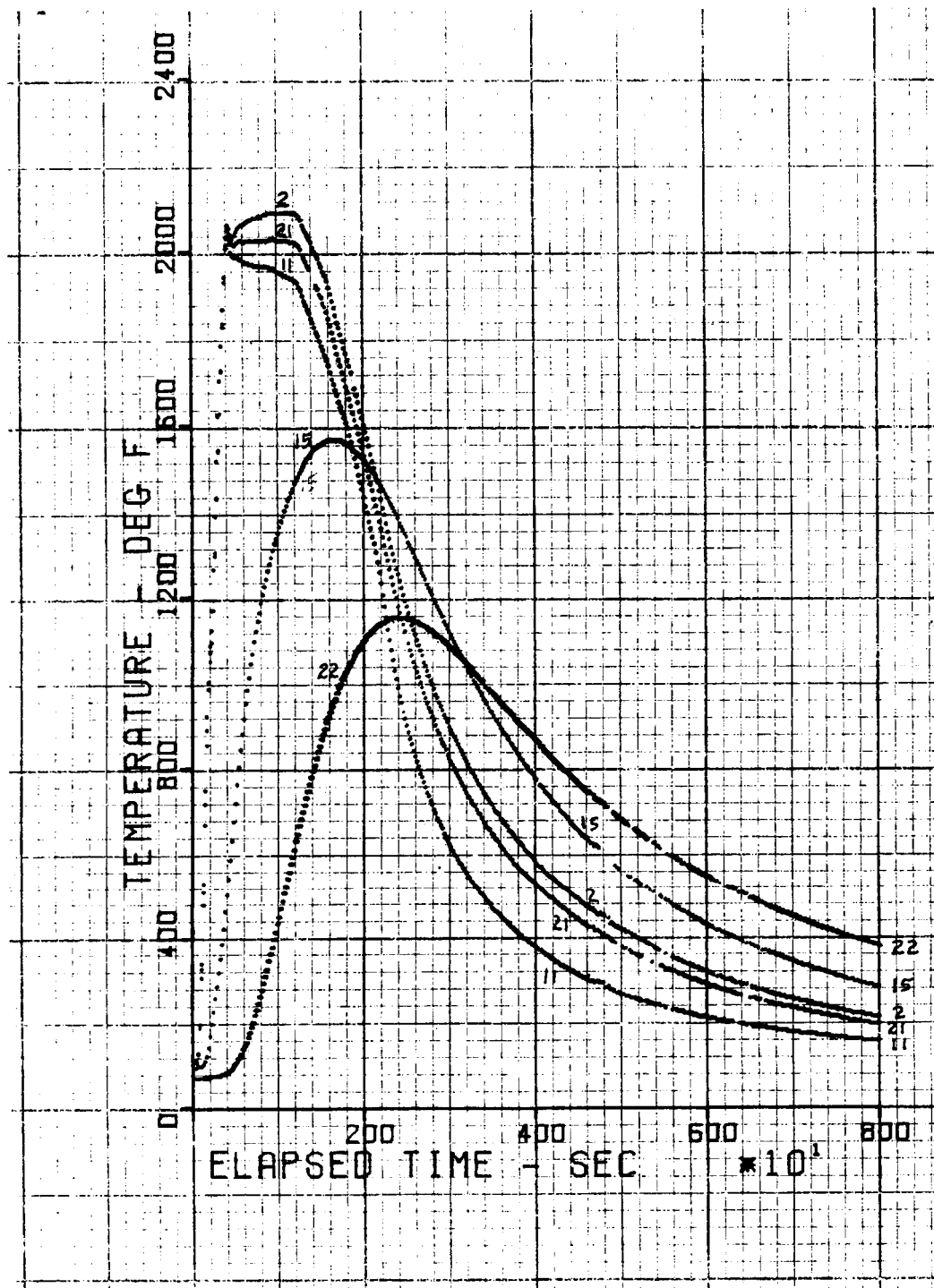


FIGURE 17

RPP WINDWARD SIDE LUG TEST - NOVEMBER 8, 1972

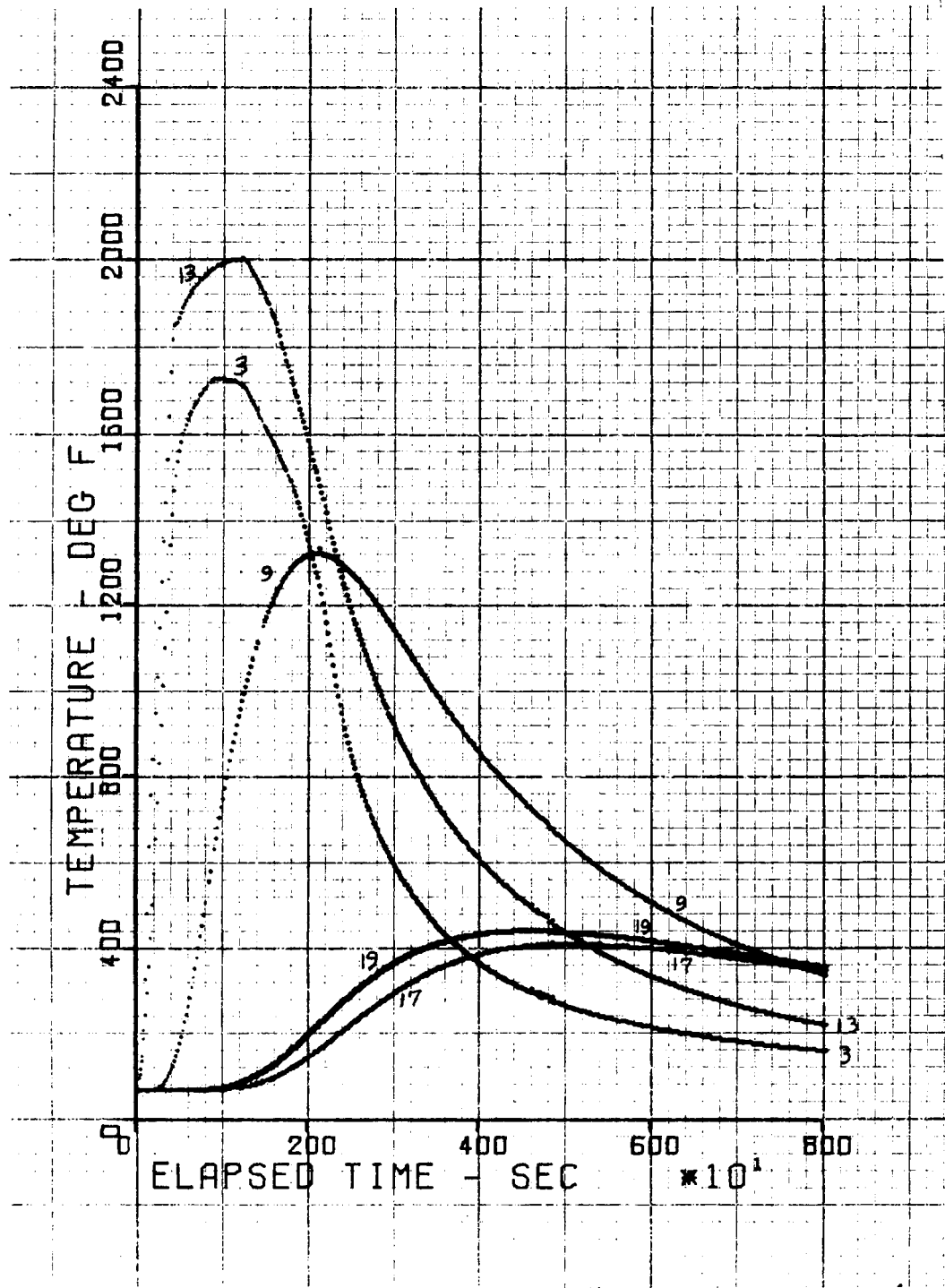


FIGURE 18

RPP WINDWARD SIDE LUG TEST - NOVEMBER 8, 1972

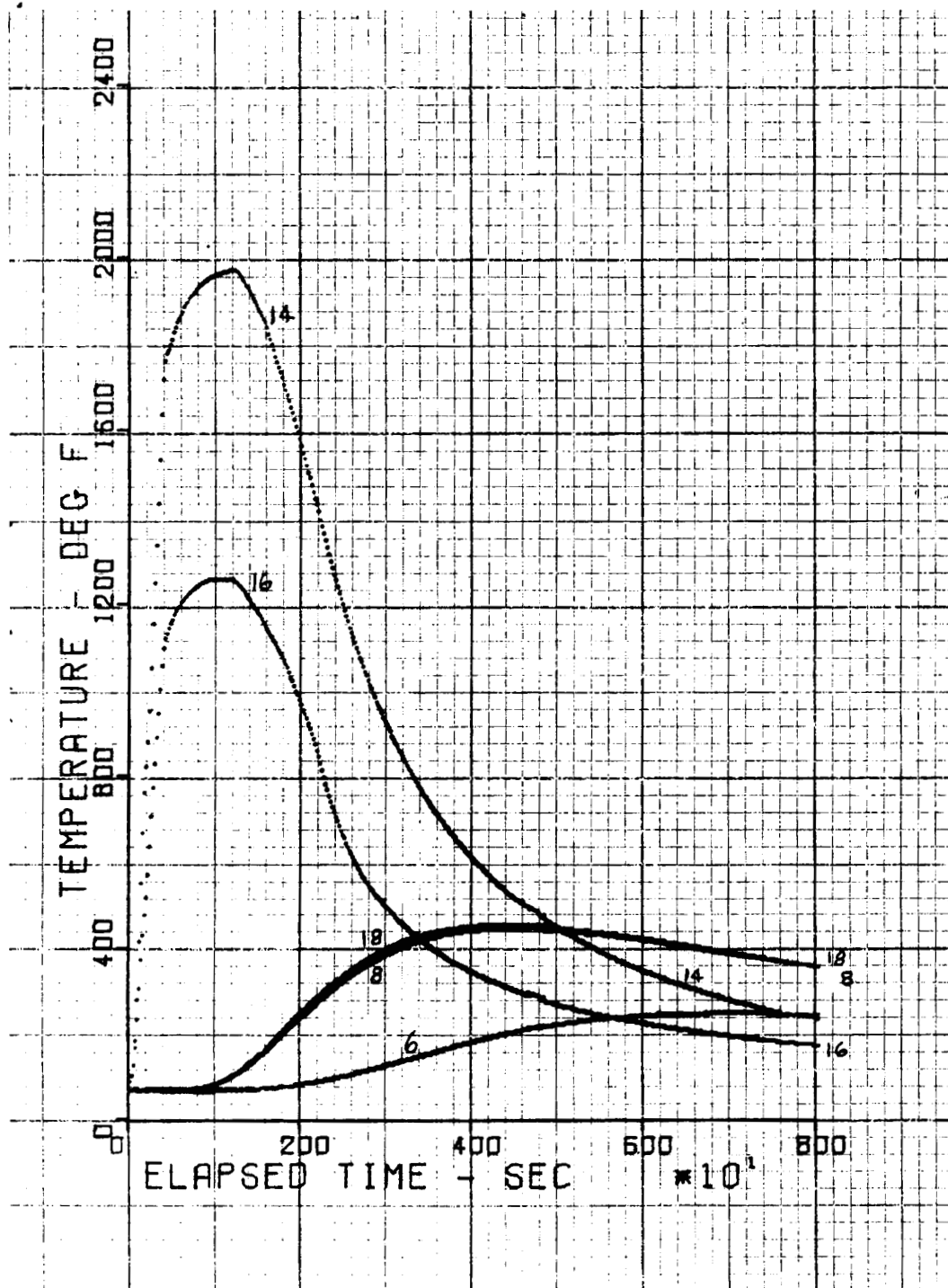


FIGURE 19

RPP WINDWARD SIDE LUG TEST - NOVEMBER 8, 1972

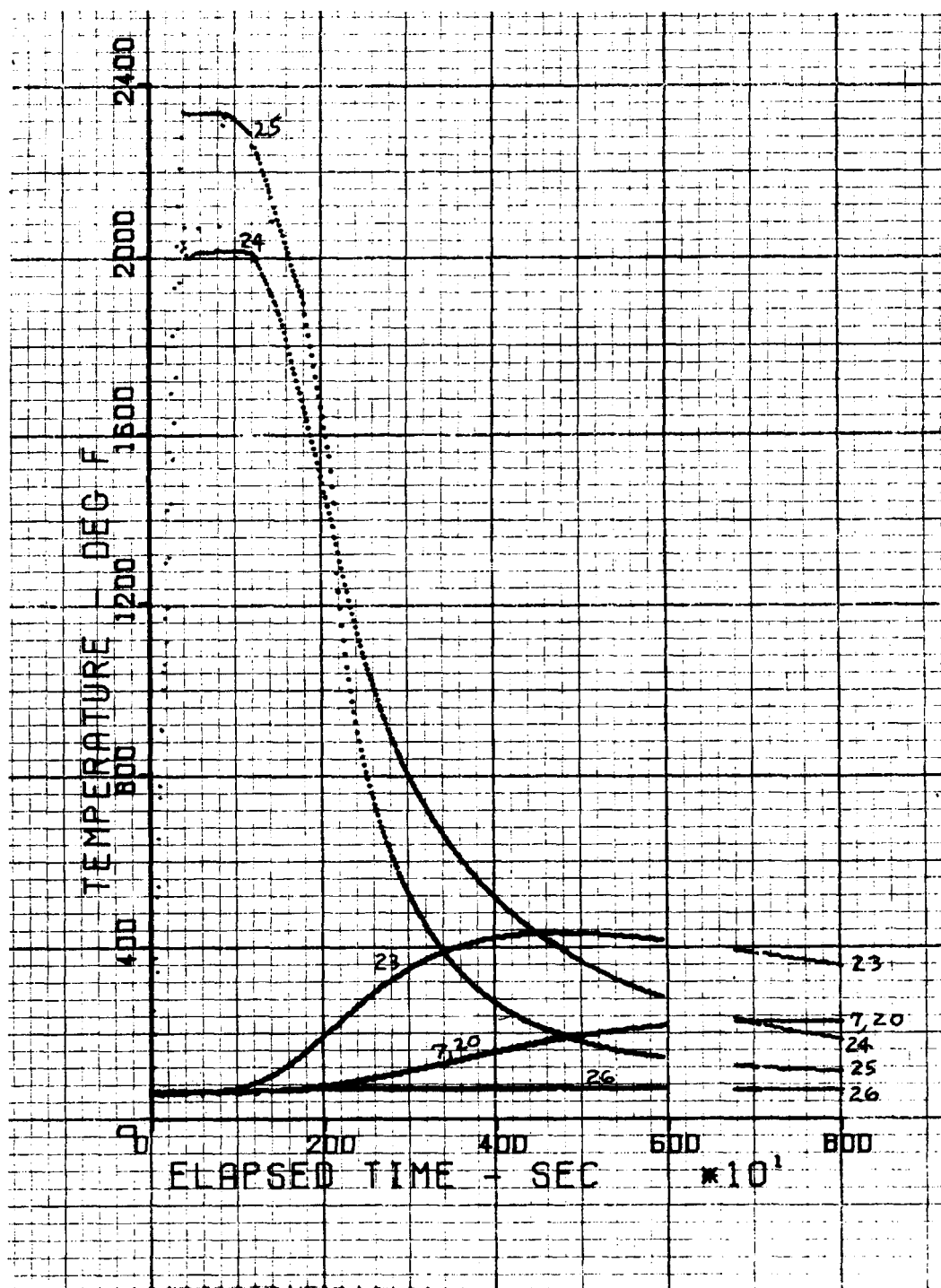


FIGURE 20

RPP WINDWARD SIDE LUG TEST - NOVEMBER 8, 1972

Thermocouple number 16, positioned at the surface of the insulation on the side, peaked at 1260°F. Graphite heaters were placed at the front of the insulation only, therefore the maximum temperature at the side was less than on the front. In the actual flight conditions the sides of the insulation will receive approximately the same thermal radiation as the front of the insulation so its temperature will be about the same as the front face. Since the test heating setup resulted in quite a difference in temperatures for the side and front surfaces, analysis was done to determine the effect of the reduced side heating on the expected peak temperatures at the aluminum and polyimide. Results of the analysis showed less than 10°F difference in the predicted temperatures of the aluminum and polyimide with the higher temperature of the side insulation.

Although actual test temperatures for the second retest were much closer to predictions than the previous test, the actual maximum temperature of the polyimide was still 100°F higher than predicted.

Post-test analysis was performed to determine changes required in the thermal model to make it give better predictions, so that it will be a more useful tool in flight analysis. This post-test analyses will be discussed in the next section.

THERMAL MODEL DEFINITION

The thermal analyses were performed using a three-dimensional thermal model and a VMSC computer routine which accounted for heat conduction along the skin and RPP rib, across the contact surfaces at the support joint, through the steel bolt and the bracket, and across the insulation into the aluminum wing structure. Cross radiation from the skin to the portion of the RPP rib outside the bulk insulation and radiation along the expansion gap between the rib and sealing strip was considered, as was the heat conduction through the bulk insulation and into the support joint.

The three-dimensional thermal model used in the analysis is shown in Figures 3,4,5, and 21 through 23. The model for the rib area, Figure 21, is similar to that which was used in Reference 5 to predict temperatures of the ribs in the support joint area. The aluminum structure is represented by a block

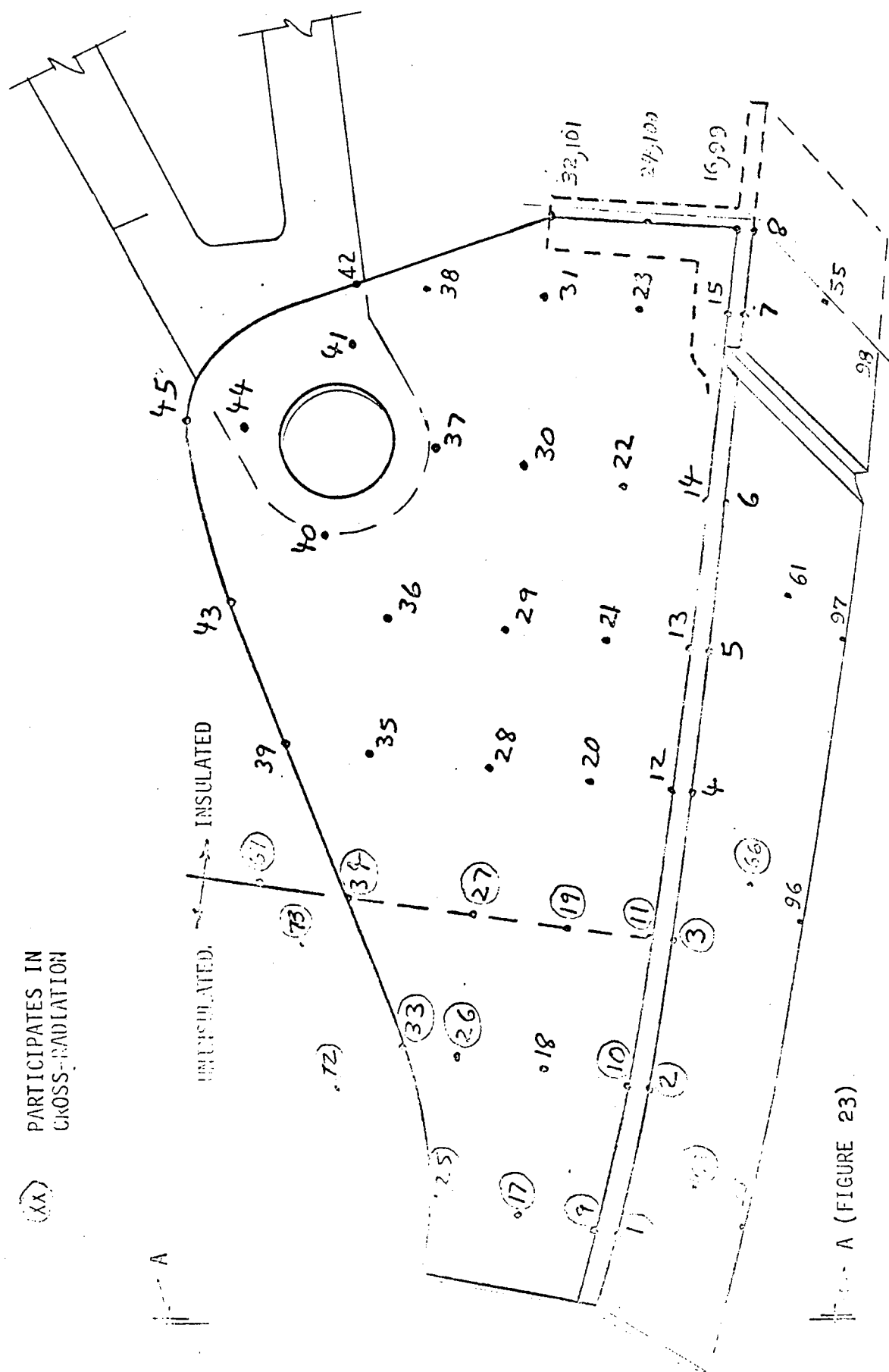
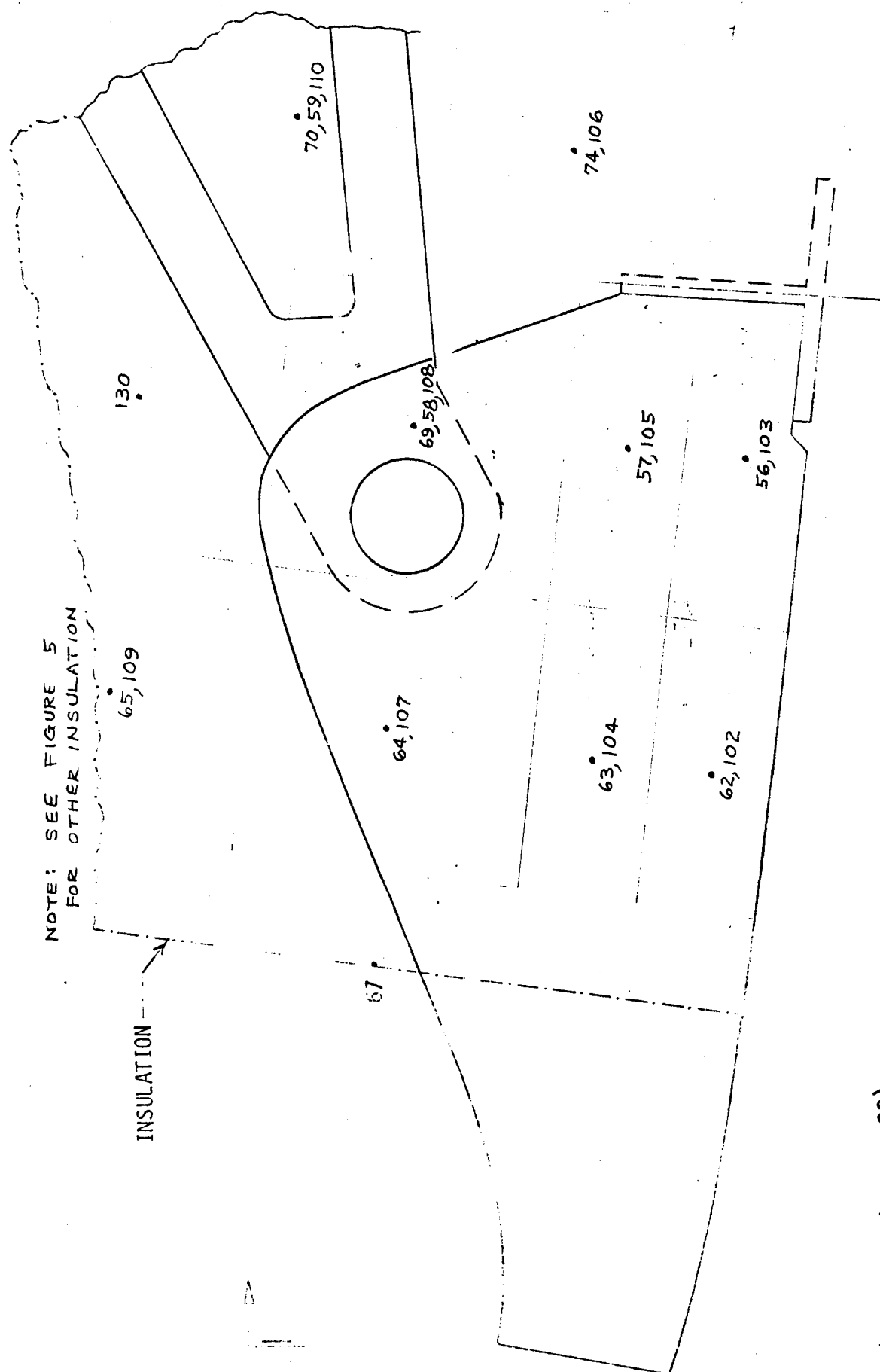


FIGURE 21 THERMAL MODEL OF CARBON-CARBON RIB AND SKIN



A (FIGURE 23)

FIGURE 22 - THERMAL MODEL OF BULK INSULATION

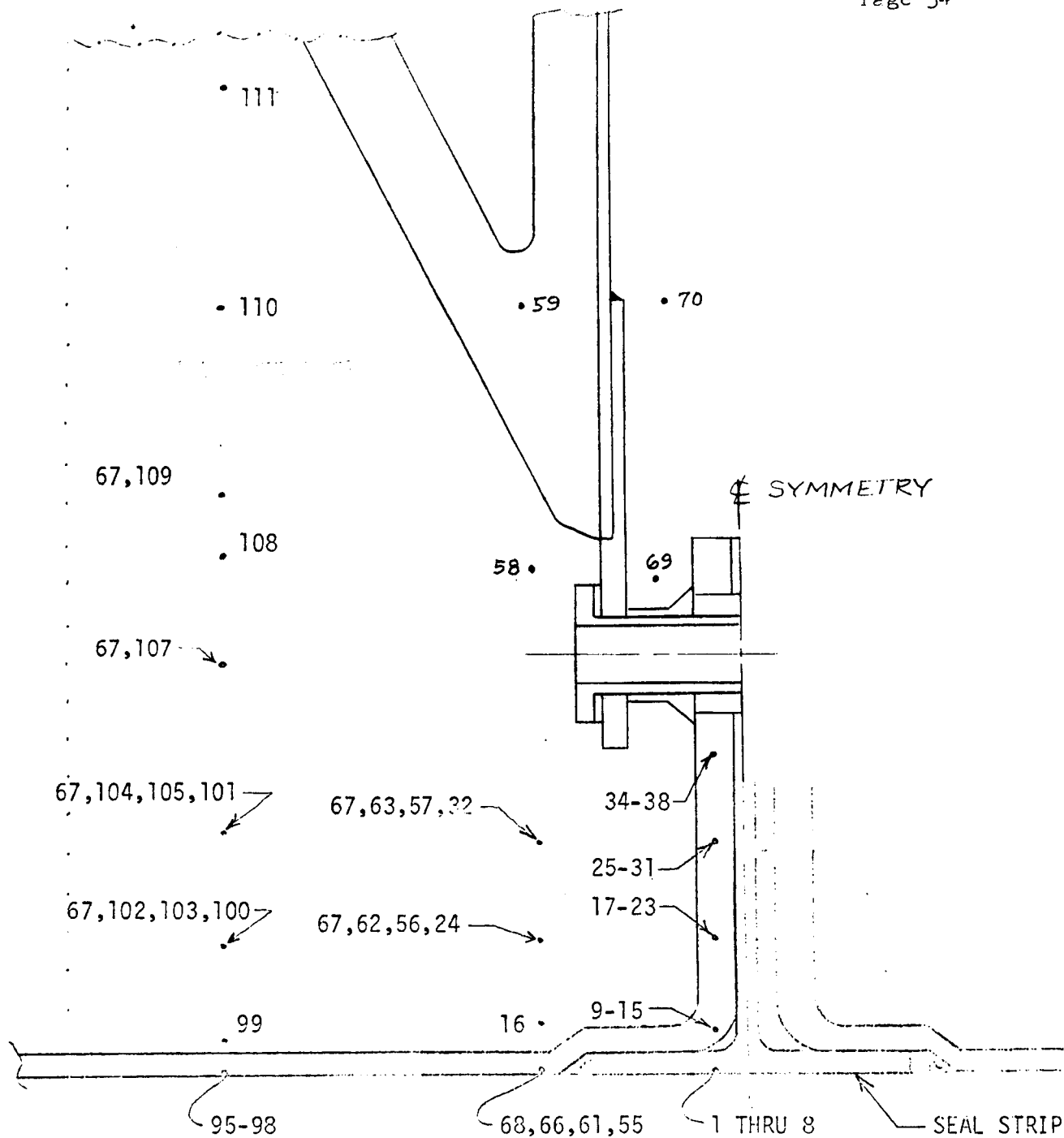


FIGURE 23 - THERMAL MODEL - SECTION A-A

of aluminum with adiabatic boundaries except at the bracket. Also the effect of the titanium brace (Figure 1) upon the bracket is neglected for this analysis.

The recovery temperature and the convection heat transfer coefficients used for the external skin nodes were the same as those used in the rib analysis of Reference 5. The external temperature of the bulk insulation was input as a function of time as given in Figure 24. Thermal property data used in the analysis and not presented in Reference 2 are presented in the Appendix.

The thermal analyses performed in support of the September test of the lug joint are summarized in Table 1, which gives the peak temperatures. Details for three of the runs are presented in Figures 25, 26 and 27. Figure 25 for Run A, is for zirconia insulators at the bolt. The predicted maximum temperature of the cold end of the bracket (polyimide interface temperature) is 582°F. This is 136°F greater than the maximum predicted for silica insulators at the bolt for Run C. Figure 26, for Run E, shows a predicted maximum of 618°F at the polyimide interface for an all inconel joint (hollow bolt and bushings.).

Peak temperatures obtained in the test are included in Table 1 for reference. Post-test analysis was done to determine thermal model modifications required to make the model predictions match test results. Increasing the joint contact coefficient from 100 BTU/hr ft²°F for Run 12 to infinity for Run 14 improved the predicted polyimide temperature by 100°F. Figure 27 shows the results for Run 14. Run 15 was made using infinite joint coefficient and forcing the temperature of the RPP at the lug joint to follow the test values. Predicted maximum temperature of the polyimide was still 367°F below the test value. As noted in the previous section this difference was attributed to convection effects.

Table 2 is a summary of the peak temperatures obtained when varying various parts of the joint and bracket configuration. These runs were made in order to determine the influence of the system variables upon the predicted temperatures of the polyimide and aluminum and to provide pre-test predictions for the retest. Figure 28 shows the pre-test predictions for Run 22.

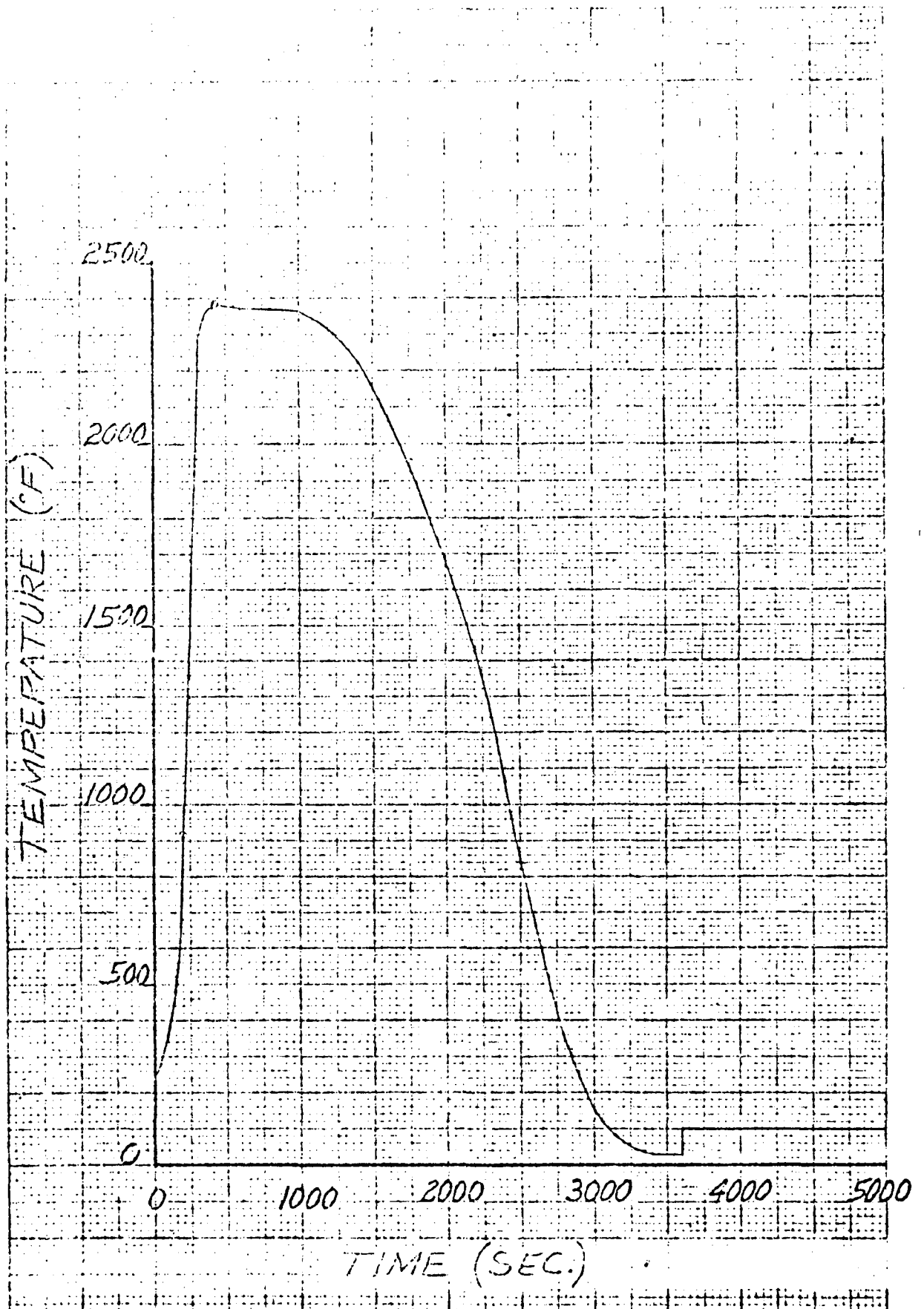


FIGURE 24 RADIATING STRUCTURE TEMPERATURE

SUPPORT JOINT PEAK TEMPERATURES, °F PREDICTIONS FOR SEPTEMBER TEST

TABLE 1

CONFIGURATION	Same as for Run A except longer in Inconel - shorter polyimide		Aluminum Polyimide F.G.		Inconel Sleeve RPP		Aluminum Polyimide F.G.	
	Inconel Insulation Bolt RPP	Aluminum Polyimide F.G.	Inconel Insulation Bolt RPP	Aluminum Polyimide F.G.	Inconel Sleeve RPP	Aluminum Polyimide F.G.	Inconel Sleeve RPP	Aluminum Polyimide F.G.
RUN NO. (See Figure XX)	A(25)	B	C*	D	E (26)	TEST (8)	POST-TEST ANALYSIS 12 13 14(27) 15	
PEAK TEMPERATURES:								
NODE NO. LOCATION								
37 RPP at Joint	1540	1710	1699	1545	1555	1761	1506	1436 Controlled
46 Attachment Bolt	1289	1437	1366	1298	1335	1640	1341	1378 1658
51 Hot End of Bracket	860	650	604	886	935	1579	1120	1258 1510
52 Cold End of Bracket	582	466	446	448	618	1426	784	880 1059
81 Aluminum **	-	-	-	< 263	-	450	-	-
NOTES:								
Joint Coefficient	100	100	100	100	100	-	100	∞
Misc.	Zirconia Bolt Insulation	Silica Bolt Insulation	Silica Bolt Insulation	Zirconia Bolt Insulation			400	∞
* The results for this run was presented in Reference 2 and designated Attachment 2, Variation 9.								
** Some runs were not run long enough to obtain peak.								

FIGURE 25
PRE-TEST PREDICTIONS
ZIRCONIA BOLT INSULATORS
RUN NO. A

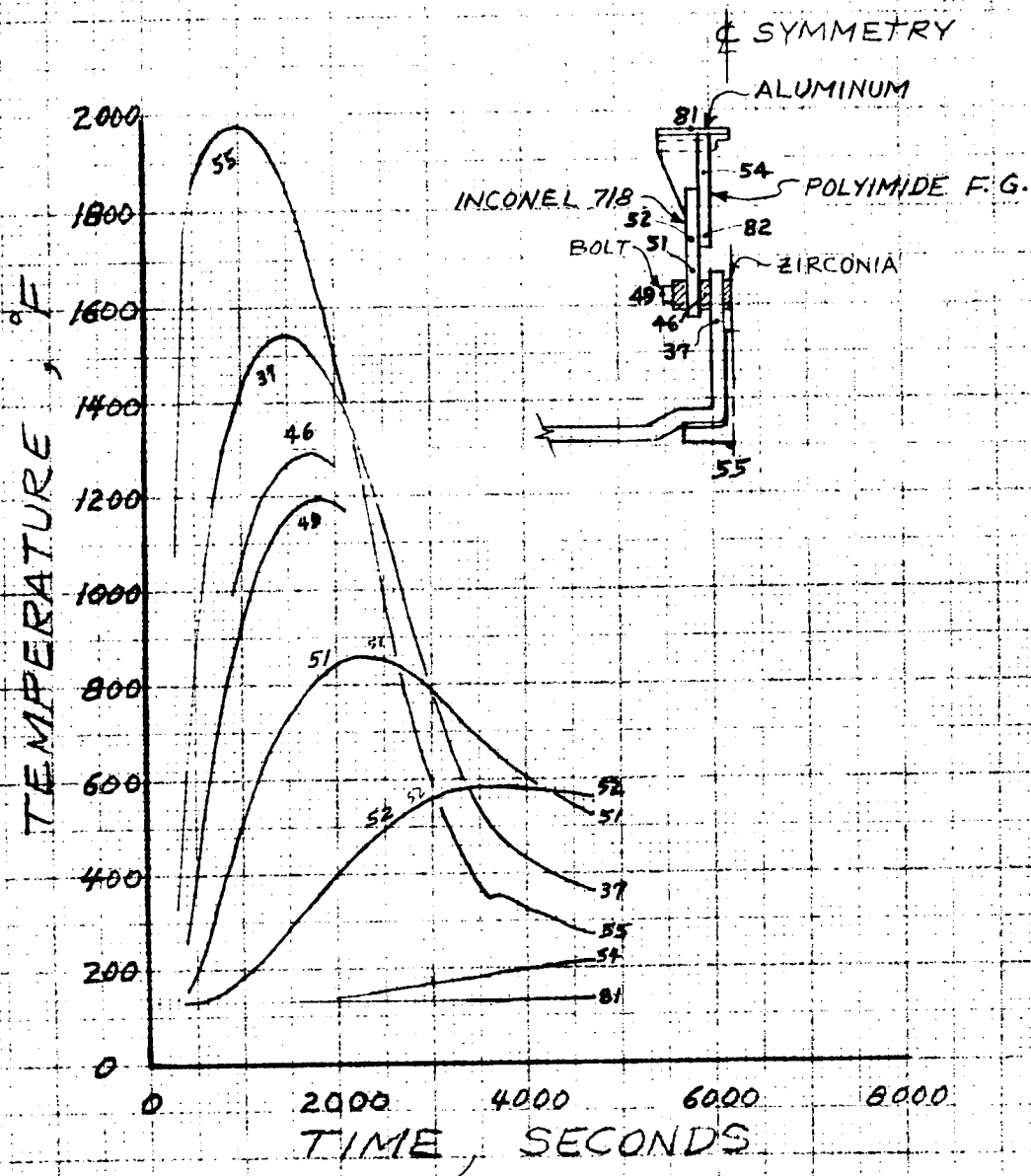


FIGURE 26
PREDICTED TEMPERATURES
PRE-TEST PREDICTIONS
ALL INCONEL JOINT RUN E

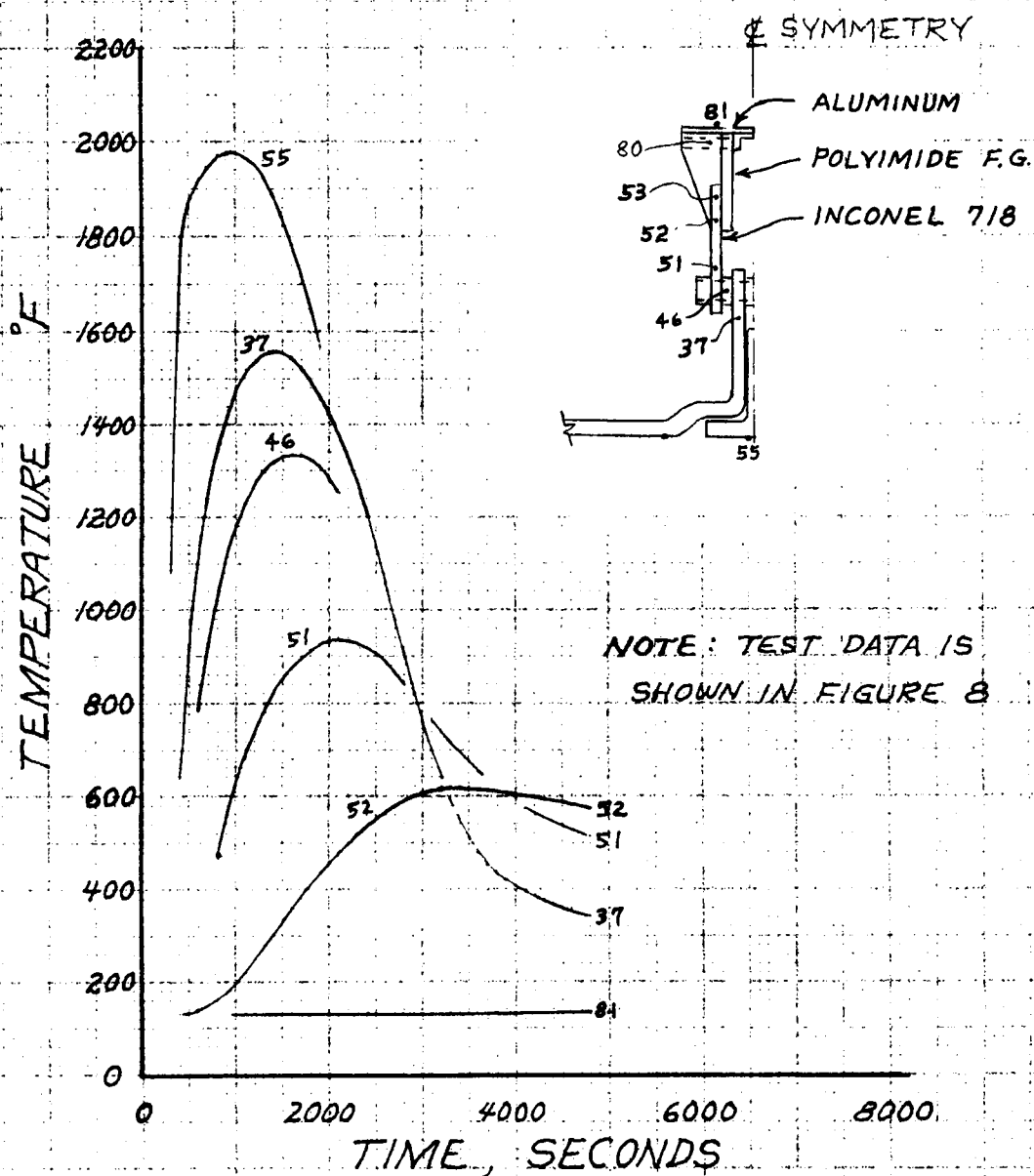
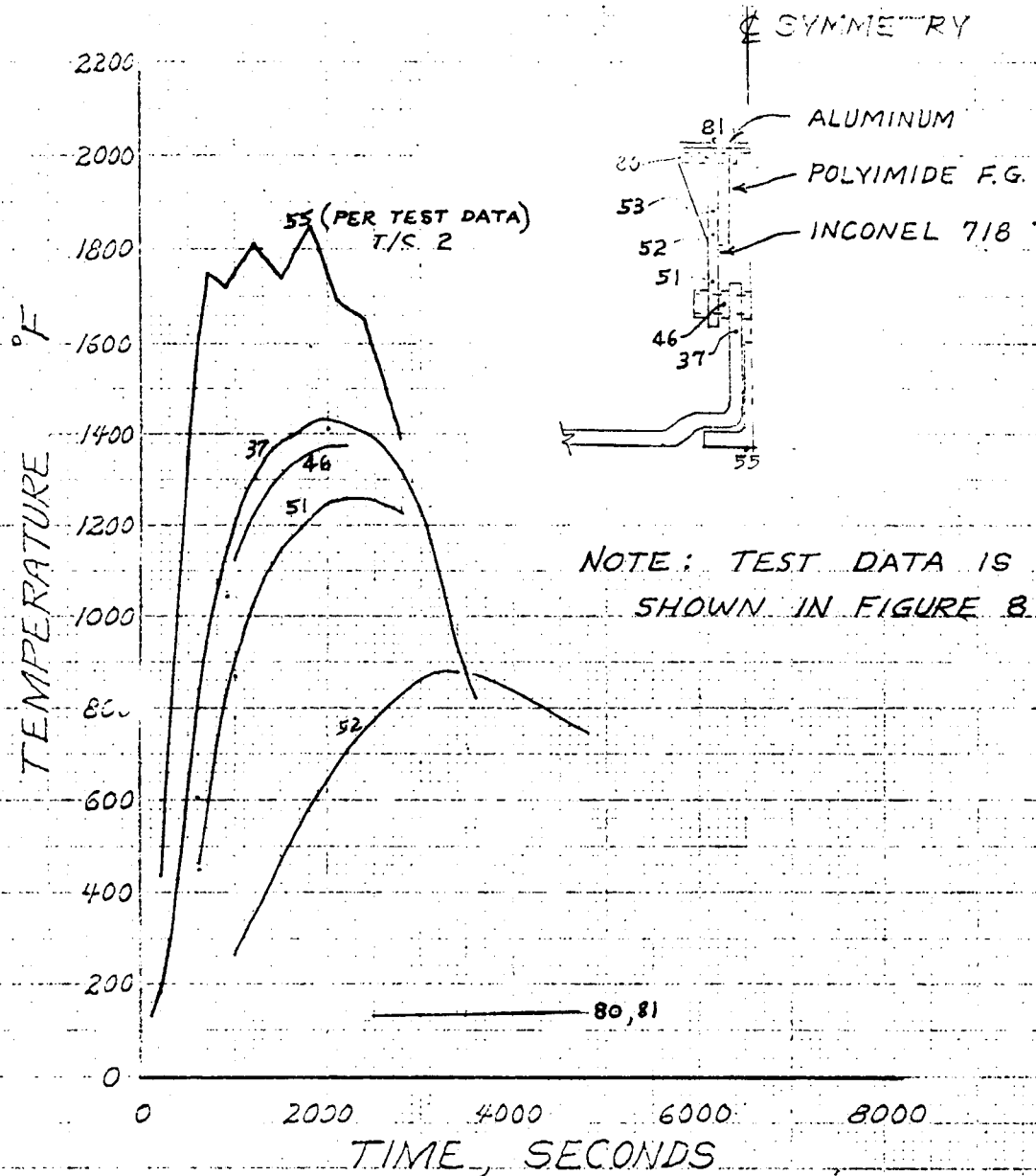
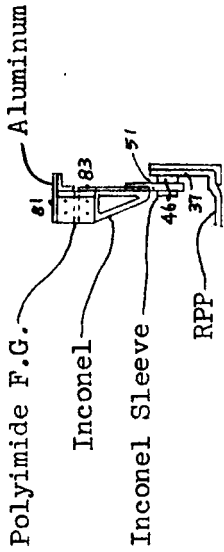


FIGURE 27
PREDICTED TEMPERATURES
POST-TEST PREDICTIONS
ALL INCONEL JOINT RUN 14
(SEPTEMBER TEST)



SUPPORT JOINT PEAK TEMPERATURES, ° F PRE-TEST PREDICTIONS
(RETESTS)

CONFIGURATION:



PEAK TEMPERATURES:	17	18	20	21	22	24	27	28	29
NOTE NO. LOCATION									
37 RPP at Joint	1389	1389	1444	1463	1444	1459	1448	1448	1648
46 Attachment Bolt	1325	1325	1393	1365	1393	1409	1397	1397	1249
51 Hot End of Bracket	1177	1177	1283	1238	1282	1295	1286	1286	846
83 Cold End of Bracket	678*	677*	382	369	346	349	381	425	-
81 Aluminum	< 268	< 234	< 227	< 213	< 234	**	< 236	< 231	-
Joint Coefficient	∞	∞	∞	∞	∞	∞	∞	∞	25
Misc.		1.5 times the mass of aluminum of Run 17	Rerun No. 17	Sprayed ZrO ₂ at bolt	Add extra .078" inconel at polyimide interface	Same as 22 but add radiation at gap between T-seal & lug.	Similar to 20 but add heat input from side of insulation.	Same as 27 but decrease conductivity of polyimide to 1/2 nom.	Compare to 27.

** Was not run long enough to obtain peak.

* Runs 17 and 18 inadvertently contained a heat short in the bracket representation. Results are presented here only to show the effect of increased mass of aluminum.

FIGURE 28
PREDICTED TEMPERATURES
PRE-TEST PREDICTIONS
ALL INCONEL JOINT RUN 22
(RETEST CONFIGURATION)

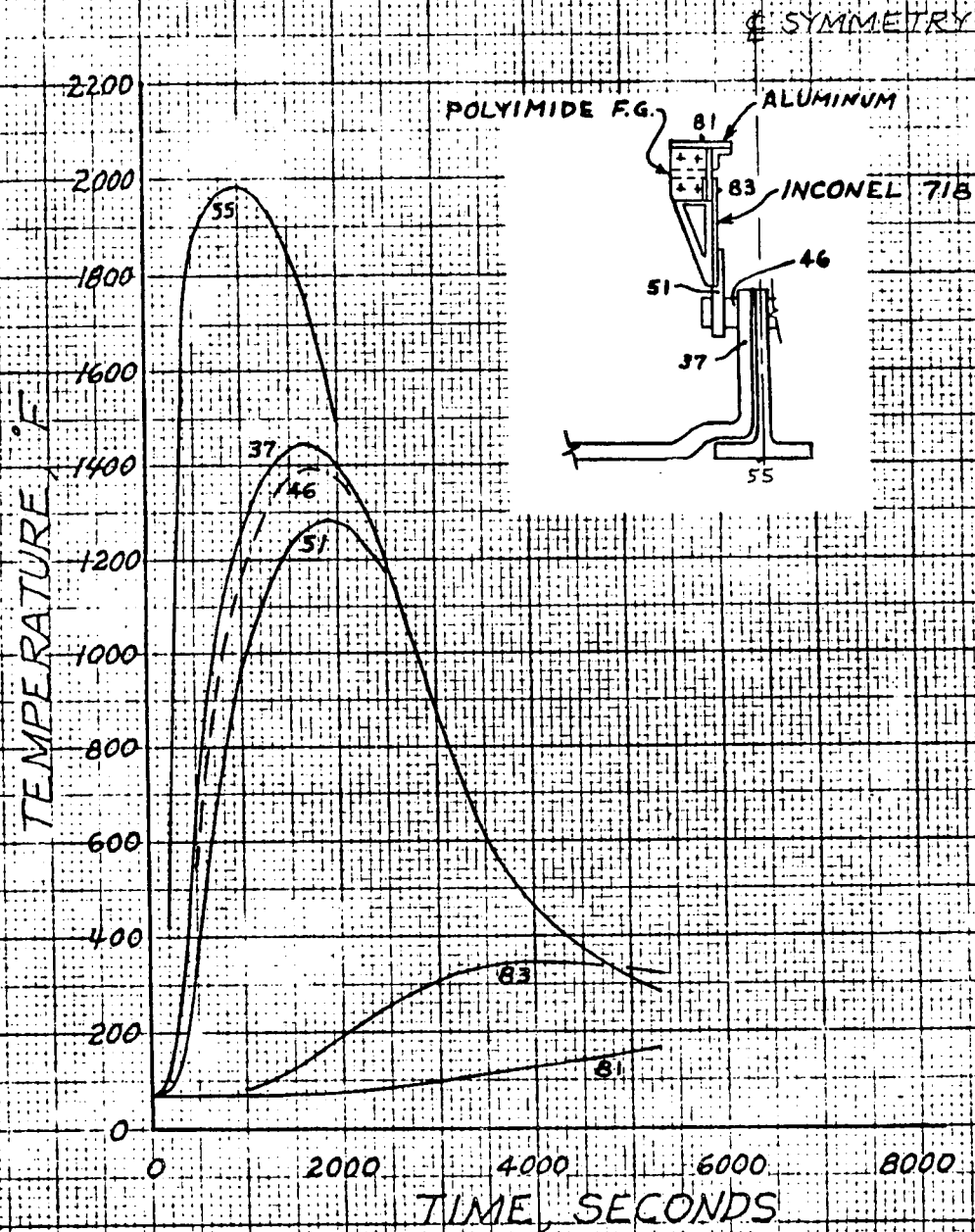


Table 3 is a summary of the peak temperatures obtained for the post-test analysis of the November tests. Pre-test predictions did not adequately represent the test results so these runs were made to determine required model modifications. RPP skin temperatures were input as a function of time per test data. A number of thermal model variables were changed independently of each other in order to determine the required changes. The results of this parametric analyses are summarized in Table 4. As a result of the analyses it was determined that two major modifications to the model needed to be made. The first was to increase the thermal conductivity of the inconel bracket by 20%, and the second was to make the joint coefficients at the bolt dependent on the temperature at the joint.

Increasing the thermal conductivity of the inconel by 20% improved considerably the predicted temperature drop from the hot to the cold ends of the bracket as shown by Runs 30 and 35. (see Figures 29 and 30). The change had only a small effect on the predicted temperature at the hot end of the bracket. A review of the literature showed that the 20% increase was reasonable for the family of nickel chromium alloys based on the spread of conductivity test data. There is also the possibility that part of the increase was required to account for the effect of thermal radiation down the gap between the insulation and the sides of the bracket. This radiation was not included in the thermal model because of the large number of nodes involved and computer run times requirements. As a further check on the suitability of using 20% increased inconel conductivity, Runs 38 and 39 were made with the temperature at the hot end of the bracket (node 51) held at the test data values. Results of the runs, see Figure 31, show that using the increased conductivity yields satisfactory predictions of the temperature drop in the inconel bracket. The model for Run 39 was the same as for 38 except the conduction area between the sides of the bracket and the bulk insulation was reduced to more accurately represent actual test conditions. Thermocouple leads along the bracket made it difficult to have good contact between the

TABLE 3

SUPPORT JOINT PEAK TEMPERATURES, °F POST-TEST PREDICTIONS (RETESTS)

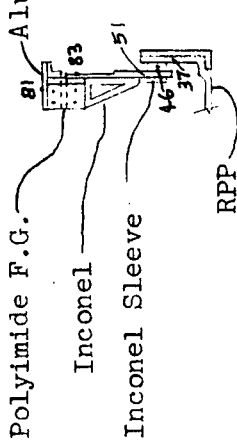
CONFIGURATION:												Test
IN NO. (See Fig. xx)	PEAK TEMPERATURES:	30(29)	31	32	33	34(33)	35(30)	37	38(31)	39(31)	44(34)	
37 RPP at Joint	1461	1462	1462	1462	1456	1443	1437	1443	-	-	1486	1565
46 Attachment Bolt	1401	1403	1402	1402	1395	1385	1473	1384	-	-	1401	1320
51 Hot End of Brkt.	1286	1289	1288	1281	1281	1272	1265	1272	Controlled			1220
33 Cold End of Brkt.	387	375	374	371	371	376	428	376	434	475	417	450
31 Aluminum	<198	<200	<189	<189	<189	<213	189	<228	<250	<247	<217	231
NOTES:												
Joint Coefficient	∞	∞	∞	∞	∞	∞	∞	∞			$h=f(\text{temp})$	-
Inconel Conductivity	Nom.	Nom.	Nom.	Nom.	Nom.	Nom.	1.2 Nom.	Nom.	1.2 Nom.	1.2 Nom.	1.2 Nom.	-
Misc.	Include cross radiation inside bracket cutouts.	Cross radiation inside bracket cutouts not included.	Include insulation inside the bracket cutouts.	This run only, use insulation thermal K for atmosphere conditions.	Start at 500 sec. using temperatures from Run 29	Compare to Run 30.	Same as 34 except reduce conduction from aluminum specimen support.	Reduce conduction from brackets to insulation.				

TABLE 4
PREDICTED TEMPERATURES - EFFECTS OF SYSTEM VARIABLES

<u>VARIABLE</u>	<u>EFFECTS OF CHANGE</u>
<u>Relative Lengths of Inconel Bracket and Polyimide Fitting (Runs A & D)</u>	The maximum temperature of the polyimide was reduced from 582°F to 448°F by increasing the length of the inconel between the center of the bolt and the polyimide interface from 2-1/4" to 4-1/2" and reducing the length of the polyimide by the same amount.
<u>Thickness of RPP Skin Panel (Runs B & C)</u>	All the results reported herein were for Phase II thicknesses of the RPP (the test panels had Phase II thicknesses) except for Run B presented on Table 1. Run B had Phase III RPP thicknesses. The effects of the different RPP thicknesses upon the predicted temperatures are small, as can be observed by comparing results of Run B to Run C. The maximum temperature of the polyimide fiberglass is only 20°F greater for the Phase III thicknesses than it is for the thinner Phase II thicknesses.
<u>Contact Coefficient at Joint (Runs 12, 13, and 14)</u> (Runs 27 & 29)	Increasing the contact coefficient from a constant value of 100 BTU/hr ft ² °F to a constant value of 400 BTU/hr ft ² °F increased the maximum polyimide temperature by 63°F (Runs 12 and 13). Further increase in the coefficient yield smaller increases; changing from 400 to infinity (perfect contact between the parts of the joint) increased the maximum polyimide temperature by only 33°F (Runs 13 and 14). Reducing the contact coefficient from infinity to a value of 25 BTU/hr ft ² °F (loose fitting parts) greatly improves the computer predictions for the hot end of the inconel during the first 700. seconds of test time. (Runs 27 and 29).
<u>Mass of Aluminum Included in the Model (Runs 17 and 18)</u>	Increasing the mass of the aluminum by 50% reduces the maximum temperature of the aluminum by 34°F. Note that this result was not obtained using the latest thermal model. The effect would probably be even greater for the final model.
<u>Heat Sink at Polyimide F.G. Inconel Interface (Runs 20 and 22)</u>	Using an extra .078" strip of inconel at the interface location results in a 36°F lower maximum temperature of the polyimide, and a 7°F lower maximum temperature of the aluminum.
<u>Thermal Radiation in Gap Between T-Seal Strip and Panel Lug (Runs 22 and 24)</u>	Accounting for radiation in the 0.06" wide gap resulted in a 13°F increase in temperature at the hot end of the inconel and a 3°F increase at the polyimide.

TABLE 4 (Continued)
PREDICTED TEMPERATURES - EFFECTS OF SYSTEM VARIABLES

<u>VARIABLE</u>	<u>EFFECTS OF CHANGE</u>
<u>Heat Input from the Sides of the Insulation</u> (Runs 23 and 27)	Predictions using the same surface temperature for the sides of the lug insulation as was used for the front of the insulation, yield approximately the same polyimide and aluminum temperatures as obtained with no heat input from the sides of the insulation.
<u>Polyimide F.G. Conductivity</u> (Runs 27 and 28)	Reducing the conductivity to 1/2 the nominal value decreases the aluminum temperature slightly (5°F) but increases the polyimide/inconel interface by 43°F. Temperatures near the hot end of the bracket are not affected.
<u>Treatment of Cut-outs in the Brackets</u> (Runs 30 and 32)	Prediction with insulation in the cut-outs instead of cross-radiation in the cut-outs results in a decrease in the temperature of the polyimide of 13°F and a decrease of 9°F of the aluminum.
(Runs 30 and 31)	Predictions accounting for radiation in the cut-outs gives a 13°F higher maximum temperature for the polyimide and 2 °F higher maximum temperature for the aluminum compared to the predictions not accounting for radiation.
<u>Thermal Conductivity of Inconel 718 Bracket</u> (Runs 30 and 35)	Increasing the thermal conductivity by 20% results in much better agreement with the measured temperature drop in the bracket. The predicted temperature at the cold end of the bracket (at the inconel/polyimide interface) was increased from 387°F to 428°F.
<u>Dynaquartz Insulation Thermal Conductivity</u> (Runs 32 and 33)	Increasing the thermal conductivity of the insulation by about 60% (using 1 atmospheric properties instead of 10 MM Hg properties) has only a small effect upon the predicted temperatures of the aluminum and the polyimide.
<u>Conduction from Brackets to Insulation</u> (Runs 38 and 39)	Because of the thermocouple leads it was difficult to have good contact between the sides of the brackets and the insulation. Run 39 was made with the contact area reduced to approximately 20% of that for Run 38. Results showed a 21°F higher peak temperature of the polyimide for the run with the reduced contact area.

FIGURE 29 RPP LUG TEST POST-TEST PREDICTIONS

THERMAL MODEL USED FOR PREDICTIONS:

- CROSS RADIATION INSIDE BRACKET OUT-OUTS
- CONTACT COEFFICIENT ∞ INFINITY

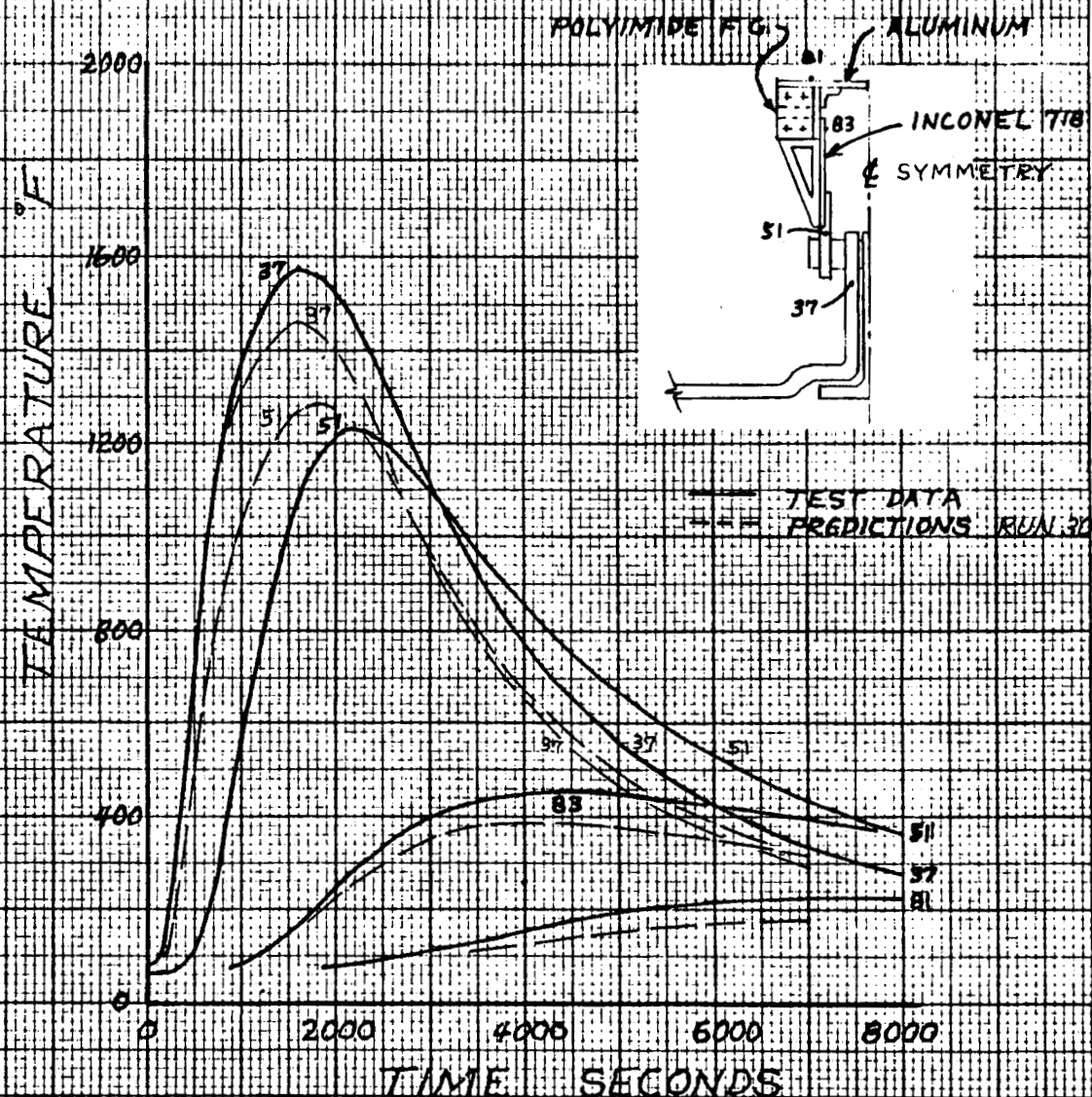


FIGURE 30 POST-TEST PREDICTIONS

THERMAL MODEL USED FOR PREDICTIONS :

- CROSS RADIATION INSIDE BRACKET CUT-OUTS
- INCONEL CONDUCTIVITY INCREASED BY 20.7%
- CONTACT COEFFICIENT = INFINITY

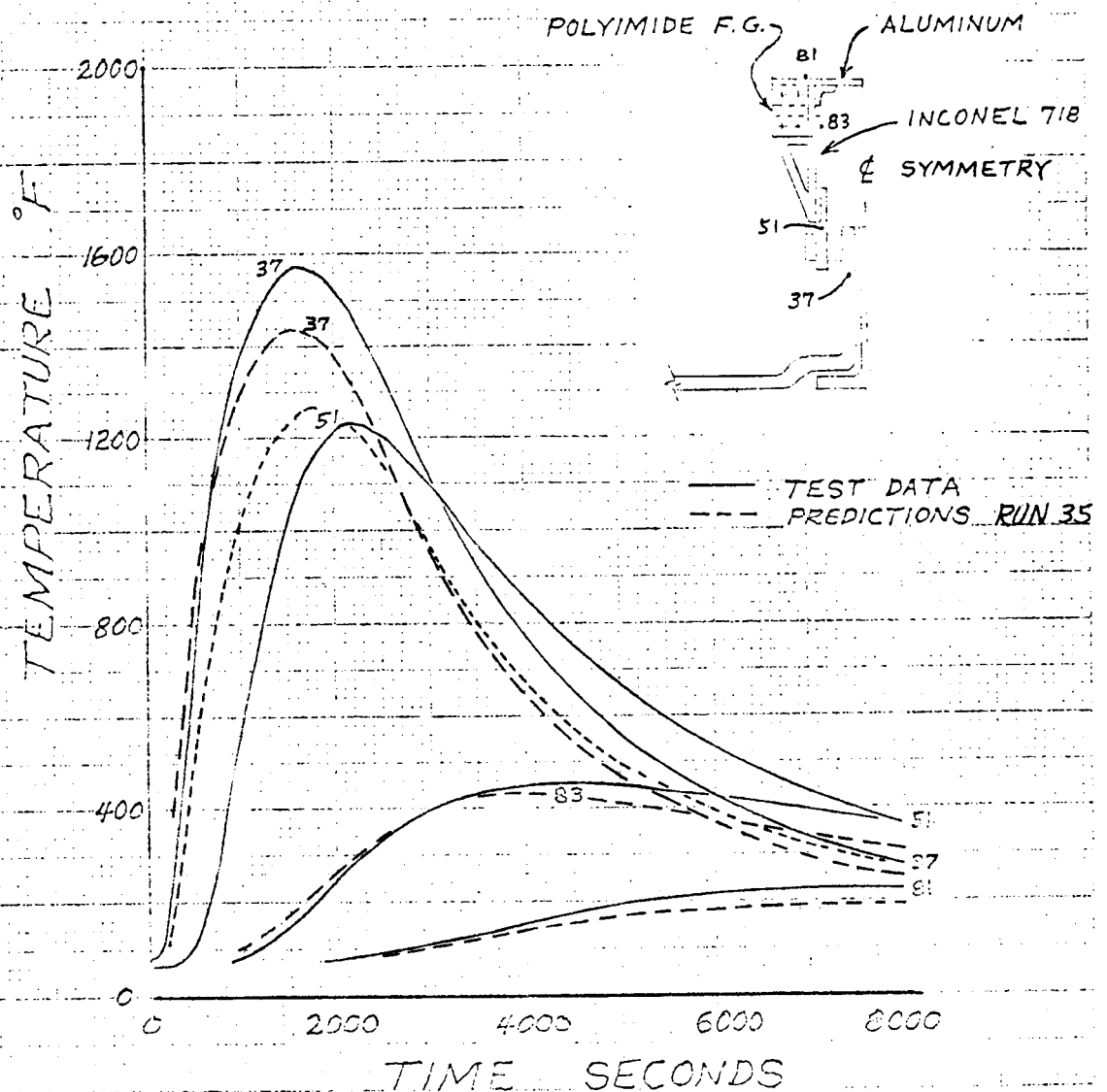
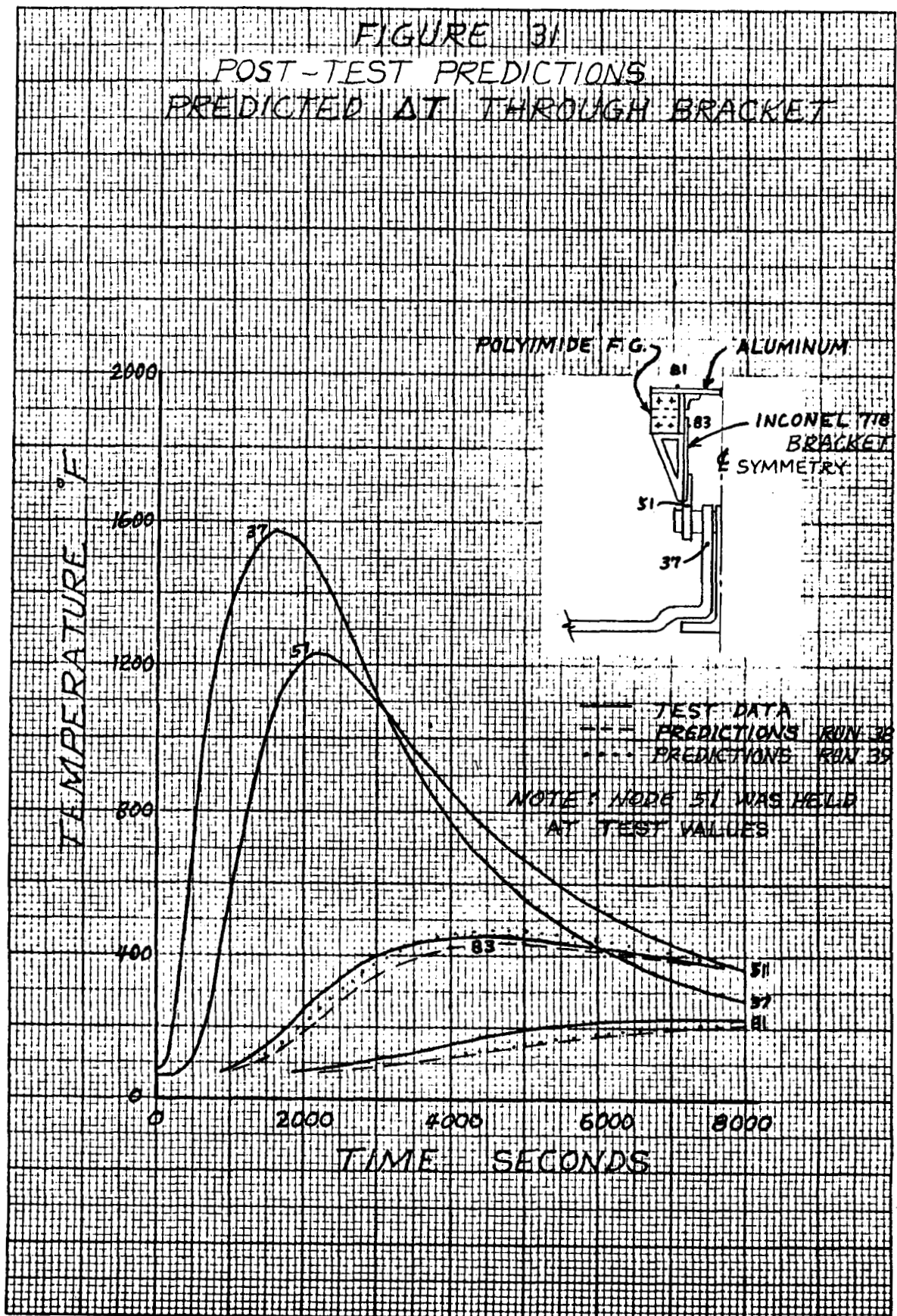


FIGURE 31
POST-TEST PREDICTIONS
PREDICTED AT THROUGH BRACKET



insulation and the bracket. All runs after 39 also used the decreased conduction to the insulation.

One of the greatest unknowns involved in the construction of the thermal model of the test configuration was the joint contact coefficients at the interface of the RPP and the inconel sleeve and spacers. A review of joint coefficient test data generated on a previous RPP program, Reference 6, indicated that a contact coefficient of $100 \text{ BTU/hr ft}^2\text{°F}$ was a reasonable value to use for the lug joint configuration. That test data, which was obtained at lower temperatures than occurred during the lug tests, also indicated that the coefficients increased considerably with temperature.

The results of Runs 27 and 29 presented on Figure 32 show that much better agreement with test data is obtained for the first 700 seconds of time by using a coefficient of $25 \text{ BTU/hr ft}^2\text{°F}$ instead of infinity. During this time the joint temperatures are relatively low. After a time of 700 seconds the use of a coefficient of $25 \text{ BTU/hr ft}^2\text{°F}$ results in a much too large predicted temperature drop across the joint (from nodes 37 to 51). This indicates that as the temperatures at the joint increase the actual contact conduction coefficient increases. Run 34 was made to show the effect of a step change in the contact coefficient from $25 \text{ BTU/hr ft}^2\text{°F}$ to infinity at a time of 500 seconds. The results of this run are plotted in Figure 33, and show that a step change does not yield satisfactory predictions.

It should be noted here that the lug test configuration is thermally satisfactory even if the contact coefficient for flight conditions is infinite throughout reentry. Results of Runs 12 and 14 showed that increasing the coefficient from $100 \text{ BTU/hr ft}^2\text{°F}$ to infinity results in about a 100°F increase in the peak temperature of the polyimide; a 150°F margin in this temperature occurred for the lug test.

The thermal model of the joint area was changed to make the thermal conductivity curve for the inconel at the contact surfaces represent a temperature

FIGURE 32
POST-TEST PREDICTIONS
EFFECT OF CONTACT COEFFICIENT
THERMAL MODEL USED FOR PREDICTIONS:
• NO INSULATION OR RADIATION INSIDE THE
BRACKET CUT-OUTS
• CONTACT COEFFICIENT = INFINITY FOR RUN 29
AND 25 BTU/HR-FT²-°F FOR RUN 27

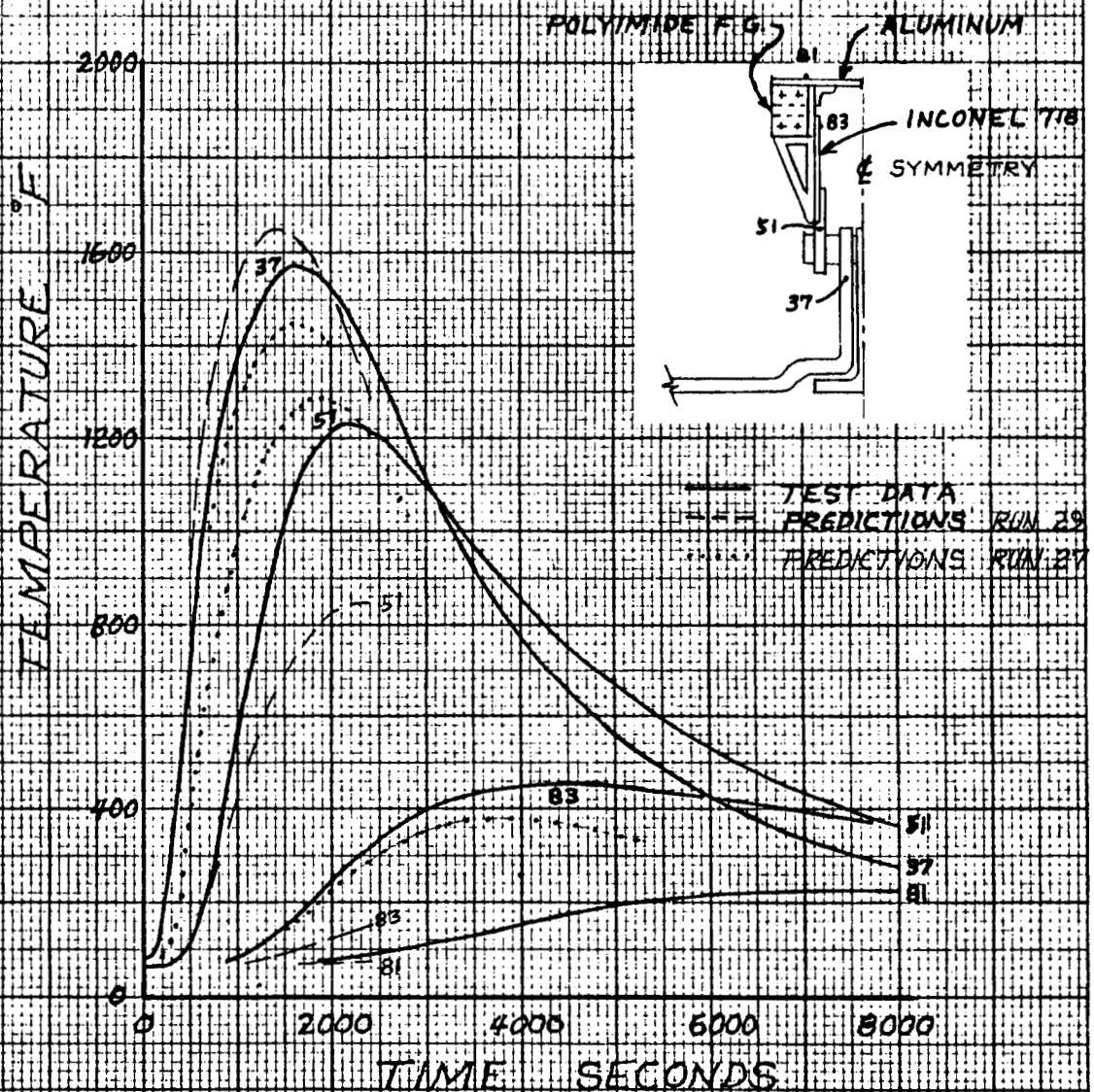
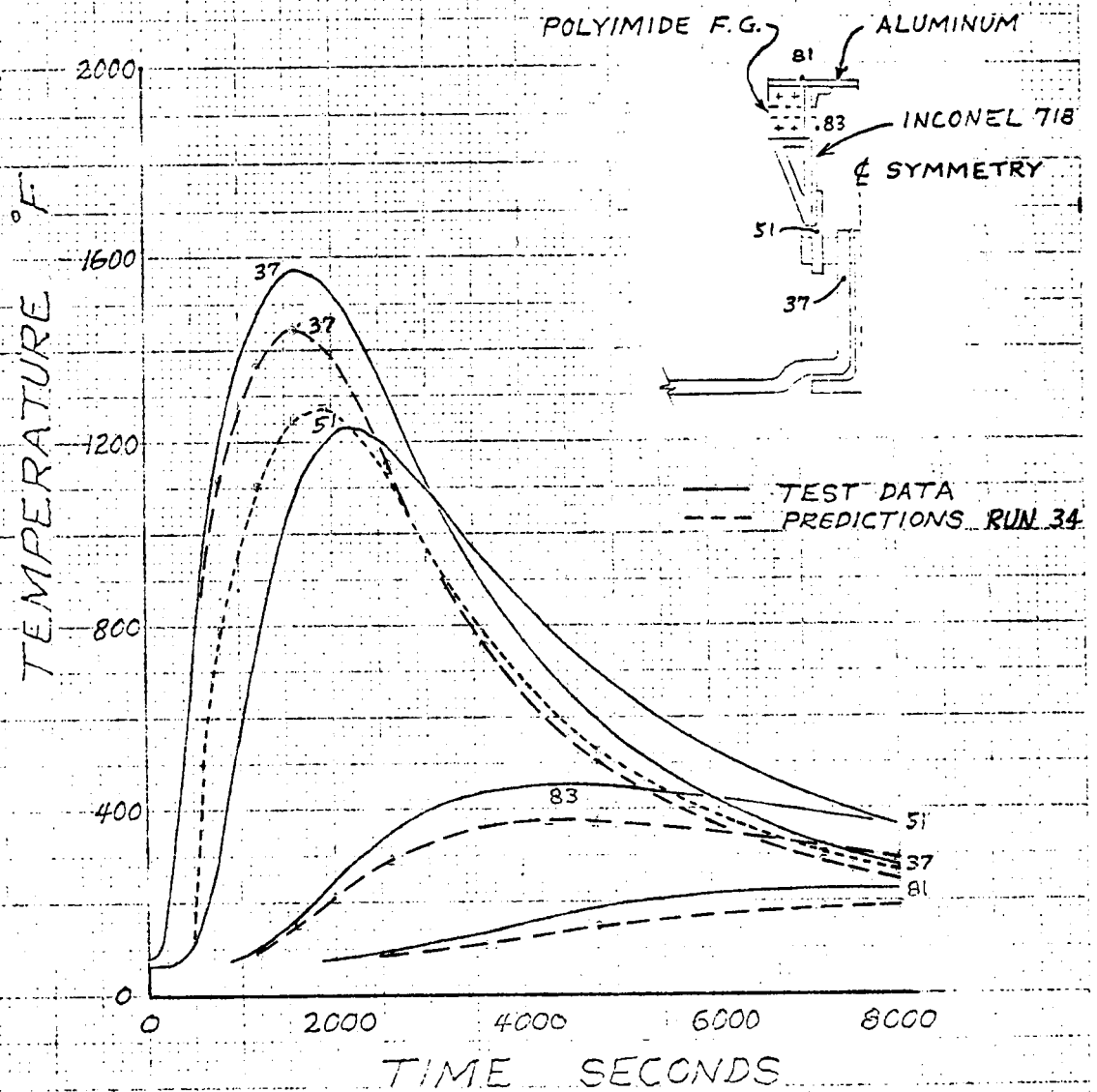


FIGURE 33
POST-TEST PREDICTIONS
EFFECT OF CHANGE IN CONTACT COEFFICIENT
• INSULATION INSIDE BRACKET CUT-OUTS
• CONTACT COEFFICIENTS = INFINITY AFTER 500 SEC
25. BTU/HR-FT²-°F FROM 0 TO 500 SEC.



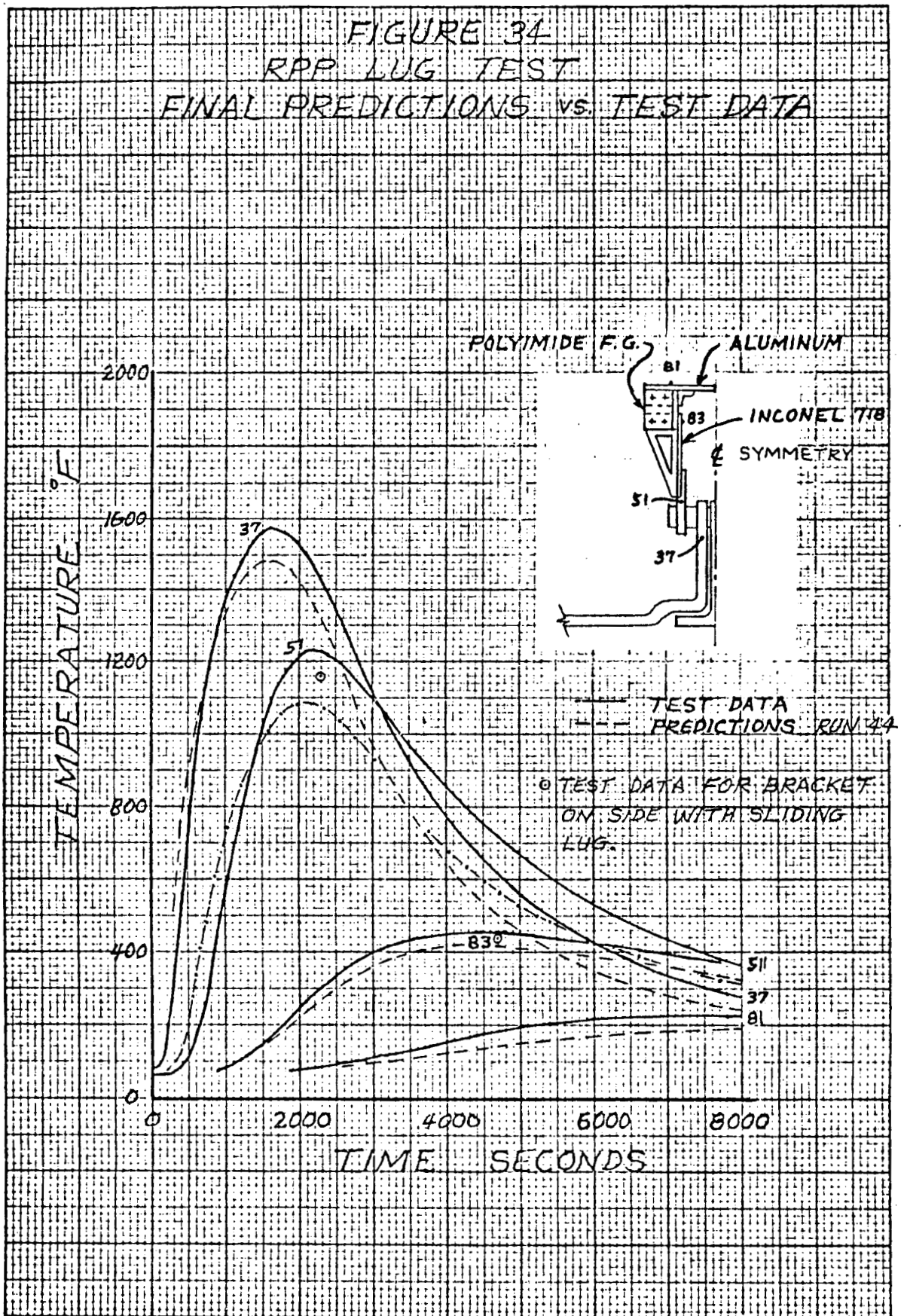
dependent joint coefficient and the results are presented in Figure 34 for Run 44. The joint coefficient varied from 25 BTU/hr ft²°F at 180°F to 40,000 BTU/hr ft²°F at 2000°F. This run also included the 20% increase in inconel conductivity which the results of Run 39 indicated to be required.

These changes resulted in much better agreement with test data. It is recommended that flight predictions be made with the increased inconel conductivity but with an infinite contact coefficient in order to be conservative.

Figure 34 shows that the predicted peak temperature of the RPP lug (node 37) near the joint is 100°F lower than test data even though the predicted temperature of the hot end of the inconel (node 51) is also 140°F lower than the test data. Part of the reason for this difference between the predictions and test data is that more than half the total heat input to the aluminum traveled through the fixed lug as was discussed previously. (Peak temperature on the hot and cold ends of the bracket for the sliding lug are shown in Figure 34 for reference. Peak temperature drop through the sliding bracket was 95°F less than for the fixed side.) The thermal model of the test configuration was prepared for the fixed lug, and it was assumed that the article was symmetrical about the center line of the T-seal strip with half of the total heat applied to each side of the center line.

Note from Figure 34 that after a time of 1500 seconds, all the predicted temperatures are considerably below the test data. This tends to indicate that more heat was input to the RPP than was simulated in the predictions. In order to increase the predicted temperatures to the test values one of the following methods would be required, (1) increase the thermal conductivity of the RPP so that node 37 would get hotter or (2) increase the RPP skin temperatures to values greater than those recorded during the test. Since there is no test data to justify making either of these changes the results of Run 43 are considered the final predictions.

FIGURE 34
RPP LUG TEST
FINAL PREDICTIONS VS. TEST DATA



CONCLUSIONS

(1) Results of the lug tests indicate that the lug design is thermally satisfactory. Thermal margins on the two critical items, the polyimide and aluminum peak temperatures, are 150°F and 120°F respectively.

(2) The final thermal model of the lug test article yields temperatures which agree fairly closely with the test data.

APPENDIX

MATERIAL THERMAL PROPERTIES

Thermal property data used in the analyses, but not presented in Reference 4, are presented herein. Material densities are presented in Table 1. Note also that Table 1 is an index to the other tables.

TABLE 1

MATERIAL, THERMAL PROPERTIES

MATERIAL	DENSITY $\rho = \text{lb/ft}^3$	SPECIFIC HEAT $C_p = \text{BTU/lb}^\circ\text{F}$ or TABLE NO.	THERMAL CONDUCTIVITY $K = \text{BTU in/hr ft}^2^\circ\text{F}$ or TABLE NO.
Dynaflex	12.	Table 2	Table 3
Dynaquartz	10.	Table 4	Table 5
Titanium	276.	0.1125	Table 6

TABLE 2

SPECIFIC HEAT OF DYNAFLEX, 12 PCF

Temp., $^\circ\text{F}$	-200.	0.	400.	1000.	1800.	2800.
C_p , BTU/LB $^\circ\text{F}$.2	.2	.229	.272	.292	.292

TABLE 3

THERMAL CONDUCTIVITY OF DYNAFLEX, 12 PCF

Temp., $^\circ\text{F}$	-200.	200.	300.	400.	500.	600.	700.	800.	900.
K , BTU-IN/HR $\text{FT}^2^\circ\text{F}$.27	.27	.33	.38	.43	.49	.55	.6	.66
Temp. K	1000.	1100.	1200.	1300.	1400.	1500.	1600.	1700.	
	.72	.79	.85	.92	1.0	1.07	1.16	1.24	
Temp. K	1800.	1900.	2000.	2200.	2400.	2600.			
	1.33	1.43	1.56	1.86	2.2	2.6			

TABLE 4
SPECIFIC HEAT OF DYNAQUARTZ

Temp., °F	-460.	0.	400.	1000.	1800.	2800.
Cp, BTU/LB°F	.2	.2	.299	.272	.292	.292

TABLE 5
THERMAL CONDUCTIVITY OF DYNAQUARTZ

Temp., °F	-200.	0.	200.	600.	800.	1000.	1200.
K, BTU-IN/HR FT ² °F	.4	.4	.45	.52	.59	.66	.73
10 mm Hg	.3	.3	.32	.36	.39	.42	.45
Temp.	1400.	1600.	1800.	2000.	2200.	2400.	
K	.81	.9	.1	1.11	1.17	1.37	
10 mm Hg	.49	.55	.62	.68	.775	.9	

TABLE 6
THERMAL CONDUCTIVITY OF TITANIUM

Temp., °F	-460.	100.	200.	300.	400.	1000.
K, BTU-IN/HR FT ² °F	50.5	50.5	51.6	54.	60.	96.

DESIGN INFORMATION REQUEST - RELEASE

A. 1-8-73
1-2-73

REL (S) AND EFF. Task 1 - Fail Safe Leading Edge Thermal Analysis		DIR. NO. T143-DIR-2-19		REV. A
		DATE 1/8/73	PAGE 1	OF 49
SYSTEM Phase III Shuttle Leading Edge		REF. G. O. NUMBER 3357-AA-1160		

Fill in block below for Information Request		Fill in block below for Information Release	
GROUP _____		IN REPLY TO DIR. NUMBER _____	
BY _____		REL. TO D. M. While GROUP 3-52000	
ASON _____		PREPARED BY J. E. Medford DATE 12/20/72	
ONLY <input type="checkbox"/> BWR <input type="checkbox"/> BUWEPs <input type="checkbox"/> _____		CHECKED BY 1-8-73 DATE 12/20/72	
		GROUP APPR. DATE 12/20/72	
		PROJ OFFICE DATE 12/22/72	

T. Esenwein, E. Matza, B. A. Forcht, W. E. Agan, R. J. Copeland

DESIGN INFORMATION:

INTRODUCTION

Thermal analysis of the fail safe leading edge includes determination of skin thickness, temperature distributions in skin and ribs, and insulation requirements for various elements of the assembly. Calculation of skin thickness and temperature distributions in skin and ribs was covered in a previous Task I document, T143-DIR-2-07. Selection and preliminary sizing of candidate insulation materials for the canted heat shield were accomplished as part of Task 2 and were documented in T143-DIR-2-13. Thermal design of the lower, windward side support lug was performed in Task 3 and documented in T143-DIR-2-11 and T143-DIR-2-18.

This DIR includes final sizing and thermal analysis of the canted heat shield and upper panel insulation, bulk insulation around support lugs, lower panel insulation, and the upper support lug thermal design. Dynaquartz insulation, in 10 PCF density for the canted heat shield, upper and lower panels, and in 15 PCF density for the support lugs, was selected over reusable surface insulation for the full scale test article considered herein, because of availability and cost advantages. Thermal properties used in these analyses are documented in the DIR's outlined above and will not be repeated herein.

Revision A has to do with only the predicted temperatures for the leeward side lug area, and affects only pages 47, 48, and 49.

CANTED HEAT SHIELD AND UPPER PANEL

These two elements of the design are considered jointly due to thermal coupling between them. Sizing of the insulation thickness in each area, which ignored this coupling, will be discussed first, followed by analysis of the coupling effect, heat shorts due to gaps in the insulation, and heat shorts due to the titanium rib truss.

Canted Heat Shield Sizing

Thermal analyses were performed to size the thickness of Dynaquartz, 10 lb/ft³ density, required on the canted heatshield for the test article. The thermal model employed is shown in Figure 1. The thickness of forward insulation was sized to limit the first bondline temperature to 600°F and the aft thickness was sized to limit the aluminum substructure temperature to 350°F. Initial temperature was assumed to be 130°F.

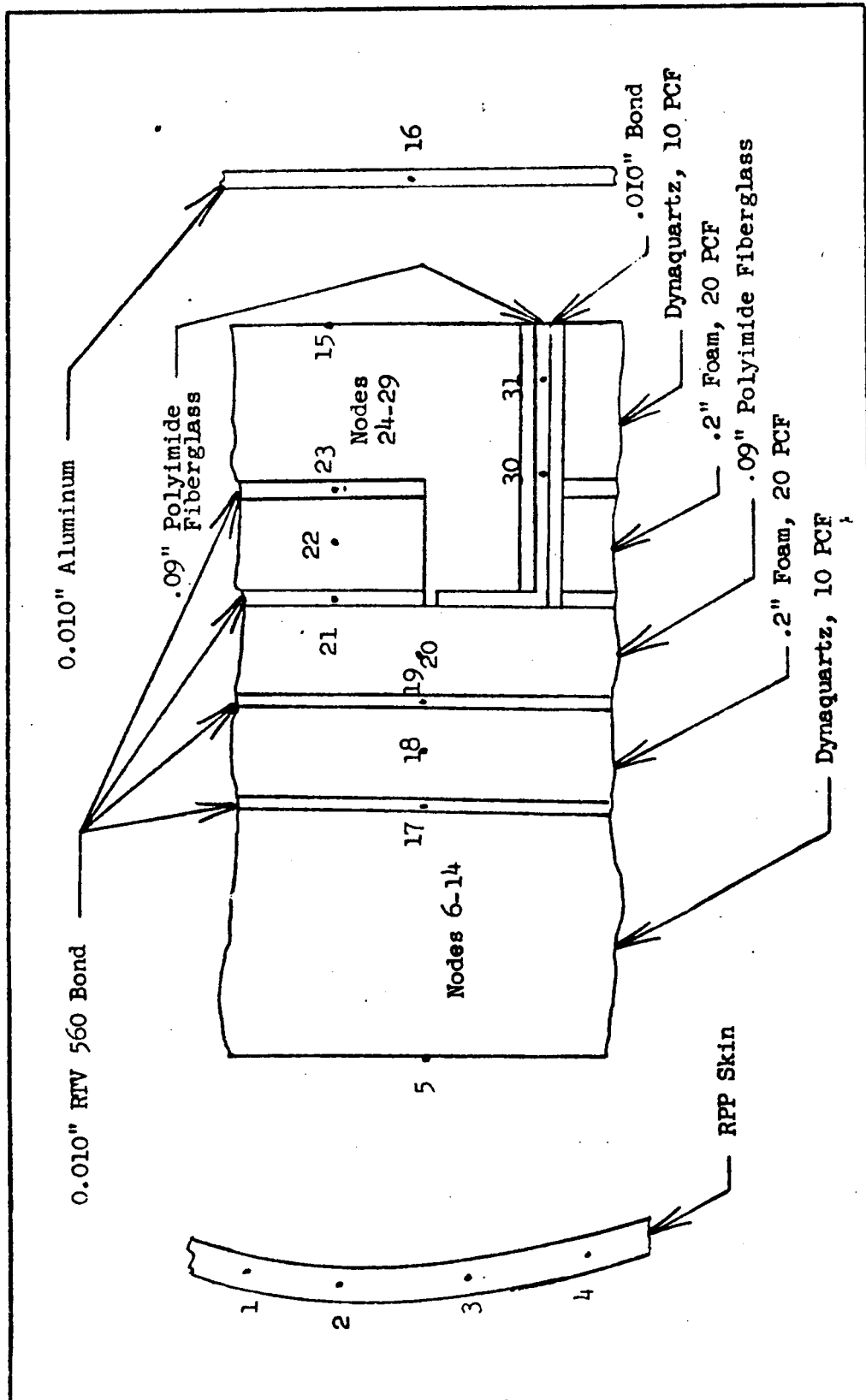
Table I presents the peak computed temperatures of the first bondline and of the aluminum for various insulation thicknesses.

TABLE I DYNAQUARTZ HEATSHIELD SIZING RESULTS

<u>Forward Insulation Thickness, Inches</u>	<u>Aft Insulation Thickness, Inches</u>	<u>Bondline Temperature, °F</u>	<u>Aluminum Temperature, °F</u>
2.5	1.0	358	275
2.0	1.0	439	297
1.5	1.0	562	346

On the basis of these results the heatshield configuration will employ 1.5 inches thick Dynaquartz forward and 1.0 inch Dynaquartz on the aft side. Since analysis is based on an initial temperature extreme of 130°F no arbitrary margins were incorporated. However, bondline temperature could be permitted to rise to at least 650°F without loss of bond integrity, based on VMSC bond tests, thus providing structural margin. Further, coupling effects between the canted heat shield and upper panel will reduce the aluminum temperature, providing additional margin as will be discussed later.

Figure 1
THERMAL MODEL FOR HEATSHIELD SIZING



Upper Panel Insulation Sizing

The inside surface of the upper RSI panel radiates to the aluminum structure (350°F temperature limit) therefore it is important that the temperature of the inside of the panel be controlled satisfactorily. The aft side of the canted heat shield also radiates to the aluminum as discussed previously in connection with the design of the canted heat shield. In the heat shield analyses it was assumed that the radiation view factor was 1.0 from the aft side of the heat shield to the aluminum. Therefore in the preliminary analyses of the upper panel the following criterion was used: The temperature of the inside surface of the panel must be equal to or less than the temperature of the aft side of the canted heat shield.

Thermal analyses were performed for the upper panel using a one dimensional thermal model. Figures 2 and 3 show the predicted temperatures of the inside surface of the panel at the forward and aft end, respectively, with no inside insulation. The temperatures of the aft side of the canted heat shield and of the aluminum are included on the figures for comparison. The panel inside temperatures increase faster and are greater than that of the insulation surface on the aft of the canted heat shield up till a time of about 3500 seconds. Thereafter, the temperatures of the panel decrease and after a time of 5000 seconds are less than that of the aft surface of the canted heat shield.

Adding insulation inside the upper panel would reduce the inside temperature, but since design considerations make it desirable to have no insulation inside the upper panel, additional analysis was performed with a more complete thermal model to determine if the initial design criterion was too severe. Results of those analyses, discussed in the next section, show that no insulation is required on the inside surface of the upper panel structure.

Combined Canted Heat Shield and Upper Panel

Thermal analyses were performed to determine the effect of coupling between the thermal response of the upper panel and the canted heat shield upon titanium and

FIGURE 2
PREDICTED TEMPERATURES
UPPER PANEL - FORWARD END

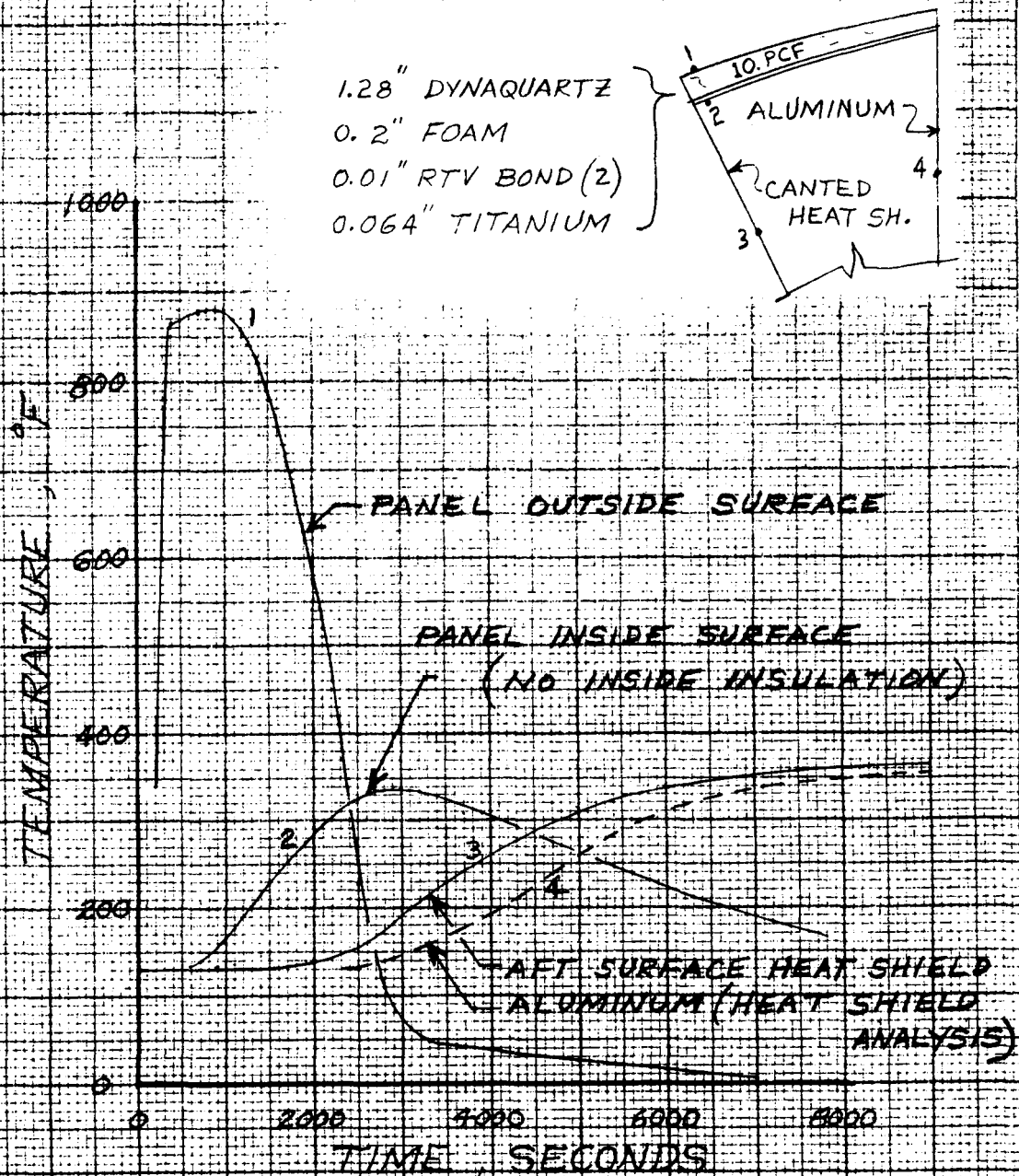
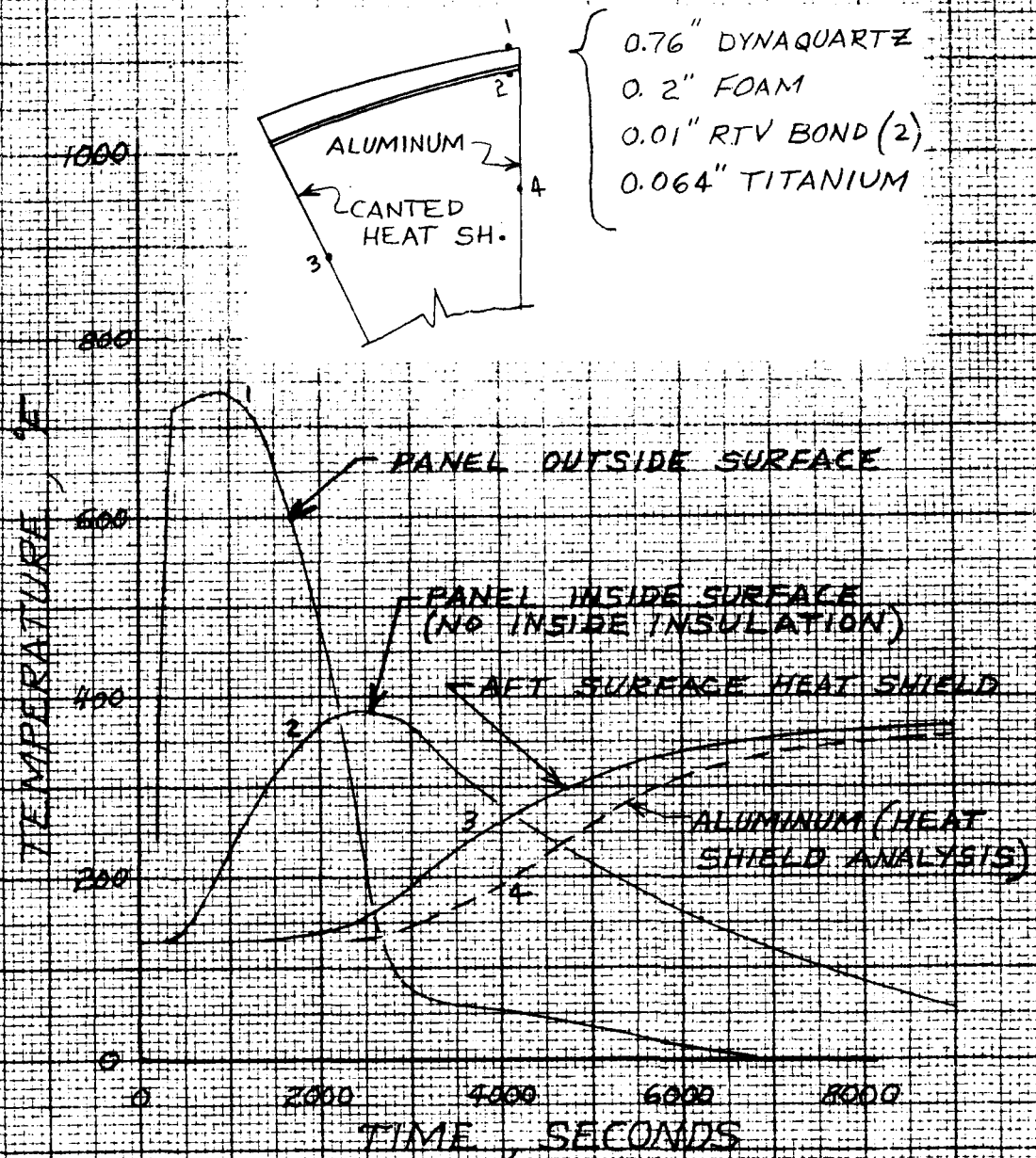


FIGURE 3
PREDICTED TEMPERATURES
UPPER PANEL AFT END

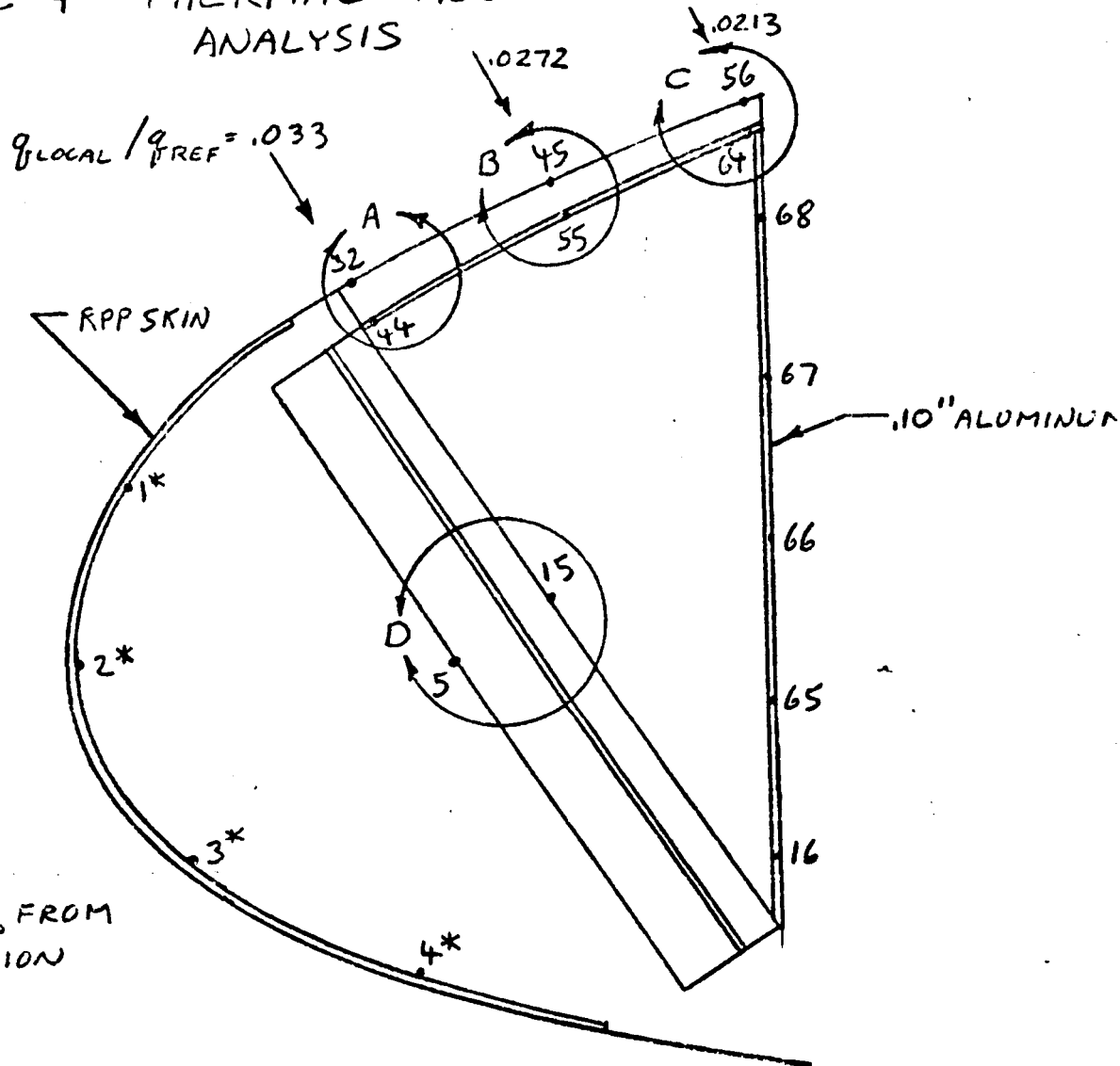


aluminum structural temperatures and insulation bondline temperatures. The thermal model employed is shown in Figure 4. Insulation thicknesses of Dynaquartz, 10 Lb/Ft³ density, were taken from results of thermal analyses discussed above. The model included effects of cross radiation between the back surface of the canted heat shield aft insulation, the titanium structure for the upper panel, and the aluminum spar. Heat conduction between the titanium and aluminum was also included, as was free convection in the forward and aft cavities.

Maximum computed temperatures are summarized in Figure 5. It is seen that the maximum bondline temperature on the heat shield is 572°F, which is 10°F higher than was computed with the previous thermal model which did not include the upper panel. However, this temperature is still within acceptable limits. The peak aluminum temperature is 293°F compared to 346°F with the previous model. The peak titanium temperature is 271°F forward and 262°F aft compared to 345°F and 382°F, respectively, computed previously. These reductions are due to heat interchange between the titanium and aluminum, whose temperatures tend to peak at different times.

Analyses discussed in the previous sections, which did not include heat transfer between the titanium and aluminum, indicated that the titanium forward end would peak at 345°F at 3000 seconds, at which time the aluminum would be at 165°F. The temperature-time curves in Figure 6 for the current analysis show that heat transfer from the titanium to the aluminum reduces the titanium temperature at this time to 260°F and increases the aluminum to 232°F. Conversely, previous analyses indicated the aluminum would peak at 346°F at 7700 seconds, when the titanium was only at 170°F. As shown in Figure 6, heat transfer from the aluminum to the titanium causes the aluminum temperature to peak earlier at 5400 seconds, and reduces the peak aluminum temperature to 293°F, while increasing the titanium to 271°F. The reason for the tendency of the titanium temperature to peak earlier than the aluminum is that the upper panel is much thinner than the canted heat shield. An additional reason for the lower temperature in the current analysis is that the aluminum spar is 12% longer than the canted heat shield, providing additional heat sink which was

FIGURE 4 THERMAL MODEL FOR HEAT SHIELD ANALYSIS



INPUT TEMPS., FROM
CROSS RADIATION
ANALYSIS

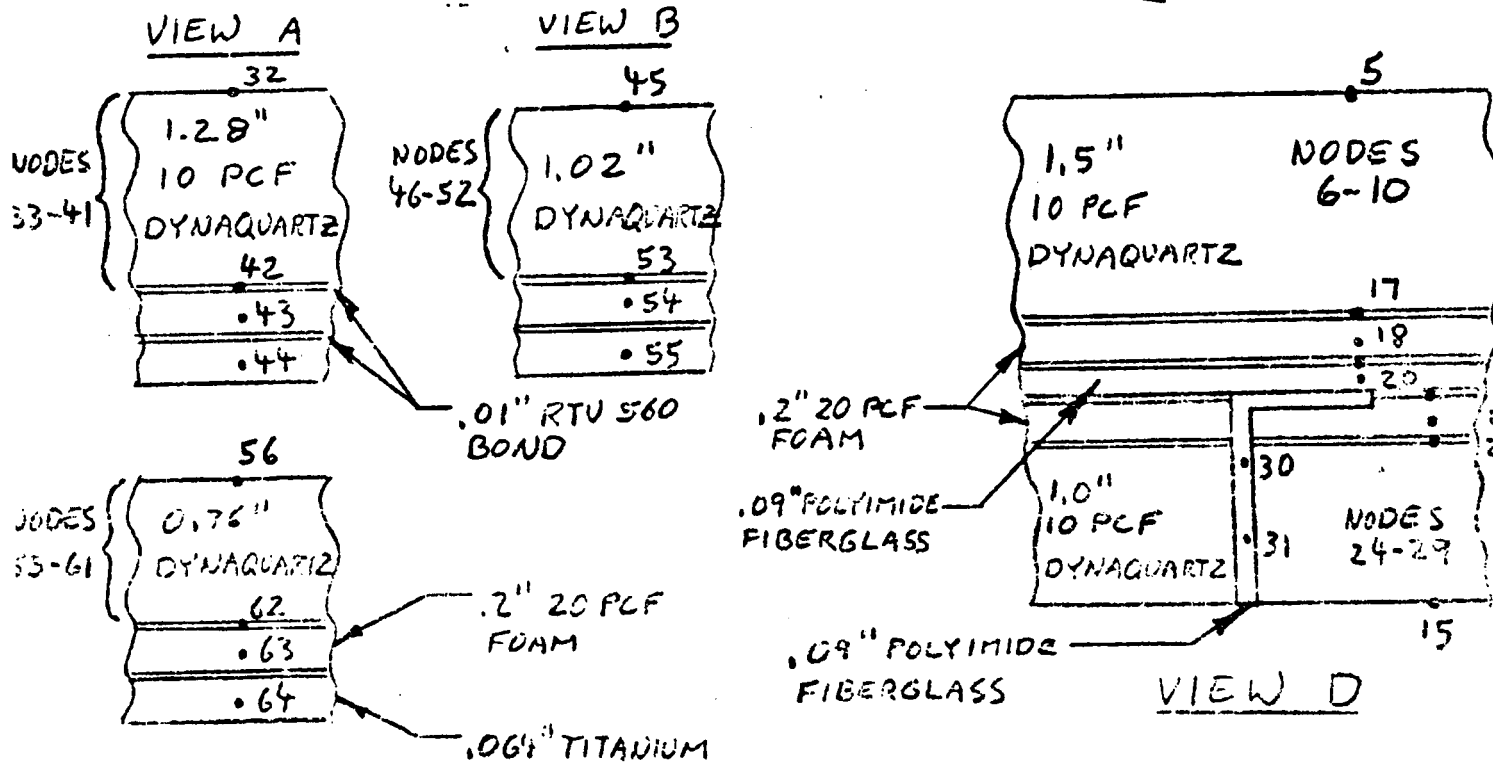
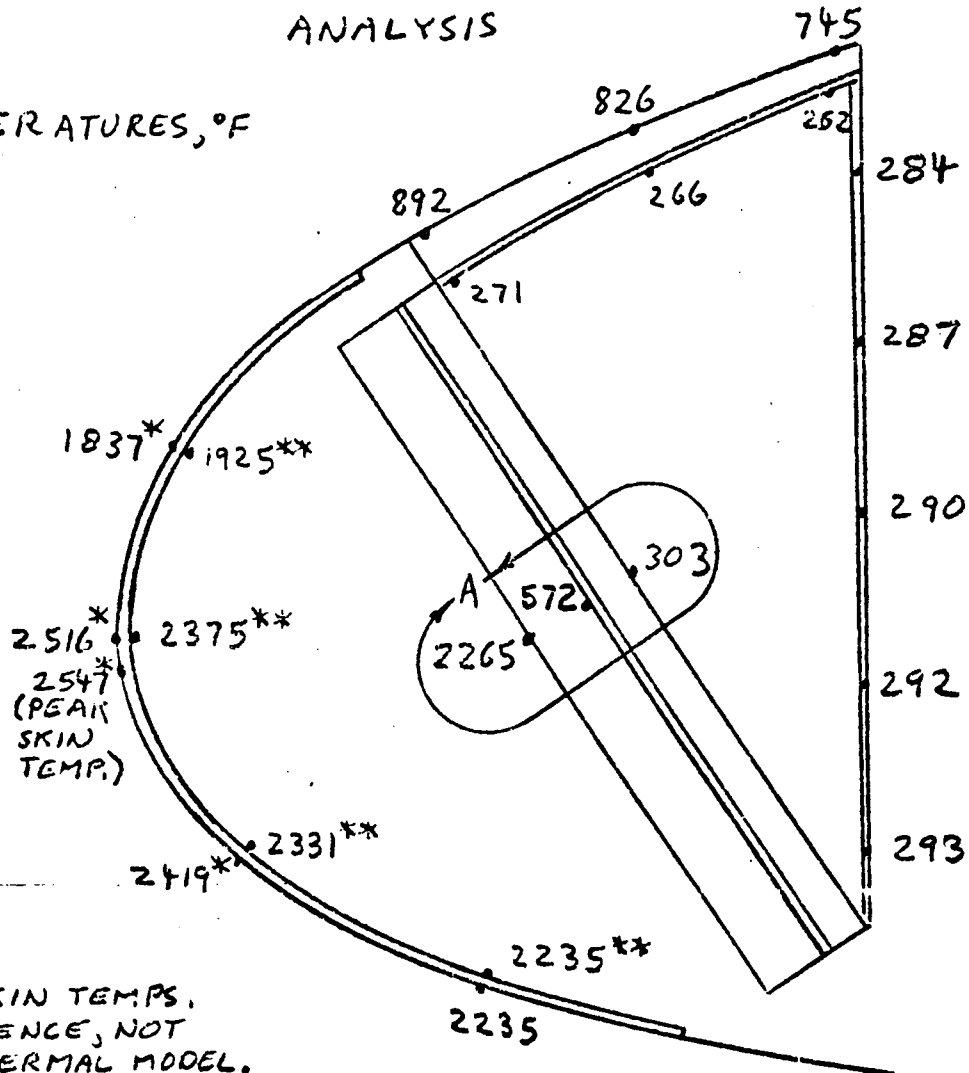


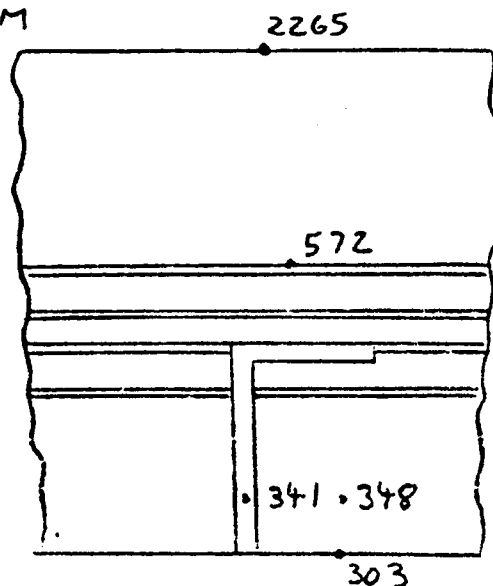
FIGURE 5 MAXIMUM TEMPERATURES FROM HEAT SHIELD ANALYSIS

TEMPERATURES, °F

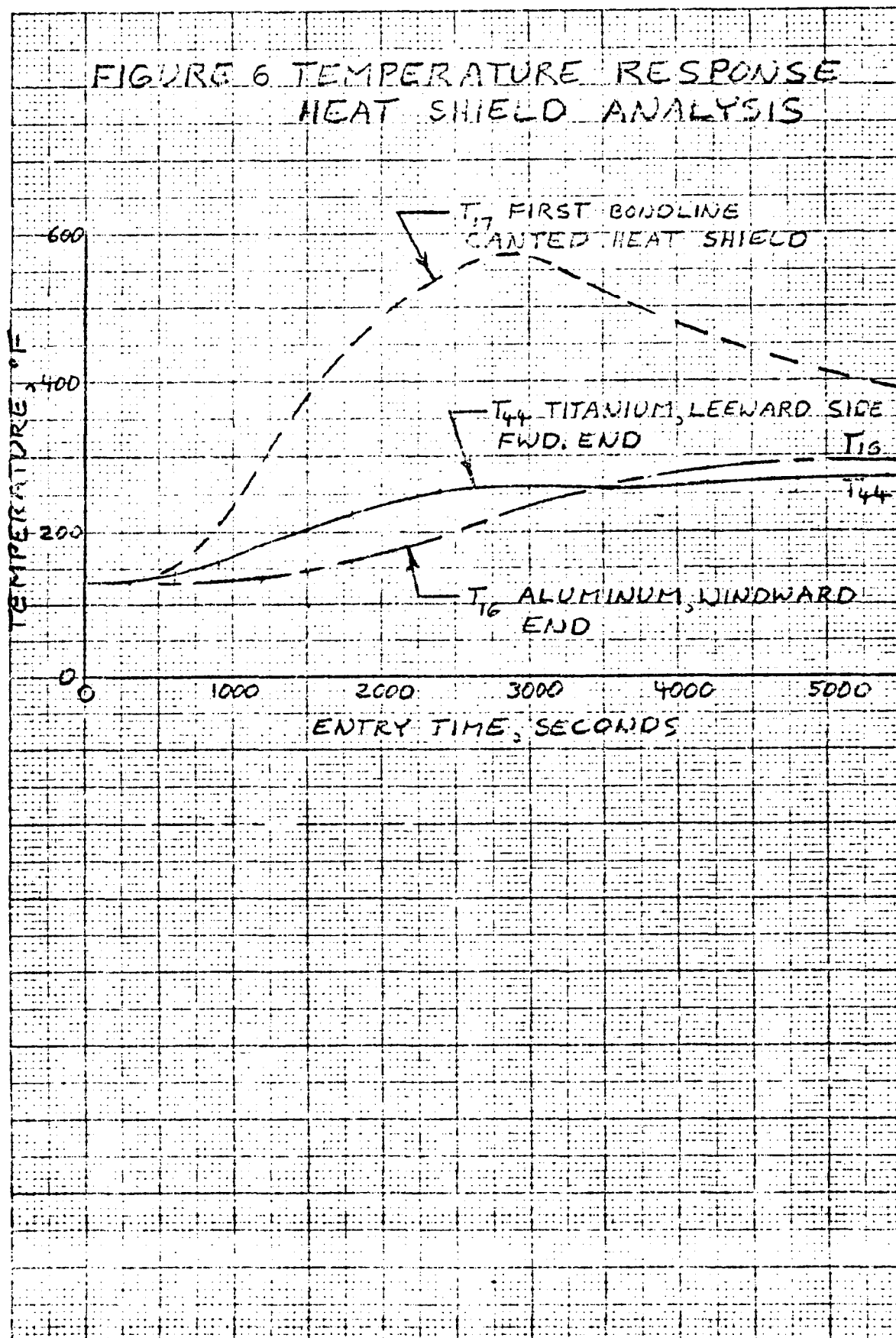


* OUTSIDE SKIN TEMPS.
FOR REFERENCE, NOT
PART OF THERMAL MODEL.

** INPUT TEMPS. FROM
CROSS RADIATION
ANALYSIS.



VIEW A



not included in the previous analyses.

In summary, results of the current analysis indicate a substantial improvement in temperature margin for the structural panels and only a slight increase in bondline temperature, as compared with previous analyses.

Titanium Rib Truss

A 94 node, three-dimensional thermal model was developed for the titanium rib truss-aluminum spar interface region on the windward side of the heatshield. The purpose of this model is to evaluate the potential heatshort across the lower portion of the rib truss into the aluminum. The model is shown in Figures 7-10 and includes not only the heat short itself, but also radiation from the aft side of the aft insulation to the aluminum and conduction across the polyimide support bracket.

Maximum computed temperatures in the aluminum are shown in Figure 11, which shows that the 0.23 inch thick polyimide rib truss insulation adequately protects the aluminum in the heat short area.

Insulation Gap Effect

Previous analysis with no radiation gaps in the aft side of the canted heat shield has shown that the predicted maximum temperature of the aluminum is well below the allowed 350°F. Since the margin on the aluminum temperature is considerable, a conservative simplified method was used to determine the predicted temperature increase of the aluminum due to radiation from the gaps in the heat shield.

The total area on the aft side of the canted heat shield is 330 square inches. The gaps are 0.03" wide with a total area of 3.9 square inches which is 1.16% of the total area. In addition to the gaps there are 11 bolt holes about 0.35 square inches each with a total area of 4 square inches, which is 1.2% of the total area.

A worst case situation was assumed: the radiating surface of the RTV was assumed to be at the aft surface of the insulation and to have an emissivity of 1.0 and a view factor of 1.0 to the aluminum. The heat balance equation is:

$$\text{Heat into aluminum} = \text{Heat radiated from gap}$$

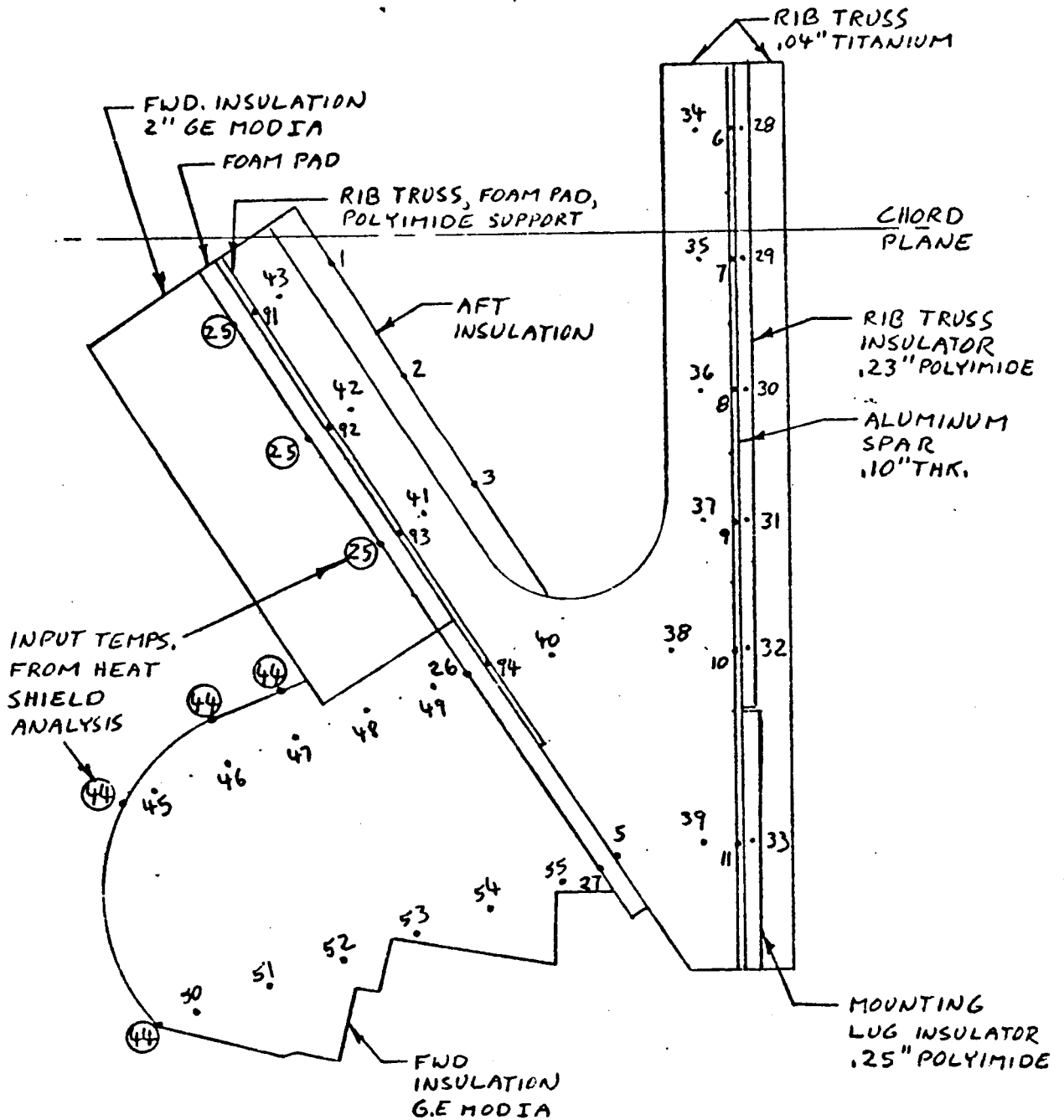
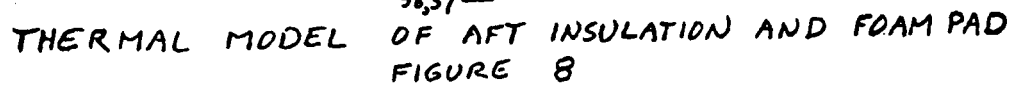
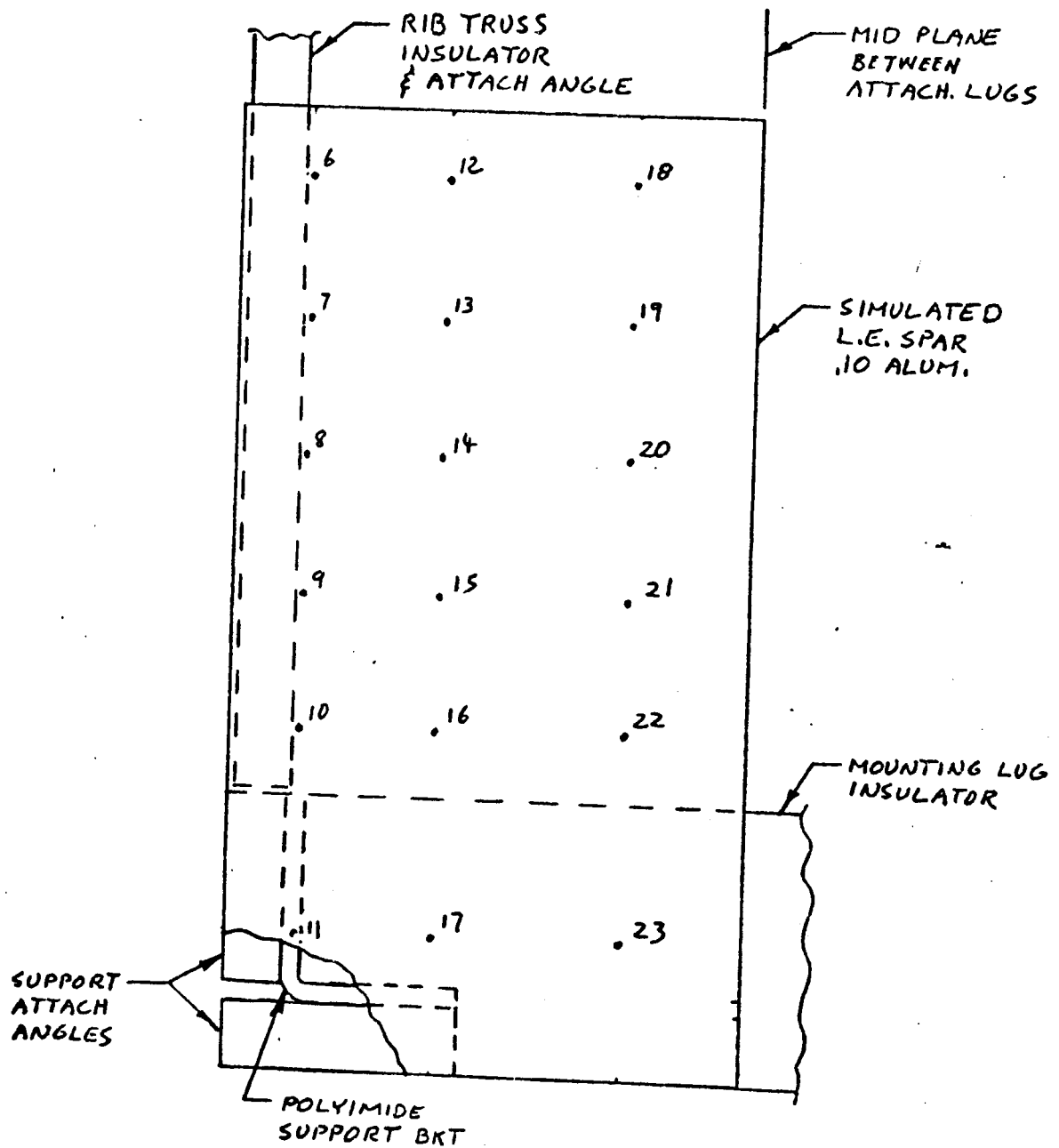
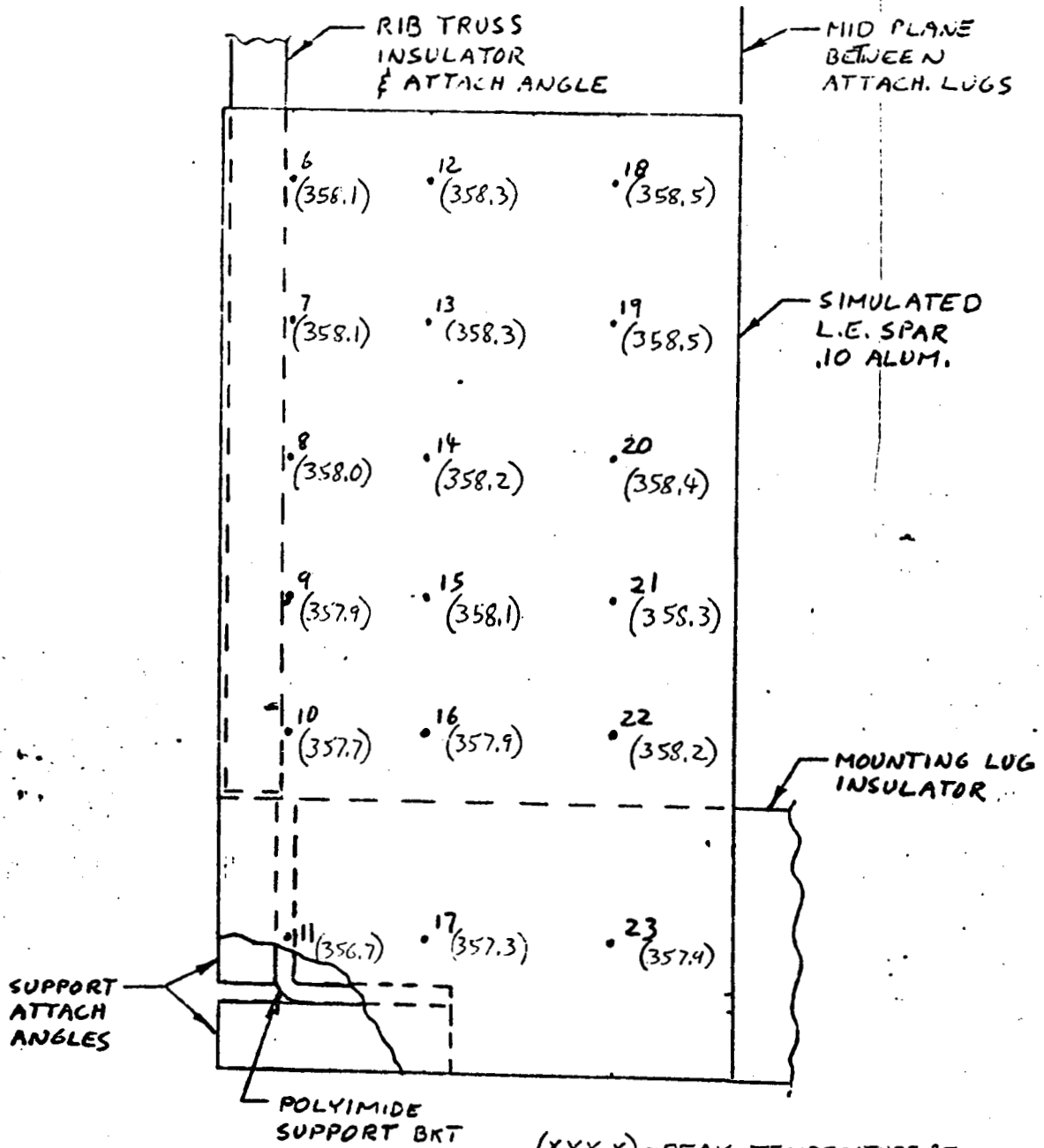


FIGURE 7
THERMAL MODEL OF RIB TRUSS, RIB TRUSS INSULATOR
AND FWD. INSULATION





THERMAL MODEL OF ALUMINUM SPAR
FIGURE 10



(XXX.X) = PEAK TEMPERATURE, °F
ENTRY TIME = 11,200 SEC. FROM 400,000 FT
INITIAL TEMPERATURE = 130 °F
PEAK TEMPERATURE OF ALUMINUM SPAR

FIGURE 11

$$(W C_p \frac{\Delta T}{\Delta \theta})_{\text{alum}} = \epsilon \sigma A F (T_g^4 - T_{\text{alum}}^4)$$

where:

$\epsilon = 1.0$ = emissivity of radiating surface

$\sigma = 0.173 \times 10^{-8}$ BTU/hrft²°F⁴

$A = 0.024$ in²

$F = 1.0$ = view factor

$C_p = 0.2$ BTU/lb°F for the aluminum

$W = .01$ lb for 1.0 in² surface by .01 inch thick aluminum

$\frac{\Delta T}{\Delta \theta}$ = change in aluminum temperature per unit of time, °R/hr

$T_g = ^\circ\text{R}$ = temperature of RTV bond surface

$T_{\text{alum}} = ^\circ\text{R}$ = temperature of aluminum

The change in temperature for the aluminum was determined in a step by step manner using temperatures for T_g and T_{alum} from previous canted heat shield analyses with no gap included. Use of these temperatures result in some conservatism since the RTV bond temperature would be slightly less with the gaps included.

Temperature increase for the aluminum using this conservative approach is calculated to be 24°F due to gap radiation. Hence, there is adequate margin in the design to account for this effect.

SUPPORT LUG BULK INSULATION

Three-dimensional thermal analyses were performed on the dynaquartz insulation around the upper and lower support lugs, including the titanium support brackets. The objectives of these analyses were to predict the insulation bondline temperatures and, for the lower lug, to evaluate the potential heat short down the titanium support bracket to the cool end of the Inconel support lug bracket.

Lower Lug Insulation Assembly

The 157 node thermal model used for analysis of the lower lug insulation assembly is shown in Figures 12, 13 and 14. This model is based on three-inch insulation

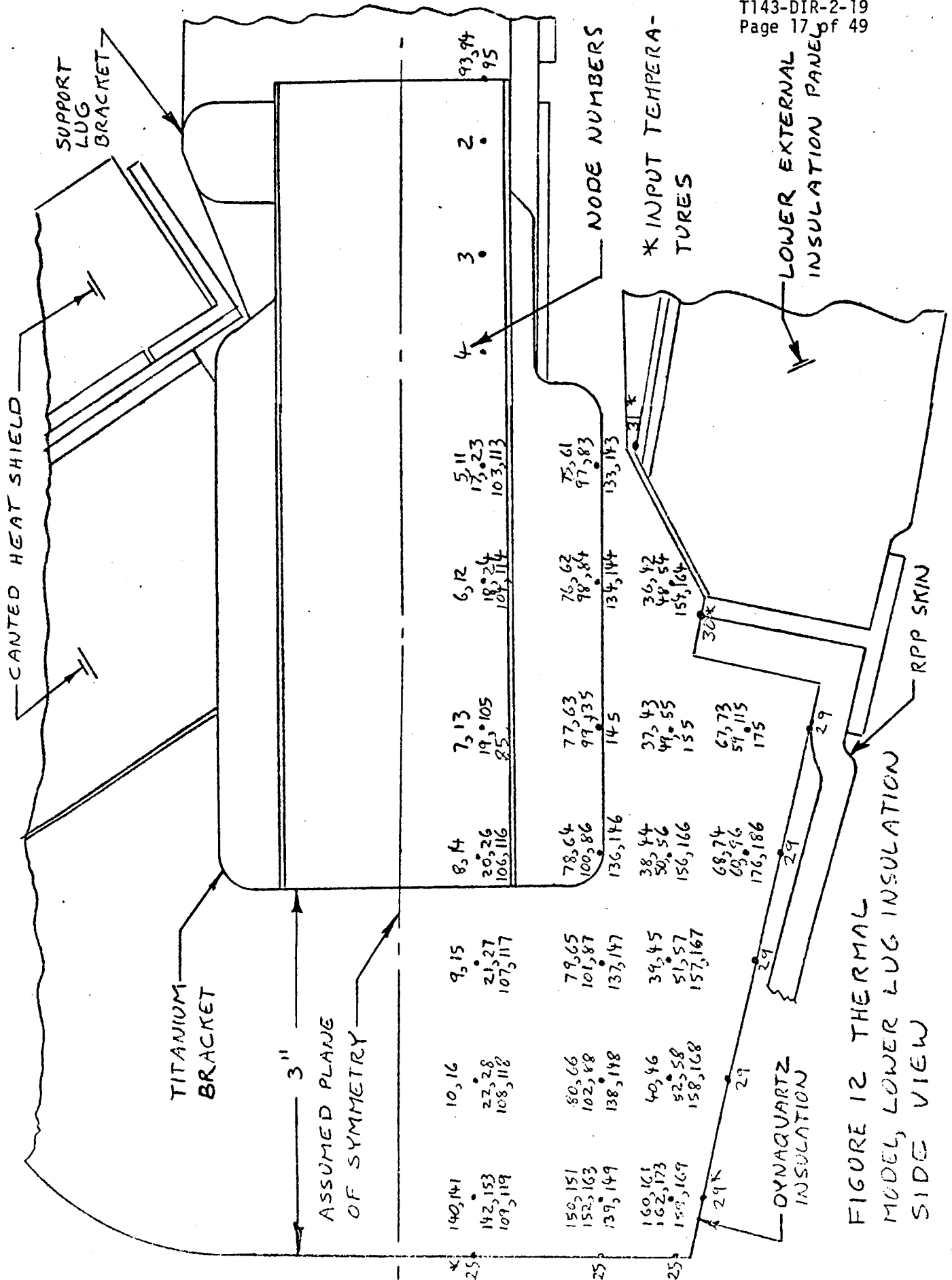


FIGURE 12 THERMAL MODEL, LOWER LUG INSULATION SIDE VIEW

FIGURE 13 THERMAL MODEL, LOWER LUG INSULATION, TOP VIEW

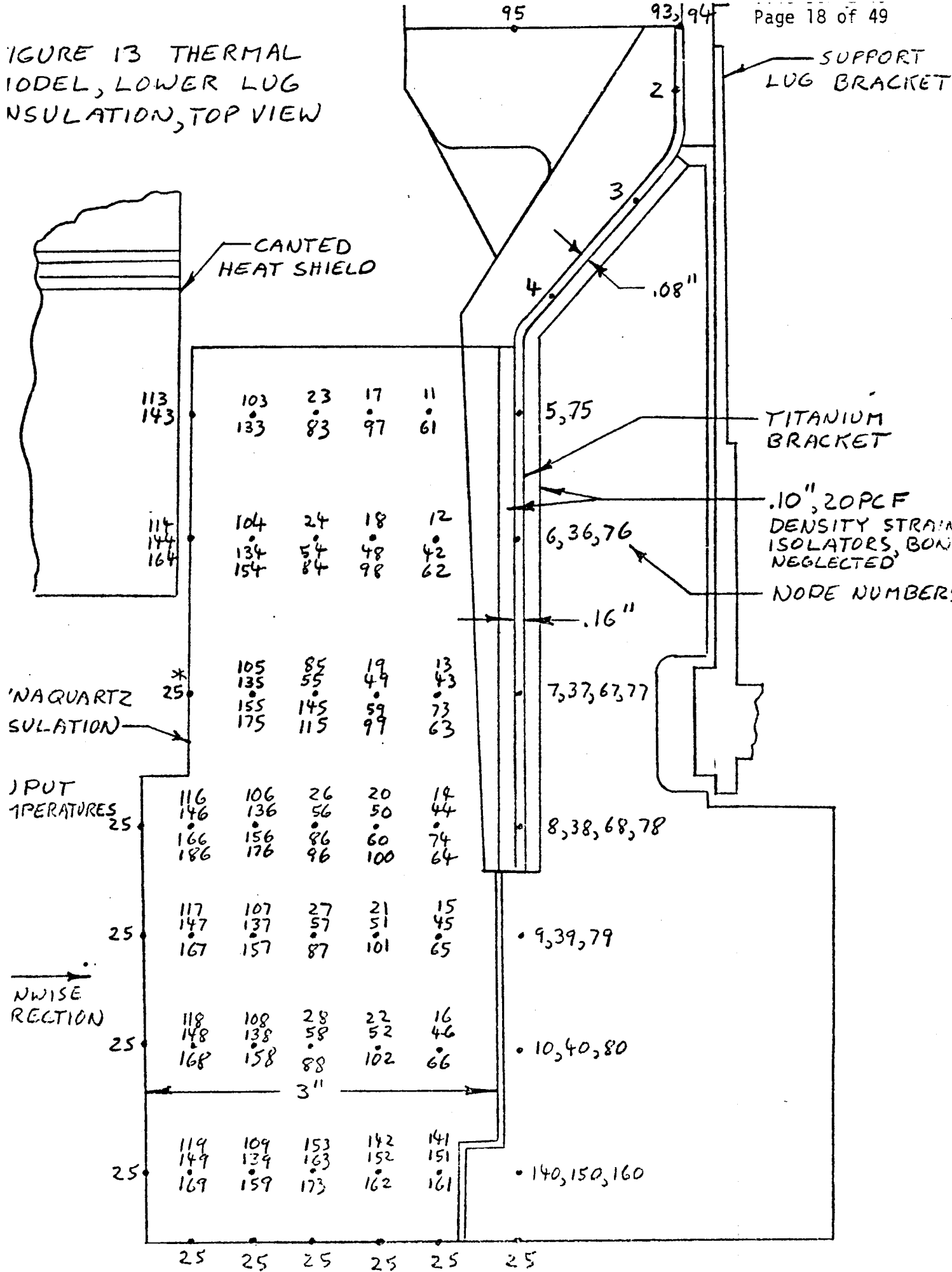
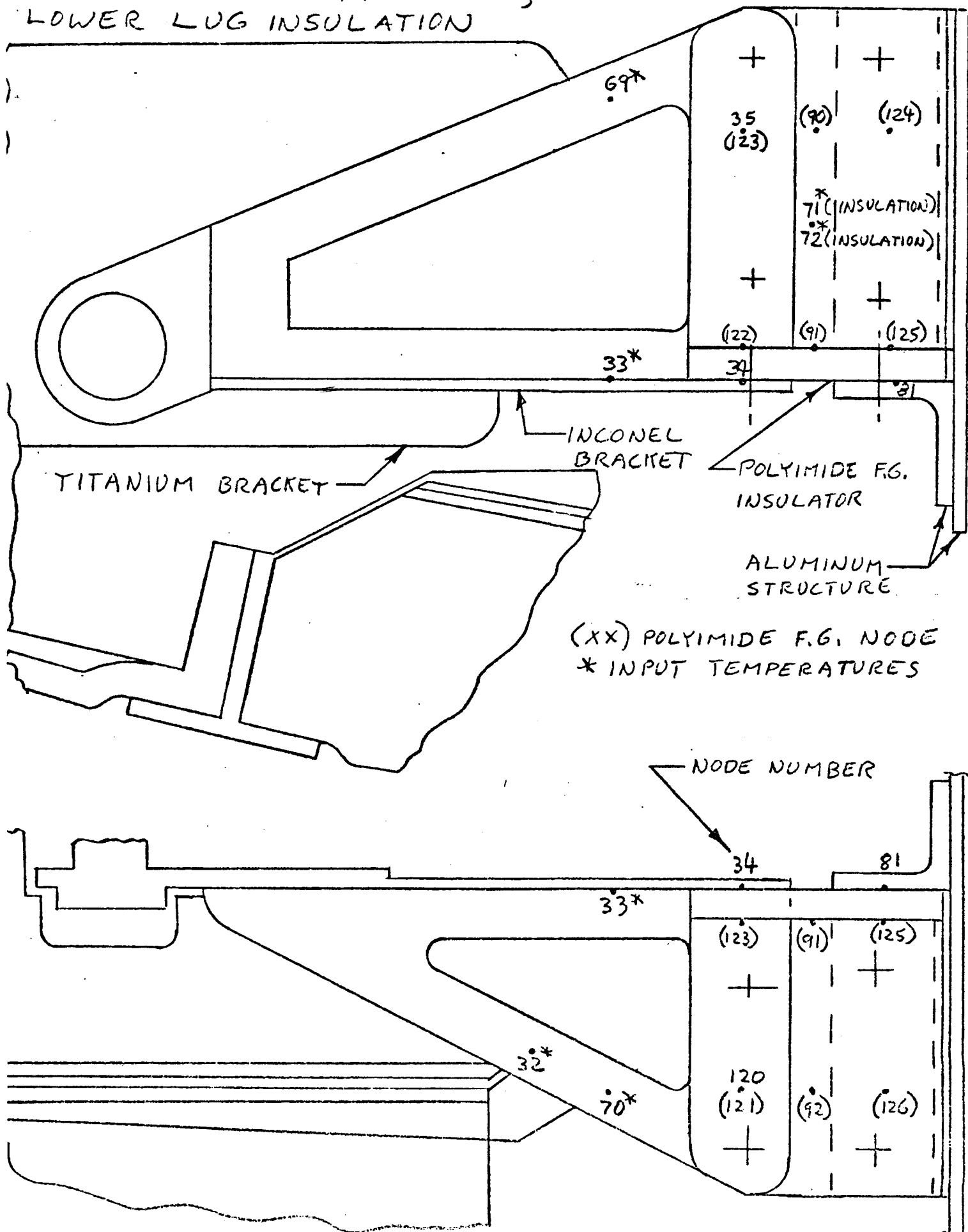


FIGURE 14 THERMAL MODEL,
LOWER LUG INSULATION

thickness, as shown in the figures. Analyses were also performed for a two inch thickness. Both 10 PCF and 15 PCF density dynaquartz were considered, as well as various thicknesses of the titanium bracket. To simplify the model, a plane of symmetry was assumed to pass through the midplane of the titanium bracket in Figure 12, and the model was constructed for the half of the bracket and insulation between this plane and the RPP skin. This simplification is conservative since the overall insulation design will result in greater heat input to the bracket from the skin side than from the inboard side.

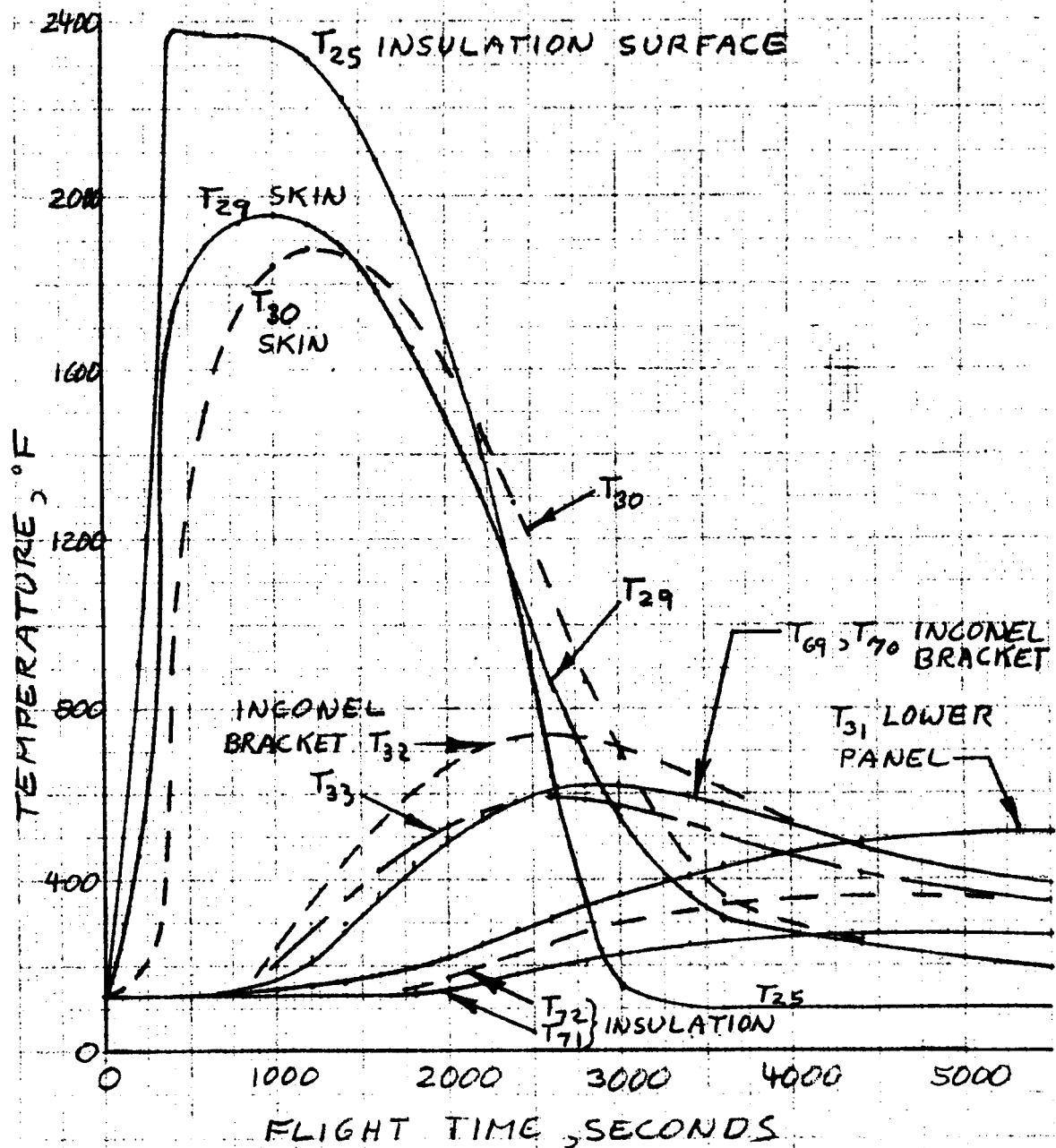
In the spanwise direction in Figure 13 the model includes the insulation between the titanium bracket and the support lug. Only one-half of the titanium bracket thickness was included for heat sink for nodes 6-8 and 76-78. The other half was allocated for heat sink in the analysis of heat input from the support lug to the titanium bracket, which is considered in a later section of this DIR.

The thermal model includes the cool end of the support lug Inconel bracket, the polyimide insulators and aluminum structure shown in Figure 14. In order to couple effects of heat conducted down the titanium bracket with effects of heat from the Inconel bracket, the Inconel bracket temperature at nodes 32, 33, 69 and 70 and the insulating temperatures at nodes 71 and 72 were taken from the support lug thermal analysis, T143-DIR-2-18, and used as input to the thermal analysis. Other input temperatures taken from that analysis are the RPP skin temperatures at nodes 29 and 30 of Figure 12. The insulation surface temperature, node 25, of Figures 12 and 13 was taken from the Task 2 heat shield analysis, T143-DIR-2-13. These input temperatures are presented in Figure 15.

The first analysis of the support lug insulation assembly was based on a 2 inch thickness of 10 PCF density dynaquartz and a 0.072 inch thick titanium bracket. Results indicated that the insulation bondline would overheat, even though the computer run was terminated prior to the time of peak bondline temperature. Three additional analyses were made with 15 PCF density dynaquartz and various thicknesses

FIGURE 15 LOWER LUG INSULATION
INPUT TEMPERATURES

NOTE: SEE FIGURES 12, 13 AND 14 FOR NODE
LOCATIONS



of insulation and titanium bracket with the results summarized below.

<u>Insulation Thickness Inches</u>	<u>Titanium Thickness Inches</u>	<u>Peak Bondline Temperature, °F</u>
2	.05	898
3	.08	647
3	.16	590

It is seen that the final design combination maintains the bondline below its temperature limit of 600°F. It was somewhat surprising that the bondline temperature was so high, considering results of the canted heat shield analysis which show temperatures below 600°F with 1.5 inches of 10 PCF dynaquantz. The high temperature for the support lug insulation assembly is due to three-dimensional heat conduction, with heat transfer to the bondline from three insulation faces. It should be noted that thermal conductivity data was not available for 15 PCF dynaquantz. Based upon conductivities of 9 and 15 PCF Lockheed surface insulation it was assumed that conductivity of 15 PCF dynaquantz is equal to that of 10 PCF dynaquantz.

Peak computed temperatures for the final configuration are presented in Figures 16-18. Maximum temperature of the polyimide insulator in Figure 18 is 397°F, which is well within tolerable limits. The aluminum substructure temperature had not peaked at the end of the computer run at 5300 seconds. However, the temperature rise of the aluminum at this time was only 113°F as compared to a temperature rise of 110°F for the previous support joint analysis which did not include heat conduction from the titanium bracket. Hence, the heat short from the titanium bracket is not considered excessive.

Upper Lug Insulation Assembly

The 152 node thermal model used for analysis of the upper lug insulation assembly is shown in Figures 19, 20 and 21. This model is based on 2.5 inch insulation thickness on one side of the insulation block and 2.0 inch on the other sides, as shown in the Figures. Analyses were also performed for a 2.0 inch thickness on all sides. The insulation was 15 PCF density dynaquantz. Various thicknesses were

FIGURE 17 PEAK
TEMPERATURES IN LOWER
LUG INSULATION AND
SUPPORT BRACKET, TOP
VIEW

NOTE: SEE FIGURE 16 FOR
LOCATION OF THIS PLANE

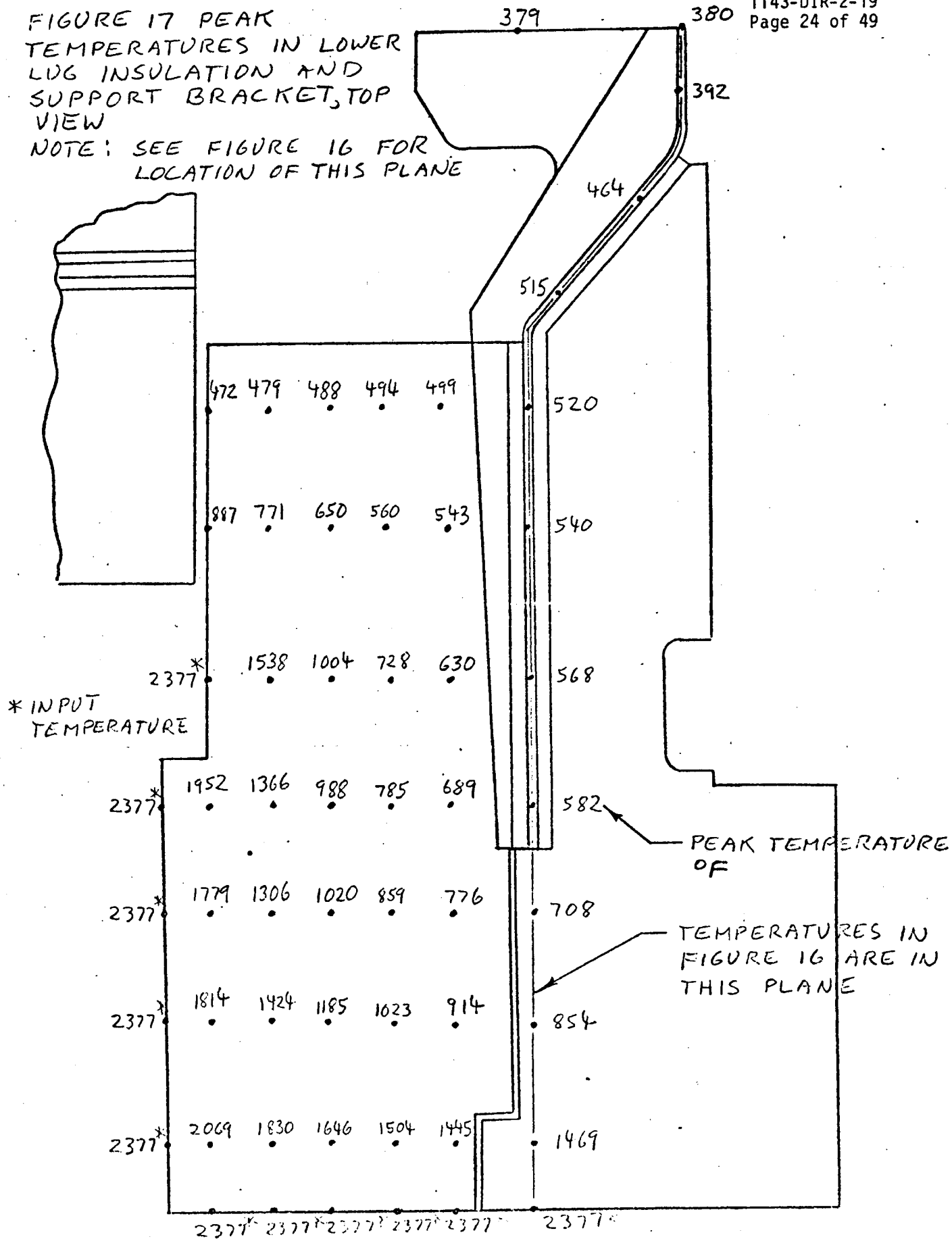
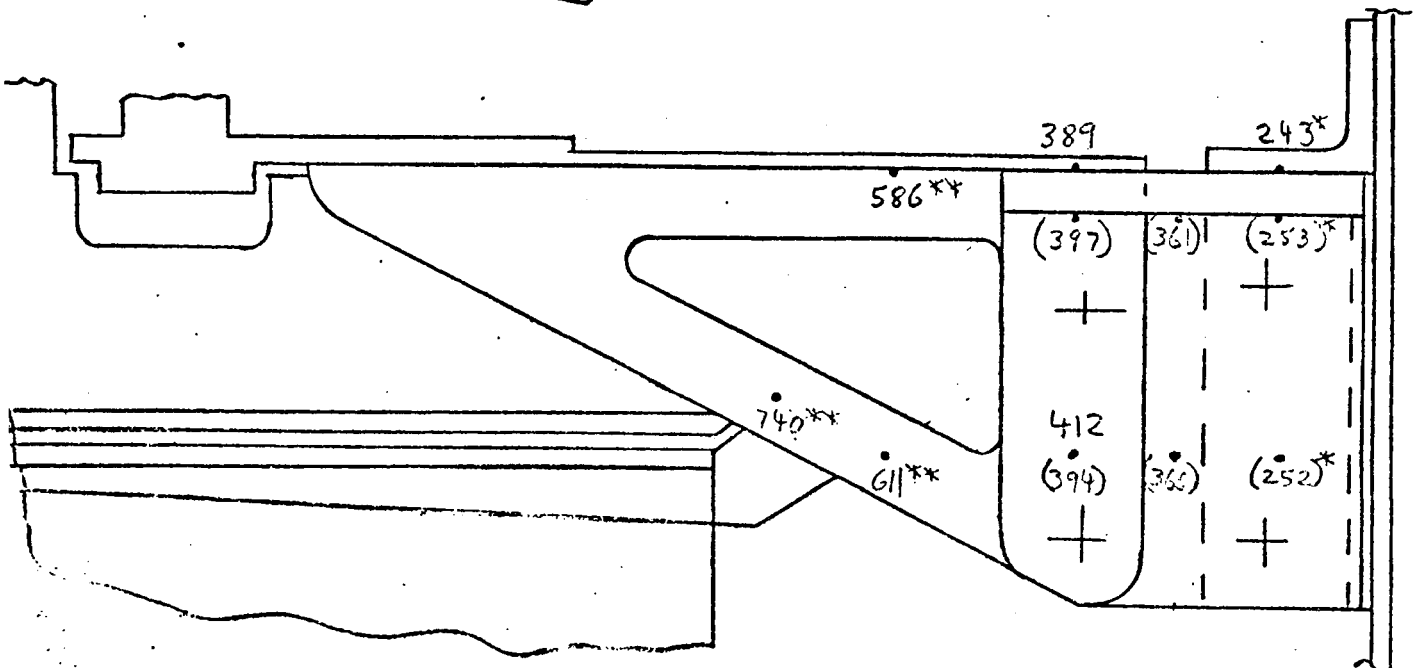
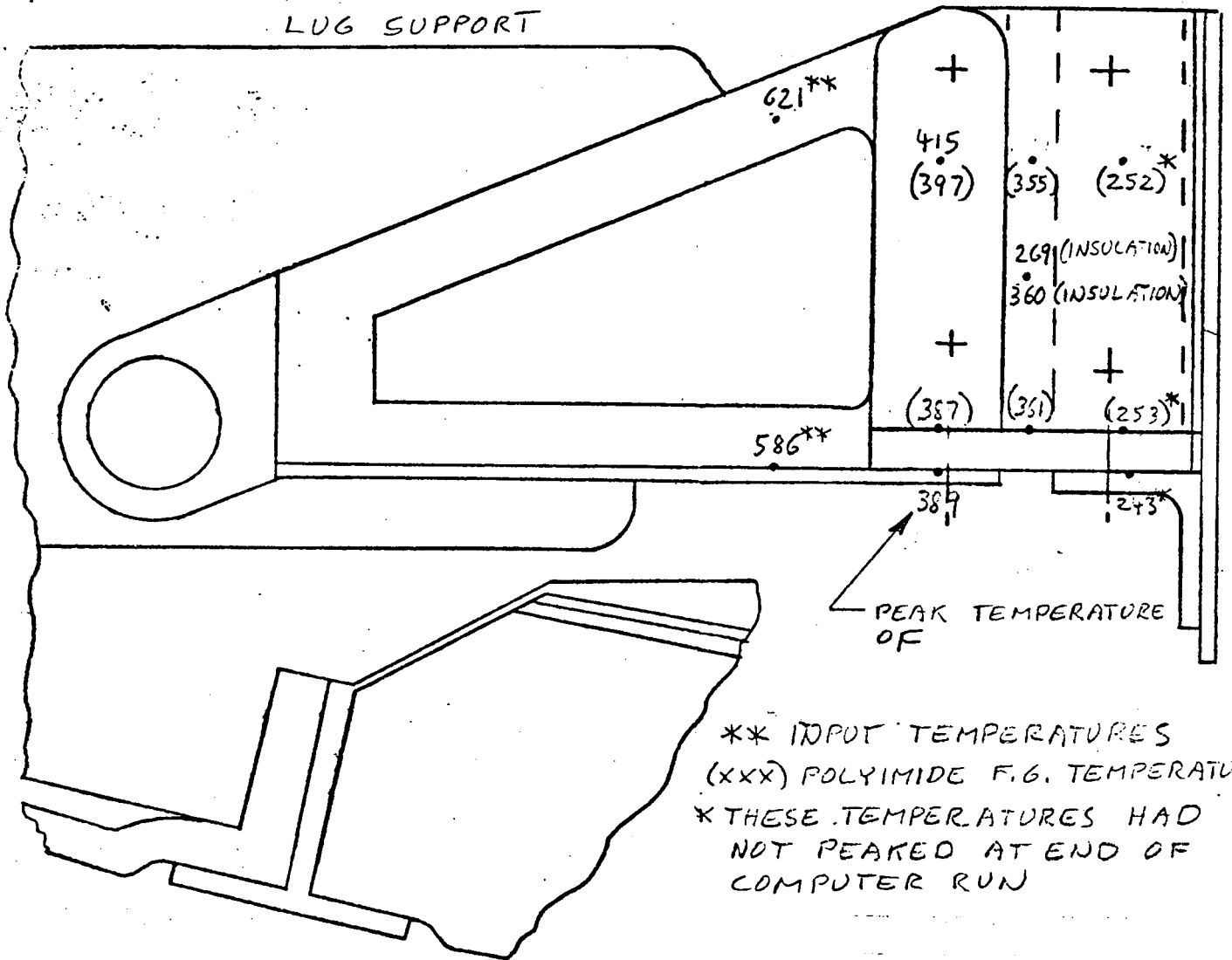


FIGURE 18 PEAK TEMPERATURES IN LOWER
LUG SUPPORT



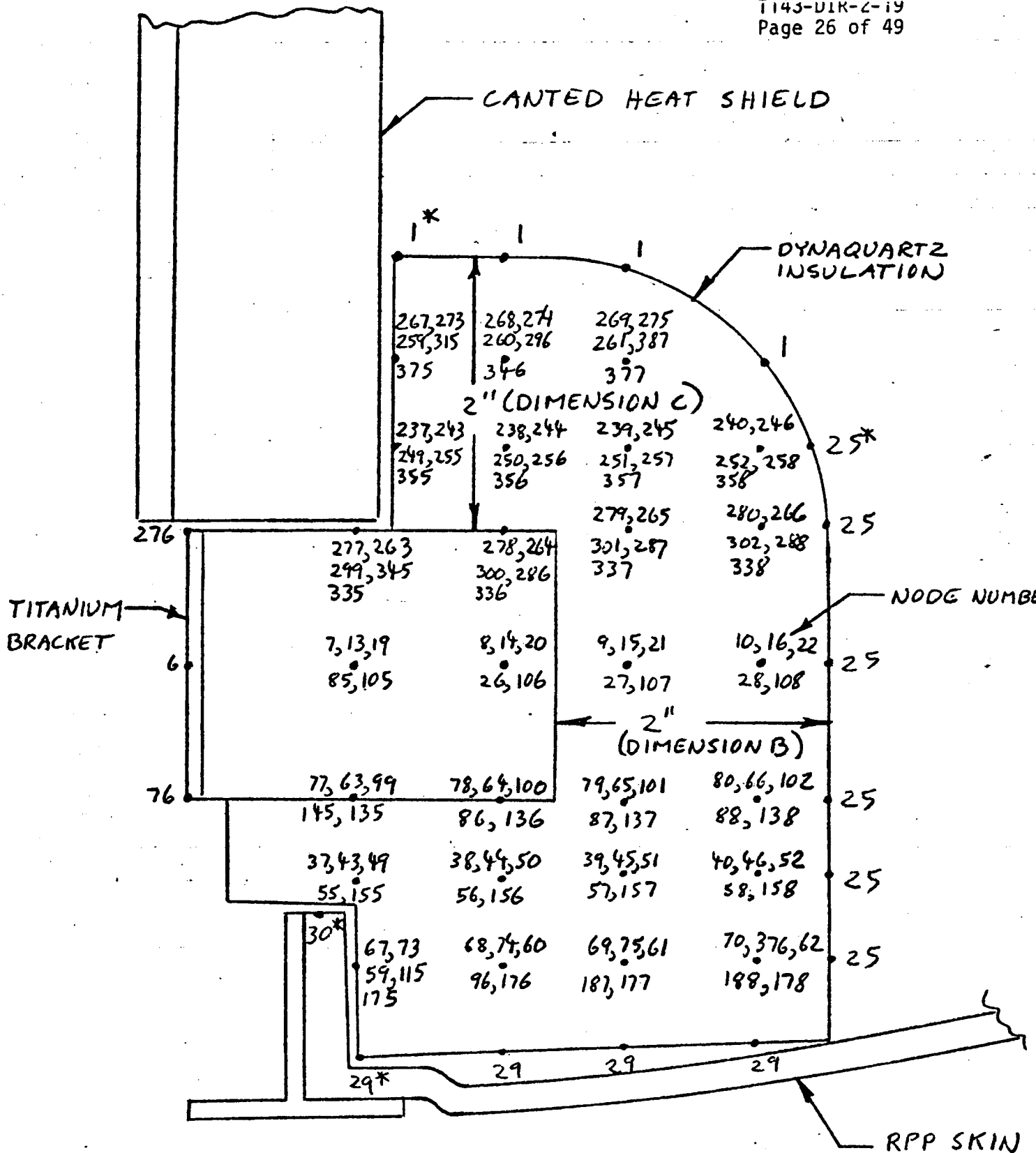


FIGURE 19 THERMAL MODEL, UPPER LUG
INSULATION, SIDE VIEW

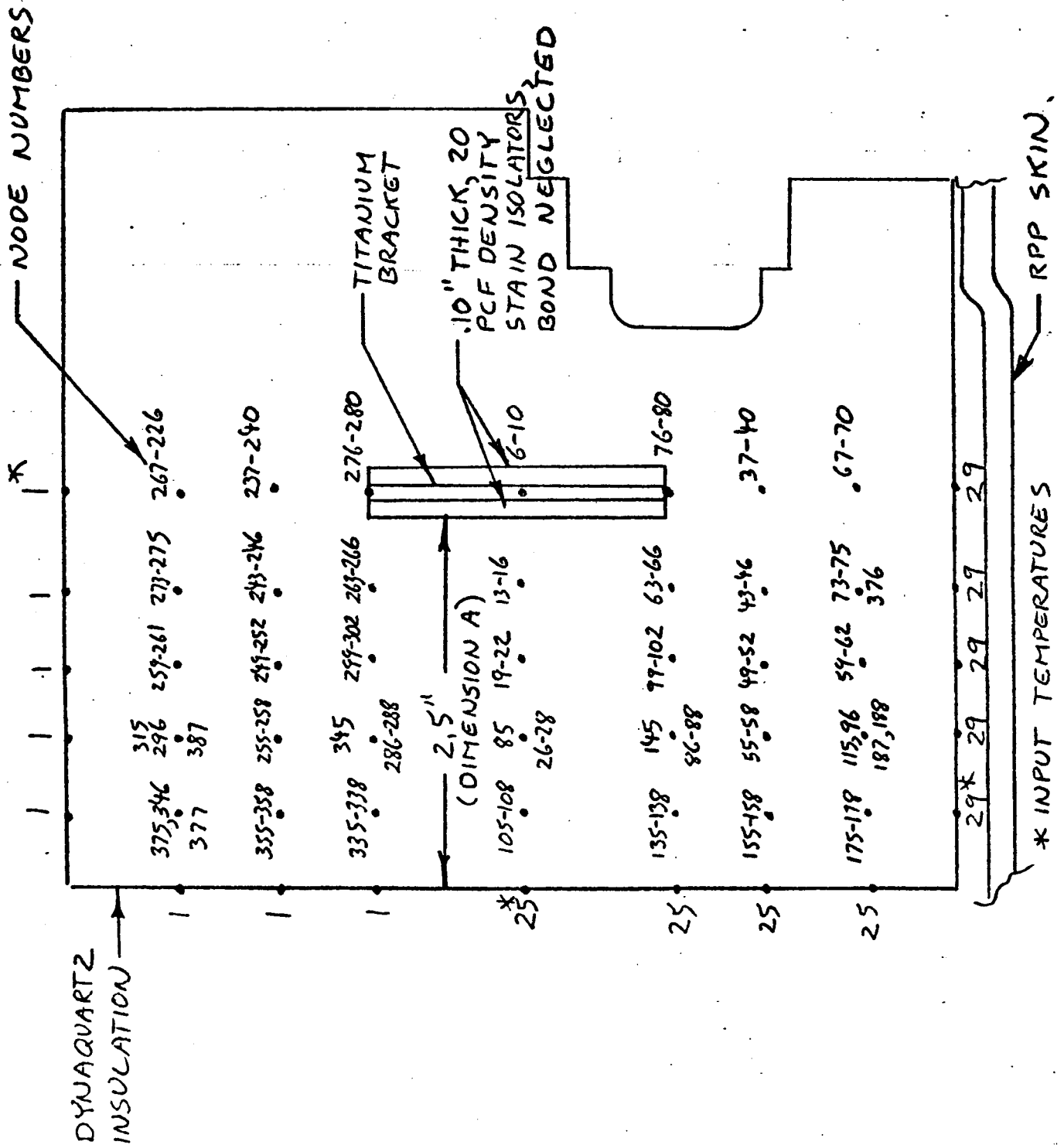
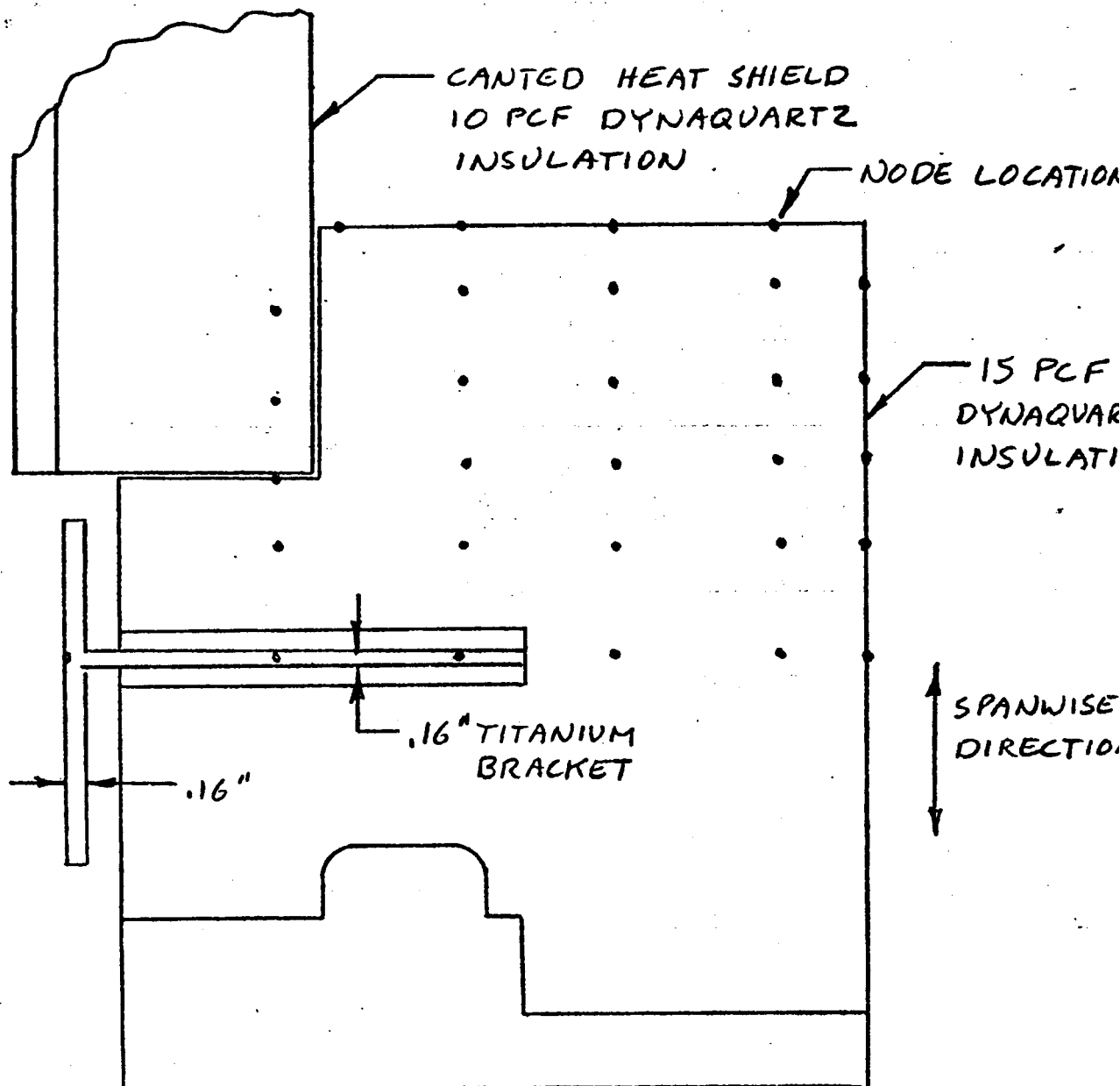


FIGURE 20 THERMAL MODEL, UPPER LUG INSULATION, END VIEW



NOTE: NODE NUMBERS OMITTED FOR CLARITY

FIGURE 21 THERMAL MODEL, UPPER LUG INSULATION
TOP VIEW

analyzed for the titanium bracket. As with the lower lug, in the spanwise direction, the model includes the insulation between its exposed surface and the titanium bracket, and one-half of the bracket thickness was included for heat sink. However, the model extends from the skin to the insulation surface opposite the skin, rather than including only half this region as for the lower lug. This is due to a lack of thermal symmetry for the upper lug, which is exposed to relatively high temperatures at the insulation surface, but much lower skin temperatures.

Insulation surface temperatures, nodes 1 and 25, were taken from Task 2 heat shield analysis, T143-DIR-2-13 and cross radiation analysis, T143-DIR-2-07. Skin temperatures, nodes 29 and 30, were taken from upper support lug thermal design analyses discussed later in this DIR. These input temperatures are presented in Figure 22.

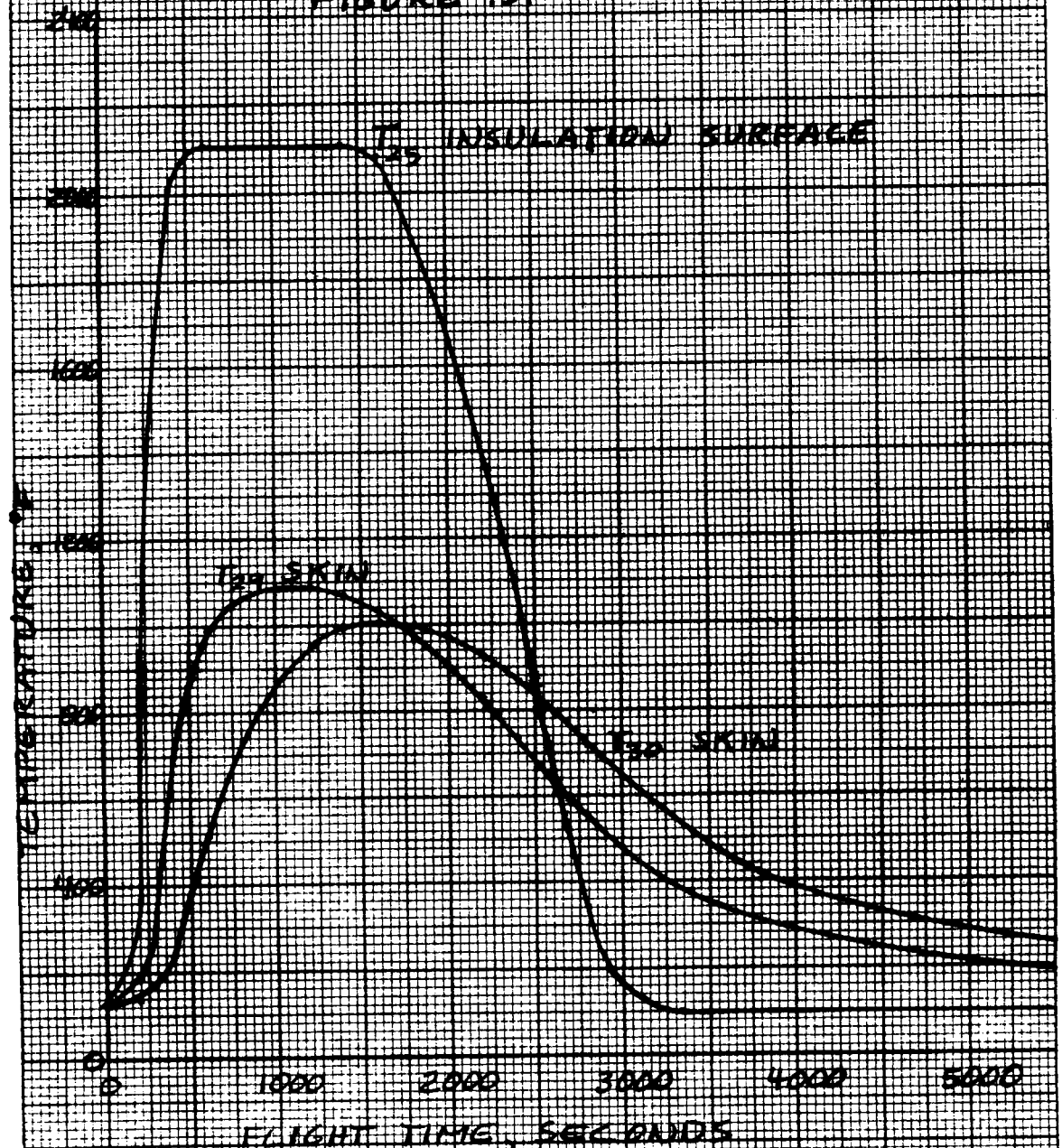
The first analysis of the insulation assembly was based on 2 inch insulation thickness on all sides of the insulation block, and a 0.10 inch thick titanium bracket. Results indicated that the insulation bondline would overheat; therefore three additional analyses were made with various thicknesses of insulation on one side (dimension A of Figure 20), a constant 2-inch insulation thickness on the other two sides (dimensions B and C of Figure 19) and various titanium bracket thicknesses. The results are summarized below.

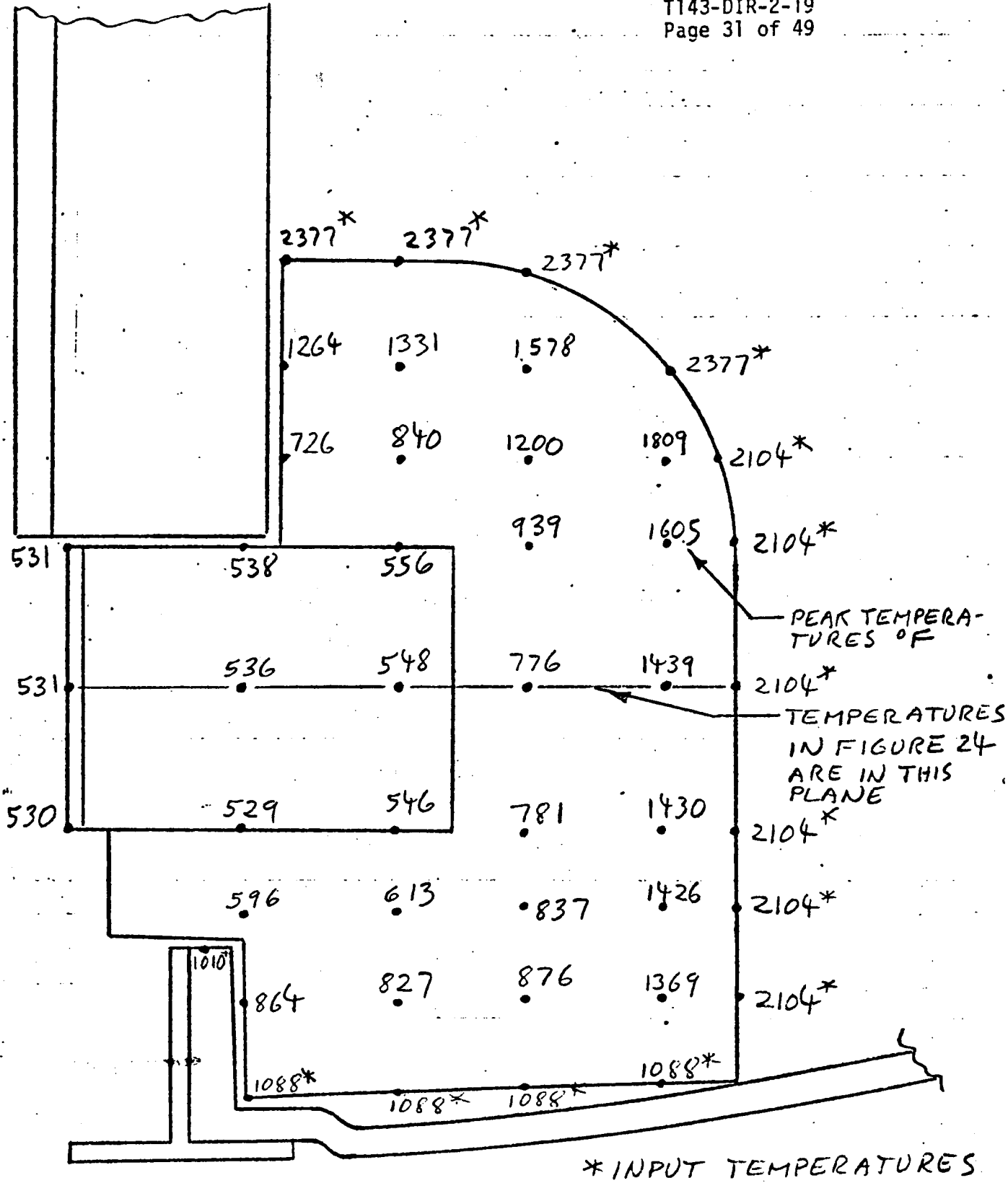
<u>Insulation Thickness (Dimension A) Inches</u>	<u>Titanium Thickness Inches</u>	<u>Peak Bondline Temperature, °F</u>
2	0.15	610
2.5	0.10	610
2.5	0.16	556

It is seen that the final design combination maintains the bondline below its temperature limit of 600°F. Peak computed temperatures for the final configuration are presented in Figures 23 and 24.

FIGURE 22 UPPER LUG INSULATION INPUT TEMPERATURES

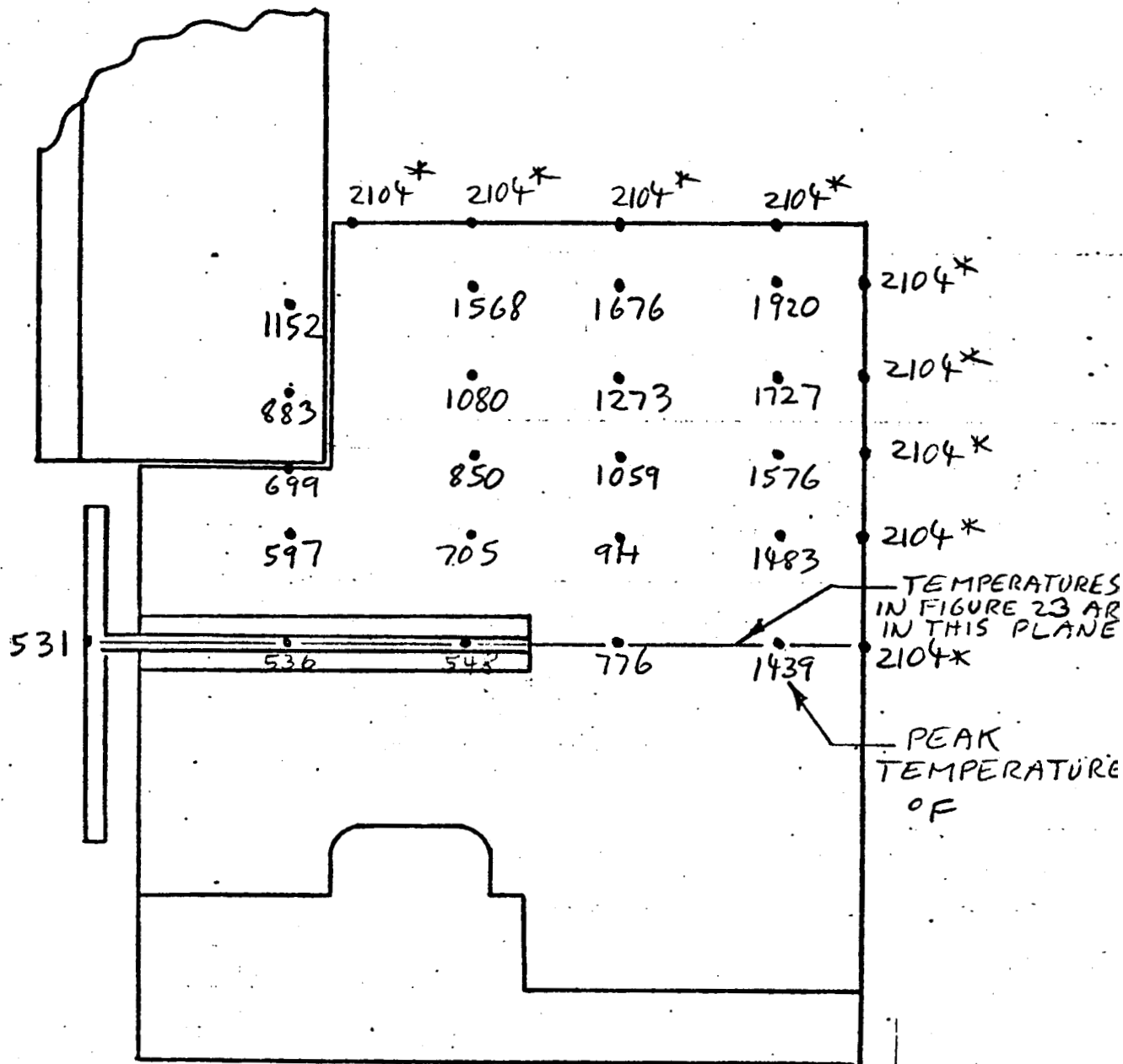
NOTE: SEE FIGURES 19 AND 20 FOR NODE LOCATIONS.
INSULATION SURFACE TEMPERATURE T_{is} IS EQUAL TO T_{is} IN FIGURE 15.





NOTE: SEE FIGURE 24 FOR LOCATION OF THIS PLANE

FIGURE 23 PEAK TEMPERATURES IN UPPER LUG INSULATION AND SUPPORT BRACKET, SIDE VIEW



NOTE: SEE FIGURE 23 FOR LOCATION OF THIS PLANE
* INPUT TEMPERATURE

FIGURE 24 PEAK TEMPERATURES IN UPPER
LUG INSULATION AND SUPPORT
BRACKET, TOP VIEW

Lower Lug Insulation Near Support Lug Bolt

The bulk insulation for the lug is held in place by a titanium bracket as shown in Figures 16 and 17. The bond used to attach the insulation to the bracket has a maximum allowed temperature of 600°F. Since the thickness of insulation protecting the bond will be a minimum near the end of the lug attachment bolt, this area was considered in detail. Only the windward side lug area was considered since heat input is greater for it than for the leeward side.

Preliminary analyses showed that a computer analysis accounting for the transient effects was required, so a thermal model of the area was constructed. Figure 25 shows the two-dimensional thermal model. Maximum temperature of the bolt during the ground test of the windward lug was 1320°F as reported in T143-DIR-2-18. Temperature versus time obtained for the bolt during the test (see Figure 26) was input in the model for node 12 representing the bolt.

Predicted bondline temperature versus time is shown in Figure 26, indicating a peak temperature of 633°F. This temperature should be quite conservative since only a 0.032 inch thickness of titanium was included in the model. As discussed in the previous section on the lower lug insulation assembly, the titanium bracket is 0.16 inch thick, and one half of this, 0.08 inch was allocated for heat sink for bolt heat transfer to the bracket. The assumed initial temperature of 130°F introduces additional conservatism, such that the bondline temperature limit of 600°F should not be exceeded.

LOWER PANEL INSULATION

The external surface of the wing aft of the RPP leading edge panel consists of an insulating panel. The insulation is attached to a titanium panel which in turn attaches to the aluminum structure of the wing. Maximum temperature allowed on the aluminum is 350°F, therefore thermal analyses were performed to determine a satisfactory method to attach the panel to the aluminum.

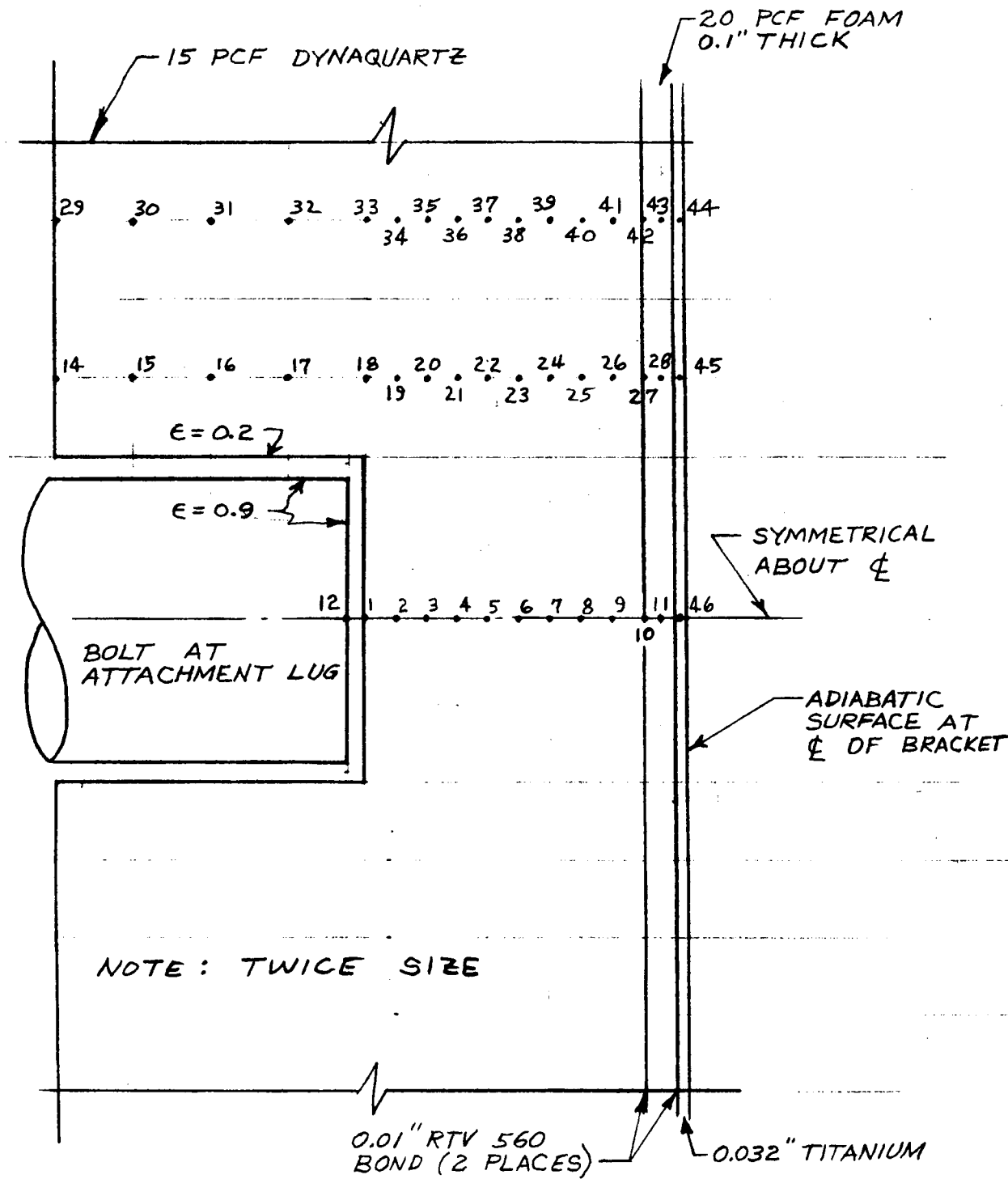
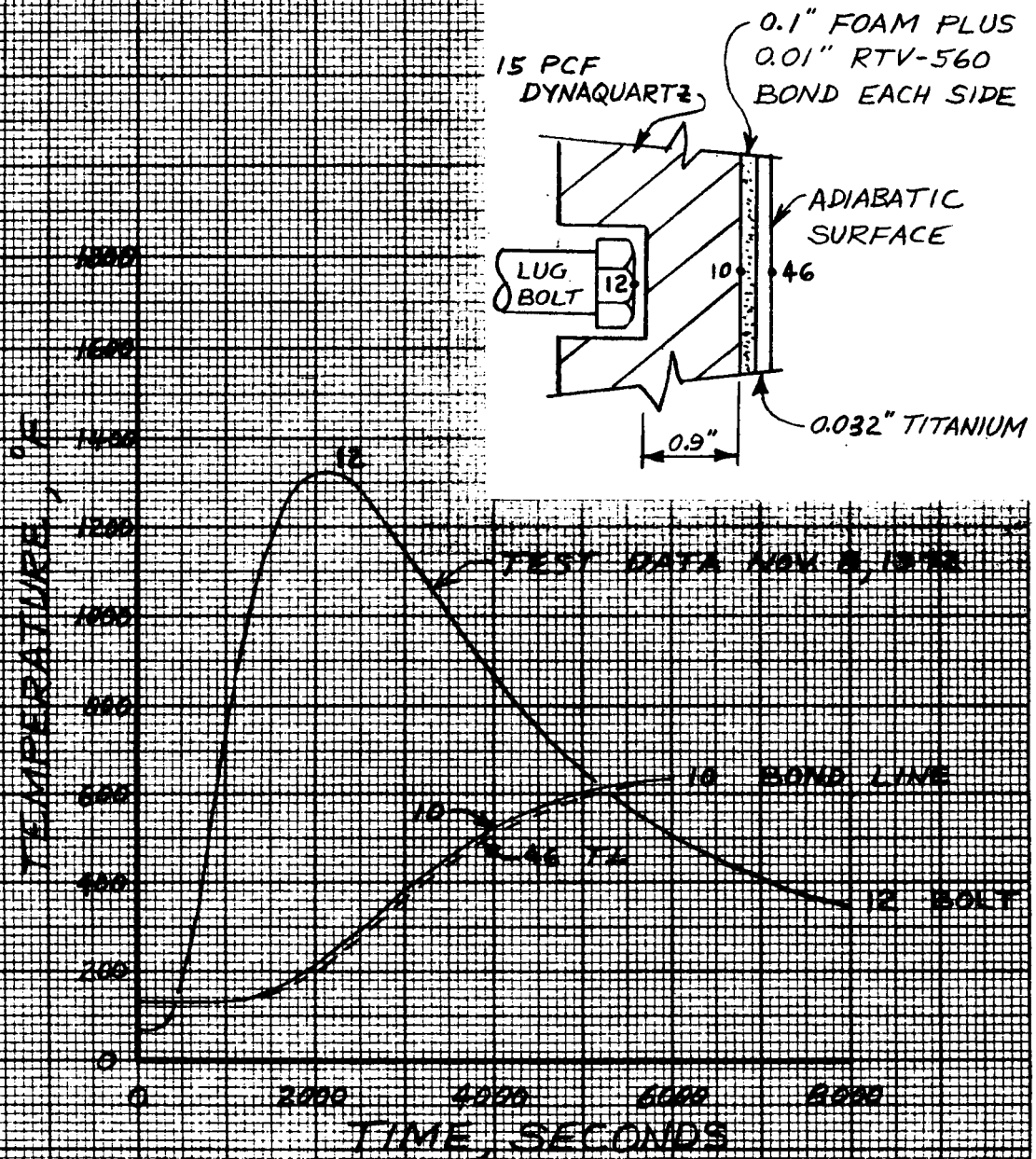


FIGURE 25
THERMAL MODEL AT ATTACHMENT BOLT

FIGURE 2.6
PREDICTED TEMPERATURES AT
WINDWARD SIDE LUG BOLT



A two-dimensional thermal model of the panel area was constructed and computer routine LVV620 was used to obtain predicted temperatures. The thermal model used in the analyses is shown in Figure 27. As explained on the Figure, the model does not represent the final design configuration, but temperatures obtained with it should be conservative based upon results obtained during analyses of the upper panel. During that analysis it was found that the following two combinations of materials resulted in approximately the same temperature response for the inner surface:

1.5" LI1500		1.28" 10 PCF Dynaquartz
0.05" Titanium		0.064" Titanium
0.09" Foam	and	0.2" Foam
		0.02" RTV Bond

Comparing the differences between the model used in the lower panel analysis and the final design of the lower panel to the differences in the models used in upper panel analysis, indicates that approximately the same temperature response would be obtained for both the final and initial designs of the lower panel.

The final design of the panel also includes bulk insulation on the inside of the titanium panel. Addition of this bulk insulation to the thermal model would also tend to result in lower predicted temperatures for the titanium and aluminum since the additional insulation would serve as heat sink. (The thermal model assumed an adiabatic surface at the titanium).

Since the actual construction details of the aluminum panel were not available, a conservative approach was taken and only the part of the aluminum in contact with the polyimide spacer was included in the model. This is probably a fairly good assumption for the location near the bracket but it is conservative for the area between brackets. It was also assumed that the aluminum had adiabatic surfaces except at the polyimide spacer.

The recovery temperature and the convection coefficients used for the

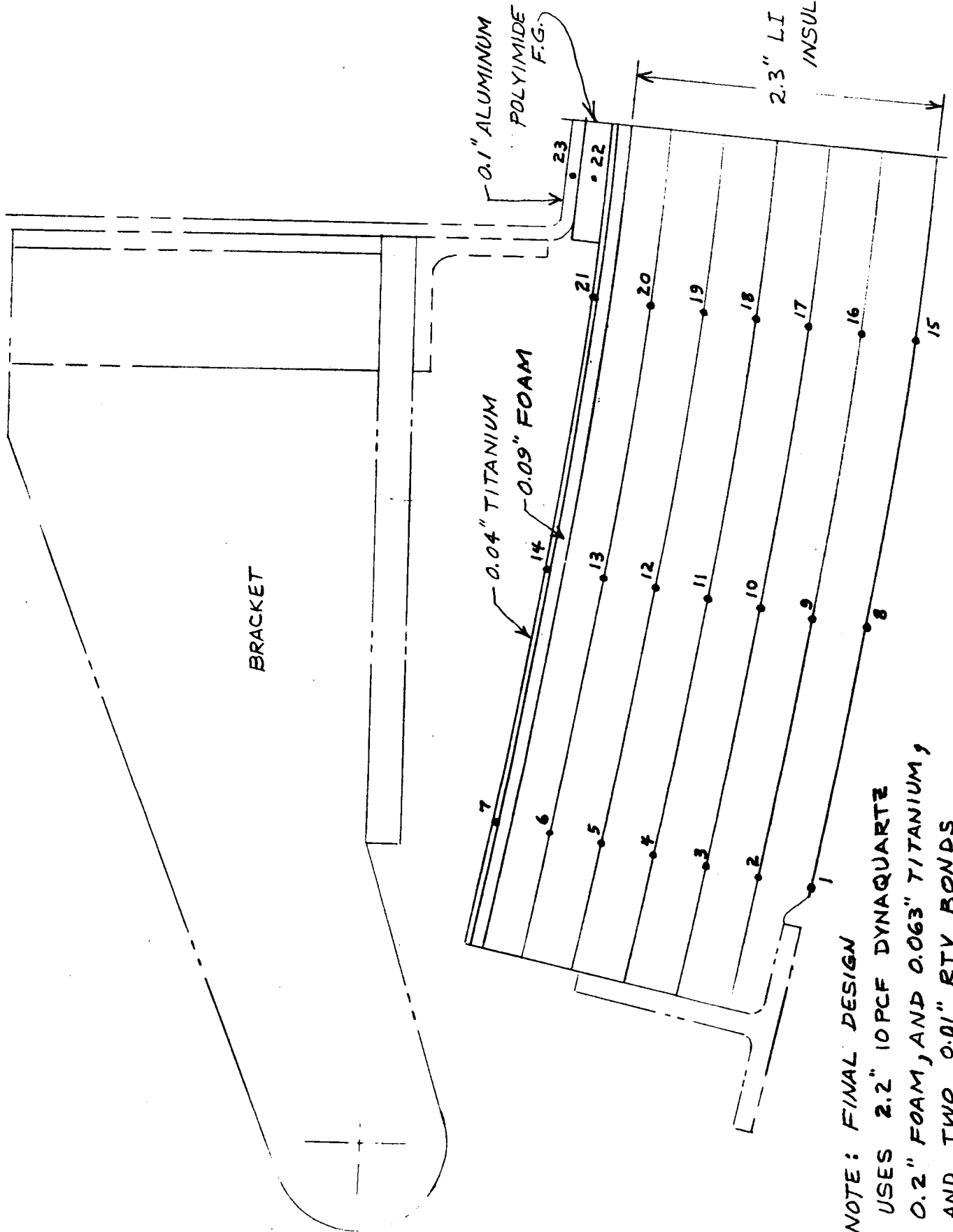


FIGURE 27, THERMAL MODEL - WINDWARD RS1 PANEL

external nodes were the same as those used in the rib analyses of T143-DIR-2-07. Multiplication factors used to modify the convection coefficients (which were for the maximum heating location) were 0.423 at node 1, 0.411 at node 8, and 0.406 at node 15.

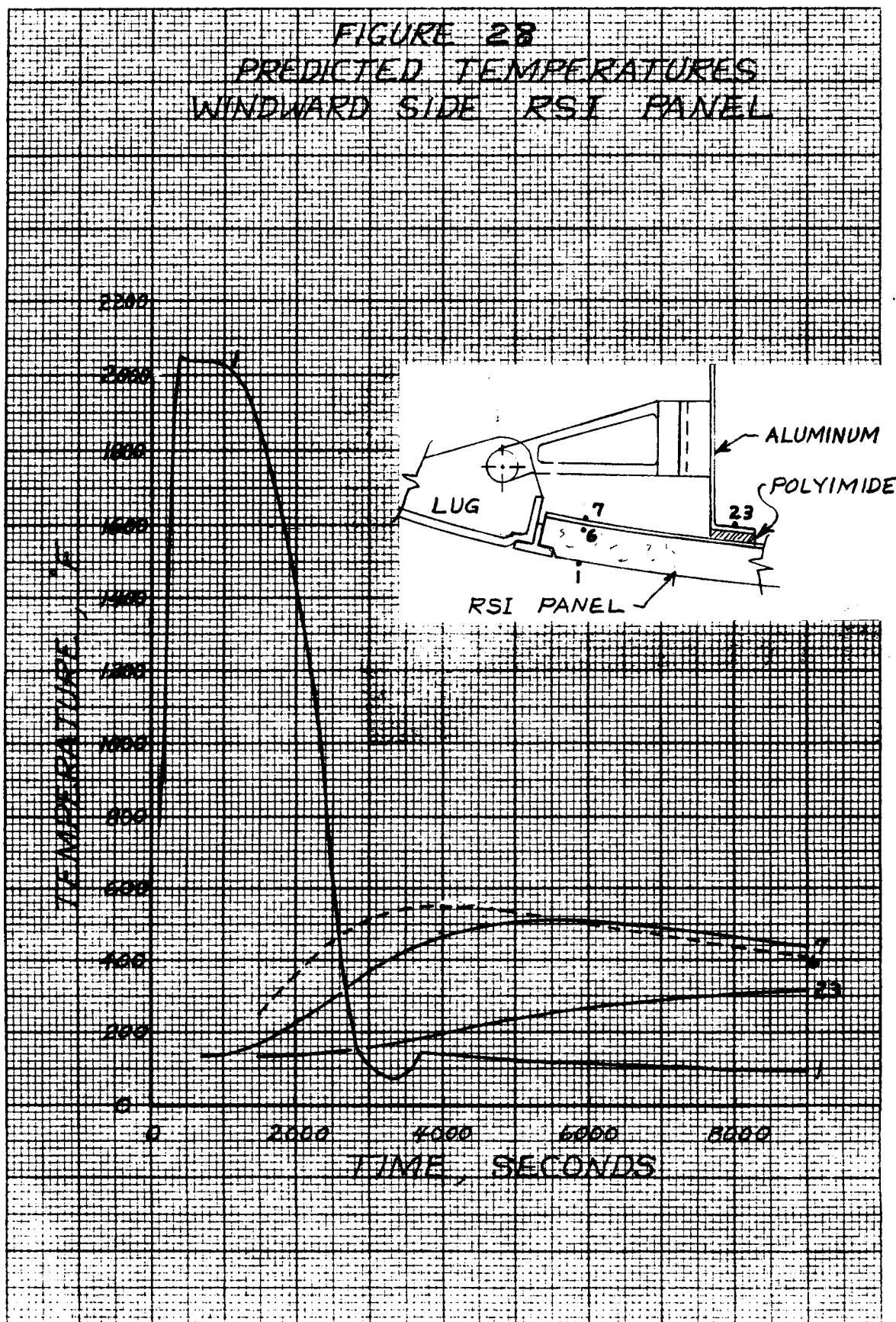
Predicted temperatures are shown in Figure 28 for the configuration with a 0.25" thick strip of polyimide insulation between the aluminum and the titanium panel. Temperatures of all the critical locations are below the maximum allowed. Peak temperature at the bondline between the insulation and the foam is about 550°F, 50°F below the 600°F maximum allowed. Peak temperature at the interface between the polyimide and the titanium is less than 510°F which is well below the 700°F maximum allowed. Also the peak aluminum temperature, extrapolated to be 333°F, is below the allowed 350°F.

An additional run was made with the thickness of the polyimide insulation strip reduced from 0.25" to 0.125". Peak aluminum temperature increased from 333°F to 381°F which is above the allowed 350°F. Interpolation between the two thicknesses indicates that a 0.2" thickness of polyimide fiberglass insulator is adequate to prevent the aluminum temperature from exceeding 350°F.

UPPER SUPPORT LUG

Thermal analyses and ground test results for the windward side lug were reported in T143-DIR-2-18. An all metal joint was designed to connect the RPP lug to the aluminum structure. The thermal requirements for the leeward side lug are different from those for the windward side lug in the following ways: (1) the temperatures of the RPP in the area of the leeward side lug are considerably lower than for the windward side, (2) the distance from the RPP surface to the wing structure is less for the leeward side than it is for the windward side, and (3) the wing structure at the leeward joint is titanium with a design temperature limit of 600°F, whereas the wing structure at the windward joint is aluminum with a design temperature of 350°F.

FIGURE 28
PREDICTED TEMPERATURES
WINDWARD SIDE RSI PANEL



The net effect of the differences in thermal requirements for the two joints is to make the windward side joint the critical one from the thermal design standpoint. In order to simplify the overall design and keep the number of different kinds of parts to a minimum the leeward side joint was made similar to the windward joint where practical, even though this may result in thermal over design.

A three-dimensional thermal model of the leeward side joint area was constructed and computer analyses were performed with VMSC routine LVV 620. The routine accounted for heat conduction along the skin, the RPP rib, across the support joint and the bracket into the titanium wing structure. Cross radiation from the skin to the portion of the RPP rib outside the bulk insulation was also considered, as was the heat conduction through the bulk insulation into the support joint and bracket. The nodal division of the model is shown in Figures 29, 30 and 31. The model for the rib area, Figure 29, is similar to that which was used in T143-DIR-2-07 to predict temperatures of the ribs in the support joint area.

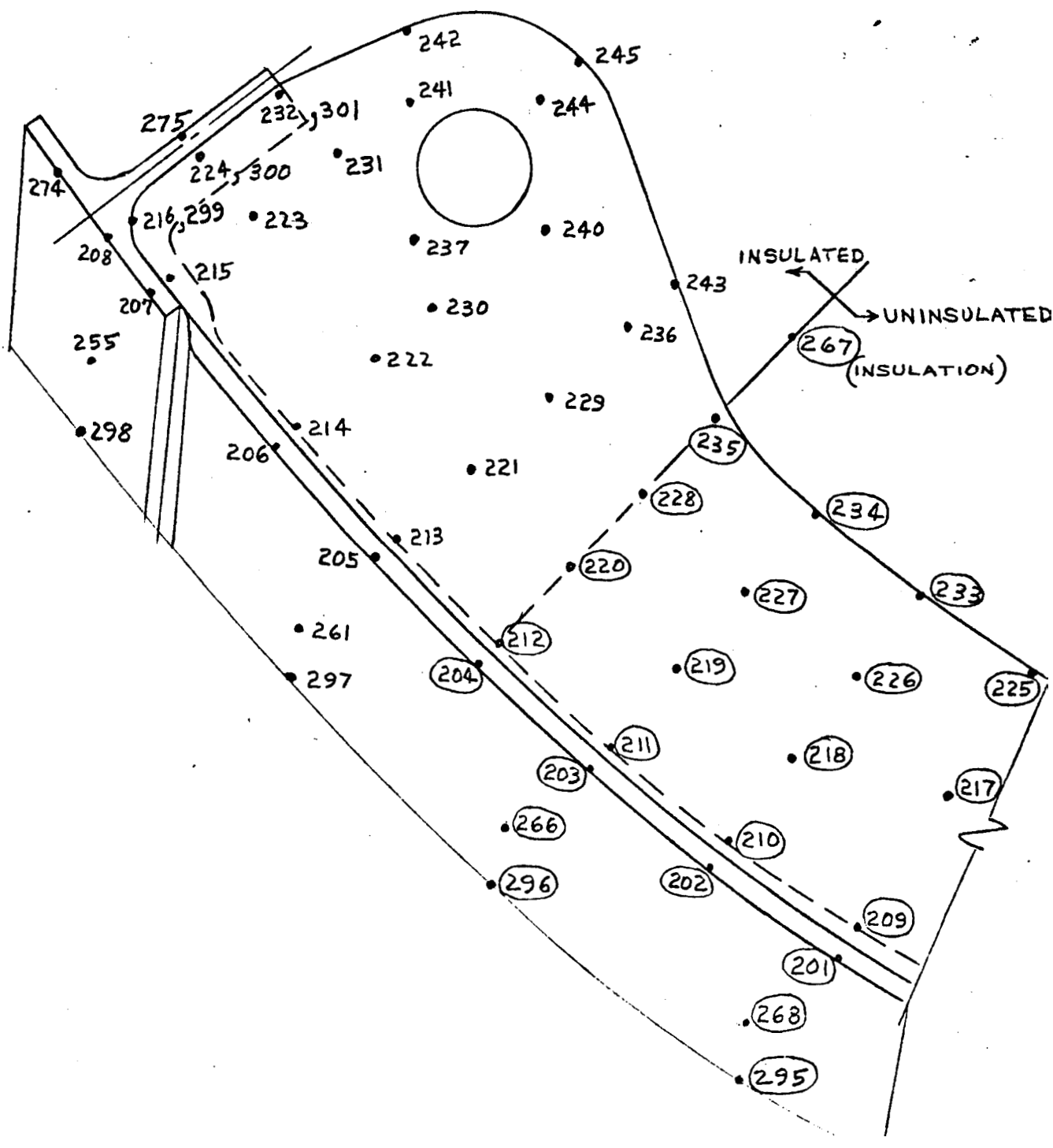
The recovery temperature and the convection heat transfer coefficients used for the external skin nodes were the same as those used in the rib analysis of T143-DIR-2-07. The external temperature of the bulk insulation was input as a function of time as given in Figure 32. Thermal property data used in the analysis are documented in the appendices of T143-DIR-2-11 and T143-DIR-2-18.

Prior to the windward side analyses showing that an all metal joint would be satisfactory, a computer run was made with a joint composed of an Inconel bolt and silica insulating washers. The results of this run are presented in Figure 33. Peak temperature of the titanium is only 329°F for this type joint.

Figure 34 shows predicted temperatures for the all metal joint. Peak temperature of the titanium is 452°F. This run was made with joint contact coefficients of 100 BTU/hr-ft²°F and nominal conductance for the inconel. Also a preliminary design of the bracket which was considerably lighter than the final design was used.

FIGURE 29. - THERMAL MODEL OF CARBON-CARBON RIB AND SKIN.

ⓧ PARTICIPATES IN CROSS-RADIATION



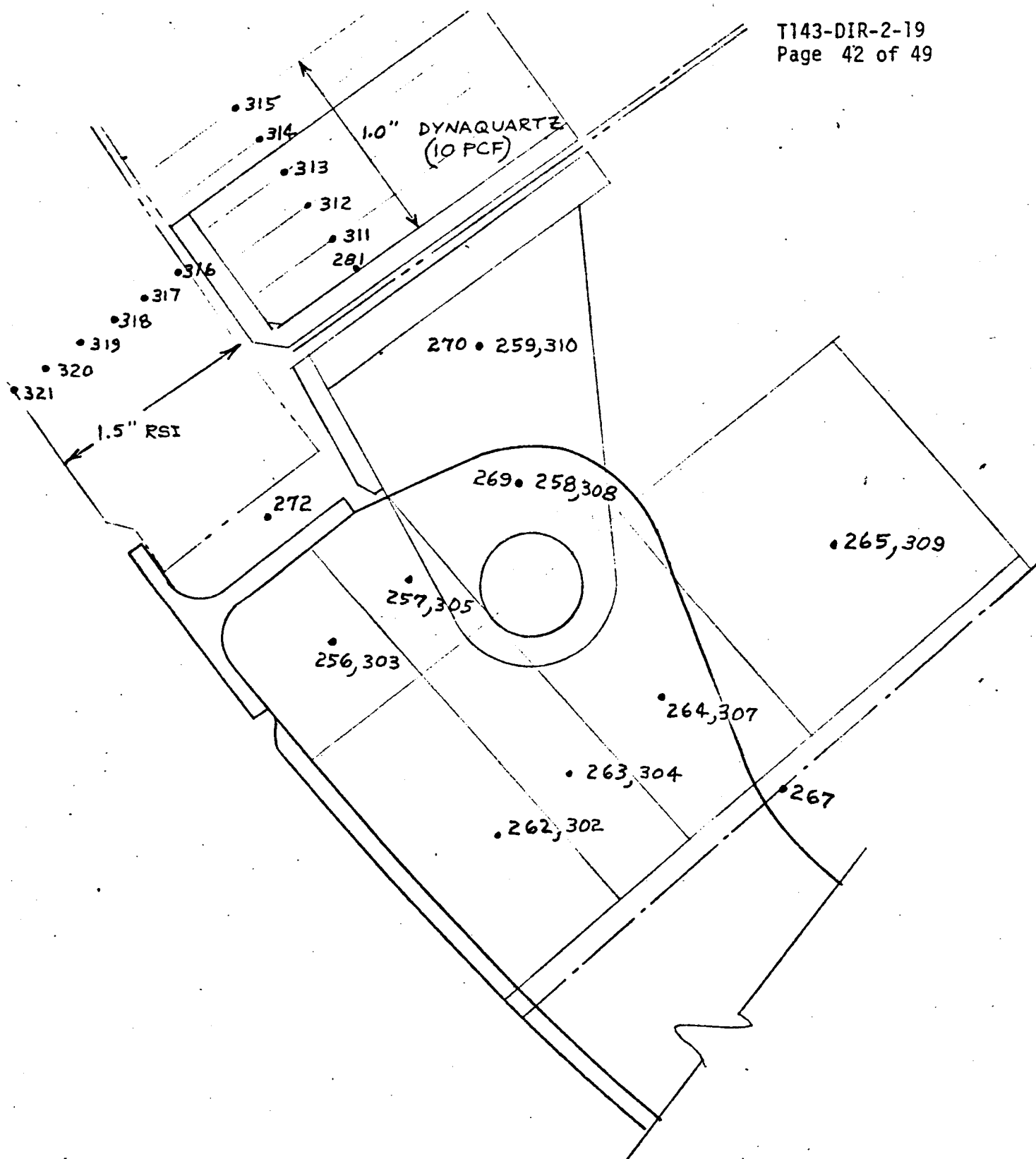


FIGURE 30 - THERMAL MODEL OF BULK INSULATION

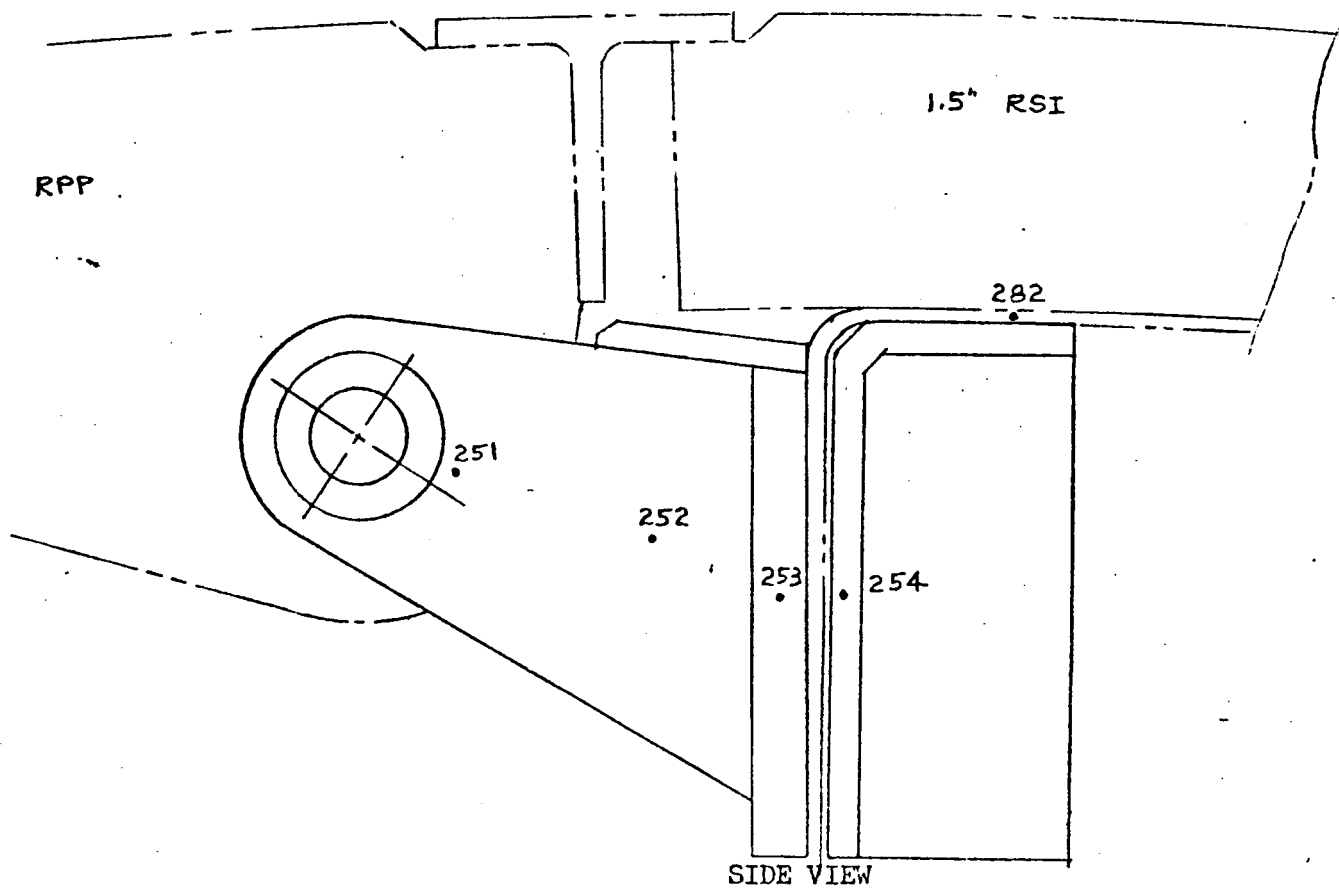
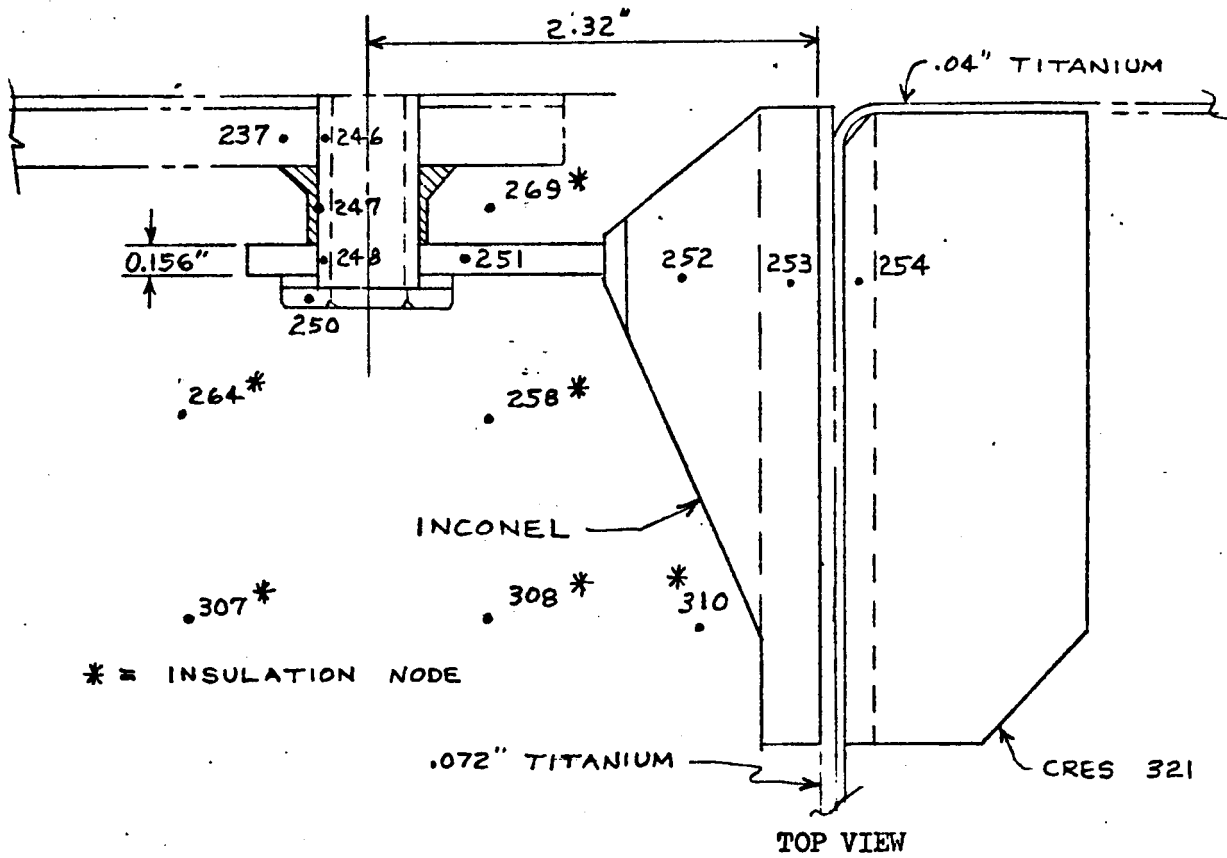


FIGURE 31 - THERMAL MODEL OF BRACKET AREA

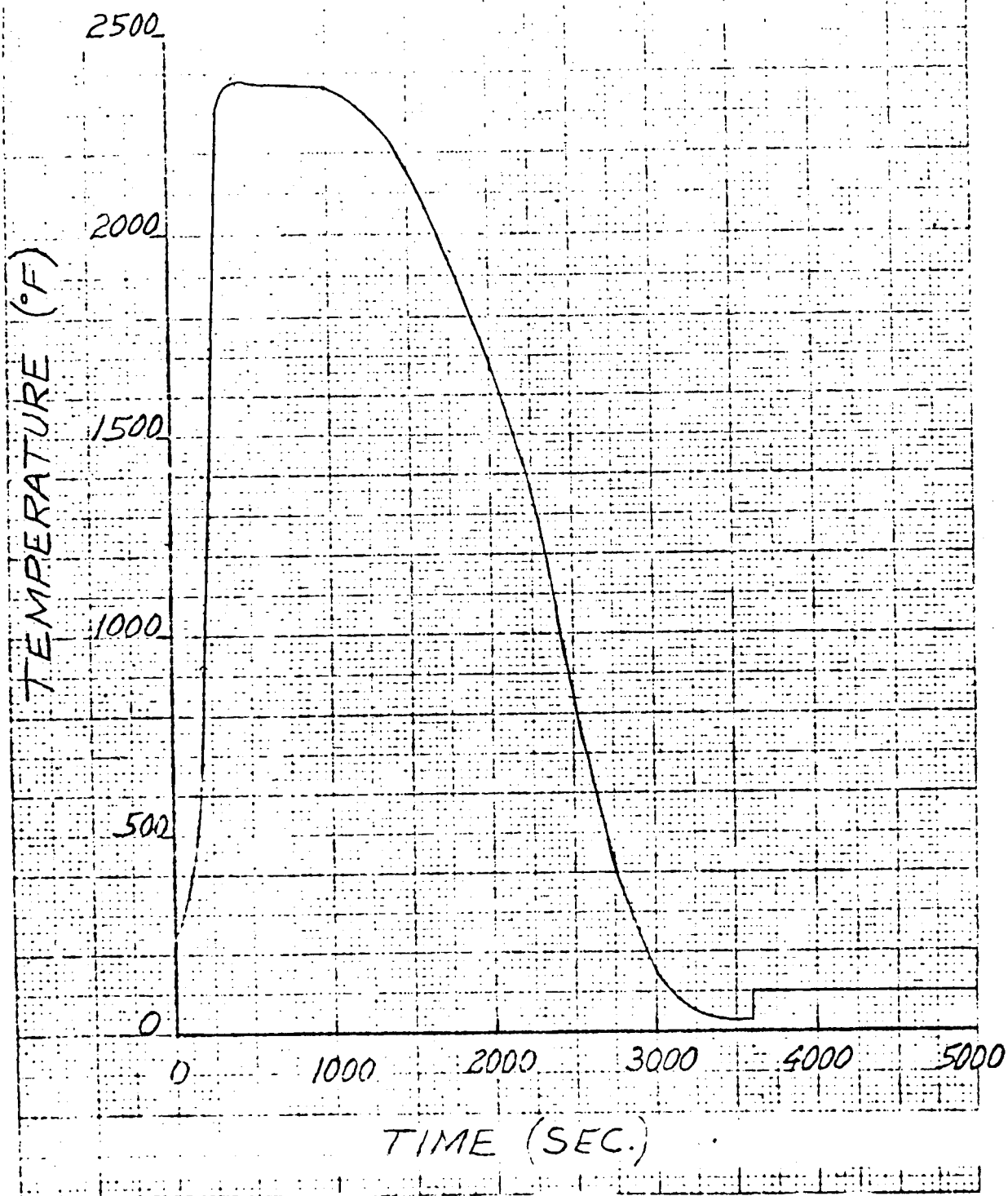


FIGURE 32 RADIATING STRUCTURE TEMPERATURE

FIGURE 33
PREDICTED TEMPERATURES
LEEWARD SIDE LUG AREA -
SILICA INSULATING WASHERS

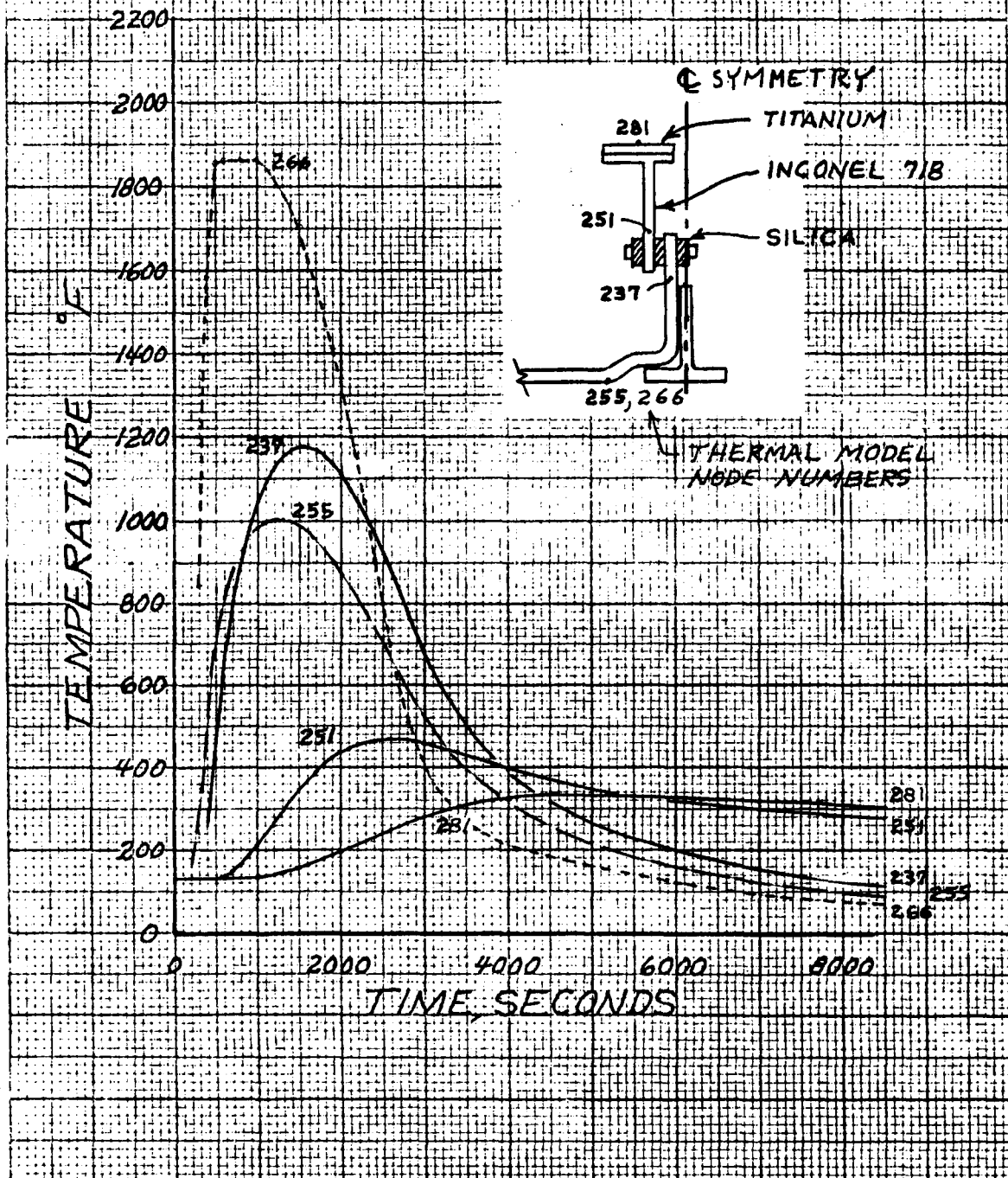
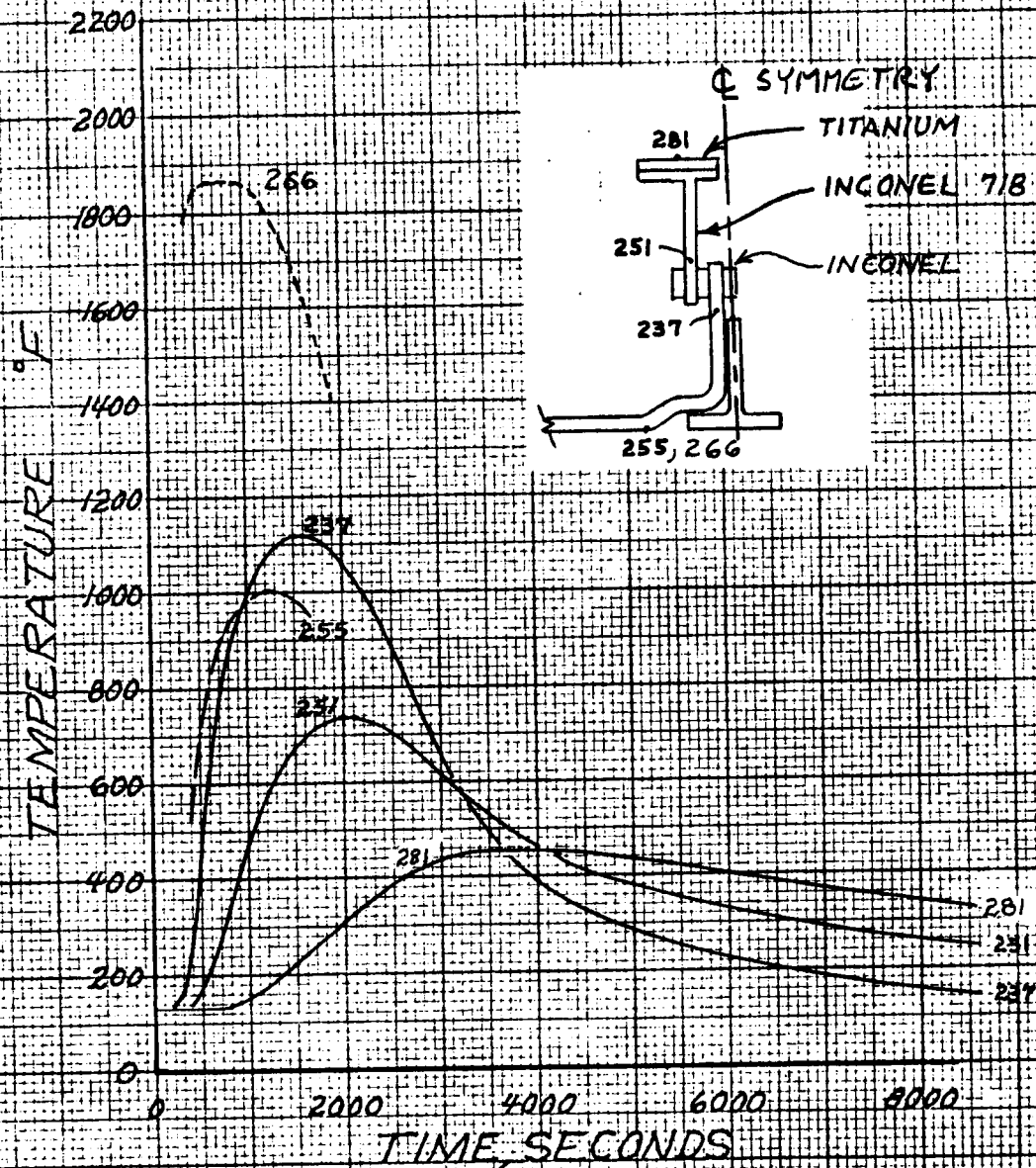


FIGURE 34
PREDICTED TEMPERATURES
LEEWARD SIDE LUG AREA
PRELIMINARY DESIGN BRACKET
JOINT COEFFICIENT = 100 BTU/HR FT² °F



Predicted temperatures for the final bracket design are shown in Figure 35. Peak temperature of the titanium is 438°F which is well below the allowed 600°F. This temperature should prove to be conservative since a joint coefficient of infinity (perfect contact at the joint bushings) was used.

It was determined during the analyses of the lower support lug thermal test that a 20% increase in the thermal conductivity of Inconel yielded better agreement with the test results. It was recommended that this modification be included in future analysis. Therefore, a run was made with the increased conductivity and the results are shown in Figure 35. Peak temperature of the titanium increased by 22°F to 460°F which is still below the allowed 600°F.

The predicted peak temperatures for the runs are summarized in Table II. The final design of the bracket is thermally satisfactory and has considerable margin for the peak temperatures.

FIGURE 35
PREDICTED TEMPERATURES
LEEWARD SIDE LUG AREA
FINAL DESIGN OF BRACKET
JOINT COEFFICIENT = INFINITY

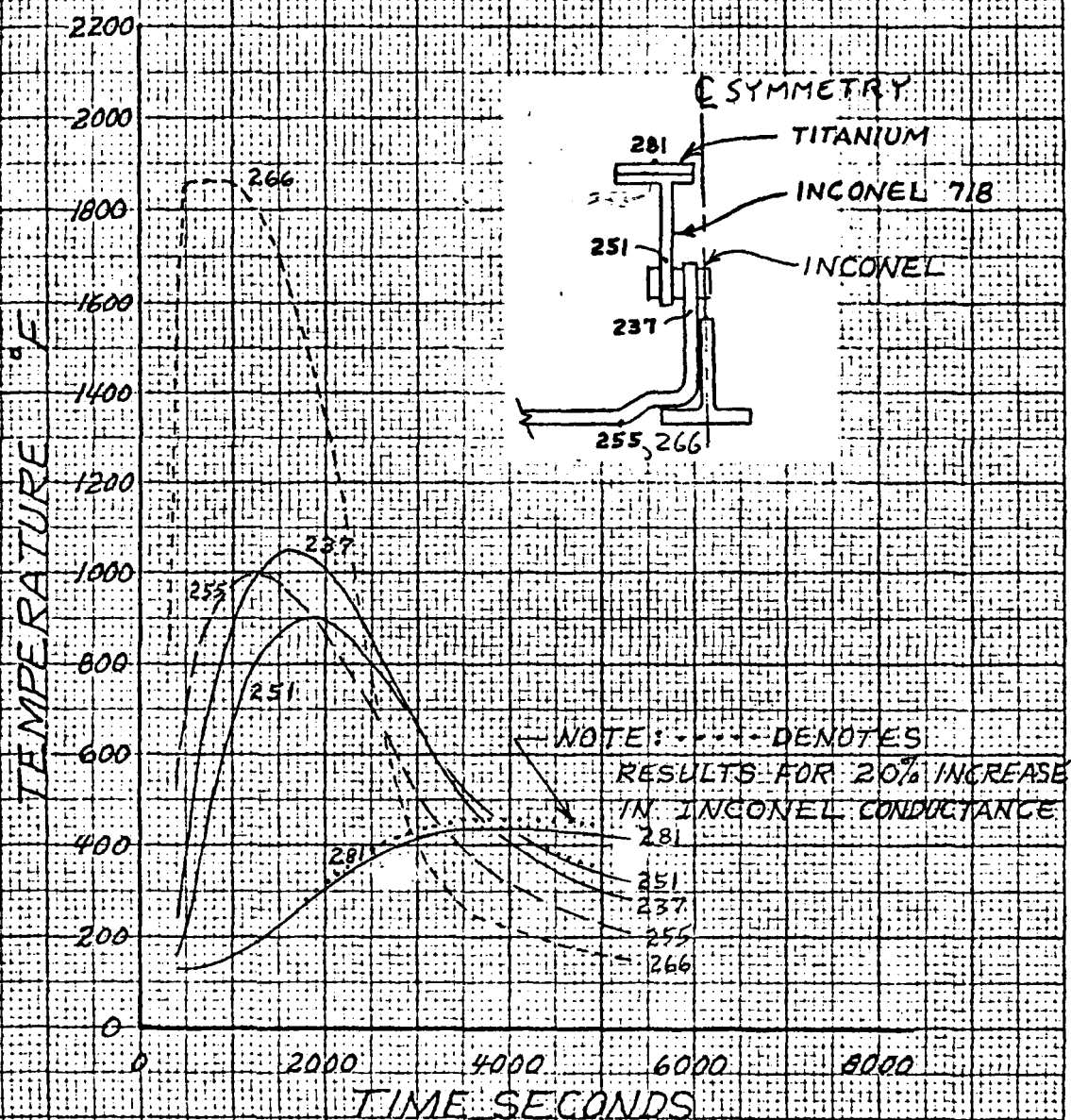


TABLE II
PREDICTED PEAK TEMPERATURES OF LEeward SIDE LUG

FIGURE NO.	33	34	35
PEAK TEMPERATURES (°F)			
Node No. Location			
237 RPP at Joint	1117	1118	1049
251 Hot end of Bracket	470	735	901
281 Titanium	329	452	438 (460)*
NOTES:			
Joint Coefficient	100	100	Infinity
Misc.	Silica Insulating Washers at Bolt	Preliminary Design of Bracket	Final Design of Bracket

* The higher temperature was obtained using 20% increased thermal conductivity for Inconel.

DESIGN INFORMATION ~~REQUEST~~ RELEASE

2-15-73

MODEL (S) AND EFF. GAP HEATING TEST		DIR. NO. T143-DIR-3-02		REV.
		DATE 2-1-73	PAGE 1	OF 37
SYSTEM Shuttle Leading Edge Phase III		REF. G. O. NUMBER 3357-DA-1160		
Fill in block below for Information Request		Fill in block below for Information Release		
TO _____ GROUP _____ REQ. BY _____ GROUP _____ REASON _____ TV ONLY <input type="checkbox"/> BWR <input type="checkbox"/> BUWPS <input type="checkbox"/>		IN REPLY TO DIR. NUMBER _____ REL. TO D. M. While GROUP 3-52000 PREPARED BY J. E. Medford DATE 2-1-73 GROUP APP. DATE 2-1-73 CHECKED BY DATE 2-1-73 PROJ. OFFICE DATE 2/4/73		

F. T. Esenwein, E. Matza, B. A. Forcht, W. E. Agan, W. A. Whitten, J. C. Utterback

DESIGN INFORMATION:

INTRODUCTION

A series of tests were performed on October 17-26, 1972 in the NASA MSC 10 MW plasma arc facility upon a model of the shuttle wing leading edge, in accordance with test plan T143/5L-20202. The objectives of these tests were as follows:

- Determine the magnitude of the gas leakage heating through the seal strip.
- Provide parametric data on effect of flow and seal design variations upon model temperatures.
- Provide confirmation or correction to gas leakage analysis methods.
- Evaluate potential methods of eliminating or reducing gas leakage heating.

This DIR includes discussion of the test model, test conditions, procedure, measurements and results. A post test thermal analysis of the test model is also presented.

TEST MODEL

A single test model, shown in Figures 1 and 2 and defined in detail in VMSC drawing T143T00008, and a calibration model, defined in VMSC drawing T143T00016, were evaluated. This model was a full scale section of the MSC 25K shuttle orbiter vehicle wing tip leading edge represented by the NACA 0010-64 air foil. This configuration was selected for the following reasons:

- 1) Consistency with test facility.
- 2) Desirability of employing a model which will represent entire gas leakage flow pattern.
- 3) Pre-test analysis results reported in T143-DIR-2-04 indicate model configuration provides reasonable simulation of reentry boundary layer flow.

Basic model size was 12.5 inches wide by 5.25 inches long with a 1.61 inch leading edge radius and model material was bare RPP-1. The width of the model was split into two sections by a seal strip which provided for adjustable seal geometry. Four seal strips were constructed to obtain the nine seal geometries in Figure 3. Model ends were closed out with graphite aerodynamic fairings and the downstream fairing included a vent to free stream. Mounting to a sting adapter assembly was accomplished with a graphite back closure. This closure was insulated with graphite felt. The model was instrumented with sixteen thermocouples, the locations of which will be shown in the test results.

Size and external contour of the calibration model was identical to the test model, but the material was graphite. The model was instrumented with nine pressure taps and nine calorimeters.

TEST CONDITIONS

The model was oriented at an angle of attack of 25° and a sweep angle of 60° to the flow as shown in Figure 4. This orientation results in a local theoretical angle of attack normal to the leading edge of 43° . Nitrogen test gas was used to avoid oxidizing the bare RPP model. Calibration runs were made with the graphite model to establish flow conditions required to meet the three tests points called for in the test plan. Two of these were achieved, and these are defined in Table I. The high pressure test condition could not be met.

TABLE I TEST CONDITIONS

Test Point	Enthalpy BTU/Lb	Pitot Pressure PSIA	Wing Stag. Line Press PSIA	4" Dia. Flat Face Heating Rate BTU/Ft ² Sec	Wing Stag. Line Heat- ing Rate* BTU/Ft ² Sec	Expected Wing S Line Heating Ra BTU/Ft ² Sec
1	16,500	.18	.071	102	24.8	100
2	11,000	.11	.041	55	24	60

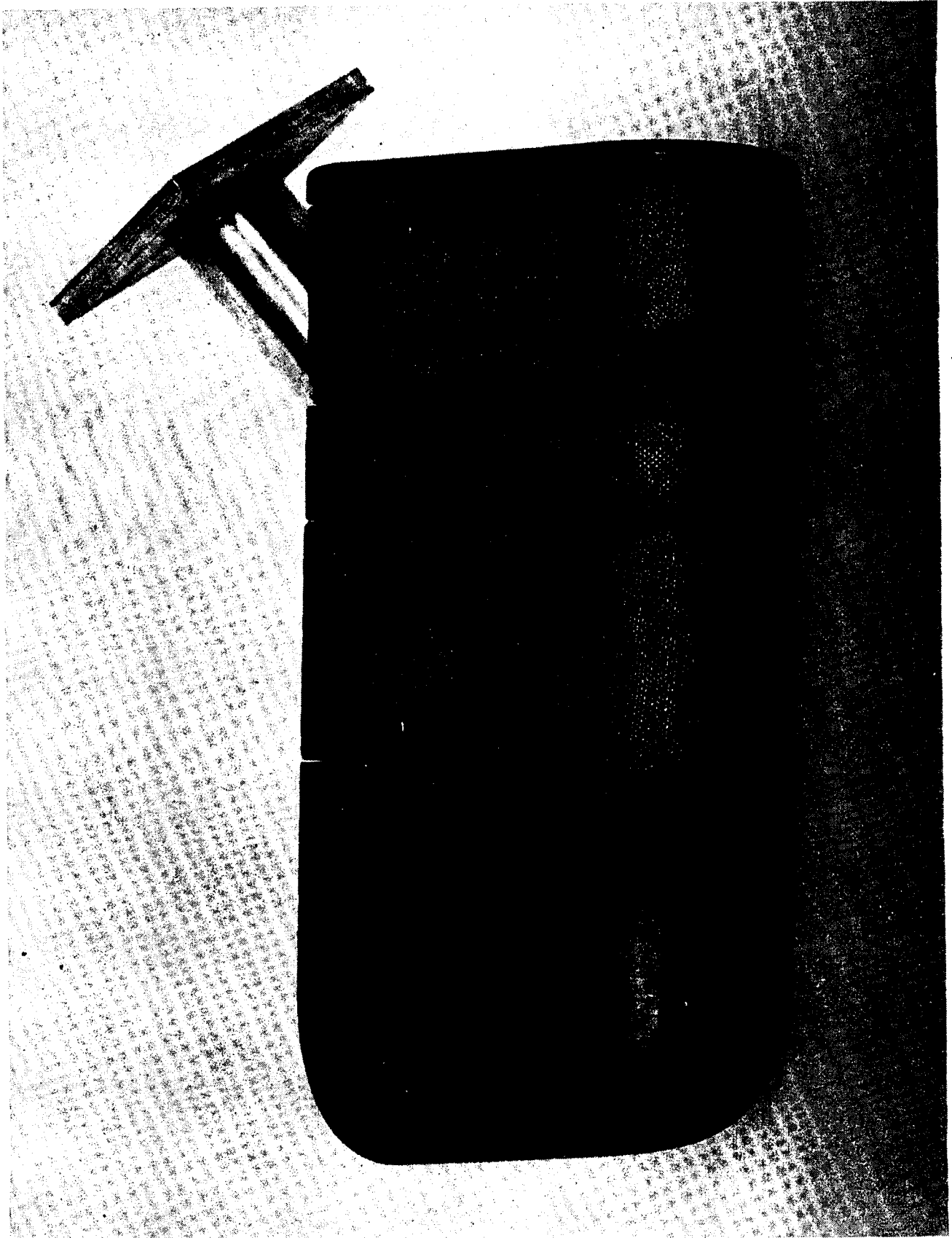


Figure 1 GAP HEATING MODEL

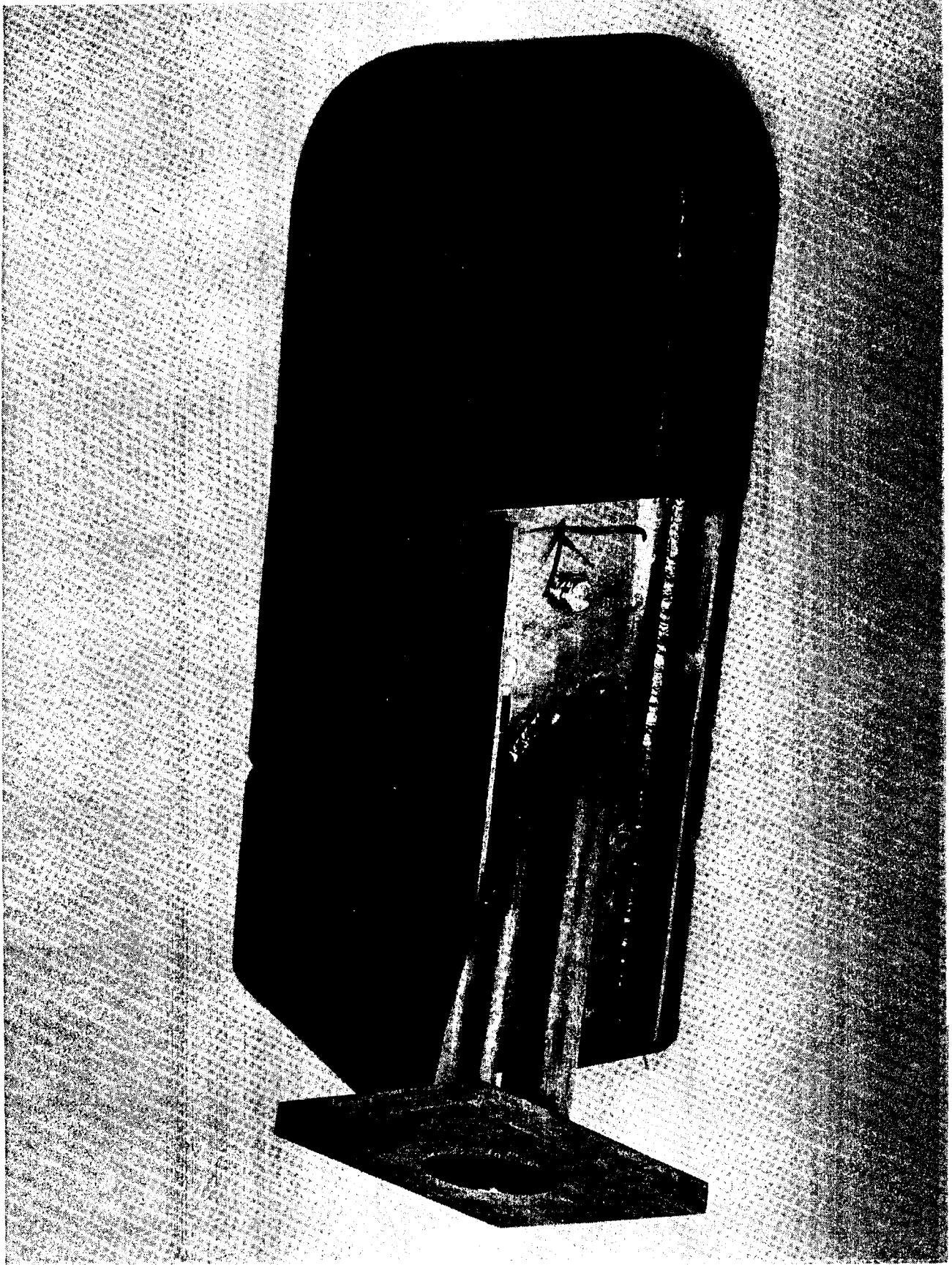
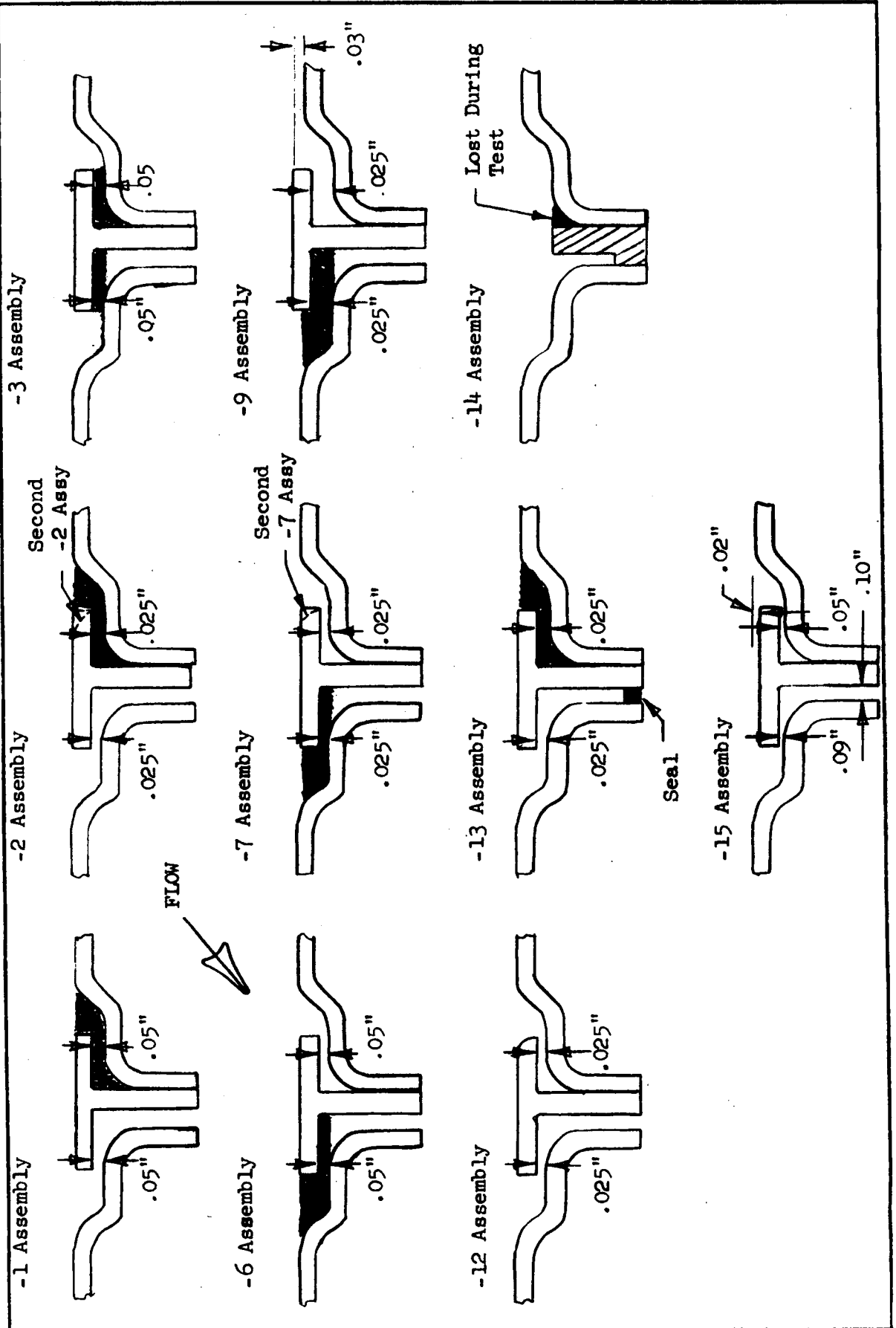


Figure 2 GAP HEATING MODEL REAR VIEW

Figure 3 SEAL CONFIGURATION



Bulk of the testing was performed at test point 1; one test was performed at test point 2. As can be seen, stagnation line heating rates, as measured by calorimeters on the calibration model, were 1/3 to 1/4 of expected values, and the reason for this is not presently known. The principal parameters requiring simulation are enthalpy and pressure, because of their influence on boundary layer thickness. Since the values of these parameters for the two lower pressure test points in the test plan were achieved, it was decided to accept the low heating rates. It will be seen in the discussion of post test thermal analyses that in order to obtain agreement between computed model skin temperatures and thermocouples in areas undisturbed by gap effects, it was necessary to assume a stagnation line heating rate of $42 \text{ BTU/Ft}^2 \text{ Sec}$ at test point 1, which is in somewhat better agreement with expectations than the calorimeters.

Heating rate and pressure distributions around the model for test point 1 are defined in Figure 5. When test facility operating conditions for each test point were established, a four inch diameter, flat face model with a transfer reference calorimeter was inserted to establish a correlation between heating rate on the model and that on the reference calorimeter.

It should be noted that the enthalpies in Table I are preliminary values. A recent NASA MSC memorandum indicates that the actual enthalpy may be either higher or lower than the preliminary values, with an uncertainty range of 7200 to 35,000 BTU/Lb.

TEST PROCEDURE

When plasma arc operating conditions for a given test point were established the reference calorimeter was inserted to confirm the heating rate. The test model was then inserted, held for 120 seconds, and removed. This provided time for stabilization of thermocouple readings with time. In the first test run only exposure time was 60 seconds and thermocouples did not stabilize, therefore this run was repeated. During each test run surface temperatures were obtained at selected points by optical pyrometer.

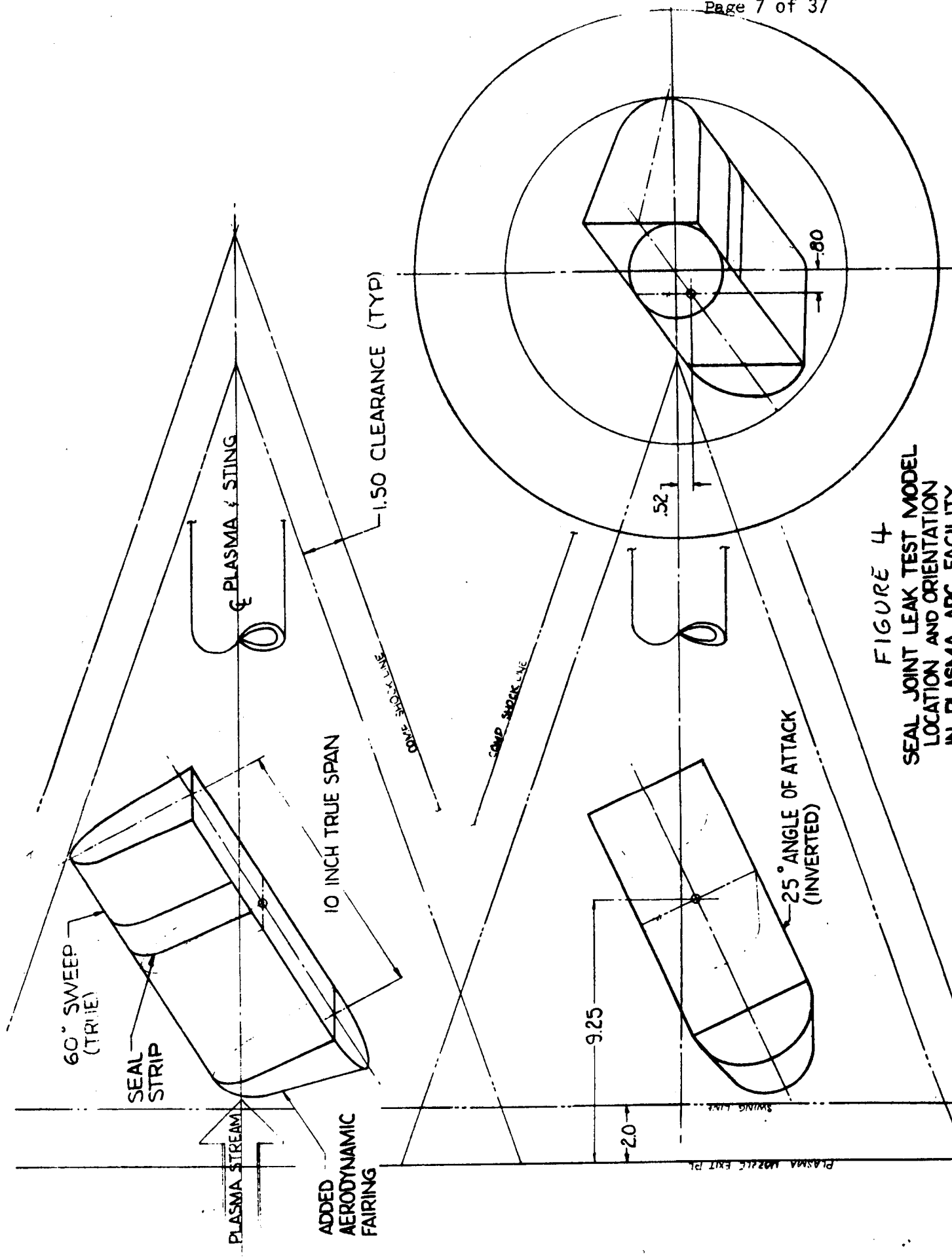
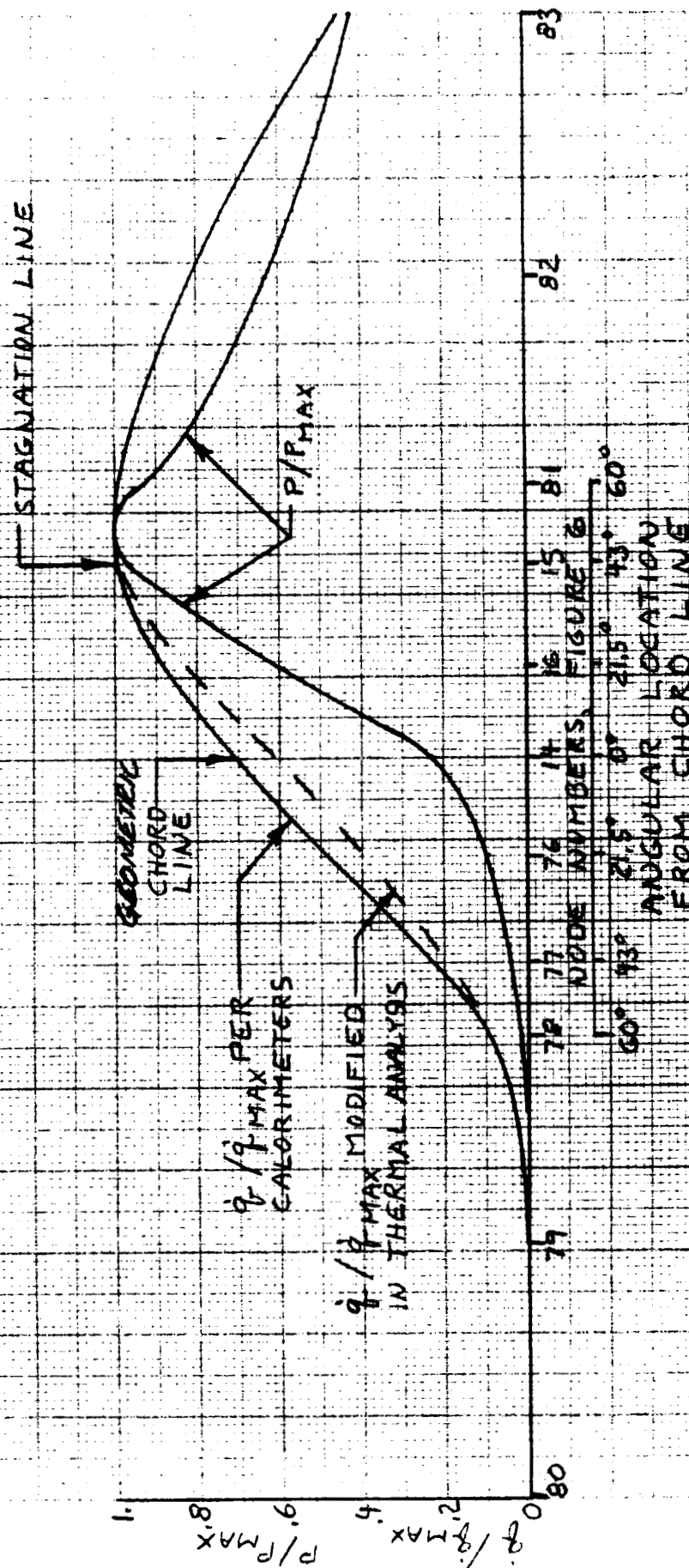


FIGURE 4
SEAL JOINT LEAK TEST MODEL
LOCATION AND ORIENTATION
IN DIAGRAM ABO FACILITY

FIGURE 5
CHORDWISE HEATING AND PRESSURE DISTRIBUTIONS
FROM CALIBRATION MODEL

q, q_{MAX} = LOCAL, MAXIMUM HEATING RATES
 P, P_{MAX} = LOCAL, MAXIMUM PRESSURES



TEST RESULTS

Test results are summarized in Tables II and III for the seal configurations shown in Figure 3. Thermocouple measurements for the reference thermocouples upstream of the tee, T_{17} and T_{18} , and downstream, T_{14} and T_{15} , were quite repeatable and in reasonable agreement with pyrometer measurements. The upstream reference thermocouples read 160 to 180°F higher than the downstream thermocouples, indicating higher heating rates upstream, although another contributing factor was higher cross radiation relief on downstream thermocouples due to radiation out of the vent hole on the downstream end of the model. For a preliminary evaluation of the data, undisturbed reference temperatures at the tee leading and trailing edges were established by interpolation between measured values for T_{18} and T_{19} on the stagnation line and T_{17} and T_{14} on the chord line.

The highest temperature area in the seal region was the leading edge of the tee, which ran about 180°F higher than the undisturbed value at the stagnation line and 160°F higher at the chord line, for a 0.025 inch upstream gap between the tee and the skin. This temperature was not affected significantly by rounding the edge of the tee. On the stagnation line it was increased about 140°F over the value for a 0.025 inch gap by increasing the gap to 0.05 inch and about 70°F by protruding the tee 0.03 inch above the skin surface. Filling the gap with carbon filler material increased the temperature of the seal leading edge at the stagnation line by 90°F, over the value for a 0.025 inch gap, presumably due to suppressing cross radiation cooling effects.

The next highest temperature area on the seal was the trailing edge of the tee, which ran about 110°F above the undisturbed value at the stagnation line and 100°F higher at the chord line for downstream gaps up to 0.05 inch. Note that these preliminary evaluations did not account for thermocouple or test environment variations.

Increasing the downstream gap to 0.10 inch (which is considered to be an unrealistically large gap) increased this temperature at the stagnation line by 450°F over the value for smaller gaps. The 0.10 inch gap also increased the skin temperature

TABLE II STAGNATION LINE GAP HEATING TEST RESULTS



Run	Assy	q_{FF} BTU / Ft ² - Sec	T ₁₅	T ₂₃ Pyro**	T ₂₃	T ₁ Pyro**	T ₁	T ₂	T ₃	T ₁₃	T ₁₀	T ₁₈ Pyro**	T ₁₈
1	- 2	100	2366	-	-	2400*	2465	2034	1256*	1719*	2671	2590	2533
2	- 2	55	1944	-	-	2100	2104	1710	1386	1681	2227	1980	2104
1 (re- peat)	- 2	100	2399	-	-	2700	2555	2044	1934	2160	2730	no data	2499
4	- 13	100	2377	2425	-	2700	2567	2094	1925	2145	2742	2500	2561
5	- 7	100	2355	2300	-	2650	2578	1905	1729	2185	2647	2380	2516
6	- 1	100	no data	2600	2432	2700	2510	2034	1955	2165	2730	2425	2550
7	- 3	100	2280	2480	2366	2650	2555	1905	1826	2135	2742	2585	2555
8	- 6	100	2275	no data	2323	no data	2590	1876	1807	2217	2790	no data	2556
9	- 9	100	2323	2490	2312	2540	2567	1876	1846	2186	2718	2600	2613
10***	- 14	100	2433	no data	2790	-	-	2421	2377	-	-	2660	2660
10*** (re- peat)	- 14	100	2476	2900	2813	-	-	2399	2333	-	-	2630	2499

* Not Stable

Carbon Felt Filler Lost During Test

** Uncorrected

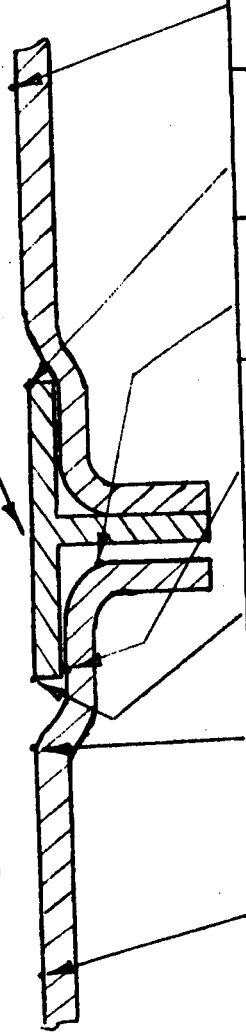
Thermocouple Bad

N. J. All Temp in OF

TABLE II STAGNATION LINE, (Cont'd.)

Run	Assy	$q_{FF}^{BTU}/Ft^2\text{-Sec}$	T ₁₅	T ₂₃ Pyro**	T ₂₃	T ₁ Pyro**	T ₁	T ₂	T ₃	T ₁₃	T ₁₀	T ₁₈ Pyro**	T ₁₈
1	-12	100	2301	-	2338	2640	2366	2004	1975	2227	2648	2600	2323*****
1	-12	100	2301	-	2421	2700	2410	1985	1975	2248	2648	2575	2323*****
repeat)													
2	- 2'	100	2280	-	2399	2700	2454	1965	1945	2217	2718	2560	2522
3	- 7'	100	out	-	2312	2650	2488	1827	1807	2259	2682	2630	2533
4	-15	100	2377	-	2642	2600	2960	2135	2095	2269	2625	2540	2510

TABLE III 43° OFF STAG. LINE GAP HEATING TEST RESULTS



Run	Assy	q_{FF} BTU/Ft ² - Sec	T ₁₄	T ₂₄ Pyro	T ₇	T ₈	T ₉	T ₁₁	T ₁₇	T ₁₇ Pyro	T ₇ Pyro
1	- 2	100	2104	-	2074	1566	1089*	2290	no data	-	-
2	- 2	55	1734	-	1816	1509	2124	1974	1816	-	-
1	- 2	100	2114	2280	2237	1885	2825	2432	2258	2215	-
(repeat)											
4	-13	100	2084	-	2237	1905	1758	2432	2185	-	-
5	- 7	100	2059	-	2237	1758	1585	2399	2135	-	-
6	- 1	100	2034	-	2196	1866	1739	2095	2185	-	-
7	- 3	100	2024	-	2216	1748	1652	2095	2201	-	-
8	- 6	100	2024	2220	2248	1739	1633	2125	2186	2250	2240
9	- 9	100	2014	-	2176	1729	1643	2344	2165	-	-
10	-14	100	2145	-	-	2217	2105	-	2186	-	-
10	-14	100	2114	-	-	2206	2135	-	2135	-	-
(repeat)											
11	-12	100	2024	-	2054	1827	1720	2280	2206	-	-
11	-12	100	2024	-	2085	1846	1749	2196	2217	-	-
(repeat)											
12	- 2'	100	2004	-	2075	1846	1749	2344	2217	-	-
13	- 7'	100	1985	-	2135	1729	1652	2301	2238	-	-
14	-15	100	2044	-	2206	1975	1895	2280	out	-	-

* Not Stable

Note: All Temp in °F

immediately downstream of the tee, T_{23} , by 280°F over the value for smaller gaps. The only effect of filling the downstream gap, relative to gaps of 0.025 to 0.050 inch, was in reducing temperatures on the skin and rib underneath the tee. Blocking this gap at the interior flange of the tee and rib (-13 assembly) had no effect.

Removing the tee completely and replacing it with a filler, as shown in Figure 3 for the -14 assembly, increased the skin temperature downstream of the tee, T_{23} , by 440°F over the value for tees with small downstream gaps.

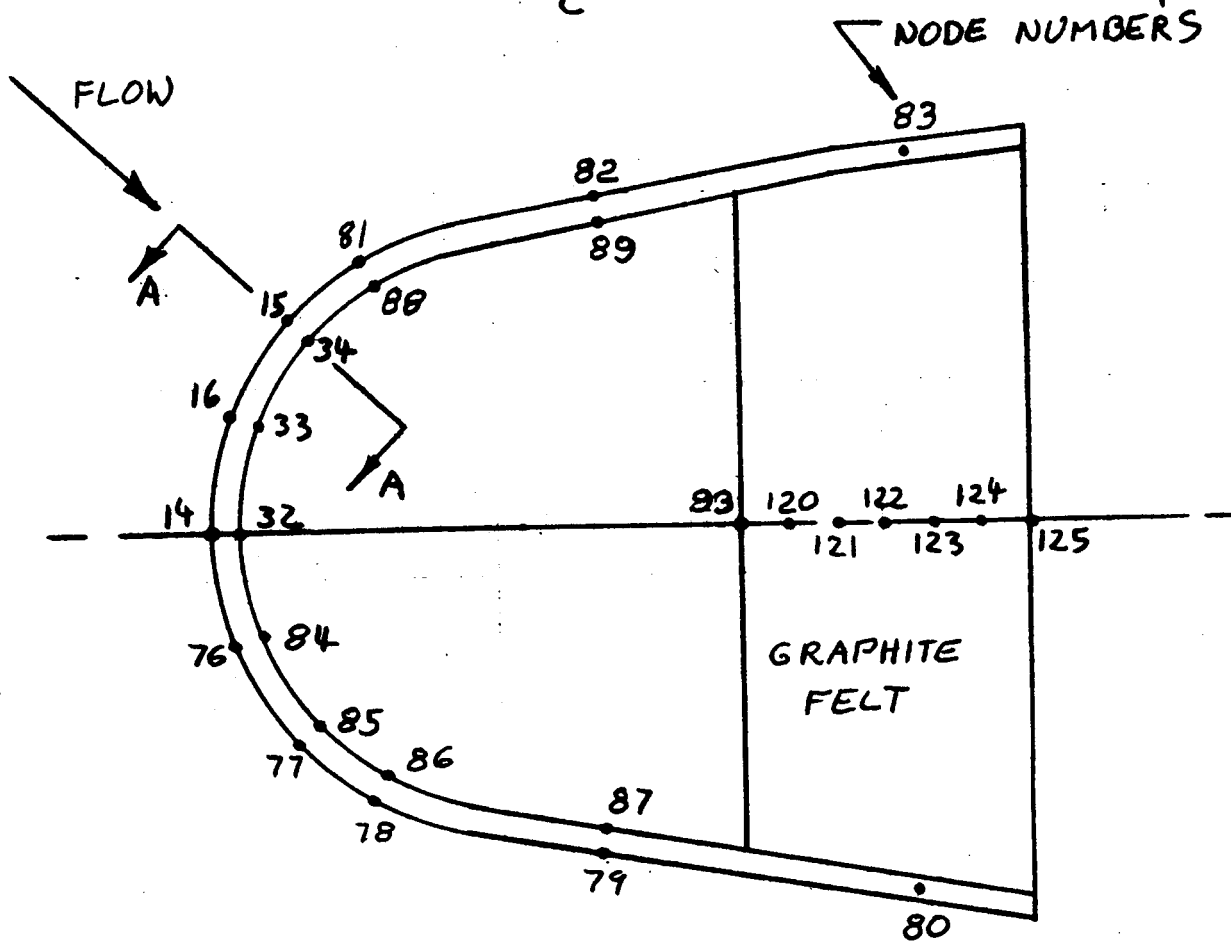
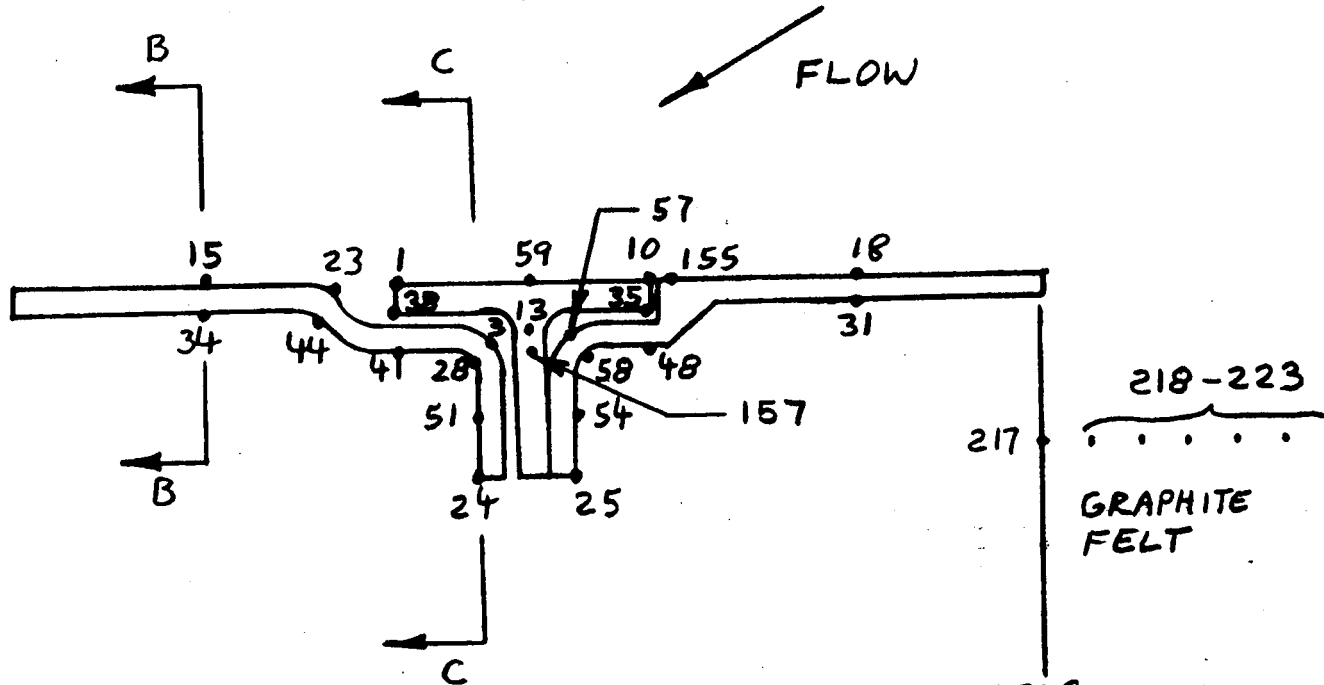
THERMAL ANALYSIS

Thermal Model

Results of the gap heating tests show that temperatures on the tee seal are higher than those on the undisturbed portion of the model skin. However, data trends indicate that a large part of this temperature increase may be due to suppressed cross radiation cooling in the seal area. It is important to separate such effects from heating due to gap air leakage and surface disturbances. A thermal analysis was therefore performed of the gap heating model to assess the relative importance of heat conduction and cross radiation effects as opposed to convective heating due to gaps.

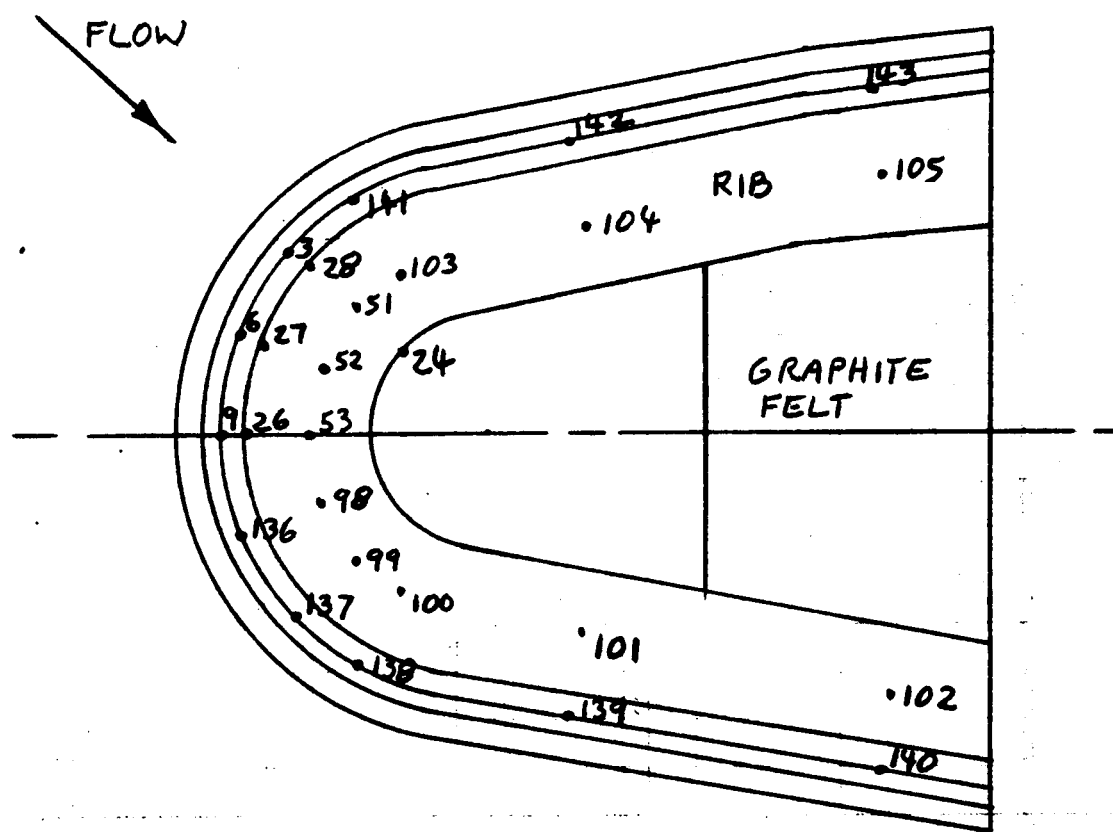
A 166 node three-dimensional thermal model was developed for the gap heating model. Three sections cut through the model are shown in Figures 6 and 7. The model includes effects of heat conduction in the RPP in spanwise, chordwise and across thickness directions. Heat transfer across gaps is by either radiation or conduction in carbon filler material, as appropriate. Cross radiation is included between the inside of the skin, ribs, graphite felt insulation, and downstream aerodynamic fairing with vent holes. Baseline computer runs were made with external convective heating rates as determined by calorimeters on the calibration model. Adjustments were then made to these heating rates to force agreement with thermocouples in undisturbed heating areas (nodes 15 and 18 at stagnation line and 14 and 17 at chord line). Heating in gaps was inferred by adjusting heating in these areas to force agreement between calculations and thermocouple readings.

FIGURE G, THERMAL MODEL
SECTION A-A STAGNATION LINE



SECTION B-B

FIGURE 7
THERMAL MODEL



SECTION C-C

Undisturbed Heating Distributions

Initial analyses to establish the undisturbed convective heating distribution were conducted for the -3 assembly tee configuration shown in Figure 3, with both upstream and downstream gaps sealed. Results using calorimeter heating rates with constant heating in the spanwise direction showed calculated temperatures to be below thermocouple readings by the following amounts.

	<u>Downstream</u>	<u>Upstream</u>
Stagnation Line	340°F	490°F
Chord Line	200°F	290°F

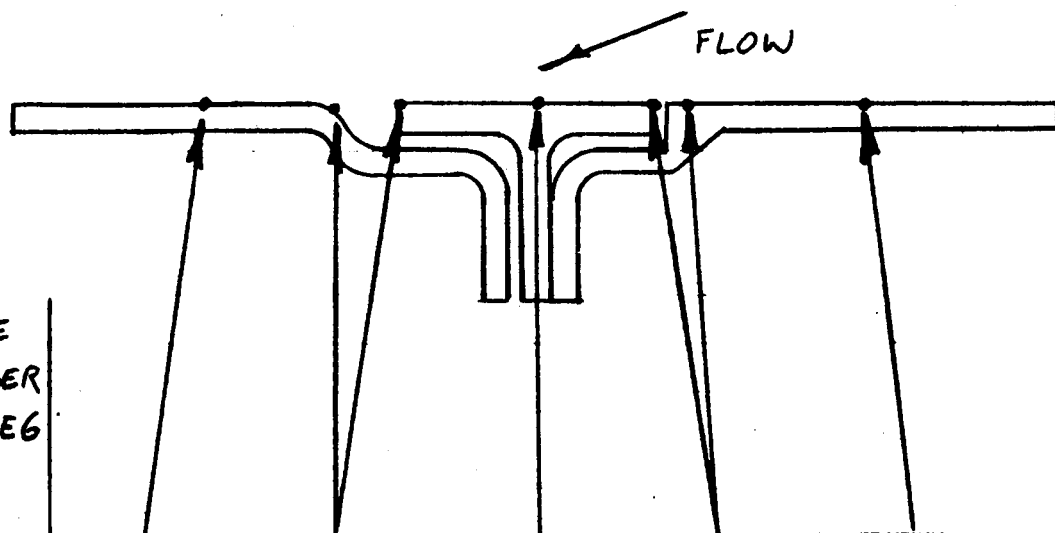
To correct these differences it was necessary to incorporate the following changes to the undisturbed heating distribution.

- Increase stagnation line heating rate at tee centerline from 24.8 to 42.3 BTU/Ft² Sec.
- Incorporate a spanwise heating distribution defined by $\dot{q} \approx L^{-.316}$ where L is wetted distance from stagnation point on upstream fairing.
- Modify chordwise heating distribution as shown in Figure 5.

It will be noted that the exponent in the spanwise heating distribution relation $N = -.316$ is intermediate between the values normally associated with purely stagnation line flow $n=0$ and wedge or flat plate flow, $n = -.5$. The final, undisturbed heating distribution is shown in Figure 8. Computed temperatures with this heating distribution are compared with measured values in Figures 9 and 10 and are in reasonable agreement.

Heating in Disturbed Flow Areas

Initial computer runs on the -3 assembly were performed with no heating in the upstream gap between the tee leading edge and skin. Results at the stagnation line gave a temperature for the tee leading edge, node 10, 73°F above that of the upstream undisturbed value, node 18. Thermocouples indicated a temperature difference of 202°F. It was concluded that part (73°F) but not all of the increased tee temperature was due to suppressed cross radiation cooling caused by the carbon filler and two thicknesses

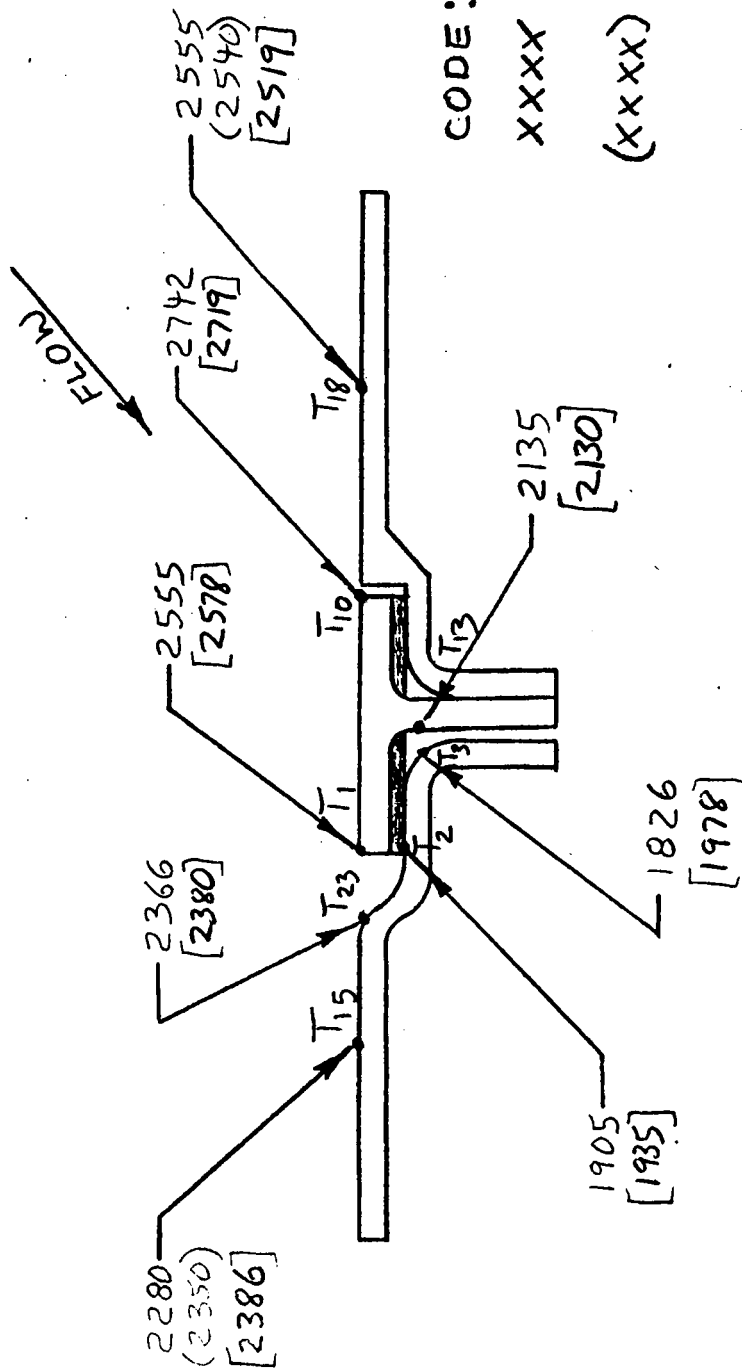


ANGULAR LOCATION FROM CHORD LINE	NODE NUMBER FIGURE 6					
	83	83 .433		113 .461		69 .500
	82	82 .759		112 .808		68 .875
60°	81	81 .938	144 .973	111 1.000	146, 156 1.031	67 1.083
43° STAG. LINE	15	15 .938	23, 1 .973	59 1.000	10, 155 1.031	18 1.083
21.5°	16	16 .760	4 .788	60 0.810	12, 154 .835	19 .876
0° CHORD LINE	14	14 .563	7 .584	61 .600	11, 153 .619	17 .650
21.5°	76	76 .376	148 .390	106 .400	150, 152 .412	62 .433
43°	77	77 .188		107 .200		63 .216
60°	78	78 .072		108 .077		64 .083
	79	79 0.0		109 0.0		65 0.0
	80	80 0.0		110 0.0		66 0.0

← NODE
NUMBER

RATIO: LOCAL TO
MAXIMUM HEATING
RATE

UNDISTURBED HEATING DISTRIBUTION
FIGURE 8



CODE:

XXXX MEASURED TEMP, °F

-3 ASSY.

(XXXX) MEASURED TEMP, °F

AVERAGE OF 12 TEST

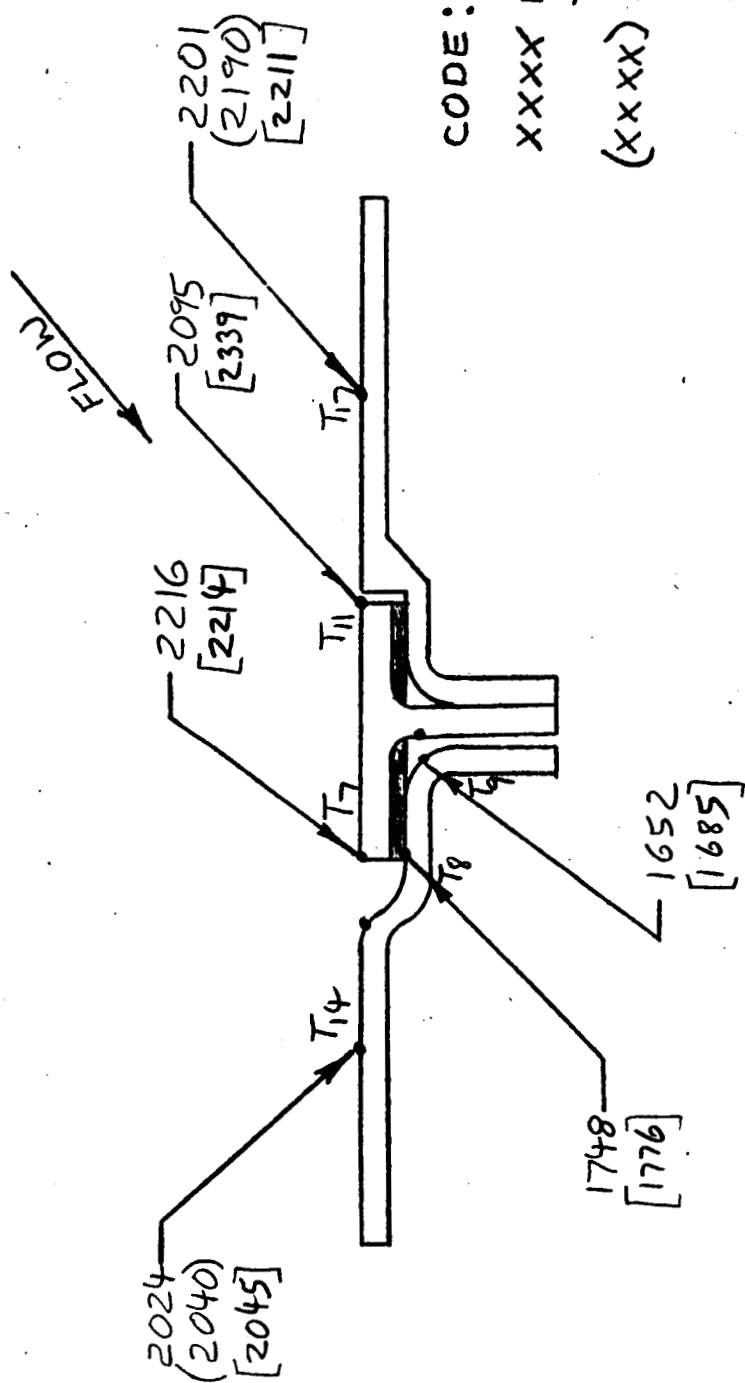
RUNS ON 10 CONFIGU-

RATIONS

[XXXX] COMPUTED TEMP, °F

TEMPERATURE COMPARISON
STAGNATION LINE, -3 ASSEMBLY

FIGURE 9



CODE:

XXXX MEASURED TEMP, °F
-3 ASSY.

(XXXX) MEASURED TEMP, °F
AVERAGE OF 12 TEST
RUNS ON 10 CONFIGU-
RATIONS

[XXXX] COMPUTED TEMP, °F

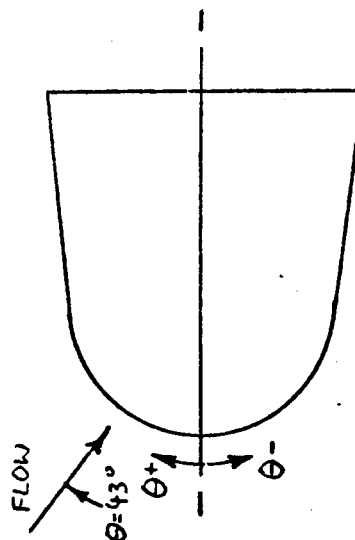
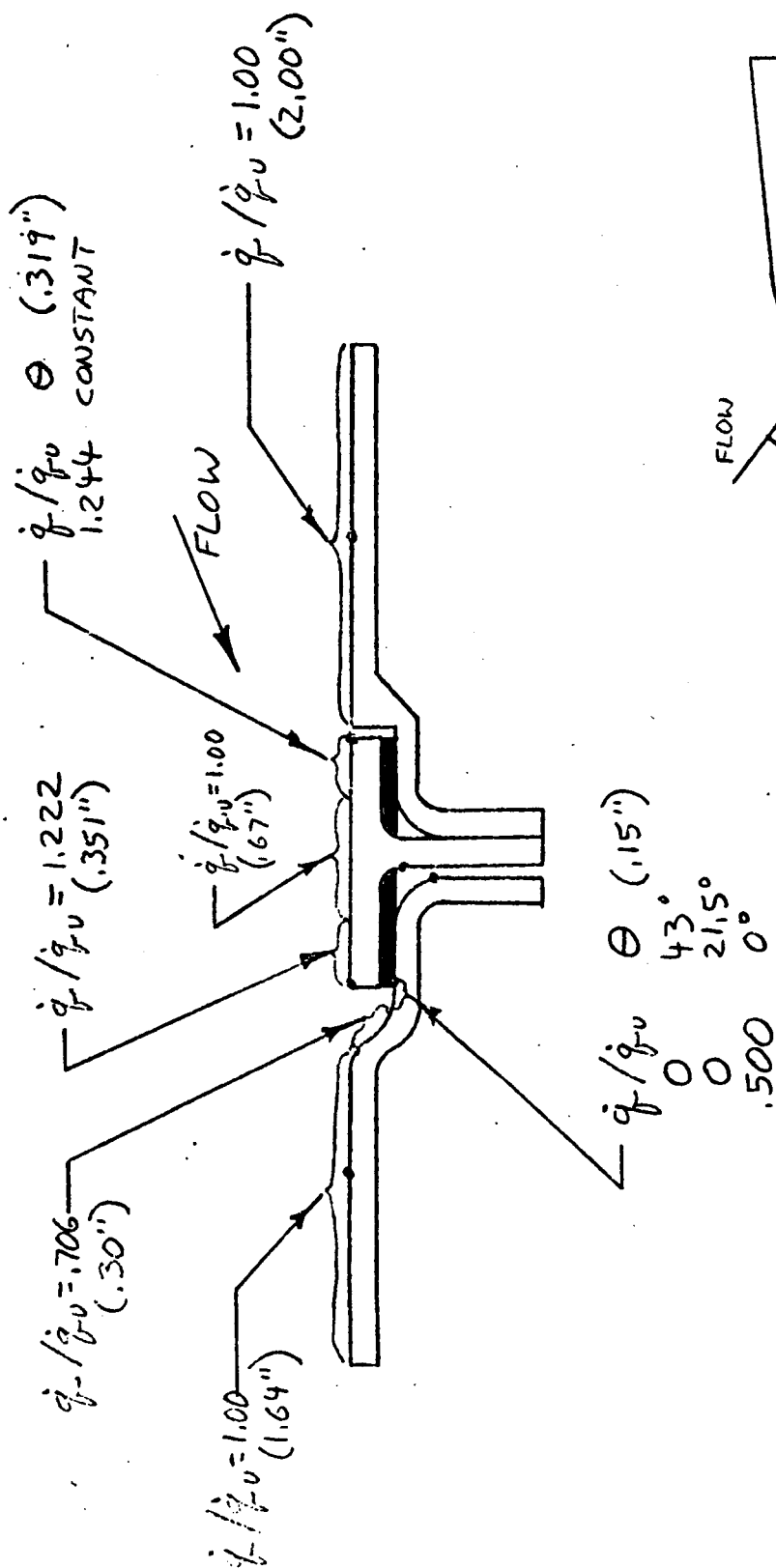
TEMPERATURE COMPARISON
CHORD LINE, -3 ASSEMBLY

FIGURE 10

of RPP (tee and skin). Hence additional runs were made with convective heating in the upstream gap. Likewise, in the downstream gap between the tee trailing edge and skin joggle, assuming no gap heating results in underpredicting temperatures.

In order to obtain agreement between computed and measured temperatures at the tee leading and trailing edges and on the skin in the downstream joggle area, the convective heating over the -3 assembly was set as shown in Figure 11. This figure presents the ratio of local heating rate to the undisturbed heating rate at the same location. The local heating rate presented is the average heating rate over the nodal heated area shown in Figure 11. The heating on the tee leading and trailing edge external nodes is 22 to 24% above the undisturbed heating. On the tee leading edge node this increased heating may be due to either heating in the 0.03 inch gap between the tee and the skin, or to increased heating over the external surface. Likewise, on the tee trailing edge node the increased heating is probably at least partially due to heating on the backward facing step of the tee. Heating in the downstream cavity varies from zero to 70% of undisturbed heating.

The temperatures computed for the -3 assembly with the heating in Figure 11 are compared with measured temperatures in Figures 9 and 10. It is seen that the agreement is generally quite good. The greatest differences are for the tee leading edge at the chord line, node 11, and the rib at the stagnation line, node 3. The computed temperature at node 11 is 295°F above the measured value. The local heating at this location was not reduced to bring about better agreement because for the -2 assembly, which also had a sealed upstream gap, the measured temperature at T_{11} was 337°F higher than for the -3 assembly. On the other hand, for node 3 there was a consistent trend for the various assemblies of computed temperature exceeding measured temperatures. The difference was greatest for the -3 assembly (150°F) and the -7 assembly, both of which had carbon filler in the downstream gap. For these two assemblies the difference is believed to be at least partially due to inaccuracies in conductivity values used for the carbon filler material. This will be discussed in more detail later.



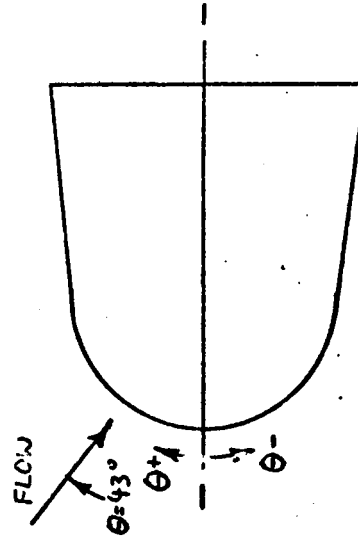
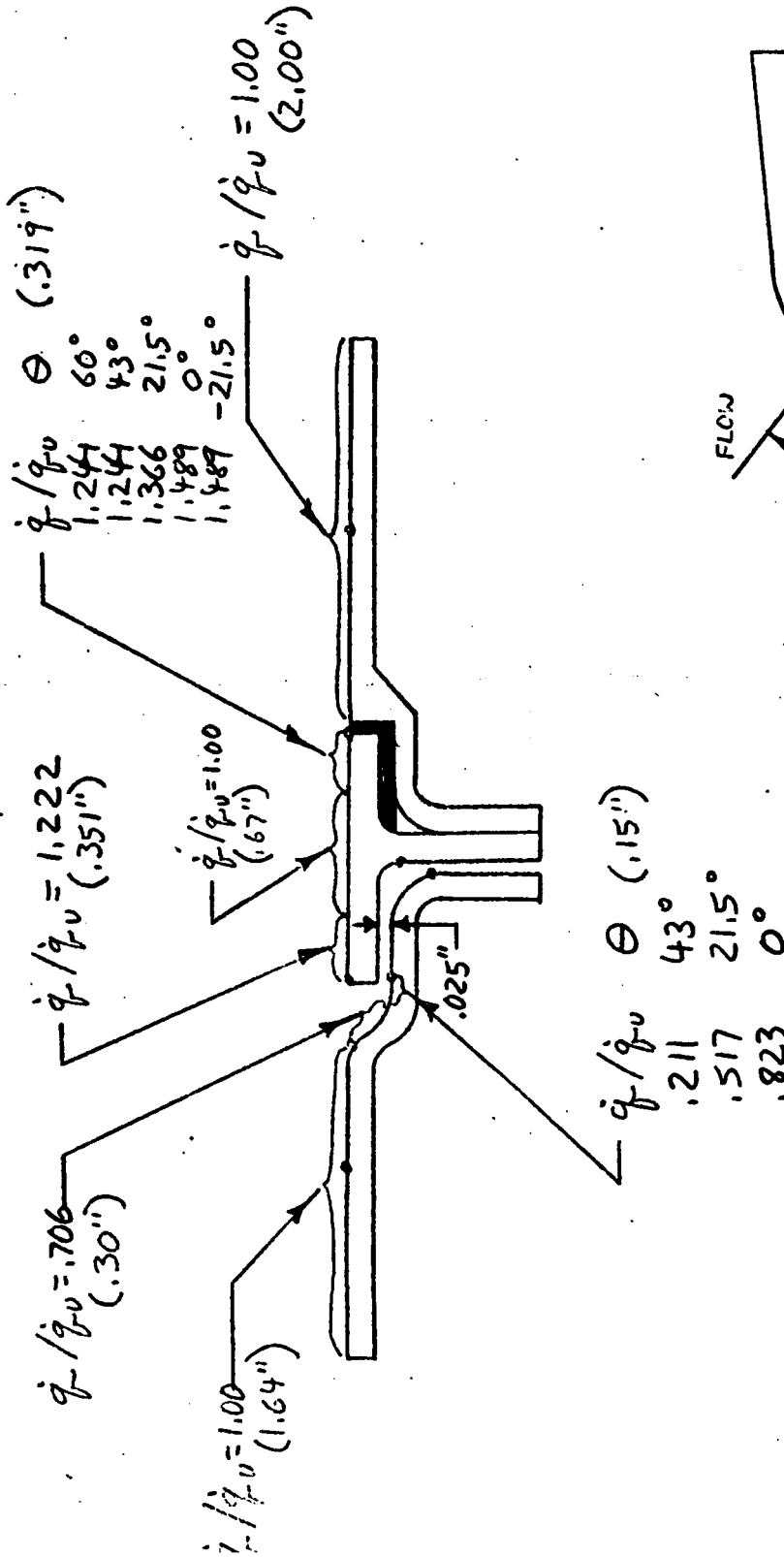
\dot{q} = LOCAL HEATING RATE
 \dot{q}_u = UNDISTURBED HEATING
 (XXX) = DISTANCE OVER WHICH HEATING OCCURS

HEATING ON -3 ASSEMBLY
FIGURE II

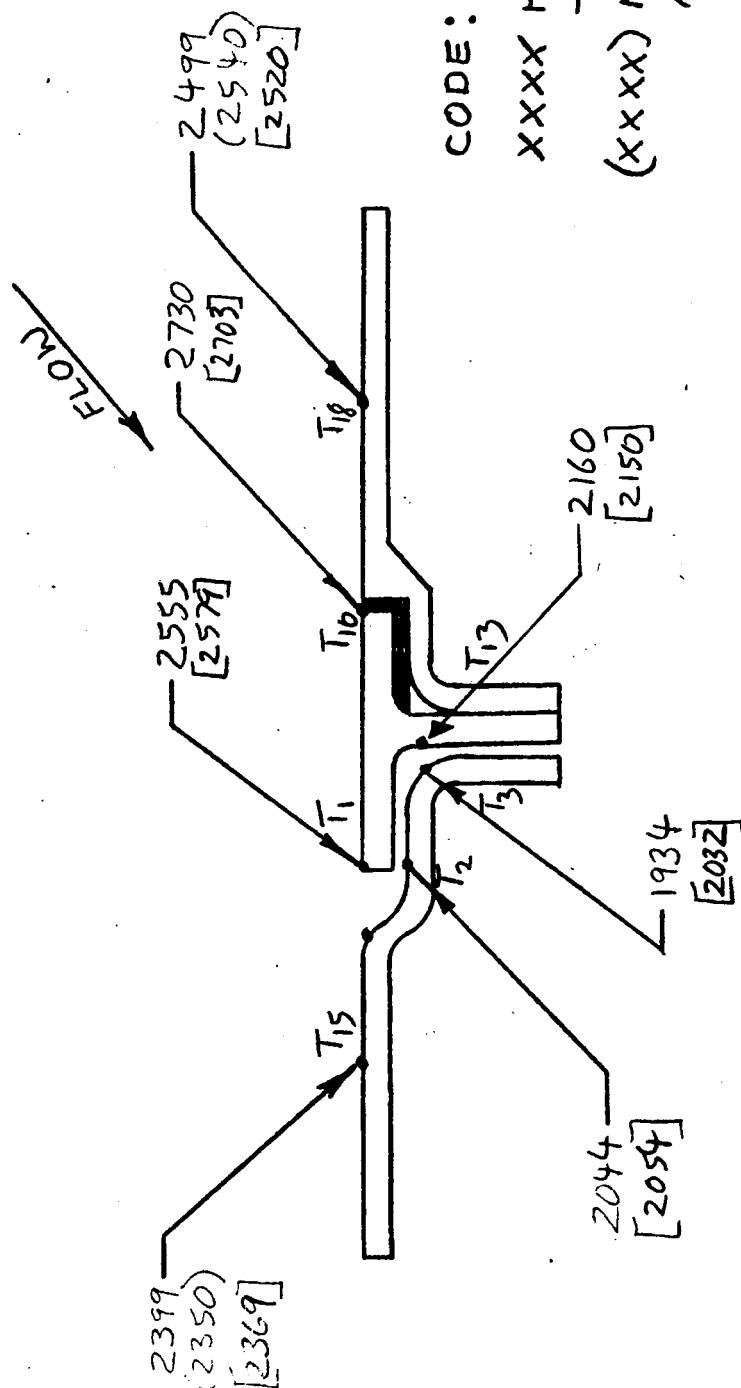
The heating distribution for the -2 assembly is shown in Figure 12. On this assembly the downstream gap was opened up to 0.025 inch. The heating on the tee trailing edge external node and on the forward facing surface of the downstream cavity were the same as for the -3 assembly. However, the heating on the cavity floor was higher, varying from 21 to 82% of undisturbed heating. This later result was surprising, since no heating was required in the horizontal or vertical gap between the tee and rib to match measured temperatures. Lack of heating in these gaps would suggest little or no gap air flow and would indicate heating in the cavity should be equal to that for the -3 assembly which had sealed gaps. This will be discussed in more detail later. The most surprising result for the -2 assembly was that in order to match measured temperatures it was necessary to impose increased heating on the tee leading edge exterior nodes, even though the upstream gap was completely sealed as shown in Figure 12. This is not understood at this time.

Comparisons between computed and measured temperatures for the -2 assembly are given in Figures 13 and 14. The agreement is quite good except for the rib at the stagnation line, node 3, where the computed temperature exceeds the measurement by 100°F. A similar, but greater difference was also noted for the -3 assembly.

The heating distribution for the -1 assembly is shown in Figure 15. This assembly is identical to -2 except that the downstream gap was further opened from .025 to .050 inch. The heating distribution is identical to that for the -2 assembly, except for a slight increase in heating to the downstream cavity. Computed temperatures are compared with measured values in Figure 16 and 17. The greatest differences are for the rib at the stagnation line Node 3 and the tee leading edge at the chord line node 11. The 77° difference for node 3 is somewhat less than that noted previously for the -3 and -2 assemblies. The 337°F difference for node 11 is similar to that noted for the -3 assembly. The heating at this location was not reduced to bring about better agreement for the same reason discussed in conjunction with the -3 assembly. There appears to be no logical reason for T_{11} to be 337°F lower on the -1 and -3 assemblies than on the -2 assembly.

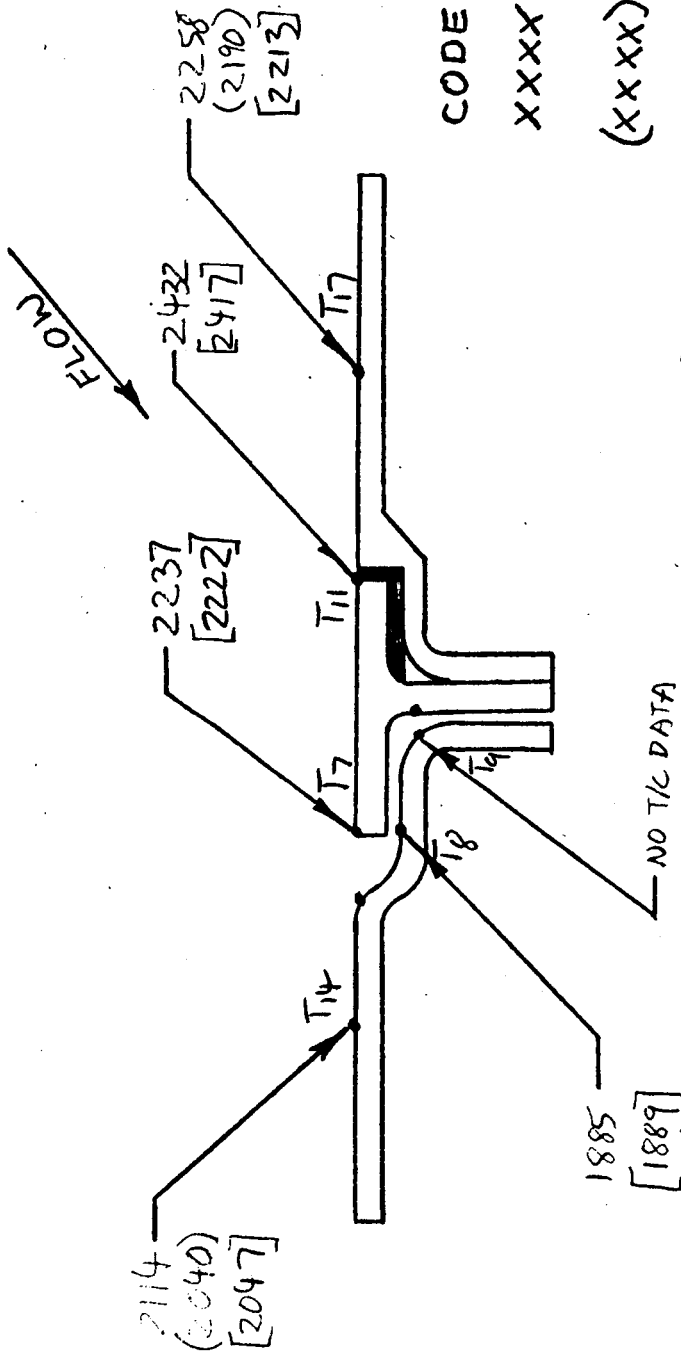


HEATING ON -2 ASSEMBLY
FIGURE 12



TEMPERATURE COMPARISON
STAGNATION LINE, -2 ASSEMBLY

FIGURE 13



CODE:

XXXX MEASURED TEMP, °F

-2 ASSY.

(XXXX) MEASURED TEMP, °F

AVERAGE OF 12 TEST

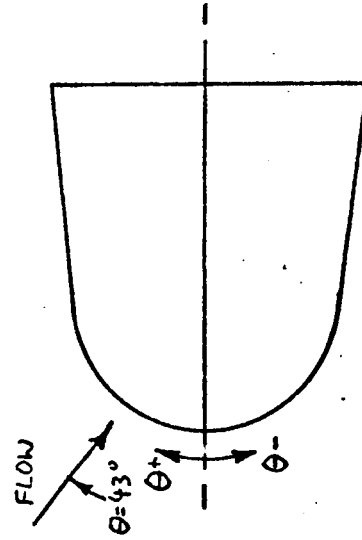
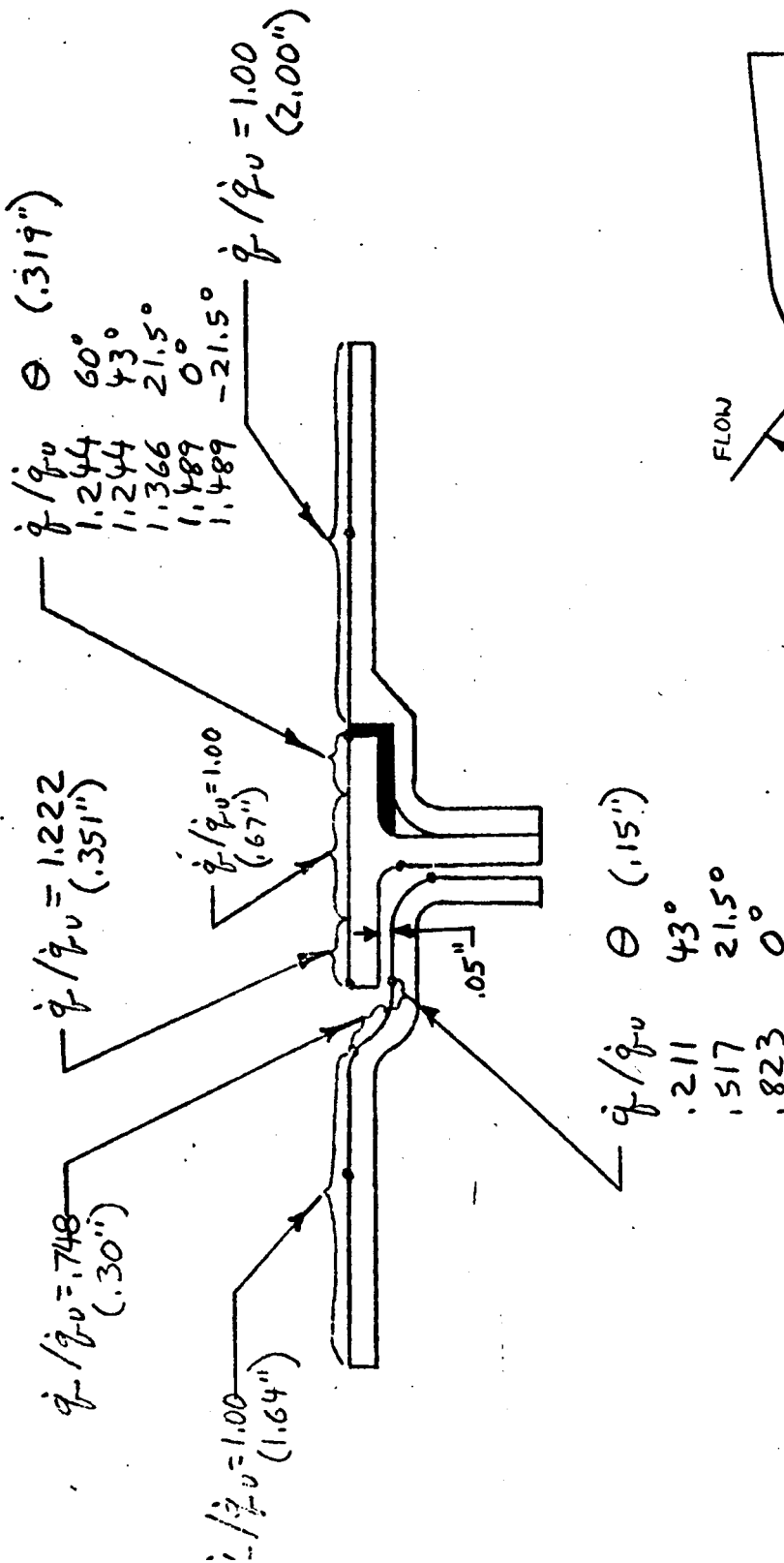
RUNS ON 10 CONFIGU-

RATIONS

[XXXX] COMPUTED TEMP, °F

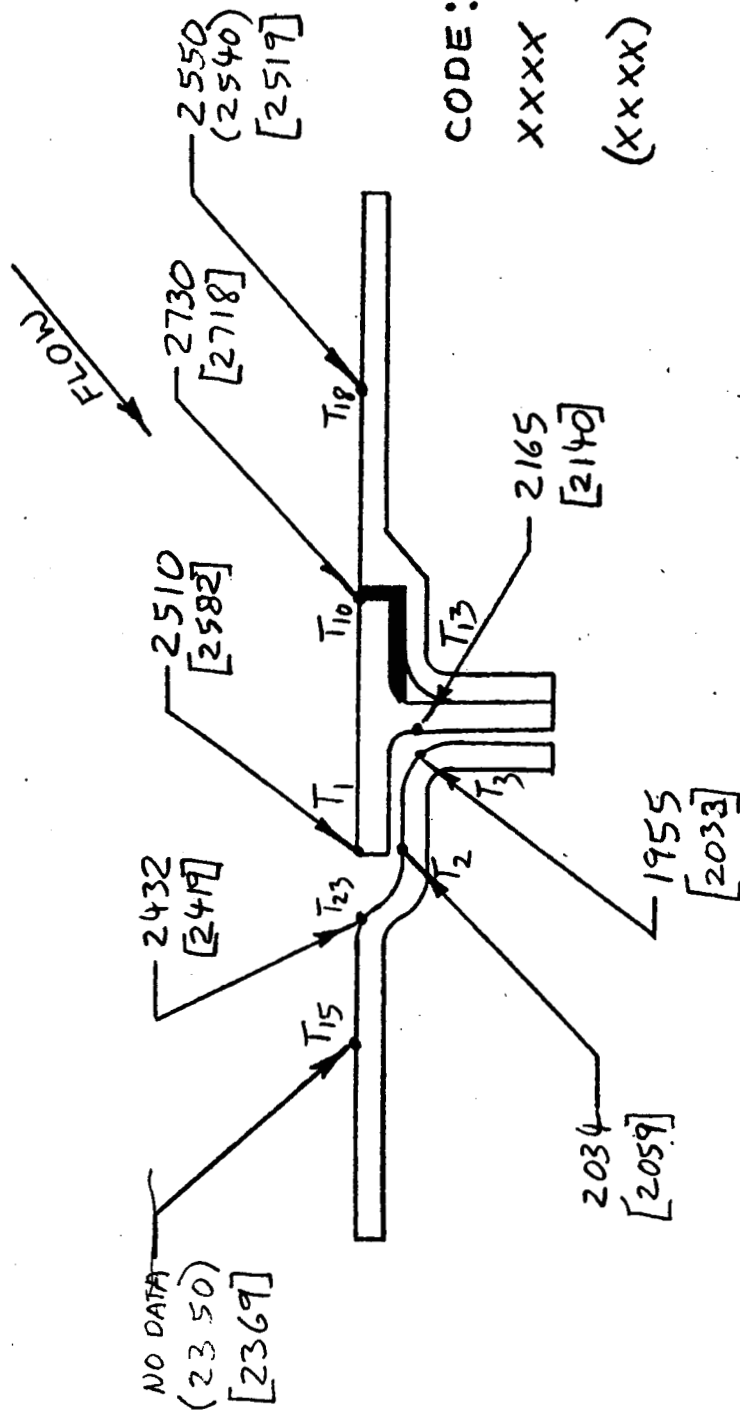
TEMPERATURE COMPARISON
CHORD LINE, -2 ASSEMBLY

FIGURE 14



\dot{q} = LOCAL HEATING RATE
 \dot{q}_u = UNDISTURBED HEATING
 (XXX) = DISTANCE OVER WHICH
 HEATING OCCURS

HEATING ON -1 ASSEMBLY
FIGURE 15

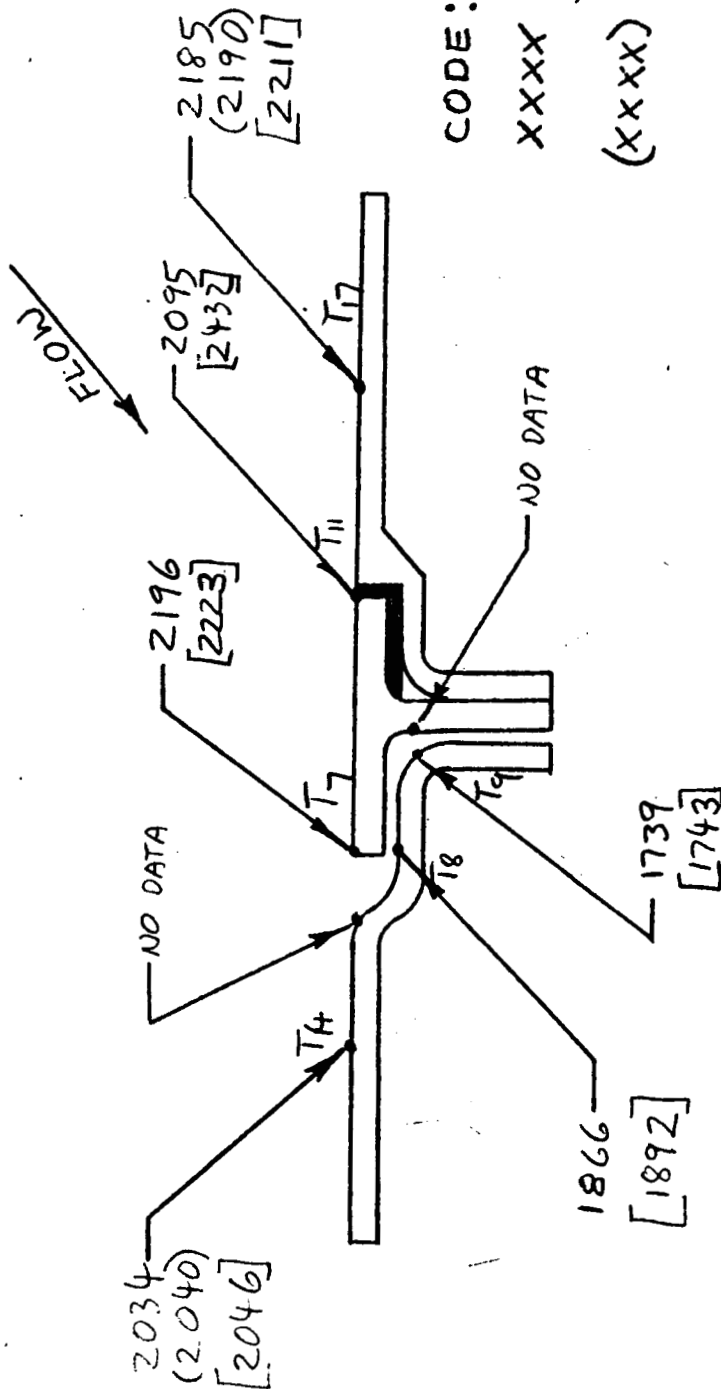


CODE:

XXXX MEASURED TEMP, °F
-1 ASSY.
(XXXX) MEASURED TEMP, °F
AVERAGE OF 12 TEST
RUNS ON 10 CONFIGU-
RATIONS
[XXXX] COMPUTED TEMP, °F

TEMPERATURE COMPARISON
STAGNATION LINE, -1 ASSEMBLY

FIGURE 16



CODE:

XXXX MEASURED TEMP, °F
-1 ASSY.

(XXXX) MEASURED TEMP, °F
AVERAGE OF 12 TEST
RUNS ON 10 CONFIGU-
RATIONS

[XXXX] COMPUTED TEMP, °F

TEMPERATURE COMPARISON
CHORD LINE, -1 ASSEMBLY

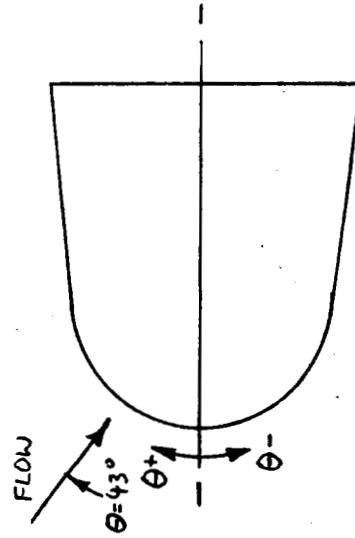
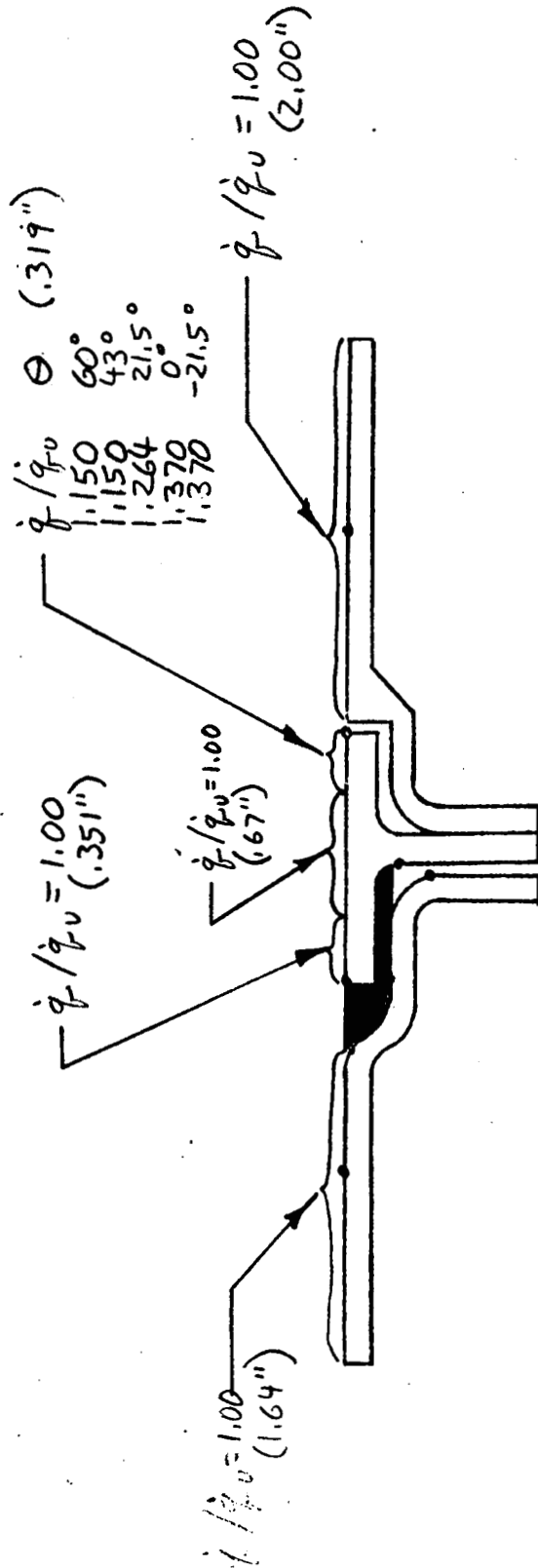
FIGURE 17

The heating distribution on the -7 assembly is shown in Figure 18. On this assembly the downstream gap was sealed and the upstream gap was opened to 0.025 inch. The only area of increased heating was the tee leading edge where the local average heating was 15 to 37% above the undisturbed value. This is in line with results for previous tee configurations and shows that opening the gap did not increase heating on the tee leading edge.

Computed and measured temperatures for the -7 assembly are compared in Figures 19 and 20. It is seen that the agreement is reasonable for external temperatures, however, computed rib temperatures significantly exceed measured values. This trend was seen for all tee configurations, but the magnitude of the differences is greatest for the -3 and -7 assemblies, both of which have carbon felt between the tee and rib in the downstream gap. It is believed that this is not due to RPP conductivity inaccuracy, since the values used for this property are measured values for RPP-0, and the RPP-1 used in the test model should have slightly higher conductivity.

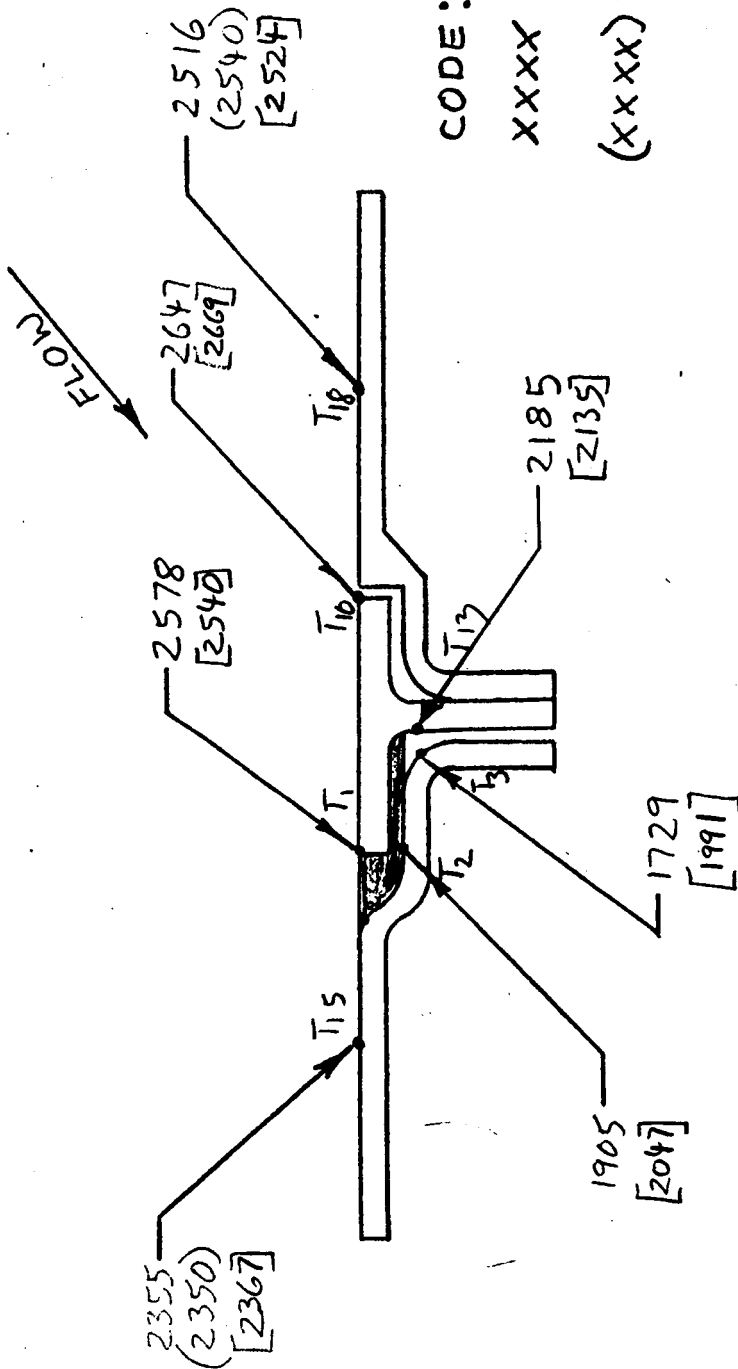
It is more likely that the felt conductivity is lower than that used in the analysis. The felt was compressed somewhat in the model installation, and limited available data indicates this would lower the conductivity. It should be noted that the computed temperatures in Figures 19 and 20 reflect a felt conductivity which was reduced by a factor of 1/2 from the "nominal" values used in analysis of the other assemblies. A previous computer run for the -7 assembly with nominal felt conductivity showed even greater differences between computed and measured rib temperatures.

It is evident that a further reduction in felt conductivity is required to bring about reasonable agreement in rib temperatures. Additional computer runs were made with further reductions in felt conductivity for both the -3 and -7 assemblies. The results showed that reducing felt conductivity significantly improves agreement between computed and measured rib temperatures and only slightly effects external tee temperatures. From the standpoint of inferring heating rates in disturbed flow areas the only area which is affected significantly is the floor of the downstream cavity for the -3 assembly. Reducing felt conductivity with no change in heating on the



\dot{q} = LOCAL HEATING RATE
 \dot{q}_v = UNDISTURBED HEATING
 (XXX) = DISTANCE OVER WHICH
 HEATING OCCURS

HEATING ON -7 ASSEMBLY
 FIGURE 18



CODE:

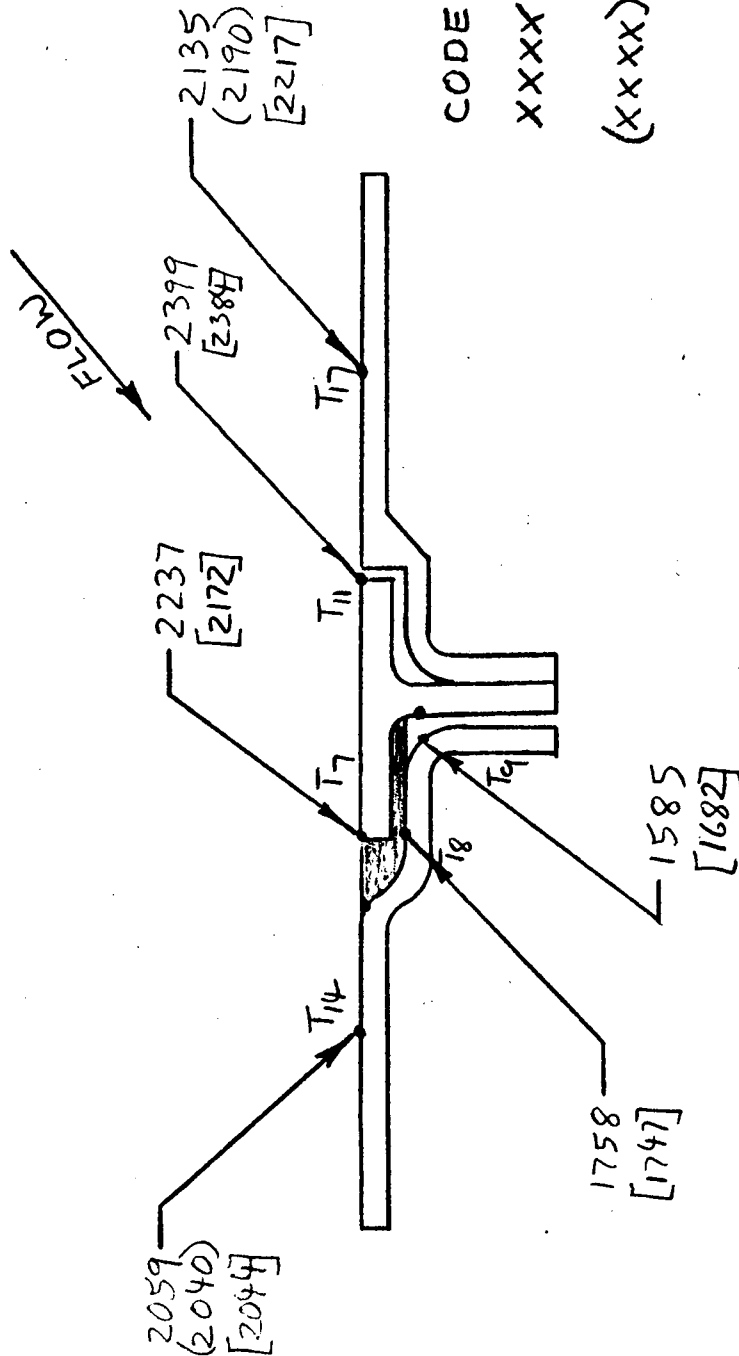
XXXX MEASURED TEMP, °F
-7 ASSY.

(XXXX) MEASURED TEMP, °F
AVERAGE OF 12 TEST
RUNS ON 10 CONFIGU-
RATIONS

[XXXX] COMPUTED TEMP, °F

TEMPERATURE COMPARISON
STAGNATION LINE, -7 ASSEMBLY

FIGURE 19

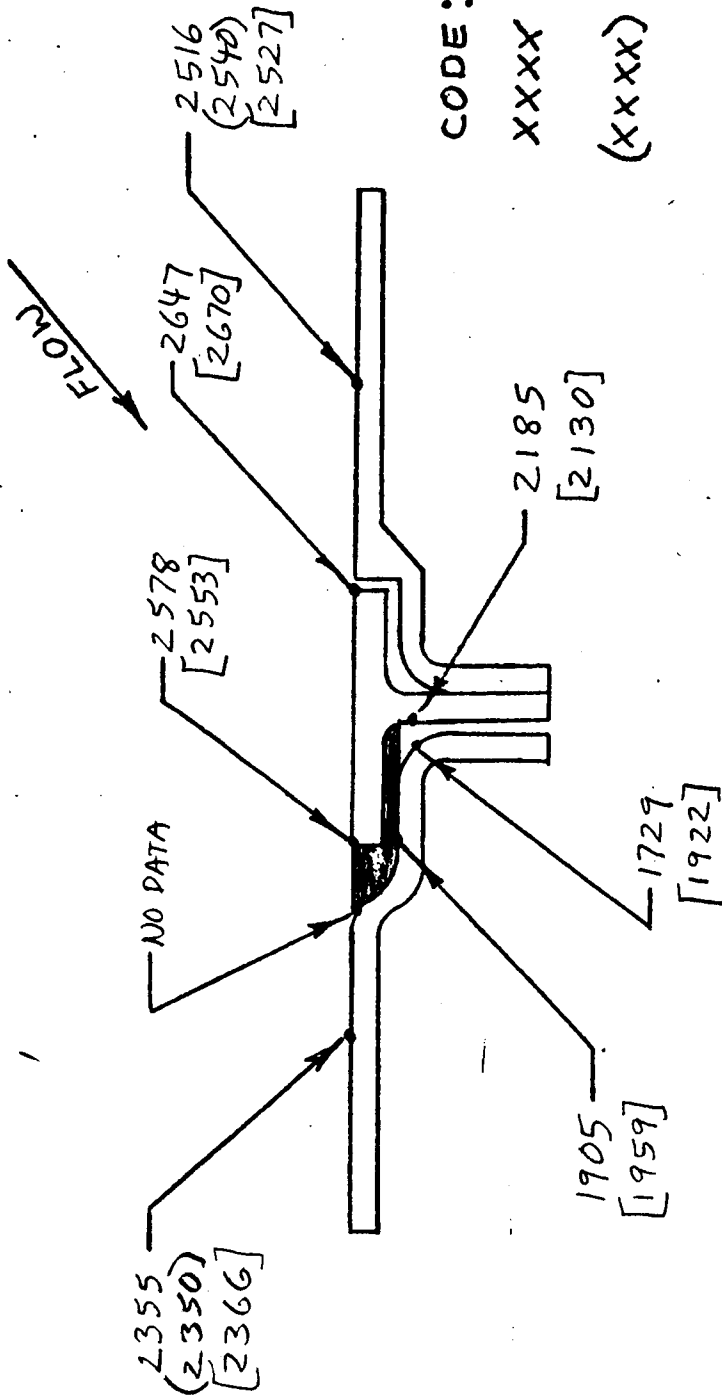


CODE:

XXXX MEASURED TEMP, °F
- 7 ASSY.
(XXXX) MEASURED TEMP, °F
AVERAGE OF 12 TEST
RUNS ON 10 CONFIGU-
RATIONS
[XXXX] COMPUTED TEMP, °F

TEMPERATURE COMPARISON
CHORD LINE, -7 ASSEMBLY

FIGURE 20



CODE:

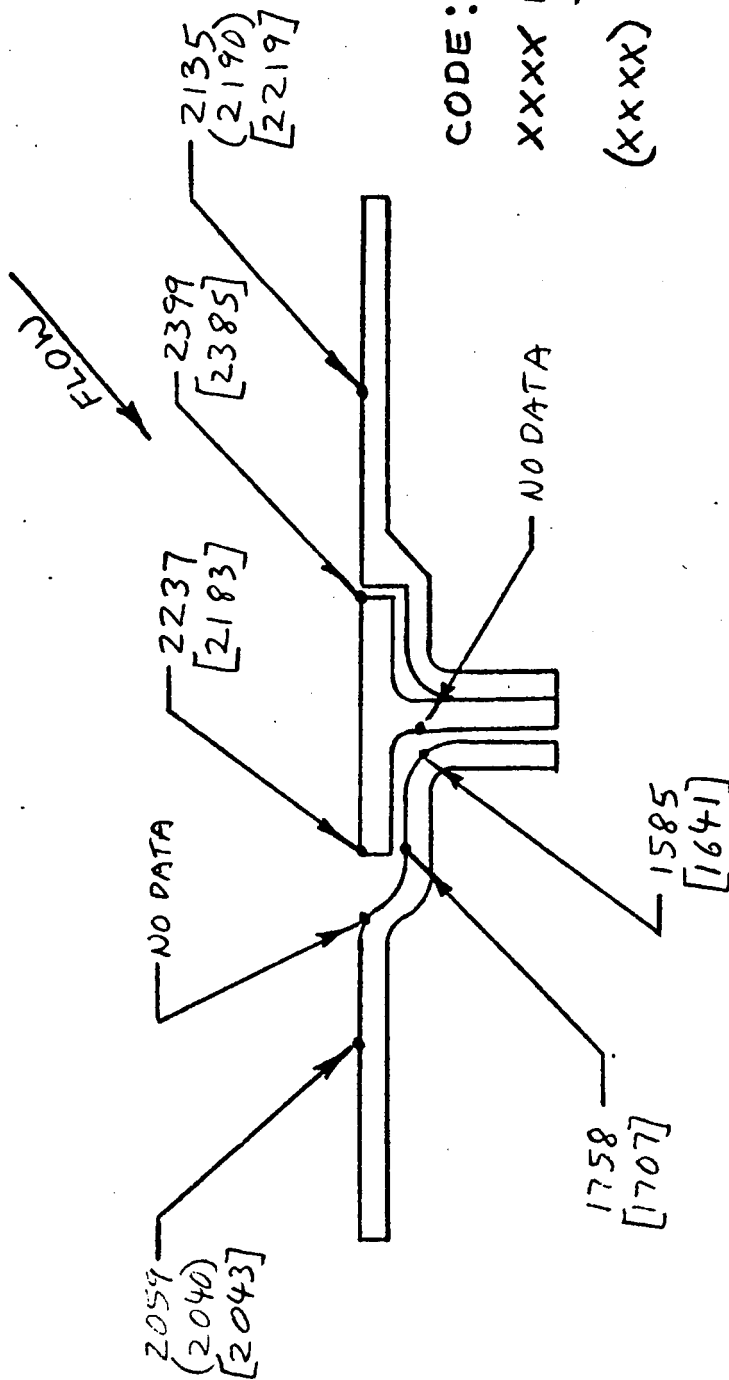
XXXX MEASURED TEMP, °F
-7 ASSY.

(XXXX) MEASURED TEMP, °F
AVERAGE OF 12 TEST
RUNS ON 10 CONFIGU-
RATIONS

[XXXX] COMPUTED TEMP, °F

NOTE: REDUCED CONDUCTIVITY OF CARBON
FILLER

TEMPERATURE COMPARISON
STAGNATION LINE, -7 ASSEMBLY
FIGURE 21



CODE:

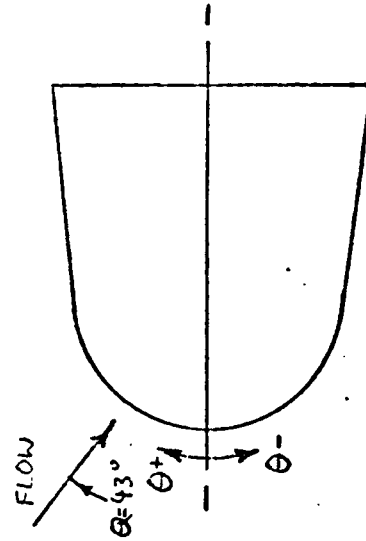
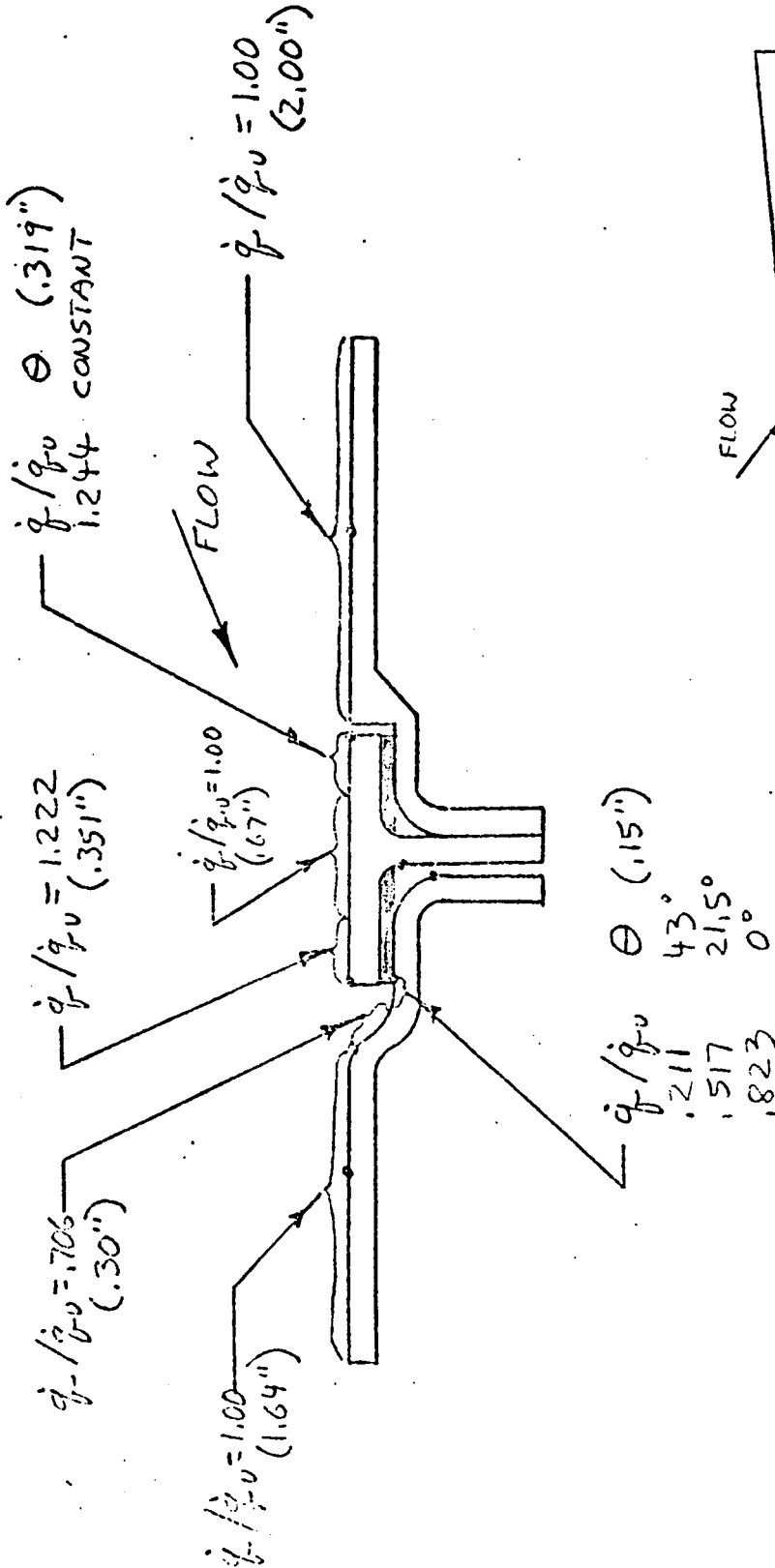
XXXX MEASURED TEMP, °F
- 7 ASSY.

(XXXX) MEASURED TEMP, °F
AVERAGE OF 12 TEST
RUNS ON 10 CONFIGU-
RATIONS

[XXXX] COMPUTED TEMP, °F

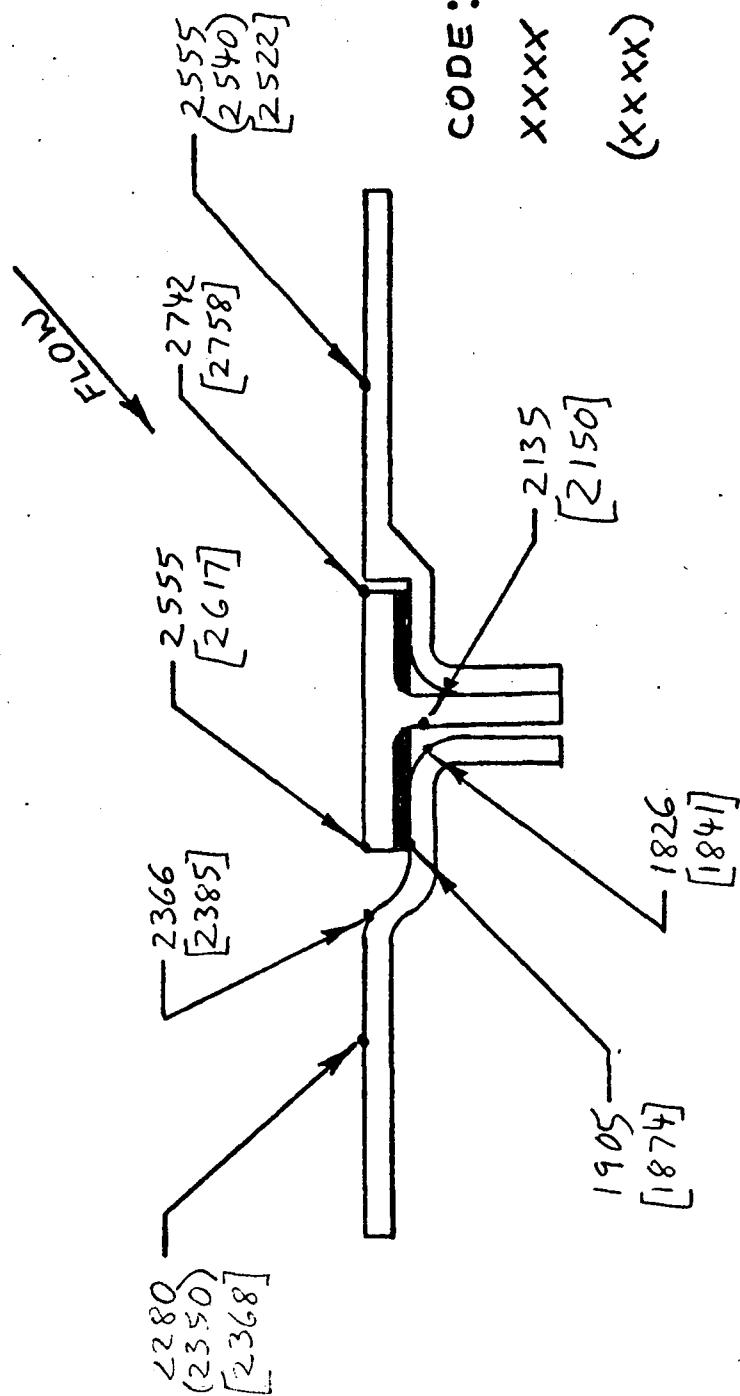
NOTE: REDUCED CONDUCTIVITY OF
CARBON FILLER

TEMPERATURE COMPARISON
CHORD LINE, -7 ASSEMBLY
FIGURE 22



\dot{q} = LOCAL HEATING RATE
 \dot{q}_u = UNDISTURBED HEATING
 (XXX) = DISTANCE OVER WHICH
 HEATING OCCURS

HEATING ON -3 ASSEMBLY, MODIFIED
 FIGURE 23

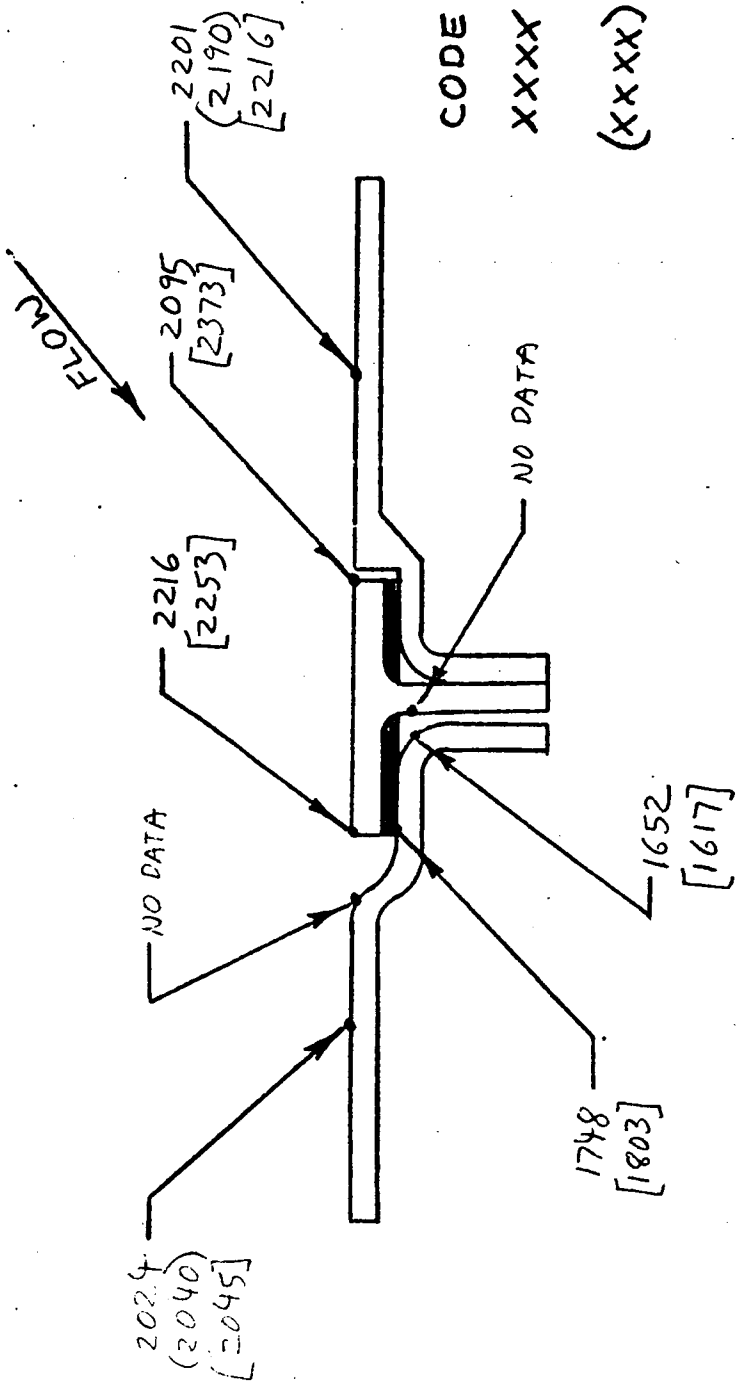


CODE:

XXXX MEASURED TEMP, °F
-3 ASSY.
(XXXX) MEASURED TEMP, °F
AVERAGE OF 12 TEST
RUNS ON 10 CONFIGU-
RATIONS
[XXXX] COMPUTED TEMP, °F

NOTE: REDUCED CONDUCTIVITY OF CARBON FILLER
HEATING PER FIGURE 23

TEMPERATURE COMPARISON
STAGNATION LINE, -3 ASSEMBLY
FIGURE 24



CODE:

XXXX MEASURED TEMP., °F
-3 ASSY.

(XXXX) MEASURED TEMP., °F
AVERAGE OF 12 TEST
RUNS ON 10 CONFIGU-
RATIONS

[XXXX] COMPUTED TEMP., °F

NOTE: REDUCED CONDUCTIVITY OF CARBON FILLER
HEATING PER FIGURE 23

TEMPERATURE COMPARISON
CHORD LINE, -3 ASSEMBLY
FIGURE 25

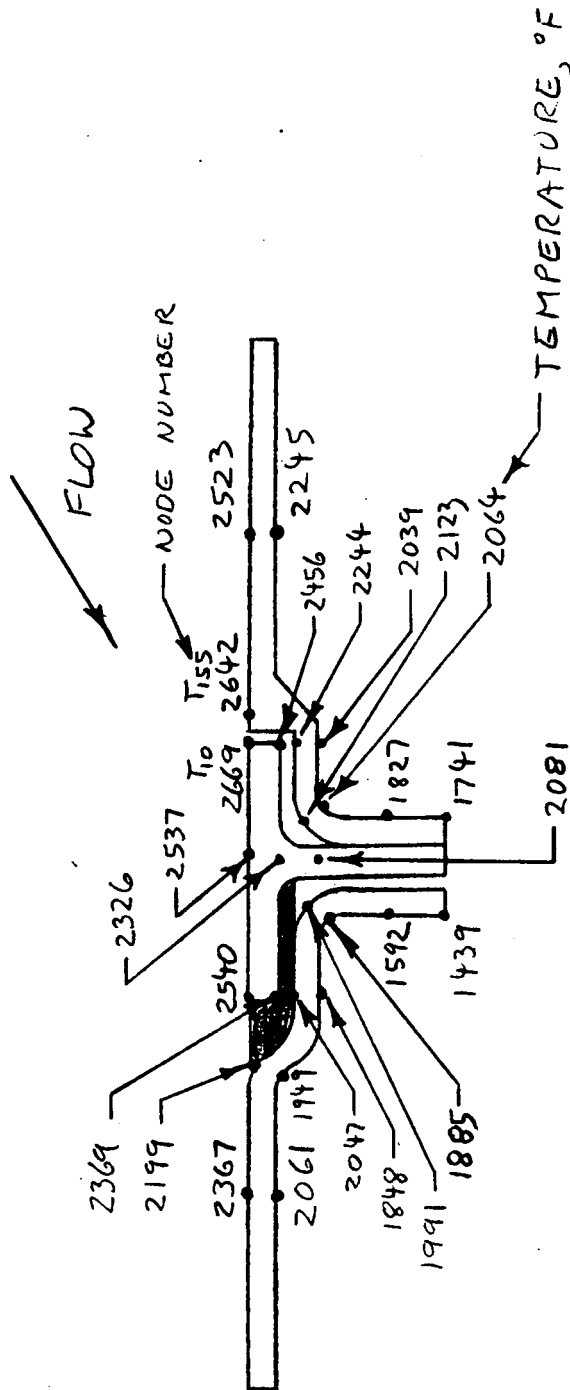
cavity floor caused computed temperatures in this area, T_2 and T_8 , to drop significantly below measurements. Hence the heating in this area is probably higher than than shown in Figure 11.

Final computer runs for the -7 and -3 assemblies were made with felt conductivity 1/3 of "nominal" values. The heating distribution on the -7 assembly was that shown in Figure 18, and computed temperatures are shown in Figures 21 and 22. Heating on the -3 assembly was modified as shown in Figure 23 by increasing heating on the cavity floor to the same values used for the -2 and -1 assemblies. As discussed earlier, it would be expected that heating in this area would be similar for these assemblies. Computed temperatures for the -3 assembly are shown in Figures 24 and 25. Computed and measured rib temperatures are in much better agreement for both -7 and -3 assemblies with the lower felt conductivity. External tee temperatures are in slightly better agreement for -7, while for -3 computed external tee temperatures slightly exceed measurements. Cavity floor temperatures for -3 are in reasonable agreement with measurements.

The other tee configurations were not analyzed in detail. The -6, -15 and -9 assemblies should be analyzed later. The -6 and -15 assemblies opened the upstream gap to 0.05 inch and the -15 assembly also opened the downstream gap to 0.09 inch. The -9 assembly introduced a 0.03 inch protrusion of the tee above the skin. The -12 assembly opened both gaps to 0.025 inch, and it was not analyzed because the effects of each gap were analyzed separately for the -2 and -7 assemblies. The other assemblies were not analyzed because, as discussed earlier in the Test Results, the parameters investigated proved not to have significant effects or the design approaches represented were found not to be favorable.

Stagnation Line Temperature Profile

Temperatures at the stagnation line of the -7 assembly are detailed in Figure 26 in order to illustrate a complete profile of computed temperatures, including locations where there were no thermocouples in the test model. This presentation reveals an important fact, that is the temperature on the skin T_{155} immediately opposite the



DETAILED TEMPERATURES, -7 ASSEMBLY STAGNATION LINE
FIGURE 26

tee leading edge T_{10} is almost as hot as the tee leading edge, 2642 versus 2669°F. This is due to radiant heat transfer across the gap, since the convective heating imposed on node 155 was undisturbed heating. This indicates that mission life of the skin will be affected by the disturbed heating to almost the same extent as the tee. It had been thought, based on thermocouple data alone, that only the tee was affected by the disturbed heating.

APPLICABILITY OF RESULTS TO FLIGHT

As part of the seal strip gas leakage analysis, T143-DIR-2-04, a comparison was made between test and entry flow parameters, as shown in Table IV. This comparison

TABLE IV
COMPARISON BETWEEN PLASMA ARC TEST AND ENTRY
FLOW PARAMETERS

Entry Time Seconds	Enthalpy for Plasma Arc Test BTU/Lb	Boundary Layer Thickness, Inches	Energy* Inflow BTU/Ft Sec	Entry Parameters Velocity Ft/Sec	Altitude Ft
400	-	1.2**	0.525	25,400	258,000
1200	-	0.54**	1.342	19,900	225,000
-	13,435	0.342	0.612	-	-
-	11,367	0.455	-	-	-
-	5,928***	0.173***	-	-	-

* 0.05 inch gap; energy inflow per foot of gap length

$$= \dot{M} (\bar{H} - H_w)$$

\dot{M} = Mass inflow per foot of gap length, Lb/Ft Sec

\bar{H} , H_w = enthalpy of air entering gap and at wall temperature, respectively, BTU/Lb

** 8.00 inch leading edge radius

*** High pressure test point which was not achieved in gap tests

indicated that boundary layer thickness in the test would be less than that in flight, and energy inflow into gaps would be comparable to the high altitude entry condition and about one-half of that for the low altitude entry condition. Test results indicate that the disturbed heating on the seal is primarily a rough body or cavity flow effect, which is sensitive to boundary layer thickness, rather than an inflow effect.

It should be noted that Scott, in a NASA Memorandum of Dec. 12, 1972, computed entry boundary layer thicknesses lower by a factor of 60 to 70 than those in Table IV

The difference appears to be primarily in assumed leading edge radius which was 3 inches in Scott's analysis and 8 inches in Table IV. Scott's boundary layer thickness calculations for the test model are comparable to those in Table IV for similar assumed enthalpy. Enthalpy for the tests, however, has been measured by various means as between 7200 and 35,000 BTU/Lb, according to a Scott memorandum of Dec. 14, 1972. It is evident that this important parameter must be defined more closely in order to make a firm comparison of entry and test flow parameters.

Correlation of the disturbed heating rates from the present study with available analytical relations and other empirical data in the literature is a most desirable next step in the analysis in order to provide a rational basis for application to flight conditions. However, it will be necessary to define the enthalpy for the tests more closely in order to perform such analyses with confidence.

CONCLUSIONS

- o The test objective of evaluating various seal configurations from a thermal standpoint was met.
- o Gaps should be maintained below 0.05 inch and tee protrusion should be avoided.
- o The magnitude of temperature increase on the tee seal compared to the unperturbed skin amounts to about 180°F for a 0.025 inch gap. Temperature increase on the skin immediately opposite the tee will be slightly less.
- o Alternate seal configurations represented by -13 and -14 assemblies are not beneficial.
- o Making the tee fully integral with the upstream panel would result in increased temperatures of about 110°F for the downstream overlap area.
- o Rounding of the tee leading edge is not beneficial.
- o Both increased convective heating and suppression of cross radiation cooling contribute significantly to the increased temperatures measured on the tee seals.
- o The technique of measuring temperatures, using tungsten-rhenium thermocouples mounted within approximately 0.010 inches of the outer surface and covered with C-34 cement, produced consistent and reproducible results. Replacement thermocouples and replacement parts produced little variance in temperature measured.

RECOMMENDATIONS

- o When the enthalpy of the flow for the tests has been more closely defined, additional analyses should be performed to correlate heating rates with available theory and empirical data in the literature, and to apply results to flight conditions.
- o The post test thermal analysis reported herein should be extended to evaluate effects of conductivity of RPP-3 versus RPP-1 and to include analysis of additional tee configurations.
- o Additional tests should be performed at high stagnation pressures, possibly by use of zero sweep angle, for simulations of low altitude entry conditions.
- o Additional tests should be performed with more thermocouples in critical areas and using infrared photography for detailed temperature maps.
- o Coated RPP-3 models should be tested for better simulation of conductivity effects and effects on the coating.